POLITECNICO
MILANO 1863

DIPARTIMENTO DI CHIMICA, MATERIALI E INGEGNERIA CHIMICA
"GIULIO NATTA"

Doctoral program in Materials Engineering, XXX Cycle

Long term fracture behaviour of HDPE for household detergent containers: a study on environmental stress cracking

Doctoral dissertation of
Marco Contino

Supervisor
Dr. Luca Andena

Tutors
Prof. Claudia Marano
Prof. Marta Rink

The Chair of the Doctoral Program
Prof. Chiara Castiglioni

A Francesco Caimmi e Dario Picenoni

per avermi mostrato cosa vuol dire avere passione per il proprio lavoro.

Alle mie due nonne, Anna e Giannina,

per tutti gli "a nonna" e gli "stûdïa" che mi avete detto in questi anni.

Acknowledgements

Come prima cosa vorrei ringraziare Fater S.p.A. per aver finanziato, con una borsa di dottorato e con un contratto di ricerca, il mio lavoro durante questi tre anni. In particolare un ruolo primario durante questo periodo lo hanno avuto Giuliano Marra e Stefano Resta con cui ho collaborato sin dal primo giorno di questo progetto e Matteo Lega che ha preparato tutte le soluzioni utilizzate durante i test meccanici e di invecchiamento.

Luca e Marta siete state le persone che mi hanno aiutato di più durante questo percorso: mi avete guidato e aiutato durante questi anni e vorrei quindi ringraziarvi per avermi fatto crescere dal punto di vista professionale con tutte le discussioni che abbiamo avuto, con tutti i consigli che mi avete dato, e per tutto il tempo che avete speso nel correggere ogni poster, ogni presentazione e ogni pagina di questa tesi. Senza di voi la qualità del mio lavoro sarebbe stata sicuramente inferiore. Claudia ringrazio moltissimo anche te, per essere diventata la mia tutor e per i preziosi consigli che mi hai dato durante questi anni. Grazie mille a Francesco Briatico, a Francesco Caimmi, al Prof. Roberto Frassine e al Prof. Andrea Pavan per essere stati sempre disponibili nell'ascoltarmi e per avermi dato il vostro punto di vista sulla mia ricerca. Oscar, ti ringrazio per avermi aiutato durante le fasi di preparazione dei provini e di test e, dato che abbiamo condiviso lo stesso ufficio durante gli ultimi quattro anni, per aver dovuto sopportare più di tutti "i pochi" lati irritanti del mio carattere…

In questo periodo io e Luca abbiamo proposto alcune tesi triennali e magistrali e ho seguito i ragazzi che hanno avuto la sfortuna di avermi come correlatore: Andrea, Sergio, Chiara, Massimiliano, Sofia, Francesca e Vincenzo avete contribuito enormemente a chiarire alcuni aspetti di questa ricerca. Vi ringrazio

per l'impegno e la serietà con cui avete affrontato il lavoro che vi abbiamo assegnato, per tutte le domande che mi avete fatto e per gli spunti di riflessione che mi avete fornito. Lavorando al PolyEngLab ho anche avuto modo di collaborare con tanti assegnisti e dottorandi e ognuno di voi mi ha, in qualche modo, arricchito: Francisco, Roberto, Nadia, Michele, Emanuele, Andrea, Tommaso, Susanna, Davide, Jacopo, Federica, Marco, Giancarlo e Stefano grazie mille per il percorso che abbiamo condiviso, per le discussioni che abbiamo avuto cercando di risolvere un problema o di chiarire un dubbio ma anche per tutte le scemate che abbiamo fatto insieme (chiedo scusa se mi sono dimenticato di qualcuno ma in più di sei anni c'è stato un certo via vai).

I switch to English to thank Prof. Thomas Pardoen for letting me work for almost six months at the pole of Materials and Process Engineering (IMAP) of the Université Catholique de Louvain in Belgium: you gave me the opportunity to study a quite complex phenomenon and to better understand some aspects of my research. I also thank Catherine Bauwens, Marc Sinneave, Catherine Doneux and all the members of IMAP pole for helping me during my permanence in Louvain La Neuve. Mrs. Georgette Vincke Noel, thank you for having graciously welcomed me to your house, for all the French lessons and for the many cultural and tourist activities you suggested me.

Dr. Bamber Blackman and Dr. Francesco Baldi I would like to thank you for your review of this thesis, for the suggestions to improve the quality of this work and for making yourself available as external members of the commission for the final dissertation of my work. I also thank Dr. Leonardo Castellani for having accepted the latter role as well.

Torno all'italiano per ringraziare gli amici che mi hanno accompagnato durante questi anni e con cui ho condiviso tantissime esperienze. Teresa e Fabio grazie mille anche a voi per l'affetto che ci lega e per tutto quello che abbiamo passato insieme da quando le nostre strade si sono incrociate. Mamma e papà, vi ringrazio per tutto l'amore che mi avete dato fino ad ora e per tutto quello che avete fatto per aiutarmi a raggiungere questo traguardo. Devo però farvi notare che i vostri rimproveri perché "quando passava Marco rompeva tutto" si sono rivelatati totalmente inutili, visto che negli ultimi tre anni mi hanno pagato proprio per rompere diverse cose, tra cui dei provini. Monica ti ringrazio per avermi fatto da chioccia come solo una sorella maggiore sa fare e per essere stata sempre un esempio da seguire e ammirare. Daniele, grazie per tutti gli hard disk cambiati poco prima di una conferenza e, soprattutto, per l'affetto e l'amicizia che ci lega ormai da troppi anni per considerarti solo come il mio "cogny". Emanuele e Nicolò un ringraziamento speciale va anche a voi, i miei "nipotini", per la vostra gioia e la vostra allegria e per avermi ricordato che, a volte, le domande più semplici sono quelle a cui è più difficile trovare una risposta. Valeria da più di tredici anni mi dai forza, mi sostieni in tutte le mie decisioni e mi sopporti: ti ringrazio per essere al mio fianco in ogni momento e per l'amore che mi dai ogni giorno. Senza di te questo percorso sarebbe stato sicuramente molto più difficile

Abstract

High-density polyethylene (HDPE) is a polymer widely used for many packaging applications. During its service life a container can be exposed to substances, like commercial bleach, which, interacting chemically and physically with the polymer, can alter its mechanical properties and can lead to a premature failure of the container itself.

Due to the great number of ingredients present in a typical commercial bleach, the determination of their individual effect on the mechanical properties of the polymer and the identification of the nature of their interaction is of particular interest to properly describe the occurring phenomena. In fact, it has to be considered that substances like sodium hypochlorite can interact chemically with the polyethylene causing its oxidation, while surfactants can be absorbed by the material in proximity of a defect thus favouring a phenomenon called Environmental Stress Cracking (ESC). However, due to the different nature of the two interactions and to the different amount of time required for their occurrence, it is not straightforward to predict which mechanism would be active under given conditions.

For these reasons, in this study, the two phenomena were considered separately. To evaluate the extent of the chemical interaction, HDPE samples were exposed to several solutions containing combinations of bleach ingredients for different amounts of time and the evolution of several properties was monitored at regular intervals. At the end of this characterization only a negligible increase of the sample mass, related to the absorption of the solution, was measured while no effect on tensile and scratch resistance properties was detected; it was hence

concluded that negligible chemical interaction could occur during the time range considered, corresponding to the expected bottle service life.

For what concerns ESC, instead, fracture tests were conducted on 11 mm thick compression moulded samples both in air and in the presence of the various environments. The influence of the bleach ingredients on the initiation and propagation phases of fracture was evaluated adopting a method based on Linear Elastic Fracture Mechanics (LEFM). It was observed that in presence of the considered environments, after a critical interaction time and below a critical propagation speed, the crack initiated earlier and propagated faster with respect to that observed in air. A time-temperature superposition reduction scheme was also adopted to predict the long term fracture and ESC resistance of the materials under study.

Subsequently, the effect of the production process was also studied obtaining samples directly from the bleach containers. Due to the reduced thickness of the bottle walls with respect to those of the samples used during the first part of the research, specimens were subjected to a different stress state during the fracture tests. Extensive plastic deformation was detected during in-air tests and, consequently, a different strategy, based on the J-integral approach, was used for the data analysis. As already observed with thick samples in the presence of the active environments, ESC occurred. Finally, tests conducted on compression moulded samples with a thickness comparable to the bottle wall showed that some difference, related to the different crystallinity degree of the two kind of samples, could be observed in the in-air fracture behaviour; for what concerns the in-environment behaviour, instead, practically no differences were detected with respect to the samples obtained from the bottles. This findings constitute an

important result since they could lead to a saving of time and money during the phase of material ranking and selection, as there is no need to manufacture bottles of a given material to obtain information on their expected lifetime.

Sommario

Il polietilene ad alta densità (HDPE) è un polimero ampiamente utilizzato in diverse applicazioni nel settore del packaging. Durante la vita di servizio di un imballo, questo può entrare in contatto con alcune sostanze, come la candeggina, che, interagendo chimicamente e fisicamente con il polimero, possono alterarne le proprietà meccaniche causando un cedimento prematuro dell'imballo stesso.

A causa dell'elevato numero di ingredienti presenti in una candeggina commerciale, la determinazione del loro effetto sulle proprietà meccaniche del polietilene e l'identificazione della natura della loro interazione con il polimero stesso risulta essere di particolare interesse per descrivere in modo appropriato i fenomeni che avvengono durante la vita di servizio dell'imballo. Bisogna infatti considerare che alcune sostanze come l'ipoclorito di sodio possono interagire chimicamente con il materiale causandone l'ossidazione mentre i tensioattivi possono essere assorbiti dal materiale in prossimità di un difetto favorendo lo sgrovigliamento delle catene polimeriche e causando un fenomeno chiamato *Environmental Stress Cracking* (ESC). Tuttavia a causa della differente natura di questi tipi di interazione e a causa del diverso tempo necessario affinché queste abbiano un'influenza sulle proprietà meccaniche del materiale, non è facile prevedere se entrambi i meccanismi siano attivi durante la vita di servizio di un flacone di candeggina.

Per queste ragioni, durante questo studio, questi due fenomeni sono stati studiati in modo separato. Per valutare l'entità dell'interazione chimica, i campioni sono stati esposti a diverse soluzioni contenenti varie combinazioni degli ingredienti contenuti in una candeggina commerciale per diversi periodi di tempo, valutando l'evoluzione di alcune proprietà dopo l'esposizione. Alla fine di questa

caratterizzazione è stato misurato un esiguo aumento della massa dei materiali considerati, dovuto all'assorbimento delle soluzioni, mentre non è stato misurato alcun effetto sulle proprietà di trazione e sulla resistenza al graffio; si è quindi giunti alla conclusione che, in termini pratici, un'eventuale interazione chimica tra candeggina e polietilene ha effetti del tutto trascurabili sul comportamento del flacone per tutta la durata della sua vita di servizio.

Per quanto riguarda l'ESC, invece, sono state condotte delle prove di frattura, in aria e in presenza delle diverse soluzioni, su provini spessi 11 mm, ottenuti per stampaggio a compressione. L'influenza dei vari ingredienti della candeggina sulle fasi di innesco e di propagazione della frattura è stato valutato con un metodo basato sulla Meccanica della Frattura Lineare Elastica (LEFM). Si è osservato che, in presenza degli ambienti attivi, dopo un certo tempo di interazione chimica e al di sotto di una velocità di propagazione critica, la cricca innesca in tempi inferiori e propaga a velocità maggiori rispetto a quanto osservabile durante le prove in aria. È stato inoltre applicato uno schema di riduzione dei dati basato sul principio di sovrapposizione tempo-temperatura per prevedere il comportamento a frattura e la resistenza a ESC a lungo termine dei materiali considerati.

In seguito, è stato analizzato l'effetto del processo produttivo ricavando dei campioni direttamente dai flaconi. A causa del ridotto spessore della bottiglia rispetto a quello dei provini utilizzati durante la prima parte di questo lavoro, il materiale si trova in uno stato di sforzo diverso durante i test di frattura. È stata inoltre osservata la formazione di una estesa zona plastica durante i test in aria e, di conseguenza, si è deciso di utilizzare una differente strategia, basata sull'integrale *J*, per l'analisi dei dati. Come per i provini più spessi, in presenza di

un ambiente attivo il fenomeno dell'ESC può essere osservato. Infine, sono stati condotti alcuni test su provini stampati a compressione aventi uno spessore paragonabile a quello delle bottiglie osservando come siano presenti delle differenze, legate al diverso grado di cristallinità dei due tipi di provino, per quanto riguarda il comportamento a frattura in aria; considerando invece il comportamento in ambiente attivo si è osservato che queste differenze tendono ad assottigliarsi. Questo fatto potrebbe portare a un notevole risparmio di tempo e denaro durante la fase di ranking e selezione di materiali in quanto potrebbe non essere necessario condurre test sui flaconi veri e propri.

Contents

1 Introduction

High-density polyethylene (HDPE) is a polymer widely used for many packaging applications. During its service life a container can be exposed to substances which, interacting chemically and physically with the polymer, can alter its mechanical properties and can lead to premature failure. An example of this kind of application are the bottles used for the distribution and sale of household detergents: during this research project, sponsored by FATER S.p.A., the case study of HDPE bottles used for bleach solutions has been considered.

In terms of the mechanical stresses to which the containers are subjected during their life, the most critical phases are the storage and the distribution. Once filled with the product, in fact, the bottles are usually packed in pallets, which are stacked one on top of the other. Hence, the bottles located at the bottom of these structures may be subjected to very high mechanical loading, even for several months, before the display of the product on the shelves of a retailer. In case of the premature failure of the containers, caused by the combined action of the mechanical stresses and of the aggressive environment, economic and reputation damage could occur and, in the worst case, the workmen safety could be threatened consequently to the exposure to high quantities of bleach.

The increase of the logistics and production costs related to the adoption of the easiest solutions to this problem, i.e. avoid stacking and increase the wall thickness of the bottle, makes these strategies inapplicable. In the same way, a re-design of the bottle done to minimize the parts of the container more prone to brittle failure, like handles and welding lines which are subjected to high residual thermal stresses, would require a huge investment for the replacement of all the moulds used during the production. Moreover, this kind of approach could also have some deleterious effect on the quantity of sold bottles, and

consequently on the profit, since, as revealed by marketing studies, the typical customer is more inclined to buy the product if its appearance stays the same.

A detailed study of the phenomena involved in the failure of the bottles and their causes appears to be necessary. Due to the great number of ingredients present in a typical commercial bleach, the determination of their effect on the mechanical properties of the polymer and the identification of the nature of their interaction is of particular interest to properly describe the phenomena occurring during the service life of the container. Considering the typical composition of a commercial bleach, in fact, it has to be considered that substances like sodium hypochlorite, which can interact chemically with the polyethylene, and surfactants, which can be absorbed by the material, are simultaneously present. The first can oxidize the material and cause chain scission [1–4] while, in the presence of a mechanical stress, if the surfactants are locally absorbed in proximity of a defect (where the surface to volume ratio is high) they can plasticize the material and favour disentanglement of the polymeric chains [5–7]; in both cases the consequence is a local decrease of the mechanical properties and, in particular, of the fracture resistance of the polymer. However, due to presence of other components in the bleach, to the different nature of the two interactions and to the different amount of time required for their occurrence, it is not straightforward to predict if both mechanisms would be active and if the various components could synergistically influence the mechanical behaviour of the polymer.

For these reasons, in this study, the two phenomena were studied separately starting from samples produced via compression moulding. To evaluate the extent of the chemical interaction the samples were exposed to several solutions

containing the various ingredients of bleach for different amounts of time (from 0 to 9 months at 23°C) and the variation of mass and of bulk and surface mechanical properties of the polymer was evaluated. For what concerns the physical interaction, known in literature as Environmental Stress Cracking (ESC), instead, tests on notched samples were conducted both in air and in the presence of the various environments to determine the influence of the bleach ingredients on the initiation and propagation phases of fracture. Although several standard methods [8–17] are available for the determination of the Environmental Stress Cracking Resistance (ESCR) of polymers, in most cases they can be used only for ranking purposes; to better understand the processes involved in this phenomenon, a method based on the Linear Elastic Fracture Mechanics (LEFM), an approach already proposed in [5–7, 18–24] for the study of the environmental resistance of various polymers, was adopted during this work.

Subsequently, the effects induced by the production process were also studied obtaining samples directly from the container considering, also in this case, both types of interaction. Due to the reduced thickness of the bottle walls with respect to the samples produced via compression moulding, the samples were subjected to a different stress state and plastic deformations extensively occurred during tests. Consequently a different strategy, based on the J-integral approach, was considered to be more adequate for the reduction of the data obtained from thin samples.

A brief description of the following Chapters is hereby given:

- Chapter 2 presents a review of the relevant scientific literature including the description of the possible interactions between bleach and polyethylene, of the experimental methods usually adopted to evaluate chemical degradation and Environmental Stress Cracking of polymers; a brief review of different Fracture Mechanics approaches is also included
- Chapter 3 describes the considered active environments and polyethylenes together with the process required for the production of plates and bottles from which samples were obtained
- Chapter 4 reports the results obtained from tensile tests performed to evaluate material orientation in plates and bottles, to measure elastic modulus and yield stress; furthermore, the material responses to complex loading histories is analysed
- Chapter 5 describes the fracture behaviour in air of the considered polymers under plane strain and plane stress conditions
- Chapter 6 presents the results obtained from tests performed to evaluate chemical interaction between bleach and polyethylene
- Chapter 7 presents the Environmental Stress Cracking results obtained under plane strain conditions
- Chapter 8 describes the effect of the temperature on Environmental Stress Cracking Resistance under plane strain conditions
- Chapter 9 presents the Environmental Stress Cracking results obtained under plane stress conditions; the effect of production process and of the stress state are also reported in this Chapter
- Chapter 10 highlights the main conclusions of this research work and possible future developments

Part of the data here presented have been already published as papers [25, 26], extended abstracts for conferences [27, 28], a bachelor degree thesis [29] and two master degree thesis [30, 31] which were co-supervised by the author of this work.

2 Theoretical background

2.1 Bleach

Bleach is a substance able to remove stains by strongly interacting with a substrate and which can also have sanitizing and disinfecting power; thanks to its properties it is commonly used in applications varying from domestic laundry and cleaning to the production of paper and to wastewater treatment [32].

When it is used for laundry purposes, the bleaching agent interacts with the molecules of a stain making them more soluble via a degradation in smaller units and via the introduction of solubilizing groups like carboxylates [33]. Considering this class of products, it is possible to define the families of peroxide and hypochlorite bleaches according to the relevant bleaching agent used. The solutions considered during this work belong to the latter group which is the most common bleaching system; consequently the main features regarding the production process and the chemical composition of this class of bleach are described below.

The production of the bleaching agent is carried out via the chlorination of sodium hydroxide or other bases like sodium carbonate and trisodium phosphate [34]. During this process, gaseous or liquid chlorine are introduced in an aqueous solution of sodium hydroxide, contained in a reactor, and the following reaction takes place:

$$Cl_2+2NaOH\rightarrow NaClO+NaCl+H_2O$$

A slight excess of alkali (pH>11) is used to reduce the possibility of formation of the hypochlorous acid, HClO, from the reaction between water and the ClO^- ion [35] and, consequently, granting the solution with the stability required for an

acceptable lifetime of the final commercial product. During storage, however, a series of chemical reactions involving the ClO^- ion occurs leading to the gradual decomposition of the bleaching agent:

$$2ClO^- \rightarrow ClO_2^- + Cl^-$$

$$ClO^- + ClO_2^- \rightarrow ClO_3^- + Cl^-$$

$$2ClO^- \rightarrow O_2 + 2Cl$$

Hence, sodium hypochlorite content, and consequently the strength of the bleach, diminishes during time, the more so as temperature is increased as shown in Figure 2.1.

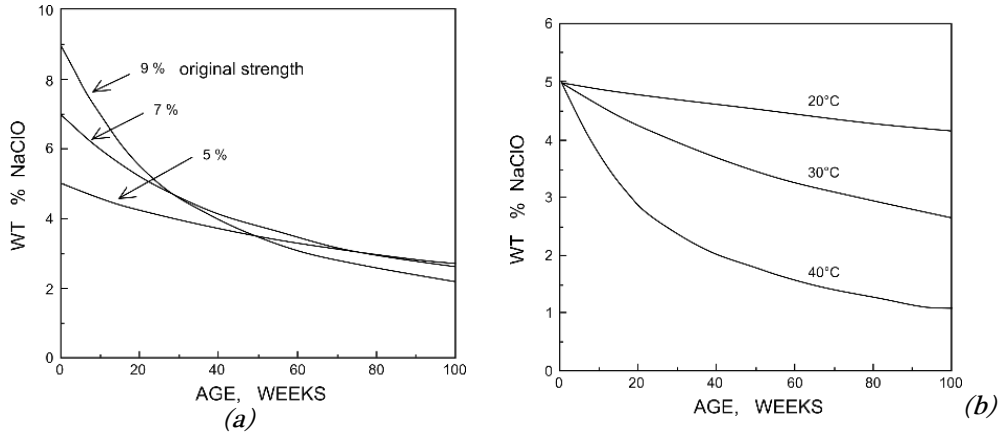

Figure 2.1 - Decomposition of sodium hypochlorite during time. (a) decomposition of bleaches with different strength at 30°C; (b) effect of temperature. [35]

One of the possible strategies adopted to reduce the loss of strength of the bleach over time is the addition of substances like silicates, bromides or calcium salts which act as stabilizers reducing the degradation rate of sodium hypochlorite [35].

Considering the chemical composition of a commercial bleach, moreover, it has to be noticed that additives other than stabilizers can be present in the solution

for several purposes. As an example, in order to reduce the strong smell typical of sodium hypochlorite bleaches, fragrances (i.e. perfume oils) could be added together with surfactants necessary to disperse them in the aqueous solution. On the other hand, different type of surfactants, together with sodium polyacrylate, clays or colloidal aluminium oxide can be present in the product to increase its viscosity and its ability to adhere to inclined surfaces assuring the contact time required to complete the bleaching or disinfection function.

Due to the different chemical species present in a commercial bleach, different kind of interactions can occur between the product and the items it comes in contact with. Among this object, the container in which the solution is stored before final usage is surely the one which stays longer in contact with the solution and, for obvious reasons, it is necessary to guarantee its integrity for the whole product lifetime. Hence, a material having adequate chemical and mechanical resistance must be selected for the production of this packaging system in order to avoid fracture phenomena limiting the container service life. For its properties and due to its low cost and ease of processing high density polyethylene (HDPE) is often selected for this purpose.

In this work the possible type of interactions occurring between a commercial bleach and the HDPE constituting the container were studied with the aim of better understanding physical phenomena, characterize the relevant material behaviour and possibly improve bottle lifetime.

2.2 Polyethylene

With more than 90 million of tons produced in 2017 [36], polyethylene is probably the most used polymer in the world for the production of pipes, wires and cables, films, household articles, several packaging systems (as for example

bleach bottles) and many other items commonly used in everyday life . It belongs to the polyolefin family and it is composed of hydrogen and carbon atoms arranged in the repeating unit $(-CH_2-CH_2-)_n$ obtained from the opening of the double bond in the ethylene molecule $CH_2=CH_2$.

Despite its simple chemical composition, different forms of this material can be obtained by changing the polymerization conditions, the catalyst or the production process. If, for example, the polymerization is conducted using a free radical initiator (usually belonging to the class of the peroxides) at pressure higher than 2400 bar and temperature higher than 310°C Low Density Polyethylene (LDPE) can be obtained [37]. If a lower pressure and temperature (10-140 bar and 70-300°C respectively) are instead adopted, Very Low Density Polyethylene (VLDPE), Linear Low Density Polyethylene (LLDPE), Medium Density Polyethylene (MDPE) and High Density Polyethylene (HDPE) can be produced depending on the catalyst used and production process parameters [38].

The differences between the various forms are mainly related to the abundance and length of the side branches present in the polymeric molecules. As sketched in Figure 2.2, going from LDPE to HDPE, the number and length of the side branches decreases and, consequently, the molecules become more linear. These different structures will influence the organization and packing of the polymeric chains within the material: in the presence of long side branches the formation of a compact structure will be hindered while for more linear molecules a higher degree of packing will be possible. Consequently, in the latter case the crystallization of a larger fraction of the material will be favoured from a thermodynamic point of view, while less crystalline materials will be obtained from highly branched molecules.

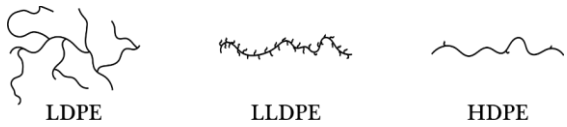

Figure 2.2 – Differences in the molecular structure of three kind of polyethylene.

A property directly affected by the different degree of crystallinity, χ_c, is the density; due to its ease of determination, it is commonly used to distinguish the main families of this material as shown in Table 2.1.

Table 2.1 - Density of the main classes of polyethylene [38, 39].

		VLDPE	LDPE	LLDPE	MDPE	HDPE
DENSITY	MIN.	0.860	0.915	0.910	0.930	0.940
[g/cm^3]	MAX.	0.915	0.932	0.930	0.940	0.970

The density, however, is not the only parameter which is typically controlled during the polymerization: the molecular weight distribution (MWD) is also of great importance, both for ease of processing and for the final properties (namely, fracture resistance). Considering the material studied during this work, i.e. HDPE, it is usually produced via slurry polymerization in which the gaseous monomer (ethylene), a comonomer (usually 1-butene or 1-hexene) and the chain transfer agent (hydrogen) are fed into a reactor together with diluents, the catalyst (Phillips, Ziegler-Natta or metallocene) and the cocatalist which are the liquid and solid components of the slurry. During the polymerization, for example, the average molecular mass can be controlled by adjusting the quantity of hydrogen present in the gas phase: for higher partial pressure of the transfer agent, higher molecular mass species are formed. Combining two reactors in cascade, moreover, it is also possible to polymerize HDPEs having a very broad bimodal molecular weight distribution (MWD) and increased long-term mechanical behaviour (while still retaining processability).

By varying only the two material parameters introduced up to now, it is be hence possible to obtain several grades of HDPE to be adopted in different applications. As described in Figure 2.3, in which a map of various HDPE products is plotted in terms of optimal density and melt flow rate (which due to the almost linear structure of this polymer can be considered as a rough indication of its average molecular weight and MWD), in fact, it is possible to tune the material structure in order to produce grades adequate both for the injection moulding process and for the production of pipes or large containers. In particular, in the middle of the graph it is possible to observe a region representing the extrusion blow moulding grade used for the production of bottles to which the polymers considered during this work belong.

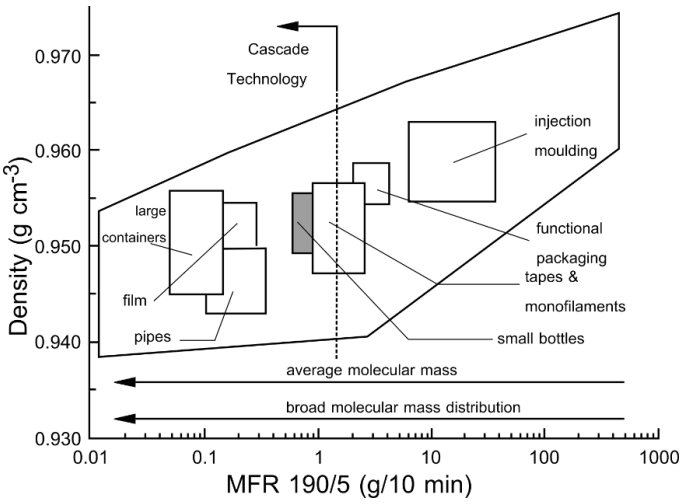

Figure 2.3 - HDPE density-melt flow rate map. The rectangles represent the different products which can be obtained for a given couple of the two parameters [38]. *The grade used for the production of small bottles, which is of particular interest during this work, is highlighted in grey.*

2.2.1 HDPE morphology and mechanical behaviour

When cooled from its molten state, HDPE can form crystalline lamellae, having lateral dimensions in the order of tens of microns and thickness in the order of

the tens of nanometres [40], consisting of a regular chain-folding arrangement of the molecular chains (also called stems) perpendicularly aligned to the lateral lamellae surfaces. Obviously, due to the complexity of the polymeric chains, to their high flexibility in the molten state and to some irregularities intrinsically present, not all the material is in the crystalline state and it is well known that the same macromolecule can be partly in the ordered crystalline phase and partly in the disordered amorphous one. The resulting material is hence constituted by stiff crystalline domains, a more compliant amorphous phase and an interphase characterized by intermediate molecular mobility and, consequently, intermediate stiffness with respect to the other two phases [41].

Considering the amorphous state, it is possible to define the three types of intercrystalline material highlighted in Figure 2.4 [42, 43]:

- **Cilia:** chains which begin in the crystalline lamella and end in the amorphous phase
- **Loose loops:** chains beginning and ending in the same lamella having the mid-section in the amorphous phase
- **Tie molecules:** chains beginning in a lamella and ending in a different one, adjacent to the first, connecting in this way the two crystalline domains

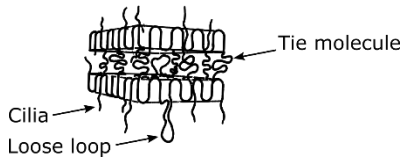

Figure 2.4 - Sketch of the amorphous layer between two crystalline lamellae highlighting the three types of intercrystalline material (Cilia, Loose loop and Tie molecules) [43].

Being located in the amorphous phase, these three types of intercrystalline material are, of course, in a disordered configuration. Hence, physical entanglements between cilia, loose loops and tie molecules are present, increasing the connections between the lamellae.

These lamellae and amorphous interlayers can be organized in superstructures whose morphology depends on several factors including, for example, the molecular weight distribution, the cooling rate, the presence of orientation in the melt, the melting temperature. One of the most known types of superstructure, usually observed in HDPE, is known by the name of spherulite and is characterized by the arrangement of the lamellae in a radial configuration as sketched in Figure 2.5 [44].

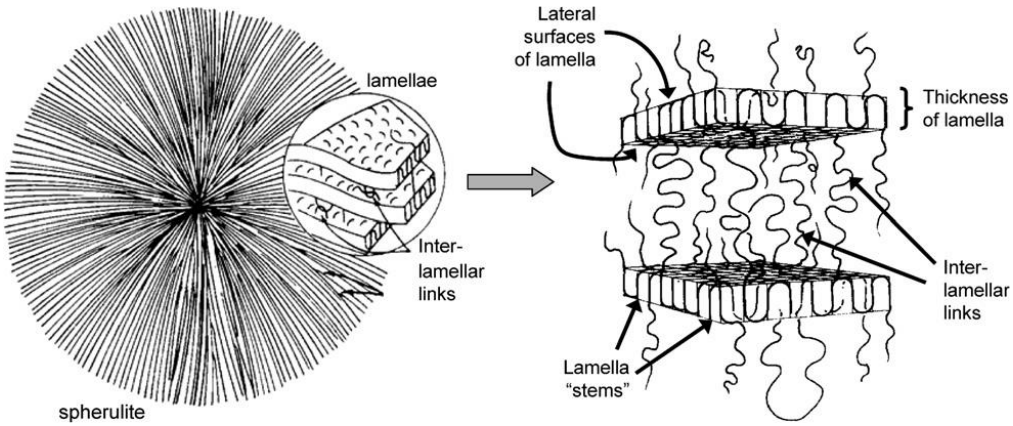

Figure 2.5 - Sketch of a spherulite, lamella and amorphous phase [44].

Having described the microstructure of HDPE it is possible, at this point, to link these aspects with the complex phenomena occurring during a deformation process, which implies a simultaneous a concurrent response of the crystalline and amorphous phases present in this material [45]. Beginning from low strains, it is reasonable to expect that the more compliant amorphous phase would deform more easily with respect to crystalline lamellae which at this stage would

remain mostly undeformed. Increasing the strain up to the yield point, instead, irreversible shear deformations, which can involve also the crystalline phase, take place.

Considering the fracture process, which is of particular interest for this work, the model proposed by Lustiger and Markham in [42, 43] clearly conceptualize the processes occurring in the material during failure. Starting from an undeformed situation and considering a tensile stress σ applied normal to the face of two adjacent lamellae, the tie molecules and the other type of chains present in the amorphous interlayer (i.e. cilia and loose loops), begin to stretch as shown in Figure 2.6.

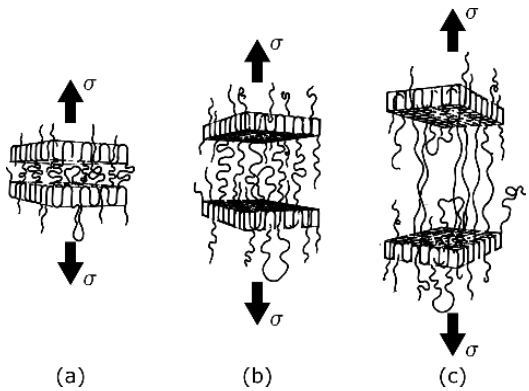

Figure 2.6 - Initial steps in the deformation of polyethylene. Adapted from [42, 43].

If the applied stress is high enough, once the tie molecules and the entangled molecules in the amorphous layer are fully extended (Figure 2.6(c)), the lamellae start to break up into smaller units called “mosaic blocks” (Figure 2.7(a)) and a fibre morphology, in which the smaller units are incorporated, forms as sketched in Figure 2.7(b). These processes will generate the typical rough fracture surface observed for ductile failure.

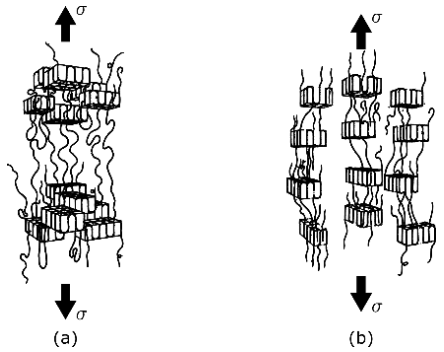

Figure 2.7 – Steps of the ductile failure. (a) break up of the lamellae in smaller units; (b) evolution of a fibrillary structure containing the smaller units themselves [42, 43].

At lower stresses, instead, fibre pull out does not occur and the molecules in the amorphous state have sufficient time to relax and disentangle leading to a brittle failure type as sketched in Figure 2.8.

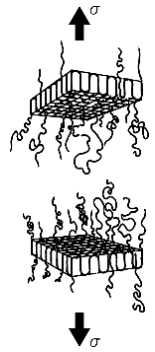

Figure 2.8 - Final step of the brittle failure [42, 43].

A further investigation on the failure modes of polyethylene has been conducted by Plummer, Goldberg and Ghanem in [46] who proposed the sketch reported in Figure 2.9. In agreement with the mechanism previously described, a decrease of the stress intensity factor K (a fracture parameter which will be properly introduced in Section 2.5) causes a variation of the damage mechanism of the polymer: for high K it is dominated by the nucleation of large cavities and by the large deformation of the crystalline domains while at low K it is characterized

by a relatively fine fibrillar structure. This model can be represented also in term of stress-time curves as shown in Figure 2.10; considering three loading conditions the following mechanisms can be activated:

- If the material is loaded according to the loading line (i) the yield stress will be reached and the failure will occur via ductile tearing
- The hatched region represents a situation of instability since the stress-time curve describing the breakdown of interlamellar fibrils is intercepted before the one of the interlamellar cavitation: if the material is loaded according to the load line (ii) a coarse fibrillation of the polymer will usually occur
- If the material is loaded according to load line (iii), instead, the interlamellar cavitation will lead to a relatively fine fibrillar structure which will subsequently break

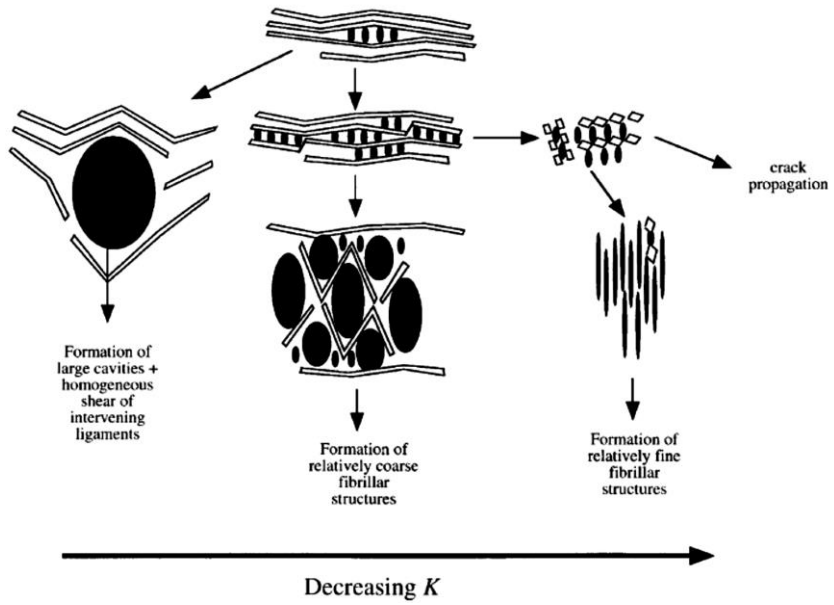

Figure 2.9 - Schematic of the damage mechanisms of polyethylene as a function of the stress intensity factor K. [46]

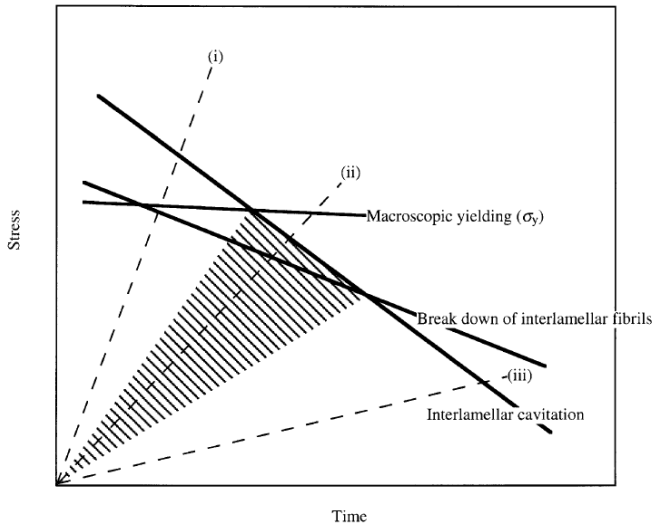

Figure 2.10 – Schematic of the stress-time dependence of the basic damage mechanisms of polyethylene. [46]

These models assume that the molecules in the amorphous phase have a key role in the brittle failure of HDPE while the crystalline phase mainly influences the ductile one. To further clarify the link between the material microstructure and the fracture resistance, the effect of some molecular parameters on the material behaviour is described below:

- **Molecular weight:** the amount of molecules in the amorphous phase increases with increasing molecular weight, leading to a higher content of tie molecules and entanglements [47, 48]; moreover the thickness of the amorphous phase and of the interface with the crystallites increases with the molecular weight itself [41]. Since polymers are polydispersed systems, the entire Molecular Weight Distribution (MWD) needs to be considered
- **Presence of side groups:** crystallinity is inhibited by the presence of these groups which can be introduced, for example, by adding a comonomer

during the polymerization phase. Moreover, since these side groups increase the probability of chain entanglement, it can be argued that increasing the content of the comonomer or its length will lead to an increase of the brittle-failure resistance [49, 50]

- **Degree of crystallinity:** the crystalline and amorphous phases are, of course, complementary; hence, the higher the crystalline content, the lower the brittle-failure resistance of the polymer
- **Lamellae orientation:** in the case of process-induced orientation of the crystalline domains, the material response to a mechanical stimulus is anisotropic and, consequently, an orientation more prone to interlamellar failure is present. This effect is minimized in case of extensive spherulite formation during the crystallization of the melt

Now that the main features regarding both bleaches and polyethylene have been introduced, the relationship between the nature of their interaction and the effect on HDPE mechanical properties can be described.

2.3 Interactions between bleach and HDPE

As described in Section 2.1, a commercial bleach contains several ingredients which can influence the mechanical behaviour of the HDPE constituting the container. In particular, it is known that chlorine based disinfectants, as sodium hypochlorite, can chemically degrade several polymers and that HDPE suffers from a physical phenomenon, called Environmental Stress Cracking (ESC), if loaded in presence of surfactants. The mechanisms with which these two kind of interactions take place and their effects on the material morphology and mechanical behaviour are presented in Sections 2.3.1 and 2.3.2 together with the techniques used in literature to study these phenomena.

2.3.1 Chemical interaction

As elucidated in different works regarding the infrastructures required for the transportation of drinkable water [1, 2, 4, 51–55], the chlorine or chlorine-based substances, added to reduce the presence of bacteria, can have deleterious effects on polymeric pipes or membranes.

When these disinfectants are added to water, in fact, they can decompose to very reactive species, including ions and radicals like HClO, ClO^-, Cl^-, HO^-, $Cl^\bullet$, $HO^\bullet$ and $ClO^\bullet$, which chemically attack the molecules of the polymeric material leading to its degradation [4, 53]. Since, for what concerns the polyolefin family in particular, a free radical mechanism can occur causing oxidation and polymeric chain scission [2], $Cl^\bullet$, $HO^\bullet$ and $ClO^\bullet$ would be the species involved in the degradation process of HDPE. Even if the chemistry of these systems is not completely understood [53], it is known that $Cl^\bullet$ exists only at acid pH and that, due to the high reactivity of $HO^\bullet$, this radical is probably consumed for the oxidation of a very thin surface layer of the polymer. It is hence supposed that, in case of massive degradation of the component, the main species acting during the chemical degradation of polyolefin systems is $ClO^\bullet$. The main chemical reactions taking place during the exposition to an oxidizing environment are the formation of double bonds between carbon atoms, the attachment of oxygen atoms to the latter and the formation of hydroxyl (OH) or carboxylic (COOH) as revealed by the infrared spectroscopy analyses conducted in [1, 4, 55–60] (see Figure 2.11).

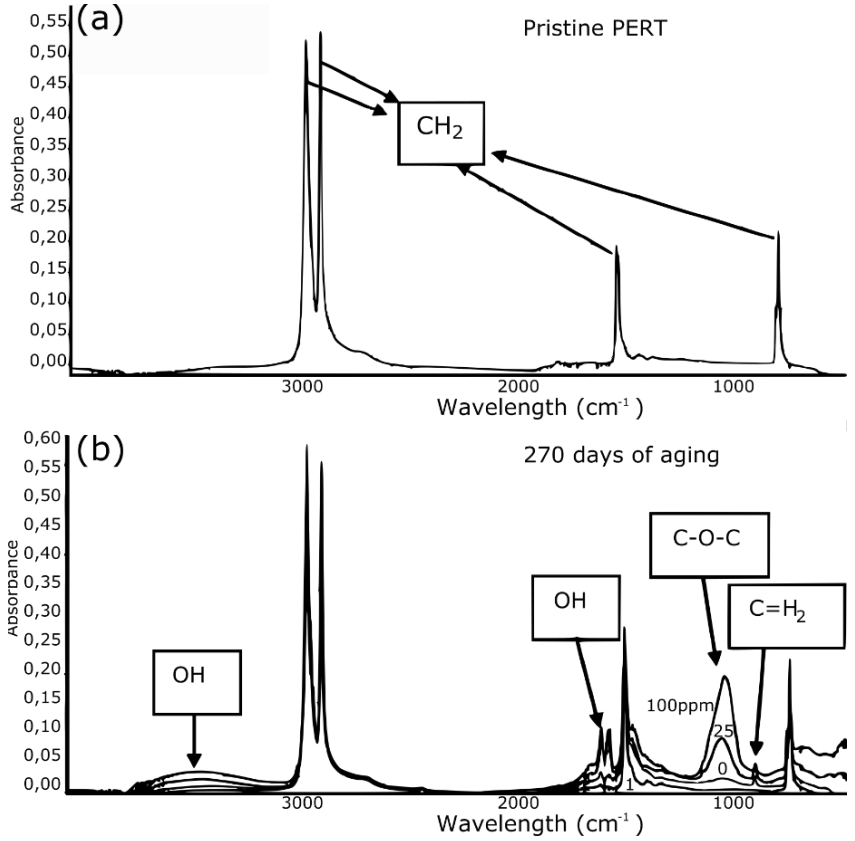

Figure 2.11 - Infrared spectra of polyethylene of raised temperature resistance (PERT). (a) unaged material; (b) 270 days aged material in aqueous solutions containing sodium hypochlorite at different concentrations of free chlorine (100 ppm, 25 ppm, 0 ppm and 1 ppm from top to bottom). [4]

The material integrity, and consequently its mechanical properties, is usually safeguarded by incorporating antioxidants or stabilizers to its formulation. These additives easily react with the oxidant species preserving, in this way, the chemical structure of the polymer. However, if the concentration of these oxidants is too high, or if there is prolonged contact with the material, the polymer itself can suffer chemical degradation with occurrence of the aforementioned reactions. In the worst cases polymeric chain scission can take place leading to a reduction of the material molecular weight [1, 56, 59, 60].

Moreover, in [1, 4, 56–60], it has been demonstrated that, in case of free radical oxidation of polyethylene, the amorphous part is more prone to chemical degradation; this can be revealed by Differential Scanning Calorimetry (DSC) analysis, showing that the crystallinity of oxidized samples is always higher than that of the unaged material. In particular, in a study on the UV and thermal oxidation of Linear Low Density Polyethylene conducted in [57], it is reported that the chain scission reaction increases the mobility of the amorphous chains. A process of secondary crystallization and the growth of the pre-existing crystals can hence occur, as revealed, for the first mechanism, by the presence of a shoulder in the thermogram of aged samples in Figure 2.12 and, for the second mechanism, by the increase of the crystallization peak area and by the shift of the X-ray diffractograms in Figure 2.13.

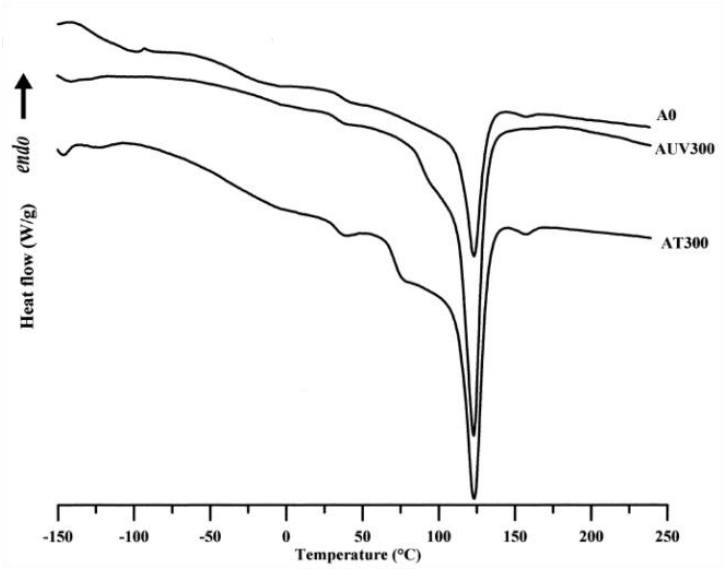

Figure 2.12 -Thermograms of LLDPE unaged (A0), UV irradiated for 300 hours (AUV 300) and thermally treated for 300 hours at 60°C (AT 300). The presence of the shoulder before the main crystallization peak reveals the formation of new domains with lower dimensions with respect to the original ones; the increase of the crystalline content is also related to the increase of the area under the main peak. [57]

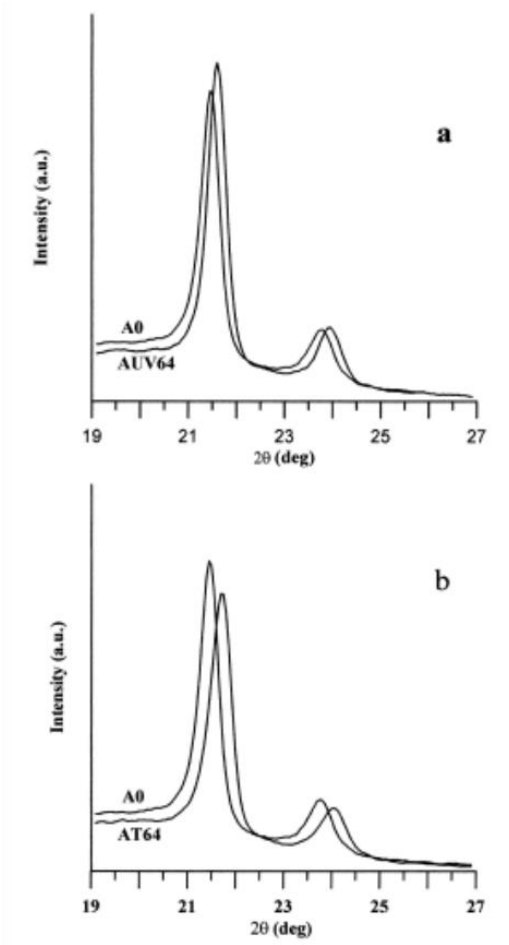

Figure 2.13 - X-ray diffractograms of (a) unaged LLDPE (A0) and UV irradiated for 64 hours (AUV 64) and (b) unaged LLDPE (A0) and thermally treated for 64 hours at 60°C (AT 64). The shift towards higher diffraction angles of AUV 64 and AT 64 indicates an increase of the dimensions of the pre-existing crystalline domains. [57]

One of the consequences of the crystallinity growth is the increase of the material density. Since the rearrangement of the polymeric chains in the amorphous phase would lead to the formation of a more compact structure, in fact, a higher value for this property has to be expected in the case of a polyethylene degraded via a free radical oxidation mechanism [55, 58]. Due to these modifications, the material mechanical properties will change: it can be

expected that a degraded component will be more stiff and fragile with respect to a pristine one. Indeed, in case of significant chemical degradation of HDPE, the hardness and the elastic modulus will increase while the strains at yield and at break and the impact resistance will decrease [52, 55, 58, 59].

The final stage of the chemical degradation process can be the nucleation of a crack or, in case of massive oxidation, of a pattern of cracks which, under the action of a mechanical stress, can grow eventually causing the sudden failure of a polymeric component [2].

Even if antioxidants are present in most commercial polyolefins and if stabilizers are added to bleaches to reduce the degradation of sodium hypochlorite, the possibility of a chemical degradation of HDPE during the service life of the bottle, leading to a decrease of the material mechanical properties, cannot be ignored. The extent of this chemical interaction was evaluated during the first stages of this work.

2.3.2 Environmental stress cracking

Environmental stress cracking (ESC) is a solvent-induced failure mode, known since the 1940s [61], which can affect, for example, polyethylene (PE) in contact with aqueous detergent solutions [5, 6, 7, 18, 19, 21, 23, 44, 46, 62–82] or organic solvents [21, 83, 84], high impact polystyrene in presence of sunflower oil [22, 23, 85–87], polycarbonate exposed to ethanol [88] or fat emulsions [86], phenolic resins in oil [88] and PMMA in organic solvents [18, 87, 89, 90]. During the exposure of the polymer to the chemical agent (commonly called active environment), if a mechanical stress acts on the material, the combined effect of these two factors can result in a brittle failure of the material even without occurrence of any chemical reactions between the environment and the polymer

which, consequently, is not chemically degraded [91, 92]. The main mechanism acting during this phenomenon, in fact, is the penetration of the environment into the material and the reduction of the intermolecular forces between the polymeric macromolecules, which causes an increase in the rate of disentanglement of the molecules themselves. As a consequence of the high surface to volume ratio of the microvoided zones or crazes that can nucleate in proximity of a flaw due to a mechanical or residual thermal stress (see Figure 2.14), the absorption of the chemical in these regions can occur easily. The result of this process is a local plasticisation of the polymer and the reduction of its fracture resistance; in other words, ESC failures are characterized by a reduced crack initiation time and an increased crack propagation rate (and thus a lower failure time) with respect to what occurs in air under the same loading conditions.

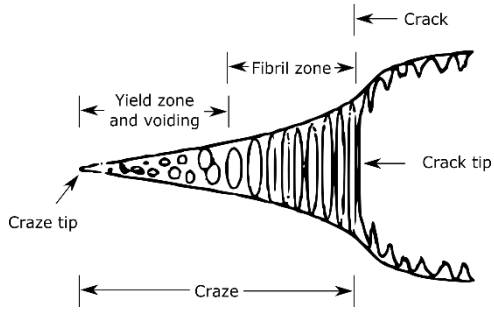

Figure 2.14 - Schematic drawing of craze structure ahead of a crack. [68]

Since ESC is linked to the absorption of the active environment in the craze region, this phenomenon will occur only if the diffusion rate is fast enough with respect to the actual rate characterizing the fracture process. Indeed if the latter is too high, there is not enough time for the fluid to penetrate the polymer and hence the fracture resistance will not be affected by the presence of the chemical. From this fact, it follows that a minimum contact time between the polymer and

the environment is required to observe a deleterious effect on the mechanical properties of the material. This characteristic time has been named "Igepal transition" in the case of polyethylene in contact with an aqueous solution of this detergent [66, 71, 93] or, more generally, "critical interaction time" or "critical initiation time" [22, 24, 87].

As reported in [91], the extent of the decrease of the fracture resistance depends on a series of factors related to the composition of the chemical agent and the microstructure of the polymer. Starting from the characteristics of the active environment it is known that fluids with moderate hydrogen bonding and low molecular weight are usually more aggressive with respect to chemicals with very high hydrogen bonding (like organic alcohols and aliphatic hydrocarbons) and having a high molecular weight, with a low possibility to permeate into the polymer. For what concerns the material, instead, amorphous polymers are generally more prone to ESC due to the high free volume contained in these materials; the ESC resistance (ESCR) increases with increasing molecular weight and, for semicrystalline polymers, with increasing degree of crystallinity.

Regardless of the interacting polymer-environment couple, if ESC occurs the material will fail in a brittle way: the fracture surface is usually smooth, indicating that Slow Crack Growth (SCG) occurred, and multiple cracks, craze remnants and stretched fibrils are usually observed. Moreover, since ESC commonly develops with a progressive crack-extension mechanism, alternating bands, corresponding to repeated cycles of crazing and crack extension, can characterize the fracture surface.

Considering the specific case of PE in contact with an aqueous detergent solution, which is of particular interest for this work, one of the first examples of ESC

failure reported in the scientific literature in 1951 is the one regarding telephone cable sheaths [94]. From that moment on, this phenomenon has been studied extensively to obtain useful information on the main parameters controlling this failure mechanism. Considering the specific properties of the active environment, in 1975 Williams and Marshall [18] demonstrated that the crack growth rate is inversely proportional to the fluid viscosity. Some years later, Tonyali and Brown [6] showed that in the range of Igepal concentration between 0 and 25% by volume the crack growth rate is directly proportional to the surfactant concentration and Tonyali, Rogers and Brown [21] discovered that the crack speed increases if the solubility parameter of the active environment approaches that of the polymer. The effect of the detergent concentration was further investigated by Fleissner [68] and Rink et al. [7] with contrasting results: the former reported failure times independent of the concentration up to 20% by weight, while the latter found a minimum of the initiation time and a maximum of the crack propagation rate for a concentration of 40% by volume. More recently, the effect of the environment on the ESC phenomenon was considered by Pinter, Haager and Lang [70] who showed that aged aqueous detergent solutions are less aggressive than fresh ones.

For what concerns aspects of the PE structure, it has to be considered that, as reported in [42, 49, 50, 95–97] and other works, the active environment plasticize tie molecules connecting the various crystalline domains. Hence, any change in the chemical structure or in the morphology of the material affecting these intercrystalline connections can, in principle, have an influence on the ESCR of PE. Some of the characteristics affecting the fracture resistance of this material have been already introduced in Section 2.2.1; these properties also influence its ESCR.

One of the more commonly accepted mechanisms for the ESC of PE in presence of detergent solutions has been described by Tonyali, Rogers and Brown in [21]. According to these authors, small amounts of nonyl phenol and polyethylene glycol, present in the detergent as impurities, are contained in the surfactant micelle as sketched in Figure 2.15. When the active environment permeates in the craze region these structures can be adsorbed on the fibril surface and the diffusion of the aggressive species (i.e. surfactant and impurities) into the material can take place.

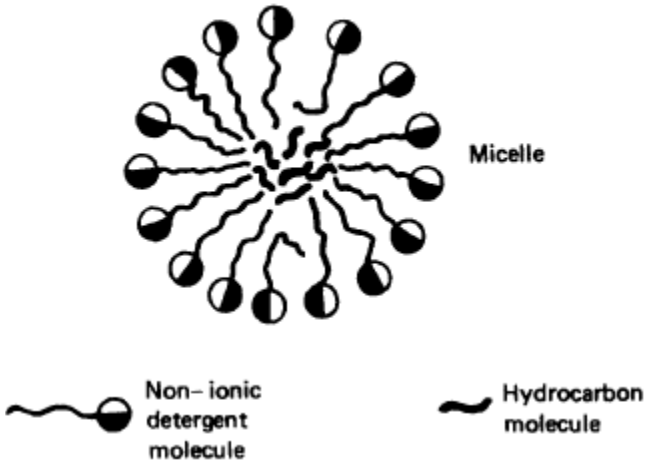

Figure 2.15 - Sketch of a micelle. [21]

Since the chain packing in the centre of the fibrils is extremely high [77], the diffusion of the environment in the shoulder of the fibrils, where the polymeric structure is more disordered, will be favoured as measured with IR analysis by Lagarón et al. in [98]. Consequently, the drawing of the polymeric molecules in the region surrounding the craze into the fibrils will be favoured (see Figure 2.16) and breakdown of these structures will occur mainly in the shoulder region, as observed in [99].

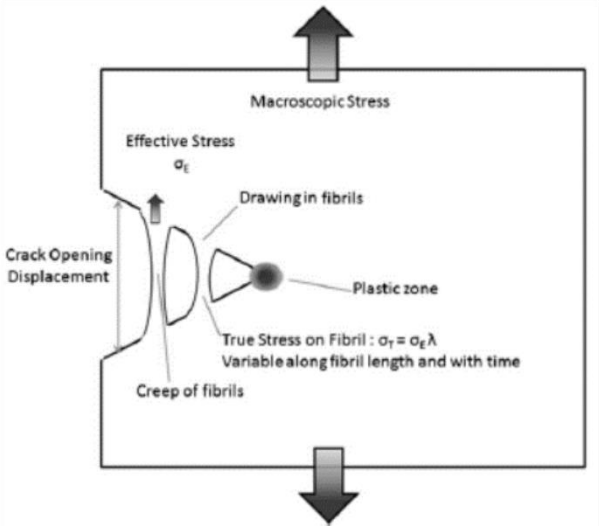

Figure 2.16 – Sketch of an opening craze. The fibrils can undergo creep or part of the polymeric molecules in the region surrounding the craze can be drawn into them. [100]

More recently, to study the evolution of the material microstructure during ESC, Yarysheva et al. [84] conducted a series of experiments with Atomic Force Microscopy during the stretching of HDPE films in presence of a solution of water and ethanol. This analysis lead to the definition of the deformation model of Figure 2.17. The results obtained in this work are substantially in agreement with the two models proposed in Section 2.2.1: it is then possible to conclude that the main effect of the active environment is to increase the rate of the SCG phenomena with respect to the in air condition.

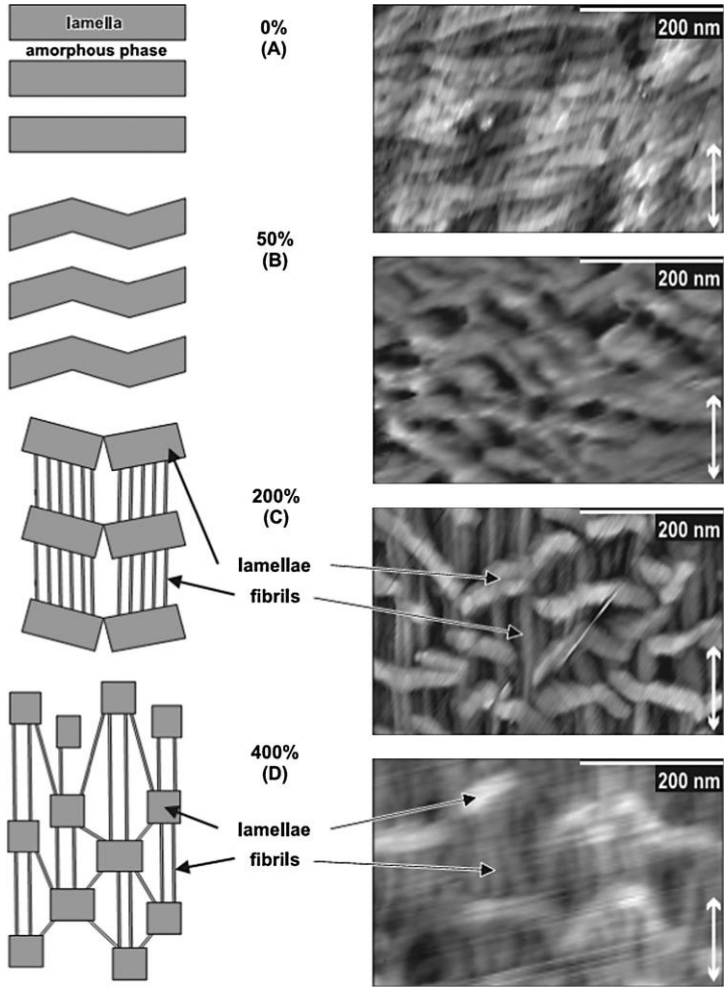

Figure 2.17 - AFM images of HDPE (A) unstretched ; (B) 50% stretched; (C) 200% stretched; (D) 400% stretched in water–ethanol solution. These Images made possible the definition of the deformation model on the left-hand part of the figure. [84]

2.4 Environmental Stress Cracking evaluation methods

The environmental stress cracking resistance of polymers can be evaluated according to different methods developed to characterize the aggressiveness of a certain environment, to rank different polymer grades or to obtain useful information for the lifetime prediction of a component. An overview of the main tests used for these purposes is reported in the next sections.

2.4.1 Standardized methods

The first method developed for the evaluation of the ESCR of PE was the "Bell telephone test" proposed by DeCoste, Malm and Wallder in [94], and which nowadays is standardized in [14, 16]. According to this procedure, longitudinally notched specimens (see Figure 2.18) are bent in an holder and inserted in a glass phial containing the active environment which, in most cases, is an aqueous solution containing the 10% by volume of Igepal. The whole apparatus is then heated at 50 °C to accelerate the process and the number of failed specimens is determined from visual observation and represented as a function of time.

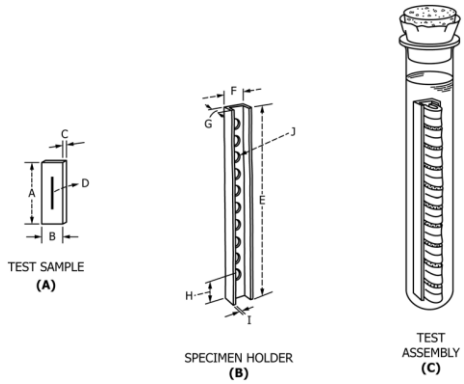

Figure 2.18 - Sample geometry and equipment for the "Bell telephone test". [16]

Another popular standardized experiment, particularly adequate for rigid materials, is the "bent strip method" described in [9]. While applying this procedure, thanks to the clamping system sketched in Figure 2.19, the specimen is bent and the whole test assembly is put in contact with the aggressive environment at a constant temperature. After a predetermined amount of time (usually 24 hours), signs of crazes, cracks, changes in colour or roughness are sought for, also in this case with the unaided eye. After this inspection the specimen can be tested, in tension or bending, to determine the variation of a

property of interest (e.g. the strain at failure) with respect to the behaviour of the unexposed polymer.

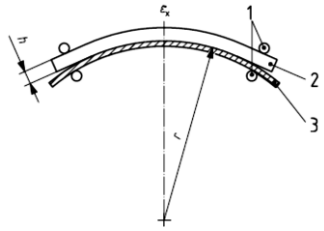

Figure 2.19 - Clamping system and specimen for the "bent strip method". [9]

A third method based on visual inspection is the “Ball or pin impression method” [10] in which a hole of specified diameter is drilled in a test specimen and an oversize ball or pin is inserted into the hole itself. After the exposure to the active environment the specimen is then inspected to observe if cracking occurred, and also in this case a variation of a property of interest can be evaluated testing the sample in bending or in tension. Moreover, varying the diameter of the pin and performing different tests at fixed exposure time, it is possible to roughly evaluate the critical strain required to observe the ESC phenomenon.

Other standardized methods for generic purposes consist in the execution of tensile tests in air and in presence of the active environment [8, 11, 12] and in the execution of Full-notch creep test (FNCT) [13] or Notched, Constant Ligament-Stress (NCLS) Test [17] to determine the nominal stress vs. failure time curve for the material of interest. Considering the specific case of extrusion blow moulded polyethylene containers, instead, the instructions proposed in [15] are to fill a certain number of bottles with the cracking agent (different amounts of this substance are prescribed depending on the selected test mode) and to place the container in an oven at a temperature of 60°C. According to this procedure

the bottle must be inspected at regular time intervals and the results are expressed in term of the ratio of failed containers as a function of time.

Most of these methods have been developed to solve a specific industrial problem and consequently a generalization of the obtained results cannot be done easily. Moreover, since the results obtained from these standards often depend on the sample geometry, only a rough indication on the aggressiveness of a substance and on the ranking of different material grades can be obtained. There is no way to compare directly results obtained from different tests. For these reasons, existing standardized methods cannot be considered as adequate for the provision of data useful during the design phase of a component or for a deep understanding of the mechanisms acting during the ESC phenomenon, and of the material parameters governing the mechanical response of the product under relevant conditions.

2.4.2 Methods based on polymer-environment affinity

One of the approaches adopted to determine the occurrence of ESC, especially used for glassy polymers but applied also to PE in [21], is based on the evidence that a polymer is dissolved and, under a mechanical stress, crazing occurs more easily if the solubility parameters of the material and of a certain solvent are similar [101–105]. As shown by Mai for PMMA [104], in fact, if the critical strain at which crazing occurs is plotted as a function of the solubility parameter of the solvent δ_s, it is possible to detect a minimum in the graph when δ_s approaches the solubility parameter of the polymer δ_p (see Figure 2.20).

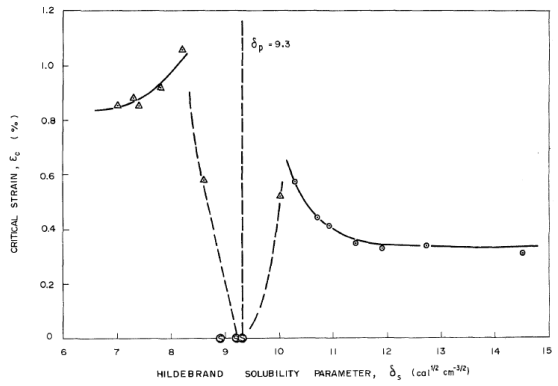

Figure 2.20 - Critical strain vs. Hildebrand solubility parameter. [104]

However, even if this approach can be a useful instrument for predicting if a certain substance can induce the ESC of a polymer, the use of solubility parameter as unique controlling factor for this phenomenon is frequently insufficient. Hence, as pointed out by Jacques and Wyzgoski [103], in many case no simple correlation can be obtained between the critical strain and δ_s; other controlling properties of the fluid, such as the solvent molar volume, have to be taken into account (see Figure 2.21).

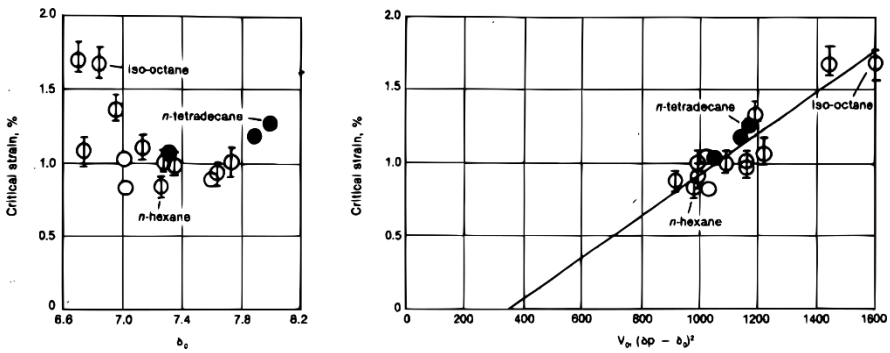

(a) (b)

Figure 2.21 – Critical strains for craze initiation in polycarbonate. (a) Critical strains vs. solubility parameter; (b) critical strains vs. molar volume times the square of the difference in the solubility parameters of polymer and solvent. [103]

A slightly different approach has been adopted by Hansen who in [105] proposed a mapping of the Relative Energy Difference (RED), a function of the difference between the solubility parameters of the solvent and of the polymer (a cyclo-olefinic copolymer in the considered case), and the molar volume of the fluid. As reported in the graph of Figure 2.22, the RED vs. molar volume plane can be divided in three regions depending on interaction between the polymer and the solvent. If the RED number is high (great difference between δ_s and δ_p) the polymer does not interact with the solvent, in the region of low RED numbers the polymer is dissolved by the solvent and, for intermediate RED numbers ESC can occur. However, since in the central region of the map some of the solvents promote ESC while others do not interact with the polymer, no certain information regarding the ESC occurrence can be obtained from this map and, for this reasons this tool should be used only for the purpose of a broad polymer selection.

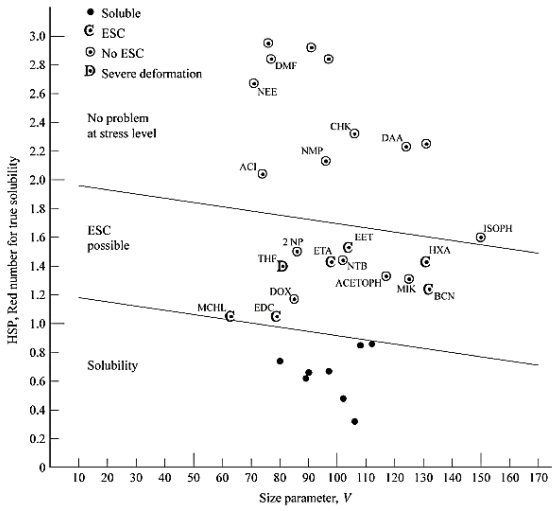

Figure 2.22 - RED number vs. solvent molar volume map for a cyclo-olefinic copolymer. [105]

The solubility parameters are not the only quantity used to predict ESC from considerations based on polymer-fluid affinity: in fact, Nielsen and Hansen tried to correlate ESC with the wettability of a polymer by different fluids in [106]. For the considered polymer-solvent couples, this phenomenon always occurs when a droplet of solvent spontaneously spreads on the polymer surface. However, also in this case no certain information can be obtained for those solvents for which spreading does not occur.

The lack of reliable results together with the inherent difficulty in the theories required for the application of the methods proposed in this Section make them of difficult practical application as industrially-ready tools for the prediction of ESC. Moreover it has to be considered that, for some applications (such as bleach containers), it is already known that the substance in contact with the polymer causes ESC and, for design or economic reasons, HDPE is still the best choice available. In this case a go-no go method, as those previously described, is completely useless while a tool for predicting which material grade is more adequate would be more convenient. Moreover a design tool to predict bottle lifetime would be extremely valuable.

2.4.2.1 Methods based on molecular and morphological investigations

A different approach for the evaluation of the ESCR of HDPE consists in the research for correlations between the molecular characteristics or the morphology of the material, usually determined by performing mechanical or thermal experiments, and the environmental stress cracking resistance, measured according to one of the methods described in Section 2.4.1.

Probably the most known example is based on the strain hardening modulus, measured from true stress-true strain curves; this approach was adopted, for

example, by Kuralec et al. [78], Sardashti [39] and Robledo, Dominguez and García-Muñoz [107] for the ranking of various polyethylene grades. The idea behind this approach is that, as proposed by O'Connell et al. [108, 109], the behaviour of the fibrillar structure within a craze can be reproduced by a tensile bar drawn to its Natural Draw Ratio (NDR). The latter can be defined as the amount of strain occurring during a tensile test in the stable neck of the specimen undergoing large plastic deformation; since it is related to the extensibility of the macromolecular network, NDR is considered, together with the strain hardening modulus, a parameter able to represent the deformation of the fibrils within the craze structure. Considering the results reported in [78], for example, it was demonstrated that the strain hardening modulus $\langle G_p \rangle$ at 80°C depends on the molecular properties also governing the slow crack growth phenomenon (see Section 2.2.1) and that a correlation can be found between this parameter and ESCR measured from a FNCT experiment, as shown in Figure 2.23. Following a similar approach, but considering the nominal stress-strain curves and conducting the experiments at room temperature, Cheng, Polak and Penlidis [44], found a correlation between the hardening stiffness (correlated with $\langle G_p \rangle$) and the ESCR, measured as the time required for the failure of a notched constant load test. Moreover, considering the model of O'Connell, Cazenave et al. [81, 82] proposed a direct correlation between the NDR and the ESCR from the Bell telephone test as shown in Figure 2.24.

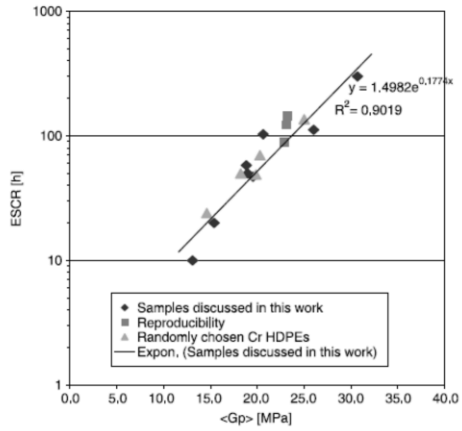

Figure 2.23 – Correlation between the ESCR measured from a FNCT experiments and the strain hardening modulus $\langle G_p \rangle$ of different HDPE grades measured at 80°C. [78]

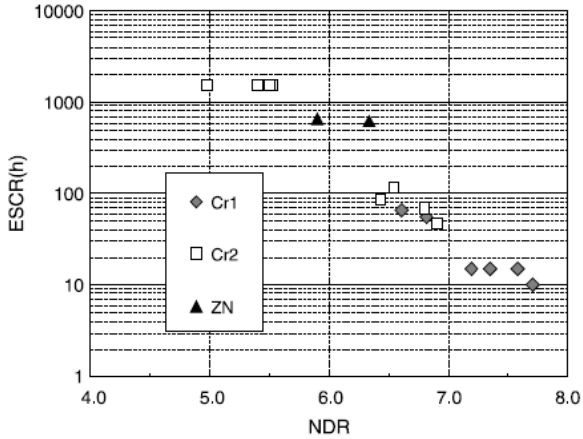

Figure 2.24 - Correlation between the ESCR measured from the Bell telephone test and the Natural Draw Ratio of several HDPE grades. [82]

Again Cazenave [82] and Nezbedová et al. [110] also used a strategy based on the analysis of the crystallization behaviour of HDPE, introduced with the name of DSC index by Hosoda and Uemura [111] and further developed by Gueugnaut and Rousselot [112] with the name of Stepwise Isothermal Segregation (SIS). According to this procedure a sample of material is placed in a DSC instrument and melted above 200°C; this temperature is maintained for a certain amount of

time to completely erase the original crystalline structure. Subsequently the material is rapidly cooled down to 120 °C, a temperature at which isothermal crystallization occurs within a few hours. After this stage the material is cooled down to room temperature at a controlled cooling rate (usually 10 °C/min) in order to crystallize the remaining crystallizable part and, in the end, the sample is reheated to record the melting behaviour. This heating scan usually reveals the presence of two endothermic peaks, which corresponds to the melting of different crystalline structure. The peak at the highest temperature corresponds to the melting of "thick" crystals formed during the isothermal step by relatively short molecules while the peak at the lowest temperature is caused by the melting of "thinner" crystals formed during the final cooling by long polymeric chains. Due to the difference in the molecular structure of the two type of crystals the former ones are characterized by a regular chain folding and few intercrystalline tie molecules and the latter present random chain folding, loose loops and a high number of tie molecules. Since, as described in Section 2.2.1, the Slow Crack Growth resistance and the ESCR of HDPE increases increasing the density of the intercrystalline molecular connections, the ratio between the melting enthalpy of the low temperature melting species and the total melting enthalpy, also called SIS ratio, can be used as a parameter for the evaluation of the Environmental Stress Cracking Resistance of this polymer. If, as shown in Figure 2.25, this quantity is expressed as a function of ESCR measured from the Bell telephone test, a good correlation exists between these two parameters at least for materials produced using the same catalytic system (Cr1, Cr2 and Zn).

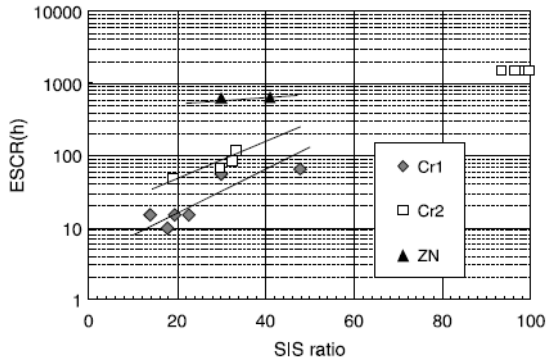

Figure 2.25 – Correlation between SIS ratio and ESCR from Bell Telephone Test. Cr1, Cr2 and Zn indicate the catalyst used for the polymer production. [82]

Finally, a third approach to find a correlation between ESCR and different molecular or morphological parameters has been adopted by Men et al. [79]. Starting from the experimental evidence the SCG and ESC resistance increases, for example, with increasing molecular weight or short branch content [50, 113, 114], they evaluated, via DMA experiments, the mobility of the amorphous phase of different PEs; this quantity of course depends on the aforementioned molecular properties, and a correlation with ESCR was found. According to the proposed procedure the magnitude of the peak corresponding to the β-relaxation in a tan δ vs. temperature graph increases with increasing mobility of the amorphous phase and this parameter, also called "dynamic glass transition", is correlated with the ESCR measured from FNCT experiments in an aqueous detergent solution. The results obtained from this analysis are shown in Figure 2.26.

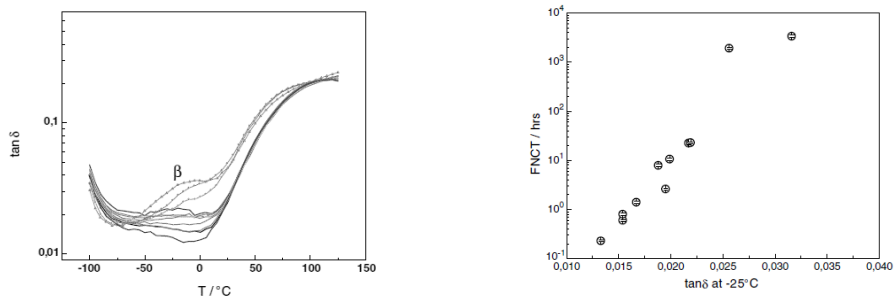

(a) (b)

Figure 2.26 – (a) graph tan δ vs. temperature; the absolute value of the β-relaxation is a measure of the mobility of the amorphous phase.
(b) correlation between tan δ at -25°C (approximation of β-relaxation) and the ESCR measured from FNCT experiments in aqueous detergent solution. [79]

The approaches described in this section, and other correlations with different material properties such as the density or the molecular weight, can be useful ranking tools; however, the ESCR measured from these tests can depend on testing conditions and, in some cases, the obtained results can be not representative of the actual behaviour of final products. Moreover the results obtained from the methods presented in Sections 2.4.1 and 2.4.2, cannot be easily used during the design phase of a component. To obtain these information a different strategy, based on fracture mechanics, has to be considered: the main features regarding this topic are presented in the next section and the application of this approach to ESC problem is treated in Section 2.5.4.

2.5 Fracture mechanics

Fracture mechanics (FM) is a branch of mechanics that studies the growth and propagation of cracks in solid materials. This theory is based on the assumption that the defects contained in a body act by a concentration of the stress field caused by a given mechanical input. If the stress, magnified in proximity of the defect, reaches a critical threshold, a crack begins to propagate inside the

material, eventually causing its failure. The basic assumptions of this theory can be summarized in the following two points:

- All materials contain defects starting from which fracture can initiate and propagate to cause failure
- The crack growth process can be characterized by the energy per unit area required to produce a new fracture surface (fracture resistance R)

FM was firstly developed during the 1920s by Griffith who, using a simple energy balance and connecting the material strength to the flaw size, formulated a fracture theory, valid for glasses and ideally brittle solids [115]. After World War II this theory was modified by Irwin to take into account energy dissipations related to local plastic flows in metals [116]. Irwin also proposed the concept of energy release rate G [117] and, starting from a previous work of Westergaard [118], he showed that the stresses and displacements near the crack tip can be described by a single fracture parameter, related to the energy release rate itself and known as stress intensity factor K [119]. These approaches, which constitute the fundamentals of the Linear Elastic Fracture Mechanics (LEFM), however, cease to be valid if significant plastic deformations precede the material failure; hence starting from 1960 several researchers, including Irwin [120] Barenblatt [121] and Dugdale [122], developed adaptations of LEFM to account for large yielding and to extend its validity.

To characterize the nonlinear material behaviour ahead of a crack a different approach was taken by Rice [123] who, in 1968, developed a new fracture parameter, called J integral: this parameter will be described in detail in Section 2.5.3.

LEFM can be inaccurate also in the case of materials whose deformation behaviour is markedly non elastic. Considering the specific case of polymers, as reported for example in [124, 125], a viscoelastic fracture approach can be more adequate; the theories proposed by Schapery [126–128] and by Williams [92] are frequently invoked to solve problems related to the fracture behaviour of this class of materials. In particular, according to William's theory, under the assumptions of a linear and only slightly viscoelastic behaviour, the equations developed for LEFM can still be valid, provided that the elastic constants are replaced with time dependent quantities representing the viscoelastic nature of the polymer; the basic concepts regarding this approach will be described in Section 2.5.2.

2.5.1 Linear Elastic Fracture Mechanics

If an elastic body containing a defect of known length a is subjected to a mechanical stress, the energy release rate G can be defined as the energy change in the system due to an increment of the cracked area dA. The energy balance of the system during a fracture growth step can be written as:

$$\frac{dU_e}{dA} - \frac{dU_d}{dA} = \frac{dU_s}{dA} + \frac{dU_k}{dA} \tag{2.1}$$

in which dU_e, dU_d, dU_s and dU_k are, respectively, the variations of the external mechanical work, of the irreversible dissipated energy, of the stored elastic energy and of the kinetic energy of the system and $\frac{dU_d}{dA}$ is the energy dissipated in propagating a fracture over an increment of area dA or, more simply, the fracture resistance R previously introduced. For a stationary body kinetic energy variations can be neglected and the energy change related to crack growth (called energy release rate) can be defined according to Equation (2.2):

$$G = \frac{dU_e}{dA} - \frac{dU_s}{dA} \tag{2.2}$$

For a crack propagating over a section of constant thickness B, equal to the thickness of the cracked body, Equation (2.2) assumes the form

$$G = \frac{1}{B}\left(\frac{dU_e}{da} - \frac{dU_s}{da}\right) \tag{2.3}$$

Considering the sketch of Figure 2.27, if the body is mechanically loaded with a load P which causes a displacement u, dU_e and $\frac{dU_s}{da}$ can be written as

$$dU_e = Pdu \tag{2.4}$$

$$\frac{dU_s}{da} = \frac{1}{2}P\frac{du}{da} + \frac{1}{2}u\frac{dP}{da} \tag{2.5}$$

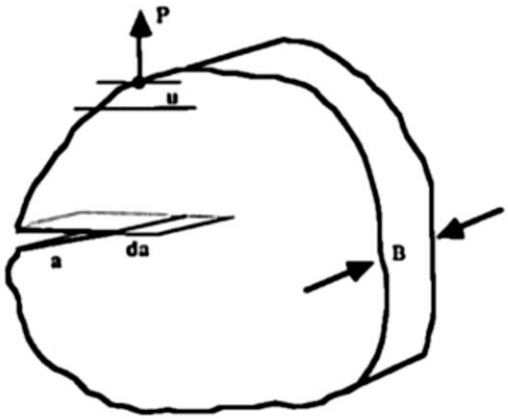

Figure 2.27 – Loaded body with a crack. [129]

Combining Equations (2.3), (2.4) and (2.5) G assumes the form

$$G = \frac{1}{2B}\left(P\frac{du}{da} - u\frac{dP}{da}\right) \tag{2.6}$$

which, explicitly introducing the compliance of the body

$$C = \frac{u}{P} \tag{2.7}$$

can be rewritten as the general expression proposed by Kies and Irwin [130]:

$$G = \frac{P^2}{2B}\frac{dC}{da} = \frac{U_s}{B}\frac{1}{C}\frac{dC}{da} \tag{2.8}$$

which is valid for loading conditions different from the constant load one from which it has been derived. The term $\frac{dC}{da}$ represents the variation of the compliance due to an increment da of the crack length; in many cases this quantity can be determined experimentally allowing the evaluation of the energy release rate. If the width of the body W is introduced in this expression, Equation (2.8) can be rewritten in a form useful for the experimental evaluation of G:

$$G = \frac{U_s}{BW} \cdot \frac{1}{C} \cdot \frac{dC}{d\left(\frac{a}{W}\right)} = \frac{U_s}{BW} \cdot \frac{1}{\psi\left(\frac{a}{W}\right)} \tag{2.9}$$

in which $\psi\left(\frac{a}{W}\right)$ is the energy calibration factor, whose expression depends on the test configuration. The derivation of the energy calibration factor for the four-point bending test, used during this work, will be presented in ANNEX A.2.

When an analytical expression of the compliance is not available, however, the determination of G is not simple and a different approach, based on the analysis of the stress field around the crack tip might be used instead. As demonstrated by Irwin in [119], the fracture parameter obtained from this kind of analysis is related to the energy release rate; therefore the following approach has to be considered as an alternative method for the evaluation of the fracture behaviour of solids which, in the context of LEFM, is equivalent to the one based on the energy release rate. Confining the attention to mode I crack loading (see Figure 2.28) and considering the coordinate system of Figure 2.29, it can be demonstrated that the stresses around the crack tip can be described by the following equation:

$$\sigma_{ij} = \frac{K_I}{\sqrt{2\pi r}} f_{ij}(\theta) \tag{2.10}$$

in which K_I is the stress intensity factor for mode I crack loading and $f_{ij}(\theta)$ is a dimensional function of θ. For mode I crack loading the stresses in the x and y direction are equal, hence evaluating $f_{ij}(\theta)$ along the crack plane ($\theta = 0^{\circ}$) and in direction normal to it ($\theta = 90^{\circ}$) the stress along the two directions ($\sigma_{xx}$and σ_{yy}) can be defined:

$$\sigma_{yy} = \sigma_{xx} = \frac{K_I}{\sqrt{2\pi r}} \tag{2.11}$$

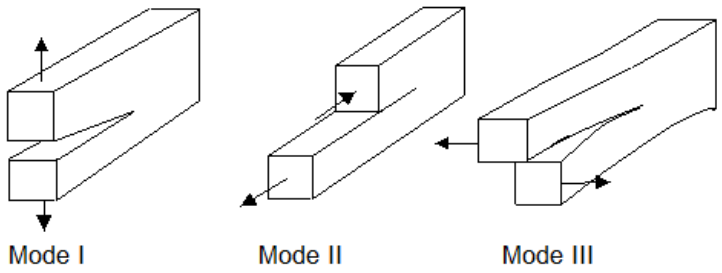

Figure 2.28 - Crack loading modes.

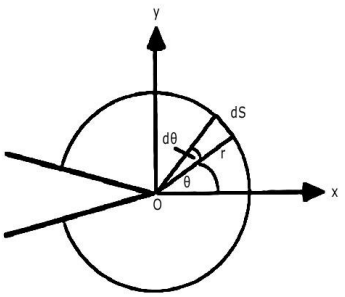

Figure 2.29 - Crack tip with polar coordinate systems. [129]

From Equation (2.11) it turns out that the stress would go to infinity when r approaches zero. A fracture criterion based on the stress at the crack tip is therefore not applicable but, since the product $\sigma_{yy} \cdot \sqrt{r}$ is finite, a critical value

of the stress intensity factor K_{IC}, above which crack extension occurs, can be considered as an elastic criterion for fracture known as fracture toughness.

In order for the stress intensity factor K to be of practical use from an engineering point of view, however, expressions linking this parameter to the geometry of the body and to the applied boundary conditions have to be obtained. These equations, available as closed-form analytical solutions in the simplest cases or determined experimentally or with numerical analysis, can be usually written in the form

$$K = Y \cdot \sigma \cdot \sqrt{\pi a} \tag{2.12}$$

where Y is the shape factor for a certain configuration and σ is a reference nominal stress applied to the boundary of the body.

As previously reported, the equivalence of the two approaches previously described has been proved by Irwin [119] who linked the energy release rate and the stress intensity factor with the formula

$$G = \frac{K^2}{E'} \tag{2.13}$$

where $E' = E$ in plane stress state and $E' = \frac{E}{1-\nu^2}$ in plane strain state, E and ν being the Young's modulus and the Poisson's ratio respectively. These two states arise, respectively, when the stress in one dimension can be neglected or when the deformation is constrained in one dimension.

As pointed out before, the elastic stresses introduced of Equation (2.11) reach an infinite value when the distance from crack tip approaches zero. Actually, it is necessary to consider some non-linearity in the material, which will yield in a region around the crack tip before the failure of the body. LEFM holds true only if the dimension of this plastically deformed zone is limited with respect to the

dimensions of the linear elastic continuum of the body or, in other words, if small scale yielding conditions are satisfied. To estimate the dimensions of a circular plastic zone Irwin [119] proposed Equation (2.14) while Dugdale [122] developed Equation (2.15) for long and slender plastic zones ahead the crack tip:

$$r_p = \frac{1}{\pi}\left(\frac{K_I}{\sigma_y}\right)^2 \tag{2.14}$$

$$r_p = \frac{\pi}{8}\left(\frac{K_I}{\sigma_y}\right)^2 \tag{2.15}$$

Of course, the dimension of the process zone is influenced by the applied stress state, being larger in the case of plane stress with respect to plane strain. Equations (2.14) and (2.15) were derived for the plane stress condition but they can be adapted to the plane strain state dividing them by 3. Plane stress state is typical of external surfaces while plane strain is relevant for the bulk of the material: along the specimen thickness, following the crack tip from the surface to the center, the stress state thus goes from plane stress to plane strain as shown in Figure 2.30.

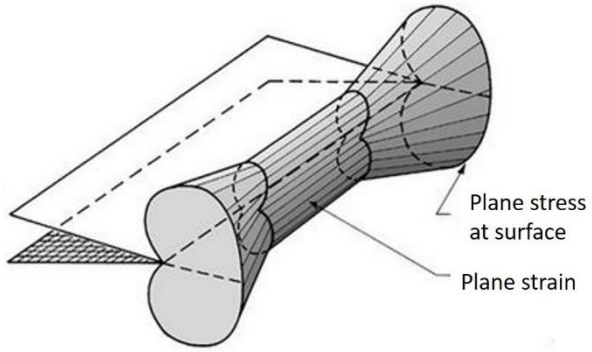

Figure 2.30 - Stress states near the crack tip. [131]

Plastic deformations represents a further dissipative mechanism with respect to those introduced at the beginning of this Section for the definition of the energy

release rate G and therefore they are related to the material capability of resisting to crack growth: since the plastic zone is larger in plane stress, in this condition K_{IC} will be higher than in plane strain. In a real body, the apparent fracture toughness is an average of the two contributions, with the plane strain one becoming predominant with increasing thickness. In a mainly plane strain condition, when the contribution of the surfaces can be neglected, a limit, constant value of K_{IC} is approached: this value can be regarded as the intrinsic fracture toughness of the material and it represents a conservative estimate, useful in many cases for design purposes. However, its value can be too conservative for products operating under plane stress conditions, as is the case for bleach bottles. In these cases, a plane stress fracture toughness should be used instead.

2.5.2 Viscoelastic Fracture

According to LEFM theory the bulk of material is assumed to be linear elastic. Polymers, however, are viscoelastic materials, exhibiting time dependent behaviour. Several theories have been formulated to describe the fracture behaviour of this material class. In this section the simple theory proposed by Williams [92] is introduced. The basic assumption is that the material behaviour is linear and only slightly viscoelastic; if this hypothesis is verified, the equations developed for LEFM theory can be employed by replacing the constant material properties typical of a linear elastic material with time-dependent quantities which effectively characterize the behaviour of polymers.

Another key assumption is that the crack tip opening displacement δ_c is constant over the time window considered. Fracture toughness can be then expressed as

$$G_{IC} = \delta_c \sigma_y(t) \tag{2.16}$$

In the case of polymeric materials crack initiation is supposed to occur after a certain time t_i. The relationship between fracture toughness and incubation or initiation time can be simply derived from Equation (2.16) considering the fact that for this material class the yield stress time-dependence (but also the relaxation modulus one) can be expressed with a simple power law:

$$G_{IC}(t_i) = \delta_c \sigma_y(t_i) = \delta_c \sigma_{y0} \cdot t_i^{-m} \tag{2.17}$$

For what concerns crack propagation, instead, a more complex analysis needs to be performed. Starting from Dugdale's plastic zone concept, introduced in the previous section, an useful expression for the shape of this region under plane strain conditions can be obtained if Equation (2.13), which links K to G, and Equation (2.16) are introduced in the generalized form of Equation (2.15):

$$r_p = \frac{\pi}{\alpha \cdot 8}\left(\frac{K_{IC}}{\sigma_y}\right)^2 = \frac{\pi}{24}\frac{G_{IC} \cdot E(t)}{(1-\nu^2) \cdot \sigma_y^2(t)} = \frac{\pi}{24}\frac{\delta_c \cdot E(t)}{(1-\nu^2) \cdot \sigma_y(t)} \tag{2.18}$$

which, considering a power law time-dependency also for E can be rewritten as:

$$r_p = \frac{\pi}{24}\frac{\delta_c \cdot E_0 t^{-n}}{(1-\nu^2) \cdot \sigma_{y0} t^{-m}} = \frac{\pi}{24}\frac{\delta_c \cdot E_0}{(1-\nu^2) \cdot \sigma_{y0}} \cdot t^{-n+m} \tag{2.19}$$

Moreover, the time necessary for a crack moving at a constant speed $\dot{a}$ to go through the process zone can be expressed as

$$t = \frac{r_p}{\dot{a}} \tag{2.20}$$

Substituting Equation (2.20) into Equation (2.19), solving for t and substituting in Equation (2.16), a relationship between G_{IC} and $\dot{a}$ can be obtained:

$$G_{IC} = \delta_c \sigma_{y0} \cdot \left(\frac{\pi}{24}\frac{\delta_c \cdot E_0}{(1-\nu^2) \cdot \sigma_{y0}}\right)^{\frac{-m}{1+n-m}} \cdot \dot{a}^{\frac{m}{1+n-m}} \tag{2.21}$$

Similar expressions, linking K_{IC} to the crack initiation time and the crack growth rate can be obtained in terms taking advantage of Equation (2.13):

$$K_{IC}(t_i) = \left(\delta_c \sigma_{y0} E_0\right)^{\frac{1}{2}} \cdot t_i^{-\frac{n+m}{2}} \tag{2.22}$$

$$K_{IC} = \left(\delta_c \sigma_{y0} E_0\right)^{\frac{1}{2}} \cdot \left(\frac{\pi}{24} \frac{\delta_c \cdot E_0}{(1-\nu^2) \cdot \sigma_{y0}}\right)^{-\frac{n+m}{2(1+n-m)}} \cdot \dot{a}^{\frac{n+m}{2(1+n-m)}} \tag{2.23}$$

Summarizing, Equations (2.17), (2.21), (2.22) and (2.23) predict that a power law dependency between G_{IC} and the crack initiation time or the crack growth rate exists and that the related exponents depend on that of the relaxation modulus and of the yield stress.

Irrespectively of the considered fracture parameter (K or G), the failure time t_f of a polymer hawing an initial flaw can be expressed as

$$t_f = t_i + t_p \tag{2.24}$$

where t_p is the time required for the propagation of the crack up to the complete failure of the material. This equation, combined with the others presented in this Section, is a very useful tool from an engineering point of view since it can be used to evaluate the long term fracture behaviour of a polymeric component. To clarify this point, considering the critical stress intensity factor as the fracture parameter of choice and rewriting Equations (2.22) and (2.23) in a more compact form,

$$t_i = C_1 \cdot K_{IC,0}^{C_2} \tag{2.25}$$

$$\dot{a} = C_3 \cdot K_{IC}^{C_4} \tag{2.26}$$

Equation (2.24) can be also rewritten as

$$t_f = C_1 \cdot K_{IC,0}^{C_2} + \int_{a_0}^{a_f} \frac{da}{C_3 \cdot K_{IC}^{C_4}} \tag{2.24}$$

where C_1, C_2, C_3 and C_4 are constants, $K_{IC,0}$ is the critical stress intensity factor at crack initiation and a_0 and a_f are, respectively, the initial and final (at failure) crack length. Knowing the geometry of the body and the applied boundary

conditions, it would be possible to predict the failure time of any component with simple calculations; this kind of procedure has been adopted, for example, in [87, 92, 132].

2.5.3 Elastic-Plastic Fracture Mechanics

LEFM and its extension to viscoelastic materials are valid only as long as nonlinear deformations are confined to a small region surrounding the crack tip or, in other words, when the small scale yielding conditions are satisfied. However, the behaviour of many materials is characterized by extensive plastic deformations occurring during the fracture process and, in these cases, the parameters introduced in Sections 2.5.1 and 2.5.2 would lead to an inaccurate or even completely wrong indication of the fracture resistance. Due to this fact, as already reported at the beginning of Section 2.5, starting from 1960 several researchers formulated methods to extend LEFM validity and proposed fracture parameters more adequate for materials exhibiting significant plastic deformations during fracture.

One of these parameters, introduced by Rice in 1968 [123], is called *J*-integral and it can be defined with the help of the sketch reported in Figure 2.31. Considering a two dimensional cracked body if, in contrast to what done starting from Figure 2.27 in Section 2.5.1, the mechanical stress is applied over the contour Γ surrounding the crack tip it is possible to define this fracture parameter as

$$J = \int_{\Gamma} \left[W_s dy - \left(\sigma_n \frac{du_n}{da} + \sigma_s \frac{du_s}{da} \right) dS \right] \tag{2.25}$$

in which σ_n, σ_s, u_n and u_s are the normal and shear stress and displacements where W_s is the strain energy density. This fracture parameter represents a more

general version of the energy release rate valid for both linear and nonlinear materials. In particular, for a linear elastic body Equation (2.26) holds true:

$$J = G = \frac{K^2}{E} \tag{2.26}$$

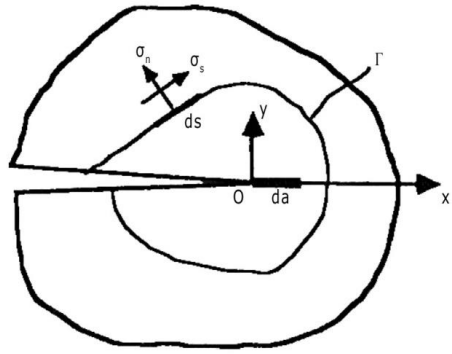

Figure 2.31 - General crack tip contour Γ. [129]

A different and, from an engineering point of view, more useful definition of the *J*-integral has been obtained by Rice in [133] starting from an energy rate interpretation of the problem; considering a body of thickness B this form of the *J*-integral can be expressed as

$$J = \frac{1}{B}\left(\frac{dU}{da}\right)_u \tag{2.26}$$

where U is the input mechanical energy up to a given displacement u. Taking advantage of this equation, Begley and Landes [134, 135] introduced the multispecimen technique as the first experimental method for the estimation of *J*. According to the original procedure, specimens having the same geometry but different crack length are deformed and the load-displacement curves are obtained. The input mechanical energy U is hence obtained by integrating each load–displacement curve up to various displacements u and U can be plotted as

a function of the crack length a at fixed u. From this graph J can be computed using Equation 2.26.

Even if the multispecimen approach is probably the most accurate method applicable in case of fracture phenomena characterized by nonlinear mechanical behaviour and extensive plastic deformations, it has the obvious disadvantage of being a highly time consuming procedure since, of course, several specimens have to be tested to evaluate J. For this reason, several researchers sought a determination of the nonlinear energy release rate directly from a load displacement curve of a single specimen. In particular Rice, Paris and Merkle [136] and Sumpter and Turner [137], generalizing the single specimen technique, separated J into elastic and plastic components according to Equation (2.27):

$$J = J_{el} + J_{pl} = \eta_{el}\frac{U_{el}}{B \cdot (W - a)} + \eta_{pl}\frac{U_{pl}}{B \cdot (W - a)} = G + \eta_{pl}\frac{U_{pl}}{B \cdot (W - a)} \qquad (2.27)$$

where U_{el} and U_{pl} are the elastic and plastic parts of the load-displacement curve, η_{el} and η_{pl} are dimensionless constants depending on the test configuration and on the ratio between the crack length a and the specimen width W whose difference $W - a$ is equal to the length of the uncracked ligament.

A further step was taken by Sharobeam and Landes [138] who noticed that both elastic and plastic part of Equation (2.27) can be rewritten as the product of two functions depending only on the geometry of the specimen and on the mechanical deformations, respectively. They found a relatively fast experimental method for the experimental evaluation of η_{pl}. Focusing on the plastic part of J, they started their analysis, called load separation method, representing the load as the product of two functions:

$$P = F\left(\frac{a}{W}\right) \cdot H\left(\frac{u_{pl}}{W}\right) \tag{2.28}$$

Where $F\left(\frac{a}{W}\right)$ is function only of the sample geometry and $H\left(\frac{u_{pl}}{W}\right)$ is a function of the plastic displacement u_{pl} (the commonly adopted notation of $G\left(\frac{a}{W}\right)$ is not applied in this work for the sake of clarity since G already represents the energy release rate). Considering two blunt notched specimens having identical dimensions with the exception of the notch length itself being equal to a_i and a_j, using Equation (2.28) they showed that the ratio $S_{i,j}$ between the load recorded from the two sample at fixed plastic displacement is constant since

$$\begin{aligned} S_{i,j} &= \frac{P(a_i, u_{pl})}{P(a_j, u_{pl})}\bigg|_{u_{pl}} = \frac{F\left(\frac{a_i}{W}\right) \cdot H\left(\frac{u_{pl,1}}{W}\right)}{F\left(\frac{a_j}{W}\right) \cdot H\left(\frac{u_{pl,1}}{W}\right)} \\ &= \frac{F\left(\frac{a_i}{W}\right) \cdot H\left(\frac{u_{pl,2}}{W}\right)}{F\left(\frac{a_j}{W}\right) \cdot H\left(\frac{u_{pl,2}}{W}\right)} = \frac{F\left(\frac{a_i}{W}\right)}{F\left(\frac{a_j}{W}\right)} \end{aligned} \tag{2.29}$$

They used this ratio, called separation constant or parameter, to determine η_{pl} for several test configurations. The first steps for this analysis are the evaluation of $S_{i,j}$ for several specimens with different blunt notch lengths, and the representation of the obtained values as a function of the ratio between the ligament length and the specimen width, as reported in Figure 2.32. Since a power law dependency can be easily determined from this procedure, this also implies that the geometry function has the same kind of dependence on the ratio between the ligament length and the specimen width:

$$F\left(\frac{W - a_i}{W}\right) = A\left(\frac{W - a_i}{W}\right)^s \tag{2.30}$$

in which A and s can be determined from the data in Figure 2.32. Since, according to Equation (2.31), η_{pl} can be defined as

$$\eta_{pl} = \frac{W-a}{W} \cdot \frac{dF\left(\frac{W-a}{W}\right) \Big/ d\left(\frac{W-a}{W}\right)}{F\left(\frac{W-a}{W}\right)} \tag{2.31}$$

it is easy to demonstrate that this parameter is equal to the parameter s of Equation (2.30).

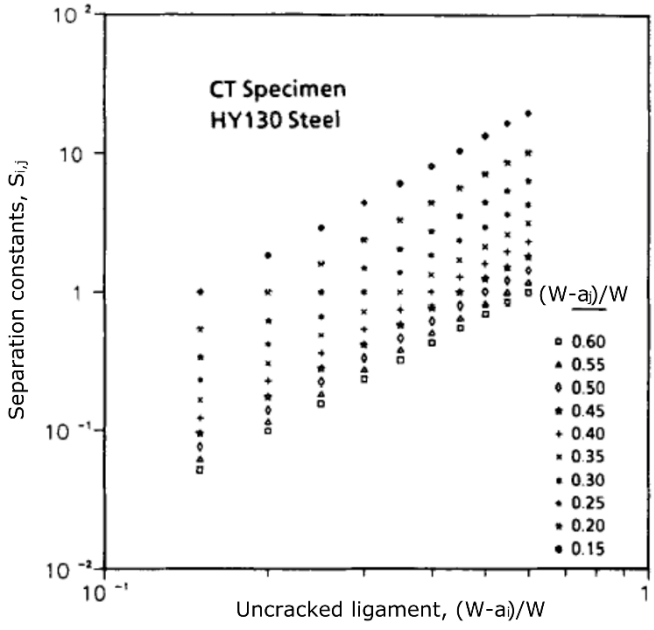

Figure 2.32 - Separation constants vs. uncracked ligament ($W - a_i$) to width ratio for different crack lengths in compact specimens. Adapted from [138]

Moreover, as reported for the first time in [139], the load separation method can be used also to determine the crack initiation point. If tests are conducted on sharp notched samples having notch length a_s, in fact, crack will initiate and propagate causing a variation of the geometrical function $F\left(\frac{a_s}{W}\right)$ and of the separation parameter $S_{s,b}$ evaluated from the geometrical function of a blunt notched sample with crack length a_b:

$$S_{s,b} = \left.\frac{F\left(\frac{a_s}{W}\right)}{F\left(\frac{a_b}{W}\right)}\right|_{u_{pl}} \tag{2.32}$$

As can be noted from Figure 2.33, if this parameter is plotted as a function of the plastic displacement three regions can be identified. At low plastic displacements an unseparable region, characterized by an increase of the separation parameter can be found; this region is followed by a zone of almost constant $S_{s,b}$, which corresponds to the region in which the crack length increases due to the tip blunting phenomenon; finally a decreasing part of the curve can be found where ductile tearing governs the crack growth. Taking advantage of this trend crack initiation can be defined as the point in which $S_{s,b}$ starts to decrease.

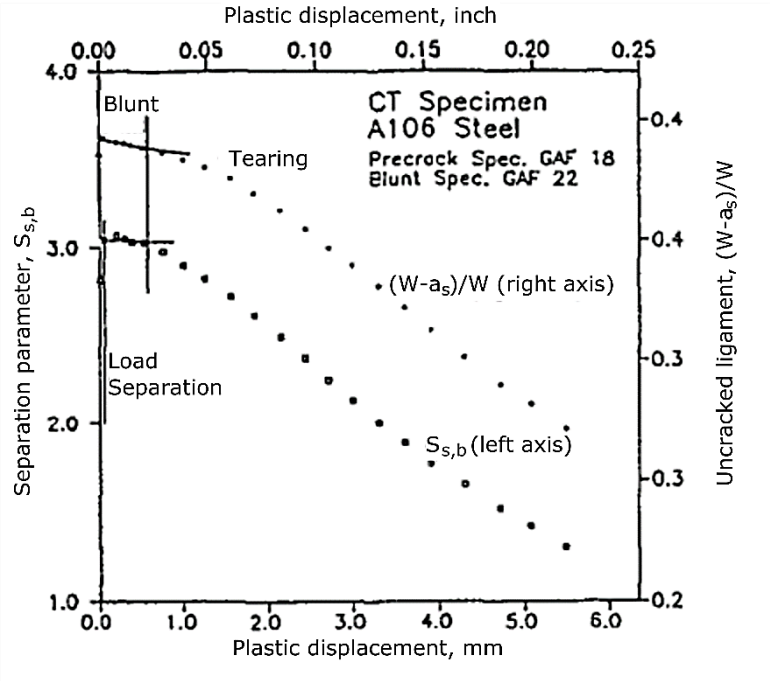

Figure 2.33 - Separation parameter and uncracked ligament of a precracked specimens versus plastic displacement. Adapted from [139].

More recently, the load separation method has found application also for the characterization of the nonlinear fracture behaviour of polymers as reported, for example, in [140–148] and, since it is a relatively fast method, it is really appealing from an engineering and industrial point of view. In fact, even if other elastic-plastic characterization methods can be found in literature, in most cases they are highly time-consuming approaches and, consequently, they turn out to be practically inapplicable to the study of a slow phenomenon as the ESC.

2.5.4 Fracture Mechanics applied to ESC

During the years, LEFM has been used to study ESC of polymers in plane strain state and in mode I crack loading conditions achieved, in many cases, with bending tests on Single Edge Notched specimens (SENB configuration).

The first to apply this approach had been Marshall, Williams and co-workers during the 1970s [18, 149, 150] who identified, for several polymer-environment systems, unique relationships between the critical stress intensity factor K_c and the crack growth rate. One of the key points of these first studies, as clearly emerges in [18], is the definition of different regimes of crack growth. If the propagation rate is low, according to the authors, the active environment has enough time to reach the crack tip and hence to reduce the fracture resistance of the polymer; whereas for high propagation rates the fluid has not enough time to reach this zone and the material behaviour will be unaffected. If the logarithm of the critical stress intensity factor and of the crack growth rate are plotted as in Figure 2.34, the slopes of the two regimes can be related to the slopes m and n of the yield and relaxation modulus vs. time curves, as described in Section 2.5.2; at low growth rates the slope is usually 0.1 and it is higher with respect to the one at high growth rates since plasticisation occurs and consequently m increases.

According to this model, the transition between these two regimes is controlled by the fluid flow velocity v: the crack growth rate is higher with respect to the rate at which the fluid flows into the crack tip region but it has, nevertheless, sufficient time to partially plasticize the material. Starting from considerations on Darcy's law for the permeability of the fluid in the crazed region and taking advantage of equations similar to those introduced in Section 2.5.2, it has been shown that the slope of this transition line should be equal to 0.5.

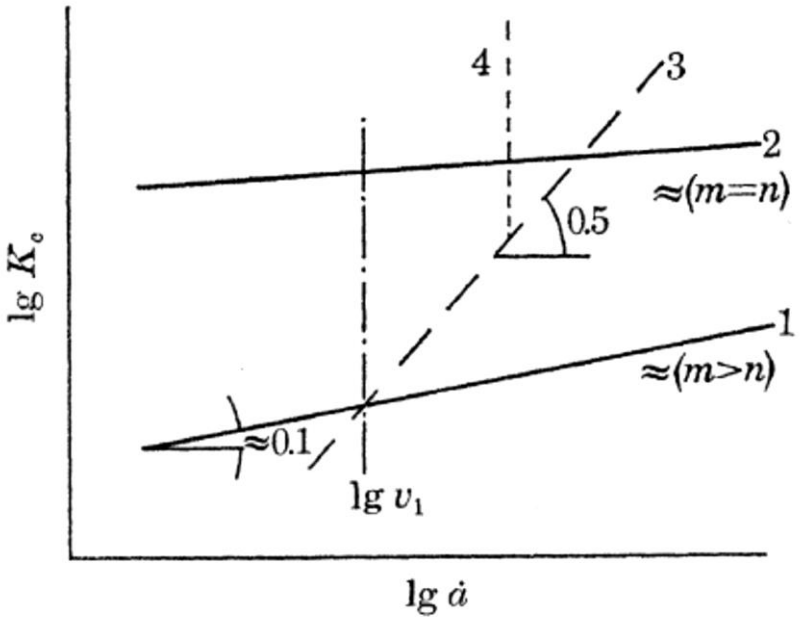

Figure 2.34 – Expected correlation between the critical stress intensity factor and the crack propagation rate for a polymeric material. [18]

A refinement of this model, with modified slopes to take into account mechanisms other than the variation of the relaxation modulus and yield stress with time, has been proposed for the case of polyethylene in contact with aqueous detergent solutions by Chan and Williams [5]. By performing tests on specimens with different dimensions, the authors obtained a unique K_c vs. $\dot{a}$ curve demonstrating that, if a proper sample geometry is selected, LEFM is

applicable to the characterization of this polymer. Moreover, as can be observed from Figure 2.35, for a HDPE grade the same slope of 0.25, related to a void growth kinetics, characterize the curves obtained in distilled water (inert environment) and at relatively low critical stress intensity factors in the active environment; the latter in turn depresses the curve towards lower value of K_c. According to Chan [151] in this region a plasticisation factor β, useful for the determination of the effect of the active environment on the fracture resistance of a polymer, can be defined as:

$$\beta = \frac{K_{c,environment}}{K_{c,distilled\ water}} \tag{2.33}$$

For increasing crack growth rates, instead, incomplete plasticisation occurs and a slope equal to 0.5 is found, in accordance with the model described before, while for $K_c > 0.7$ the environment does not affect anymore the behaviour of the polymer, since plasticisation of the crack tip region does not occur in this regime. However, in the same work slopes higher than 0.5 were also measured both in presence of the detergent solution and of distilled water meaning that the flow controlled mechanism proposed before is not sufficient to accurately describe the phenomenon. From the crack arrest line observed on the fracture surface during fractographic analysis it was suggested that the deviation of the slopes from the predicted theoretical value may be related to a stick-slip fracture propagation, with crack tip blunting occurring between the different growth stages.

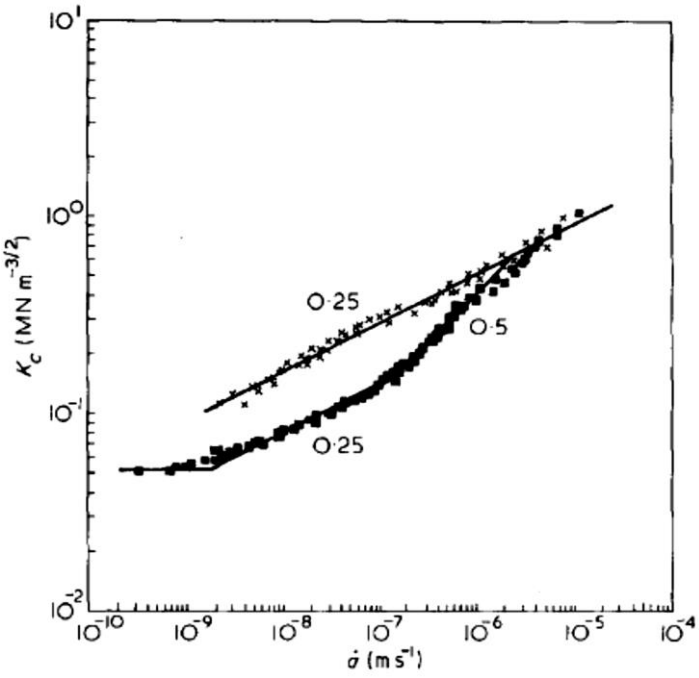

Figure 2.35 - K_c vs. $\dot{a}$ curves for a HDPE; crosses represents the fracture propagation behaviour in distilled water (inert environment) while square are data obtained in the presence of an aqueous detergent solution. Numbers indicate the slope of the lines. [5]

The applicability of LEFM to the environmental stress cracking of PE had been investigated, during the 1980s, also by Tonyali and Brown [19] who showed that, at least in the region of critical stress intensity factors lower than 1 MPa·m$^{0.5}$, a unique K_c vs $\dot{a}$ could be obtained from specimens having different dimensions and from different test configurations. In a subsequent work [6] these two authors measured an increasing crack growth rate with increasing concentration of surfactants in water and, consequently, of the viscosity of the active environment. This result is in contrast with the model proposed by Williams and Marshall since, according to their theory, an increase in the fluid viscosity would lead to a more difficult penetration of the active environment into the crazed region ahead of the crack tip. Therefore, the flow controlled crack growth explanation

turned out to be inadequate, or at least incomplete, and, due to this fact, the same Tonyali and Brown [21] proposed the model, described in Section 2.3.2, based on the diffusion of surfactant molecules in the region surrounding the craze.

A study of the ESC of polyethylene has been conducted, in 2003, also by Rink et al. [7]: adopting a compliance calibration method to four-point bending constant load tests, crack initiation was detected and the effects of the environment also on this phase of the fracture process were analysed. One of the most important results obtained from this research was that ESC occurred only below a critical stress intensity factor K_{IC}^{*}, whose value could be influenced by a diffusion-controlled plasticisation mechanism.

A different approach was adopted by Alstaeadt et al. [86] who conducted fatigue tests on Compact Tension specimens of HIPS, in presence of sunflower oil, and polycarbonate, in presence of a fatty acid emulsion. They developed a relatively fast method for the evaluation of ESC performing tests under ΔK control and they evaluated the influence of molecular weight, of material orientation and of toughness modification via the introduction of rubber particles in HIPS on the fracture and environmental stress cracking resistance of the two materials. More recently, fatigue approaches have been adopted also by Ayyer et al. [69, 71] and by Schoeffl et al. [83].

The ESC of HIPS in sunflower oil and PE in detergents was studied also by Andena et al. [22, 74]. Performing tests with different tests configuration and loading histories (i.e. three-point bending / constant displacement rate, four-point bending / constant load and buckled plate [152] / stress relaxation) the authors of this research discovered that unique K_c-t_i and K_c-$\dot{a}$ relationship could be obtained. Taking advantage of this result, the experimental window available for

the characterization of the material could be extended by performing, for example, high time-consuming tests on dedicated creep machines and faster tests on common dynamometers. The results of this study also showed that, as already pointed out in [7], ESC occurs only below a critical stress intensity factor K_{IC}^{*} and that the corresponding critical interaction time t_i^{*} and critical crack growth rate $\dot{a}^{*}$ can be easily determined from the intercept of the curves representing the material fracture behaviour in air and in the active environment. Moreover, the effect of the production process on the same HIPS grades of [22] has been conducted in [85]. Focusing on the crack initiation, it was found that toughness in air depends on the molecular orientation of the material while, in the presence of the sunflower oil, this dependency is partially or completely suppressed as shown in Figure 2.36.

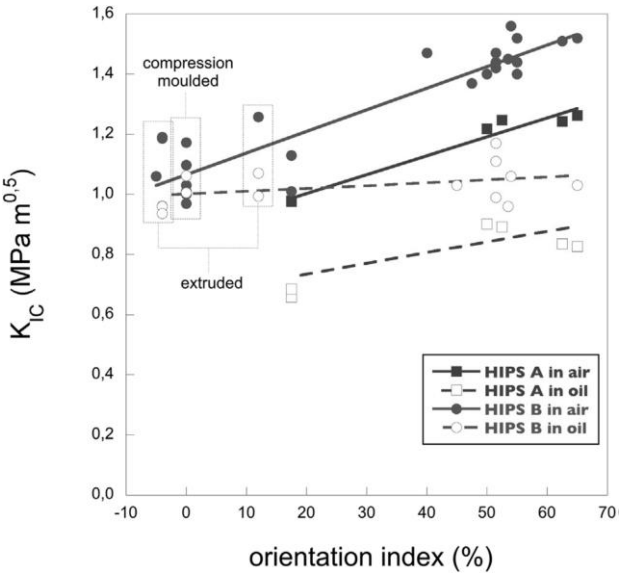

Figure 2.36 - K_{Ic} vs. orientation index curve for HIPS tested in air and in sunflower oil. [85]

Starting from 2016 the environmental stress cracking of several polymers has been studied by Kamaludin et al. [23, 87] adopting the energy release rate G as a

critical fracture parameter and considering both the initiation and propagation phases of fracture. The same authors, starting form a normalisation of t_i^* and $\dot{a}^*$ against the maximum value of crack initiation time $t_{i,max}$ and the minimum crack growth rate $\dot{a}_{min}$ measured in certain experimental window, proposed in [24] a parameter λ for the evaluation of the effect of several active environments on the fracture resistance of different polymers:

$$\lambda = \frac{t_i^*}{t_{i,max}} \cdot \frac{\dot{a}_{min}}{\dot{a}^*} \tag{2.34}$$

This parameter should be the intrinsic ESC sensitivity of a polymer: it tends to zero for materials having a low ESC resistance (low t_i^* with respect to $t_{i,max}$ or high $\dot{a}^*$ with respect to $\dot{a}_{min}$) and it tends to one for high ESC resistance (t_i^* comparable to $t_{i,max}$ and $\dot{a}^*$ comparable to $\dot{a}_{min}$). However it has to been considered that the selection of the experimental window influences the value of λ and that, consequently, if $t_{i,max}$ and $\dot{a}_{min}$ are not similar in all the considered polymer-environment couple, inaccurate indications may be obtained from this parameter.

2.6 Temperature dependence of polymer mechanical properties and time-Temperature superposition principle

It is known that the strong dependence upon temperature of the mechanical properties of polymers can be related to the variation of the free volume in the material, which lead to a change in the mobility of the polymeric chains. For many polymers, the consequence of this phenomenon is the alteration, by a scaling factor, of the kinetics of the material mechanical response but not of its nature or entity; the behaviour of this class of material is usually called “thermoreologically simple”. If a viscoelastic mechanical property of a material having this kind of behaviour is measured at different temperatures and is

plotted as a function of the logarithm of time or frequency, the various curves will have exactly the same shape but will be shifted along the time or frequency axis.

From this analysis it turns out that, obviously, the time and temperature dependence of the mechanical properties of thermoreologically simple polymers are interrelated. Selecting a reference temperature T_0 and considering, for instance, the relaxation modulus at this temperature E_{T_0}as a representative viscoelastic property, it is possible to express the so called "time-Temperature superposition principle" relating the behaviour of the material at the reference temperature with the behaviour of the material at a different temperature T as in Equation (2.35)

$$E_T(t^*) = E_{T_0}(t) \tag{2.35}$$

where t^* is an effective time at which the relaxation modulus measured at temperature T is equal to the relaxation modulus measured at t for temperature T_0. Since, as stated before, the temperature causes only a horizontal shift of the curve on a logarithmic scale, t and t^* are related through Equation (2.36):

$$Log(t) = Log(t^*) + Log(a_T^{T_0}) \tag{2.36}$$

in which $a_T^{T_0}$ is a quantity called shift factor whose logarithm indicates the entity of the horizontal translation of the viscoelastic function.

The shift factor is a material property and, once T_0 is chosen, it is a function of temperature. Its temperature dependence below the glass transition temperature T_g can be usually expressed with an Arrhenius-type expression:

$$Log\left(a_T^{T_0}\right) = \frac{\Delta H}{R}\left(\frac{1}{T} - \frac{1}{T_0}\right) \tag{2.37}$$

where ΔH is the activation energy for the specific viscoelastic process and R is the gas constant. For temperatures higher than T_g, instead, the Williams-Landel-Ferry (WLF) equation is usually considered:

$$Log\left(a_T^{T_0}\right) = -\frac{C_1(T - T_0)}{C_2 + (T - T_0)} \tag{2.38}$$

In which C_1 and C_2 are empirical constants.

From an engineering point of view, the time-Temperature superposition is a valuable tool since, performing tests at different T, it is possible to shift the obtained data and to overlap them to build the so called "master curve" making hence possible the evaluation of the polymer behaviour over a much larger time spectrum than the accessible experimental window. This principle had been successfully applied also for the reduction of fracture data as reported, for example, in [125, 132, 153, 154].

3 Materials and production processes

In this Chapter the aggressive environments and to the polymers considered during this work are presented. The main features related to the production processes involved in the preparation of plates and bottles are also treated while, for the sake of clarity, the specific operations required for the realization of the various types of specimen are described, together with the relevant experimental conditions, in the Chapter presenting the results obtained from a specific sample or test.

For reasons of confidentiality, neither the exact composition of the solutions nor the processing parameters used during bottles production, nor the material commercial names can be reported in this work.

3.1 Aggressive environments

As describe in Section 2.1, a commercial bleach could contain several ingredients. To better understand the effect of each of them on the material behaviour, eight aggressive environments, containing different combinations of the ingredients of a commercial bleach produced by Fater S.p.A., were considered. These aqueous solutions share the same main ingredients:

- sodium hypochlorite (NaClO), which is the bleaching agent
- sodium hydroxide (NaOH) and sodium carbonate (Na_2CO_3) which are present to increase the pH of the solution at a level of about 13 and, consequently, to reduce the decomposition rate of NaClO
- a perfume, added to improve the scent of the product
- a surfactant, having the function of stabilizing the molecules of perfume in the aqueous solution

The actual composition of the different solutions is reported in Table 3.1:

Table 3.1 - Main ingredients of the aggressive environments.

	NaClO	NaOH+ Na_2CO_3	Perfume	Surfactant
H+A	X	X		
H+A+P	X	X	X (-)	X (- -)
H+A+S	X	X		X
H+A+P+S	X	X	X	X
A		X		
A+P		X	X (-)	X (- -)
A+S		X		X
A+P+S		X	X	X

It can be noticed that the content of a certain species is constant for all the solutions with the exception of H+A+P and A+P in which the content of the perfume and the surfactant are, respectively, slightly and two order of magnitude lower with respect to, for example, H+A+P+S. Moreover, the same perfume and surfactant couple has been used for all the solutions containing these ingredients.

Among the eight environments, the first four (i.e. H+A, H+A+P, H+A+S and H+A+P+S) are real commercial products while the others were specifically produced for this project in order to characterize the effect of solutions without the presence of sodium hypochlorite. Due to the limited stability of the bleaching agent, the solutions containing NaClO have been completely substituted every three months to avoid variations in the aggressiveness during the chemical interaction tests (see Chapter 6). The solutions without sodium hypochlorite, instead, are chemically stable for a longer period and, consequently, less frequent shipments were required to resupply the available stock.

3.2 Polyethylenes

Two grades of HDPE, used for the production of bleach bottles, were considered during this work:

- HDPE-1, a high density polyethylene copolymer with 1-hexen as comonomer
- HDPE-2, a polyethylene copolymer with 1-butane as comonomer

Although quantitative informations were not available, the two materials are known to possess a different molecular weight distribution, with HDPE-2 having a significantly larger amount of long polymeric chains.

In Table 3.2 a qualitatively comparison of some of the properties of the two polymers is shown; this comparison is based on datasheet values of the considered materials, which, for reasons of confidentiality, cannot be reported in this work. Accordingly to the Bell telephone test [16], HDPE-2 has significantly higher ESC resistance with respect to HDPE-1.

Table 3.2 – Comparison of some properties of the two polyethylenes.

Property	Method	HDPE-1	HDPE-2
Tensile strength at yield	ISO 527-3	Lower	Higher
Tensile strain at break	ISO 527-3	Higher	Lower
Flexural modulus	ISO 178	Lower	Higher
Izod impact strength	ISO 180/A	Higher	Lower
ESC resistance (F_{50} B method)	ASTM D 1693	Significantly lower	Significantly higher

Both materials are commercial polymers and were supplied by Fater S.p.A. in form of pellets together with a masterbatch containing the rutile form of TiO_2

as white dye. After a first phase of solid mixing, performed using a rotating cylinder containing the HDPE with 3 wt.% of masterbatch, the two materials were processed with a co-rotating twin screw extruder to achieve complete mixing of the two ingredients. The melting temperature of the two polymers was determined via Differential Scanning Calorimetry measurements, applying an heating ramp at 10°C/min from 50°C to 200°C with a Mettler DSC-30 connected to a Mettler Toledo TC15 TA controller, and optimal process conditions were therefore determined; the thermograms obtained from the pellets are reported in Figure 3.1.

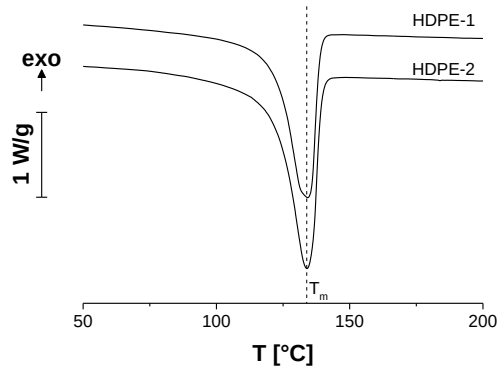

Figure 3.1 - Thermograms of the pellets of the two HDPEs.

After the extrusion process the obtained white filament was re-granulated with a specific automated cutter; flat plates were then obtained via compression moulding as reported in Section 3.2.1.

In the case of HDPE-1, a great number of bottles, produced via extrusion blow moulding, was also provided by Fater S.p.A. to characterize the behaviour of the final product; for what concerns HDPE-2, instead, a limited amount of bottles was supplied by the company and, consequently, a less through analysis was

performed. The main features concerning the bottle geometry and the relative production process are described in Section 3.2.2.

3.2.1 Production of plates

White pellets were processed via compression moulding to obtain 170 x 200 mm plates having a nominal thickness of 1 or 11 mm according to the following procedure:

- the mould was heated to 190°C
- HDPE pellets were put into the mould for 5 minutes without pressure
- a pressure of about 20 bar was applied for 5 minutes
- a pressure of about 40 bar was applied for 5 minutes
- the mould was cooled down to room temperature with a water cooling system

After compression moulding, 11 mm thick plates were placed between two flat glass slabs to be thermally treated at 140°C for 40 minutes and subsequently cooled at room temperature at a rate of 1.5 °C/min; this procedure has been developed to reduce thermal stresses in the material and avoid distortions in the final samples. 1 mm thick plates, instead, did not need a further thermal treatment after compression moulding. The thermograms obtained from the various plates are reported in Figure 3.2: very similar curves were obtained and dividing the measured melting enthalpy by the heat of fusion of 100% crystalline polyethylene (293 J/g according to [1]) a degree of crystallinity χ_c of about the 70% was calculated in all cases.

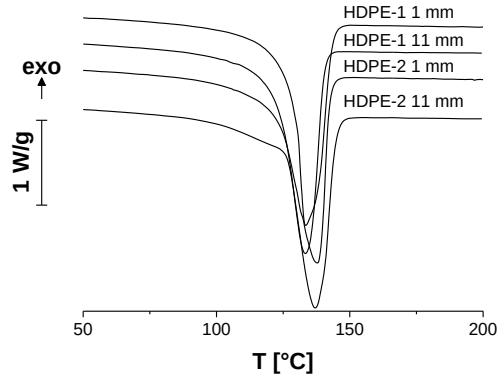

Figure 3.2 - Thermograms of 1 mm and 11 mm thick plates of the two HDPEs.

Various type of specimens, which will be described in the following Chapters, were finally obtained from these sheets as it will be explained later.

3.2.2 Production and geometry of bottles

Bleach bottles were produced by Fater S.p.A. via extrusion blow moulding. In this process the solid mix of HDPE and white masterbatch was melted and extruded into a parison which, after being closed into a metallic mould, was inflated with an air flow to obtain the final shape of a bottle. Few seconds are usually required to cool the polymer and proceed with removal of the component from the mould. Due to the high cooling rate of this process, lower χ_c values are obtained with respect to compression moulded plates. From the thermograms of Figure 3.3 a degree of crystallinity of about 60% was evaluated for both materials and practically no difference were observed performing measurements on samples obtained from different regions of the bottle (i.e. the bottom, the central region and the upper shoulder near to the neck sketched in Figure 3.5).

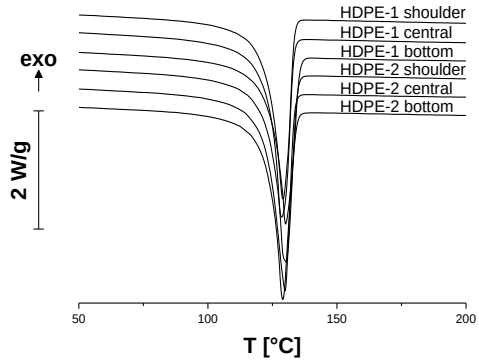

Figure 3.3 - Thermograms of various region of the bottle for the two HDPEs.

The average degree of crystallinity of compression moulded plates and of blow moulded bottles is reported in Figure 3.4; the reduced data dispersion, expressed as error bars, demonstrates that there are not significant differences in the crystallinity of plates having different thickness and of the different regions of the bottle.

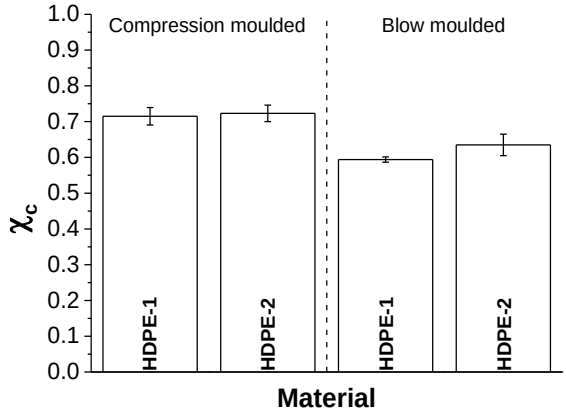

Figure 3.4 - Degree of crystallinity of compression moulded plates and blow moulded bottles.

The bottles characterized during this work belong to a unique production batch and have the geometry sketched in Figure 3.5; their nominal capacity is 1 l. The wall thickness is different in the various regions, ranging between 0.5 mm and 2 mm depending on the stretching of the parison during the inflation phase. Due to the complex shape of the bottle specimens for mechanical testing could be obtained only in the central portion of the container, having height of 105 mm and a nominal wall thickness of 0.5 mm.

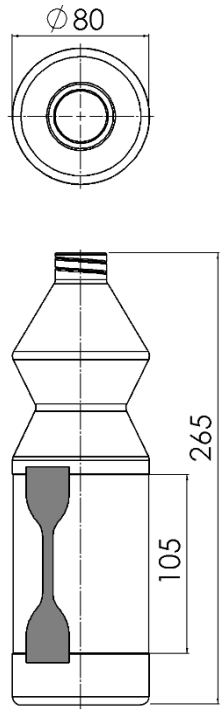

Figure 3.5 – Geometry of the bleach bottle (dimensions in mm). Specimens were obtained from the central portion of height 105 mm which has a nominal wall thickness of 0.5 mm.

4 Tensile behaviour

4.1 Aims of the study

During this work, tensile tests in air were performed for two main reasons:

- to investigate possible material orientation in the compression moulded plates and in the central region of the bottles
- to study the evolution of the relaxation modulus E and of the yield stress σ_y with time for the compression moulded materials

Moreover, during a period as visiting student at the pole of Materials and Process Engineering (IMAP) of the Université Catholique de Louvain (Belgium), the behaviour of blow moulded HDPE-1 samples subjected to complex loading histories was studied; the applicability of a viscoplastic model was first considered. Due to the great number of parameters required for the model calibration and to the unsatisfactory results obtained, the suitability of a different approach, based on viscoelasticity, was investigated. A tool for the prediction of the deformation behaviour of HDPE in bleach bottles during their service life could be very useful to develop a global model to describe fracture behaviour (whether in air or in the environment); this part of the work is, however, still open. In fact, due to the quite complex behaviour reported in the next Sections, the material response to simpler mechanical inputs (such as creep or stress relaxation experiments) could be more useful as a first step to better understand the complex phenomena occurring during the deformation of the two polymers. This analysis could be the basis for future developments of this part of the work in view of developing a numerical modelling tool.

4.2 Experimental details

Type 5 dumb-bell specimens [155], having the geometry shown in Figure 2.1, were obtained via die cutting from 170x190 mm compression moulded plates having a thickness of 1mm and also from the central part of the bottles, having an approximate thickness of 0.5 mm. To evaluate the material orientation the samples were cut in two directions: horizontally and vertically with respect to the longest side of the compression moulded plates and longitudinally or transversally with respect to the symmetry axis of the bottle (see Figure 4.2).

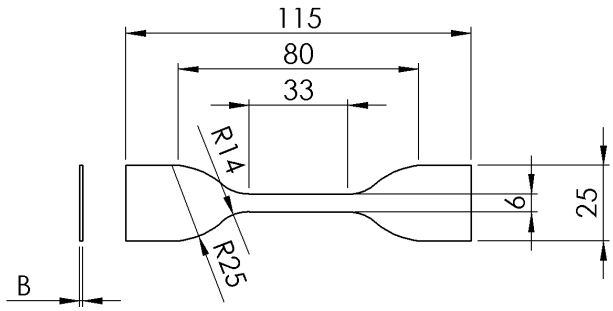

Figure 4.1 – Type 5 dumb-bell specimen geometry. B is the nominal thickness (1 mm for compression moulded samples and 0.5 mm for bottle samples).

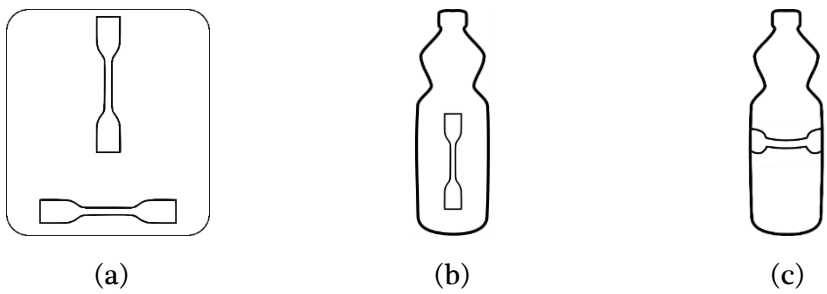

Figure 4.2 – Specimens used for the evaluation of the material orientation: (a) vertical and horizontal specimen from a compression moulded plate; (b) longitudinal specimen from a bottle; (c) transversal specimen from a bottle.

The tests for the evaluation of the material orientation and for the determination of the E vs. t and of the $\sigma_y$vs. t curves were performed on two Instron (1185R5800 and 1121) electro-mechanical dynamometers both equipped with a 10 kN load cell. A set of markers was drawn along the gauge length of the specimen and tests were video recorded with a 10 MPixel uEye UI 5490 SE camera to measure the specimen deformation. The coordinates of the centre of gravity of the various markers were measured using the software ImageJ® and a macro developed in [156] and the engineering strain was evaluated, for each frame, using an OriginPro® macro developed specifically for this purpose.

Tests for the evaluation of material orientation were conducted at 23°C and at a constant displacement rate of 10 mm/min while, for the evaluation of the E vs. t and of the $\sigma_y$vs. t curves, tests were conducted at 23, 40 and 60°C at constant displacement rates of 1, 10, 50 and 100 mm/min.

To evaluate the tangent modulus at different strains, the initial part of the engineering stress-strain curve was fitted with a two term Prony's series and its derivative calculated according to Equations (4.1) and (4.2) respectively:

$$\sigma = \sigma_1 \cdot exp\left(\frac{\varepsilon}{\varepsilon_1}\right) + \sigma_2 \cdot exp\left(\frac{\varepsilon}{\varepsilon_2}\right) + \sigma_0 \tag{4.1}$$

$$\frac{d\sigma}{d\varepsilon} = \frac{\sigma_1}{\varepsilon_1} \cdot exp\left(\frac{\varepsilon}{\varepsilon_1}\right) + \frac{\sigma_2}{\varepsilon_2} \cdot exp\left(\frac{\varepsilon}{\varepsilon_2}\right) \tag{4.2}$$

where σ and ε are, obviously, the nominal stress and strain and σ_0, σ_1, σ_2, ε_1, ε_2 are relevant fitting parameters. Since for a linear viscoelastic material σ and ε are linked through the relaxation modulus E via Equation (4.3)

$$\sigma(t) = \int_0^t E(t-\tau)\frac{\partial \varepsilon}{\partial \tau} d\tau \tag{4.3}$$

which can be rewritten as

$$\frac{\partial \sigma}{\partial t} = \frac{\partial \varepsilon}{\partial t} E(t) \tag{4.4}$$

it turns out that the tangent modulus $\frac{\partial \sigma}{\partial \varepsilon}$ at a given time t is equal to the relaxation modulus $E(t)$.

The yield point was identified conventionally as the maximum in the stress-strain curve; post-yield behaviour was not investigated. Figure 4.3 shows the stress-strain curve obtained at 23°C and 10mm/min from HDPE-1, the fitting used for the determination of the tangent / relaxation modulus and the yield point.

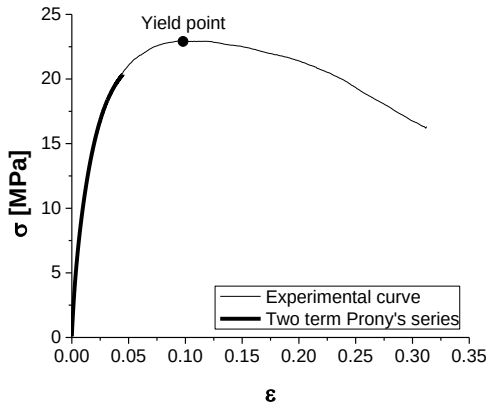

Figure 4.3 – Example of stress strain curve (HDPE-1, 23°C, 10 mm/min). The Prony's fitting of the initial part of the curve and the yield point are highlighted.

A time-temperature superposition reduction scheme was applied to both relaxation modulus and yield data and an objective criterion for the determination of the shift factor was identified. Firstly, the temperature of 23°C was considered as the reference temperature, T_0. Considering, as shown in Figure 4.4, the yield stress, $\mathrm{Log}\,\sigma_y$ vs. $\mathrm{Log}\,t$ data were linearly fitted evaluating the slope m and the corresponding intercept q. The standard error $se(m)$ was found to be

negligible in comparison with $se(q)$ which was calculated according to Equation (4.5):

$$se(q) = sd\sqrt{\frac{\sum_{i=1}^{n}(\log t_i)^2}{n \cdot \sum_{i=1}^{n}(\log t_i - \log \bar{t})^2}} \tag{4.5}$$

in which n is the number of experimental points, $\bar{t}$ is the average time and sd is the standard deviation, evaluated according to Equation (4.6):

$$sd = \sqrt{\frac{\sum_{i=1}^{n}\left(\log \sigma_{y,i} - \log \widehat{\sigma_{y,i}}\right)^2}{n-2}} \tag{4.6}$$

Here, $\log \widehat{\sigma_{y,i}}$ is the value of the interpolating function for a given experimental datum i. In accordance with the time-temperature equivalence postulate, the curves obtained at different temperatures were assumed to have the same shape and thus they were fitted linearly using the same slope m. The shift factor, $\log a_T^{T_0}$, between any given curve at temperature T and the reference one at T_0 was then evaluated using Equation (4.7):

$$\log a_T^{T_0} = \frac{q_T - q_{T_0}}{m} \tag{4.7}$$

The absolute standard error, $se_T^{T_0}$, related to the determination of $\log a_T^{T_0}$ can be defined as:

$$se_T^{T_0} = \frac{se\left(q_{T_0}\right) + se(q_T)}{m} \tag{4.8}$$

The same procedure was adopted for the E vs. t curves of the two materials.

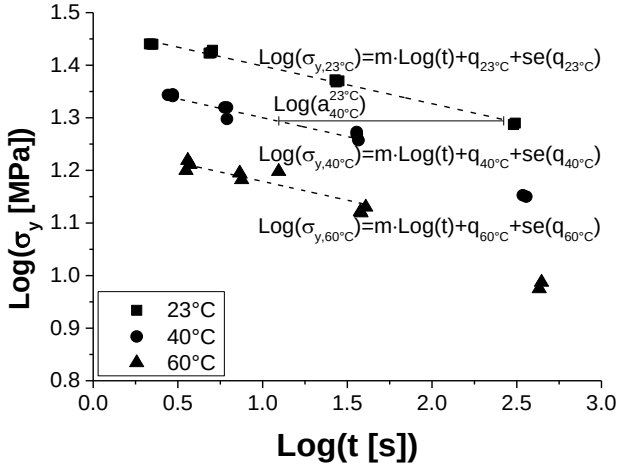

Figure 4.4 - Procedure for the evaluation of the shift factors for the σ_y vs. t curve (HDPE-2). The same procedure was used for the E vs. t curve.

To further characterize the behaviour of blow moulded HDPE-1, relatively complex loading histories were applied to this material using an available screw-driven universal testing machine Zwick-Roell equipped with a 250 kN load cell and with a mechanical extensometer. These histories, whose sketch is reported in Figure 4.5, were composed by:

- a loading phase at constant strain rate $\dot{\varepsilon}$ up to a certain strain ε_{max}
- unloading at the same strain rate down to a certain fraction $\bar{\sigma}$ of the maximum stress σ_{max} reached during the loading phase
- a hold phase at constant stress $\sigma = \bar{\sigma}$, lasting 300 s
- a second unloading at constant strain rate $\dot{\varepsilon}$ down to $\sigma = 0$

During the first two phases and the latter one the test was performed in strain control thanks to the use of a mechanical extensometer while during the third one the dynamometer worked in load control; the corresponding stress was evaluated dividing the load for the initial section of the specimen, which

practically did not vary during the tests. In the first case the input of the mechanical history was a strain while in the latter it was assumed to be the stress.

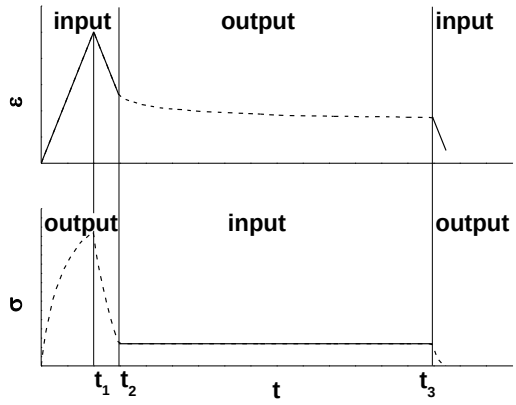

Figure 4.5 - Sketch of the test performed to evaluate the material response to complex loading histories.

Tests were performed at 23°C and at strain rates equal to 10^{-2}, 10^{-3} and 10^{-4} s^{-1}, at 40°C and 60°C at the single strain rate of 10^{-2} s^{-1}. In all cases the samples were stretched up to ε_{max} equal to 0.05 and the hold phase was conducted at stress $\bar{\sigma}$ equal to $0.2 \cdot \sigma_{max}$, $0.4 \cdot \sigma_{max}$, $0.6 \cdot \sigma_{max}$, $0.8 \cdot \sigma_{max}$ and σ_{max}; moreover for the tests conducted at 23°C and at a strain rate of 10^{-4} s^{-1} an ε_{max} equal to 0.025 was also considered.

4.3 Results and discussion

4.3.1 Evaluation of the material orientation

The stress strain curves obtained from compression moulded specimens of HDPE-1 and HDPE-2 are reported in Figure 4.6 and Figure 4.7, respectively. For both materials no differences were observed between samples cut in the horizontal and in the vertical direction of the plate meaning that, as can be expected for a material processed via compression moulding there is no

significant orientation in the plane. Therefore, no distinction will be done in the following between samples obtained from different directions of the compression moulded plates.

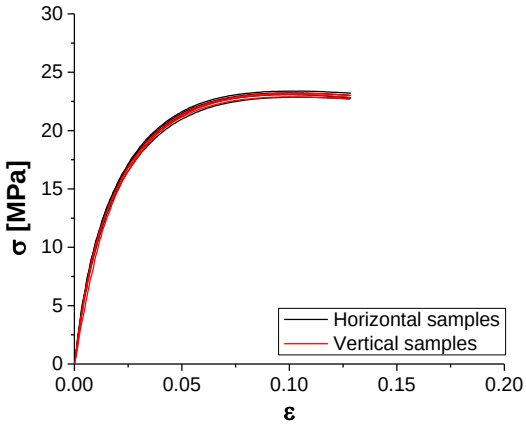

Figure 4.6 - Stress strain curves of compression moulded HDPE-1.

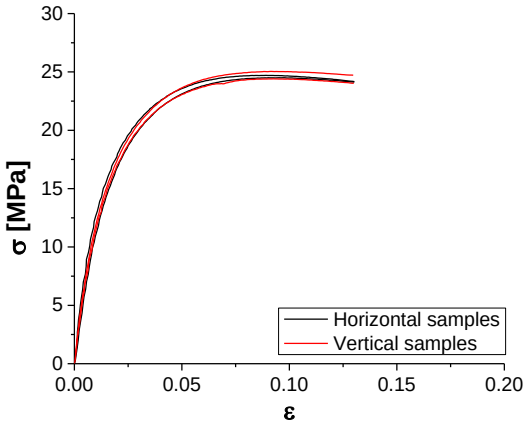

Figure 4.7 - Stress strain curves of compression moulded HDPE-2.

Also in the case of the blow moulded materials no significant differences were observed for samples obtained in the two directions of the bottles, as reported in

Figure 4.8 and Figure 4.9 for HDPE-1 and HDPE-2 respectively, at least within the larger experimental scatter of this tests, probably related to the variability of the cooling rates during bottle production and to the curvature of the samples. To confirm that there is no significant orientation of the material in the bottle, tensile properties should be measured in other direction as, for example, at 45° with respect to the longitudinal axis. However, the manufacturing of these specimens could be difficult and, considering the results obtained in the two directions, it is possible to suppose that only minor difference would be measured from these tests. Due to the greater ease of cutting in the longitudinal direction and to the higher number of specimens that could be obtained from a bottle, tensile samples were subsequently cut only form the longitudinal direction.

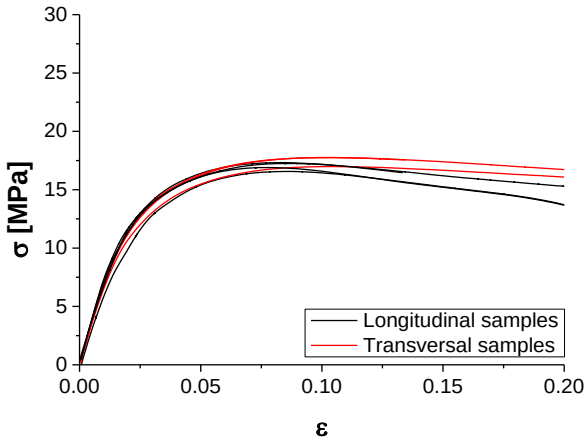

Figure 4.8 - Stress strain curves of blow moulded HDPE-1.

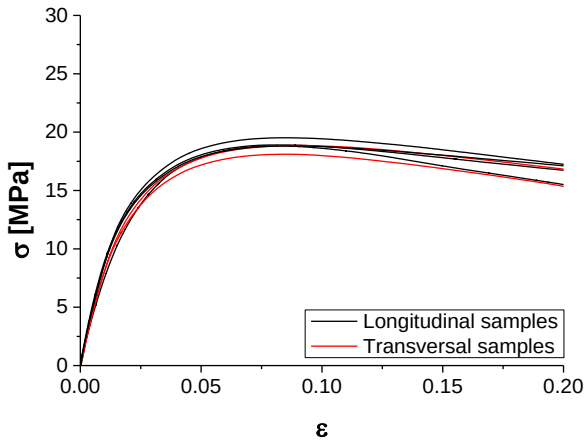

Figure 4.9 - Stress strain curves of blow moulded HDPE-2.

The elastic modulus and yield stress of the two materials processed via compression moulding and blow moulding are shown in Figure 4.10 and Figure 4.11, respectively; these values were computed as the average of all the curves reported before, irrespectively of the orientation of the sample in the plates and in the bottles. For both production processes, HDPI-BI shows slightly higher elastic modulus and yield stress with respect to HDPE-1. On the other hand, as could be expected from the lower degree of crystallinity of blow moulded samples, the specimens from the bottles are characterized by lower tensile properties with respect to their compression moulded counterparts.

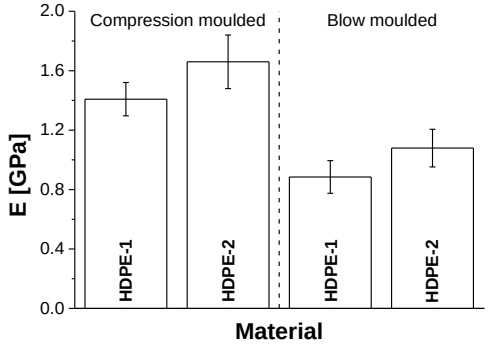

Figure 4.10 - Elastic modulus of compression moulded and blow moulded HDPE-1 and HDPE-2. T = 23°C; displacement rate = 10 mm/min.

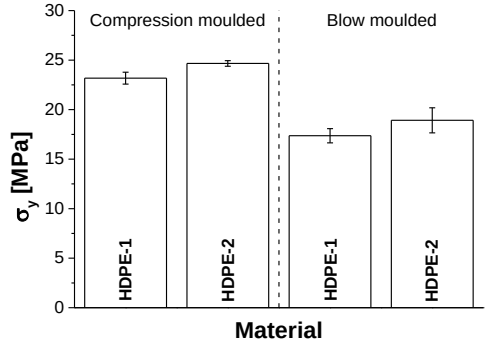

Figure 4.11 - Yield stress of compression moulded and blow moulded HDPE-1 and HDPE-2. T = 23°C; displacement rate = 10 mm/min.

4.3.2 Evolution of the relaxation modulus with time

The $Log(E)$ vs. $Log(t)$ curves of compression moulded HDPE-1 and HDPE-2, measured at 23°C and at different strains, are reported in Figure 4.12 and Figure 4.13, respectively. The two materials show a pronounced nonlinear behaviour starting from very low strains. Therefore, since the tangent modulus of the stress strain curves is equal to the relaxation modulus only for linear elastic materials, the obtained trends are only an approximation of this property.

For each strain level $\bar{\varepsilon}$, the relationship between $Log(E)$ and $Log(t)$ can be represented with a power law, according to Equation (4.9):

$$Log\left(E(t,\bar{\varepsilon})\right) = n(\bar{\varepsilon}) \cdot Log(t) + q(\bar{\varepsilon}) \tag{4.9}$$

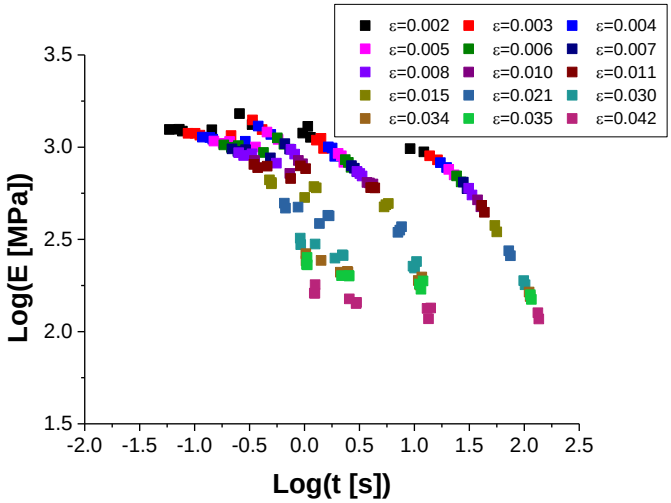

Figure 4.12 – Relaxation modulus of HDPE-1 at 23°C and at various deformations.

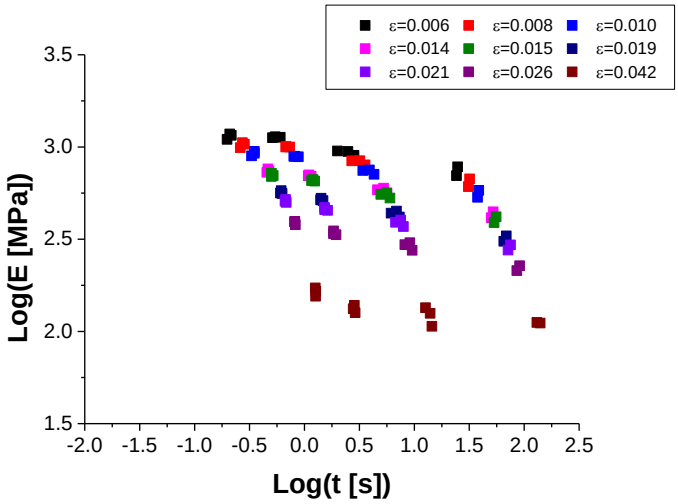

Figure 4.13 - Relaxation modulus of HDPE-2 at 23°C and at various deformations.

To better characterize the material behaviour, the evolution of n and q with the strain was investigated as shown in Figure 4.14: a minimum of the slope was found at ε of about 0.015 for HDPE-1 and 0.020 for HDPE-2 while a linear decrease of the intercept was measured. For the first parameter data were fitted using Equation (4.10):

$$n = C_1 + (C_2 - C_1) \cdot \left[\frac{C_3}{1 + 10^{(C_4 - \varepsilon) \cdot C_5}} + \frac{1 - C_3}{1 + 10^{(C_6 - \varepsilon) \cdot C_7}}\right] \tag{4.10}$$

For what concerns the intercept q, instead, the data were fitted as per Equation (4.11)

$$q = \alpha \cdot \varepsilon + \beta \tag{4.11}$$

where α and β are the fitting parameters. Combining Equations (4.9), (4.10) and (4.11), it is possible to evaluate the relaxation modulus, at a fixed strain $\bar{\varepsilon}$, as:

$$Log\left(E(t, \bar{\varepsilon})\right) = \left\{C_1 + (C_2 - C_1) \cdot \left[\frac{C_3}{1 + 10^{(C_4 - \bar{\varepsilon}) \cdot C_5}} + \frac{1 - C_3}{1 + 10^{(C_6 - \bar{\varepsilon}) \cdot C_7}}\right]\right\} \cdot Log(t) + \alpha \cdot \bar{\varepsilon} + \beta \tag{4.12}$$

Introducing the fitting parameters reported in Table 4.1 and Table 4.2, the $Log(E)$ vs. $Log(t)$ curves of the two materials, at the temperature of 23°C, can be defined at any strain of interest.

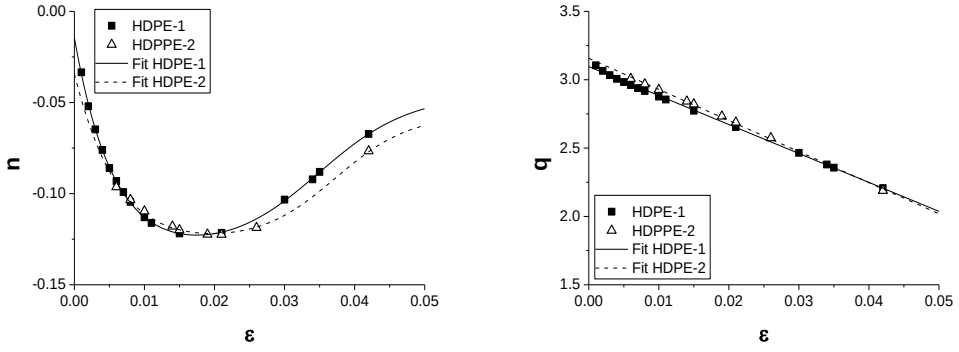

(a) (b)

Figure 4.14 – (a) Slope and (b) intercept of the $Log(E)$ vs. $Log(t)$ curve as a function of the strain.

Table 4.1 - Fitting parameters of the relationship between n and ε.

Parameter	HDPE-1	HDPE-2
C_1	-0.045	-0.056
C_2	5.400	0.485
C_3	1.016	1.130
C_4	-0.020	-0.009
C_5	-81.745	-83.494
C_6	0.035	0.037
C_7	-65.767	-79.941

Table 4.2 - Fitting parameters of the relationship between q and ε.

Parameter	HDPE-1	HDPE-2
α	-21.17	-22.74
β	3.10	3.16

To investigate the effect of temperature on the viscoelastic properties further tests were conducted at 40°C and 60°C: by applying a time-temperature superposition reduction scheme the available experimental window was extended and the master curves of the two materials, reported with the relevant shift factors in Figure 4.15 and Figure 4.16, were obtained. It is possible to observe that for both materials an Arrhenius-type expression properly represents the temperature dependence of the shift factors which, additionally, depend on the strain.

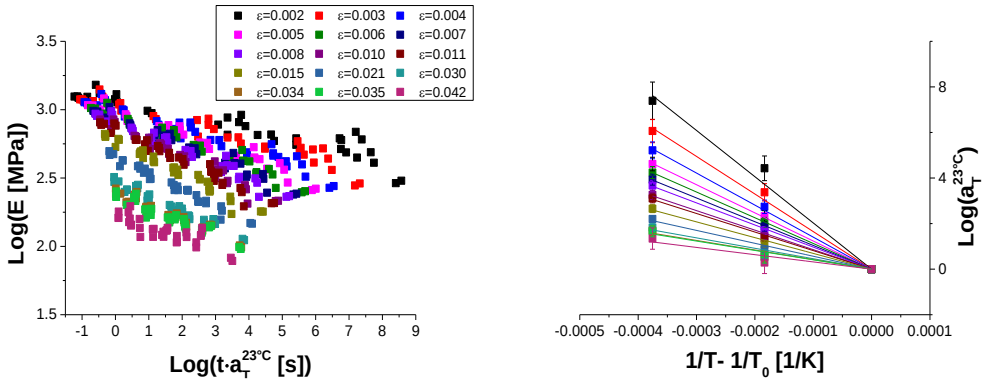

(a) (b)

Figure 4.15 – (a) Master curves of the relaxation modulus of HDPE-1 at various deformation and at the reference temperature of 23°C; (b) relevant shift factors.

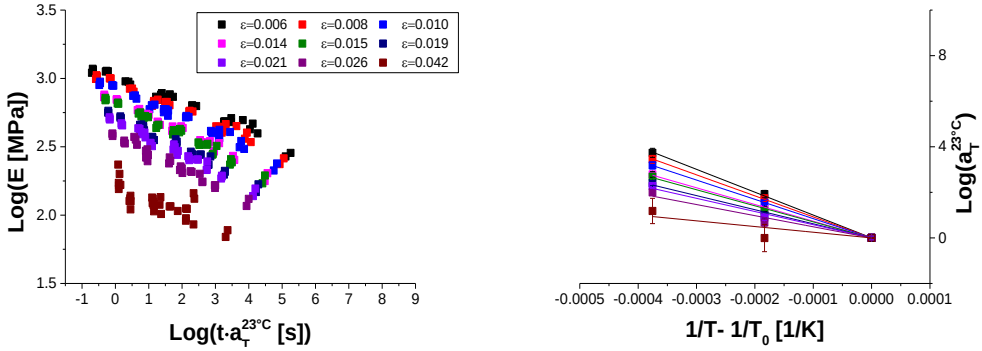

(a) (b)

Figure 4.16 – (a) Master curves of the relaxation modulus of HDPE-2 at various deformation and at the reference temperature of 23°C; (b) relevant shift factors.

Representing the absolute value of the slope of the Arrhenius plot (which, according to the original derivation of this relation, is equal to the ratio between an activation energy ΔH and the universal gas constant R) as a function of the strain as done in Figure 4.17, it can be observed that the effect of temperature on the relaxation modulus is expected to decrease with increasing the strain. These data were fitted using Equation (4.13):

$$\frac{\Delta H}{R} = \mu \cdot \varepsilon^{\gamma} \tag{4.13}$$

where μ and γ are fitting parameters reported, for both materials, in Table 4.3. Even if this equation was found empirically and it is not supported by theory at very low strains it can properly describe the experimental data in the considered range and, therefore, it can be used to introduce the temperature dependence in the expression of the relaxation modulus. Rewriting Equation (4.9) as

$$Log\big(E(t,\bar{\varepsilon},T)\big) = n(\bar{\varepsilon}) \cdot Log\big(t \cdot a_T^{T_0}\big) + q(\bar{\varepsilon}) \tag{4.14}$$

And expanding all the terms as previously done in Equation (4.12) one can obtain:

$$\begin{aligned} Log\big(E(t,\bar{\varepsilon},T)\big) = &\left\{C_1 + (C_2 - C_1) \cdot \left[\frac{C_3}{1 + 10^{(C_4 - \bar{\varepsilon}) \cdot C_5}} + \frac{1 - C_3}{1 + 10^{(C_6 - \bar{\varepsilon}) \cdot C_7}}\right]\right\} \\ &\cdot \left[Log(t) + \mu \cdot \bar{\varepsilon}^{\gamma} \cdot \left(\frac{1}{T_0} - \frac{1}{T}\right)\right] + \alpha \cdot \bar{\varepsilon} + \beta \end{aligned} \tag{4.15}$$

which can be used to evaluate the relaxation modulus at any given strain and temperature.

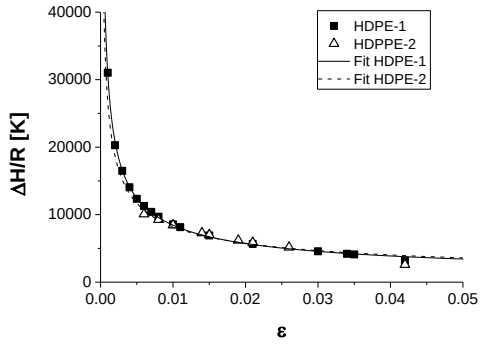

Figure 4.17 – Absolute value of the slope of the Arrhenius plot as a function of the deformation.

Table 4.3 - Fitting parameters of the relationship between $\frac{\Delta H}{R}$ and ε.

Parameter	HDPE-1	HDPE-2
μ	638.4	778.2
γ	-0.561	-0.512

4.3.3 Evolution of the yield stress with time

The correlation between the yield stress and time is shown for the two materials at the three testing temperatures (23, 40 and 60°C) in Figure 4.18. In both cases the Eyring equation properly describes the experimental data:

$$\frac{\sigma_y}{T} = \left(\frac{2}{V^*}\right)\left[\left(\frac{\Delta H}{T}\right) + 2.303R \cdot Log\left(\frac{\varepsilon_y}{t \cdot \dot{\varepsilon}_0}\right)\right] = p - m \cdot Log(t) \tag{4.16}$$

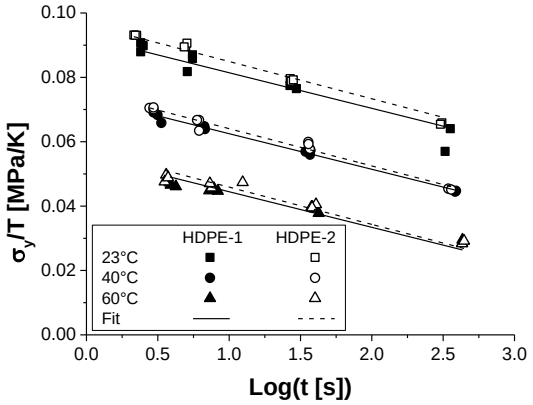

Figure 4.18 - Evolution of the yield stress with time at different temperatures.

Also in this case a time-temperature superposition scheme was applied to the experimental data and the shift factor required to overlap the curves obtained at the different temperatures and hence to build the yield stress master curves at 23°C was evaluated as shown in Figure 4.19. Also in this case, for both materials, the shift factor, follows an Arrhenius type dependency on temperature. The slope

m and the intercept *p* of the Eyring functions identified from the experimental data are reported in Table 4.4.

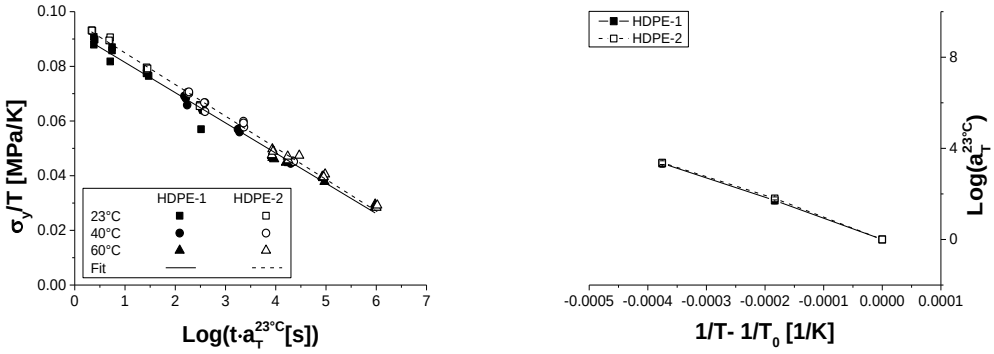

(a) (b)

Figure 4.19 - (a) Master curves of the yield stress of the two materials at the reference temperature of 23°C; (b) relevant shift factors.

Table 4.4 - Parameters of the Eyring relationship at 23°C .

Parameter	*HDPE-1*	*HDPE-2*
m	*-0.011*	*-0.012*
p	*0.092*	*0.096*

4.3.4 Material response to complex loading histories

4.3.4.1 Experimental results

During the service life of a container the material can be subjected to complex mechanical histories which, limiting the attention to static or quasi-static inputs, can include loading phases (stacking of various pallets of the product), periods during which the bottle is subjected to a constant load (storage phase) and unloading phases (removal of some of the pallets). To understand the mechanical response of the material to a combination of all these inputs the experimental procedure described in Section 4.2 and previously adopted in [157] at IMAP, where this part of the research was conducted, was followed. In light of

the complex nonlinear mechanical behaviour of the considered HDPEs, however, the analysis of the material response during simpler creep or relaxation experiments could be needed to gain a deeper comprehension of the mechanical behaviour of these materials. As highlighted during the introduction of this Chapter, these tests could be the basis for further researches related to the deformation behaviour of the HDPEs under study.

The stress-strain curves obtained from "loading-unloading-constant stress experiment" on blow moulded HDPE-1 at 23°C and at strain rate of 10^{-3} s^{-1} (described in Section 4.2) are reported in Figure 4.20. Observing the phase at constant stress, it is possible to notice that the material response quantitatively changes depending on the stress level at which the specimen is kept:

- at $\bar{\sigma} = 0.8 \cdot \sigma_{max}$ and above the strain increases with time
- at $\bar{\sigma} = 0.4 \cdot \sigma_{max}$ and below the strain decreases with time
- for $\bar{\sigma} = 0.6 \cdot \sigma_{max}$ a decrease of the strain is observed first, followed by an increase

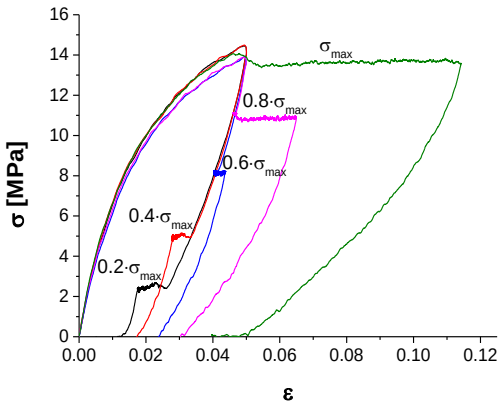

Figure 4.20 – Experimental curves obtained from the load-unload-constant stress experiments on blow-moulded HDPE-1 at 23°C and at a strain rate of 10^{-3} s^{-1}.

These different responses can be made more evident by plotting the strain evolution during the constant stress phase of the experiment, as done in Figure 4.21; to better compare the curves obtained at different stresses $\bar{\sigma}$, the strain difference $\Delta\varepsilon$ calculated from the level achieved at the beginning of the constant stress phase was considered. This representation of the data highlights the different rates at which specimen elongation or strain recovery take place: at $\bar{\sigma} = \sigma_{max}$ elongation occurred faster than at $\bar{\sigma} = 0.8 \cdot \sigma_{max}$ while at $\bar{\sigma} = 0.2 \cdot \sigma_{max}$ strain recovery was faster than at $\bar{\sigma} = 0.4 \cdot \sigma_{max}$. For what concerns the curve at $\bar{\sigma} = 0.6 \cdot \sigma_{max}$ strain recovery occurred during the first 100 s after which the specimen started to elongate. This behaviour was already known in the literature by the name of "rate reversal" as reported in [157–161]; in the present work, the effect of temperature and strain rate on the material response was investigated performing test also at 40°C and 60°C and at strain rates of 10^{-2} s^{-1} and 10^{-4} s^{-1}.

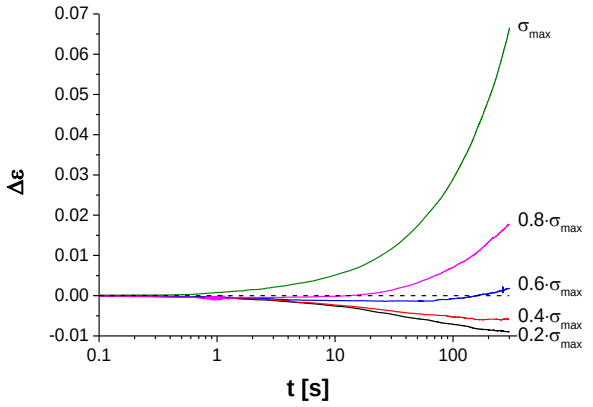

Figure 4.21 – Blow moulded HDPE-1 deformation during the constant stress phase of the tests at 23°C and with the loading and unloading phases at a strain rate of 10^{-3} s^{-1}.

The results obtained from the tests performed at 23°C and with the loading and unloading stages at the three strain rate are reported, in term of $\Delta\varepsilon$ vs. t curves in Figure 4.22. The same trend can be observed irrespective of the strain rate applied during loading-unloading but the strain values achieved during this phase strongly depend on the rate. However, due to the viscoelastic behaviour of HDPE, different maximum stresses and $\bar{\sigma}$ were obtained changing the strain rate of the first two phases; consequently no direct comparison of the data reported in these three graphs can be done.

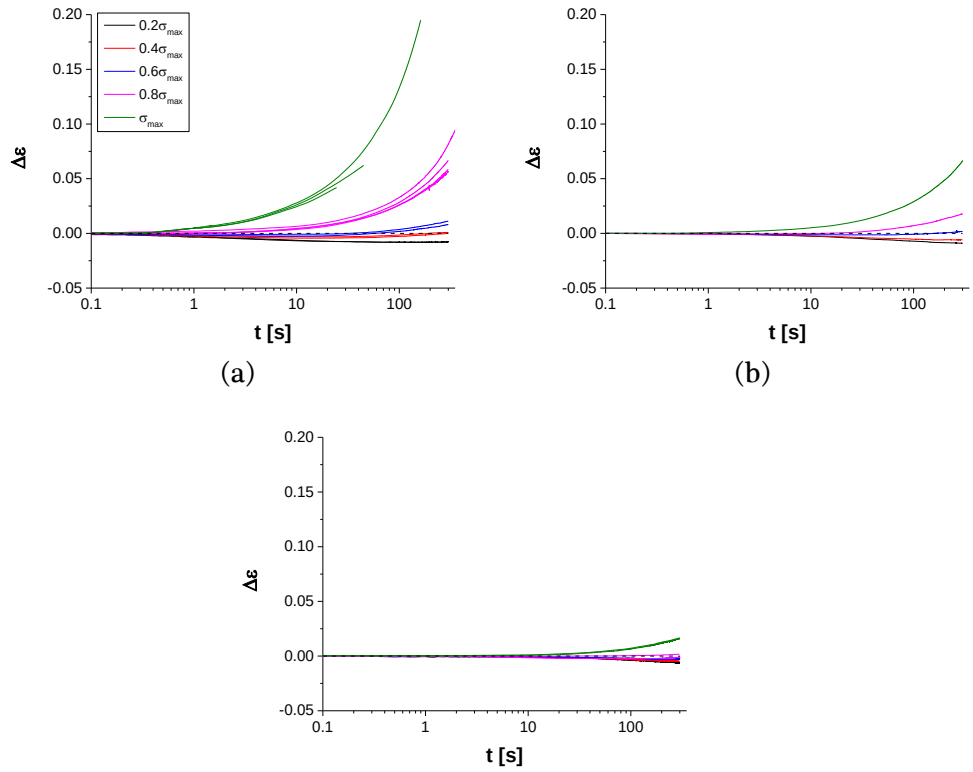

Figure 4.22 - Blow moulded HDPE-1 deformation during the constant stress phase of the tests at 23°C and with the loading and unloading phases at strain rate of (a) 10^{-2} s^{-1}, (b) 10^{-3} s^{-1}, (c) 10^{-4} s^{-1}.

To overcome this limitation, data were further analysed. At first, the value of $\Delta\varepsilon$ at different times (10, 100 and 300 s) was evaluated from all the available $\Delta\varepsilon$ vs. t curves obtained at 23°C. Hence isochronous plots for the three considered times were built (Figure 4.23 (a,b,c)), representing these data, on the same graph, as a function of the relevant $\bar{\sigma}$ which, due to the different loading rates and hold levels, is different for all samples. Finally, to further characterize the rate reversal phenomenon the derivative of the strain variation with respect to time $d\Delta\varepsilon/dt$ was evaluated at the same times considered in the isochronous $\Delta\varepsilon$ vs. $\bar{\sigma}$ curves and expressed as a function of $\bar{\sigma}$ (Figure 4.23 (d,e,f)).

Using these isochronous $d\Delta\varepsilon/dt$ vs. $\bar{\sigma}$ plots the strain rate during the hold phase for all the samples considered for this analysis can be compared. It is possible to observe that all the data fall on the same curve making hence possible the prediction of $d\Delta\varepsilon/dt$ (and consequently of $\Delta\varepsilon$) for loading rates other than those applied, for given hold stress $\bar{\sigma}$ and time t. For all considered times $d\Delta\varepsilon/dt$ is negative at low $\bar{\sigma}$ meaning that the strain is initially recovered; as higher $\bar{\sigma}$ are considered the opposite trend is observed, with increasing elongation rates. Since $\Delta\varepsilon$ does not assume a constant value in the whole time frame considered, the point at which $d\Delta\varepsilon/dt$ equals zero represents a minimum of the $\Delta\varepsilon$ vs. t curve: for longer times the sample will start to elongate and, consequently, the rate reversal phenomenon will occur. Moreover, since the value of $\bar{\sigma}$ at which $d\Delta\varepsilon/dt$ equals zero decreases with increasing the time (compare for example Figure 4.23 (d) and Figure 4.23 (f)), it is possible to conclude that irrespective of the loading rate and of the hold stress, sample elongation will occur provided that the hold phase lasts for a sufficient amount of time.

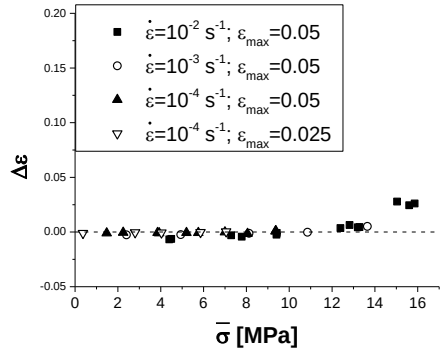

(a): 10 s

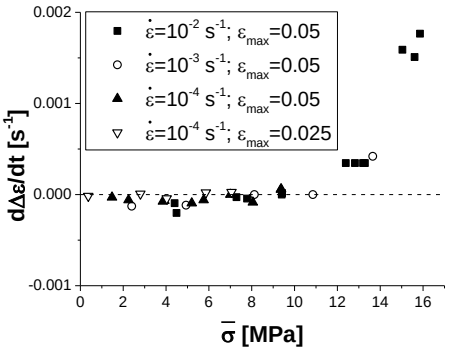

(d): 10 s

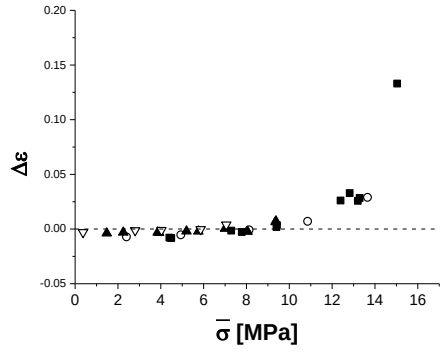

(b): 100 s

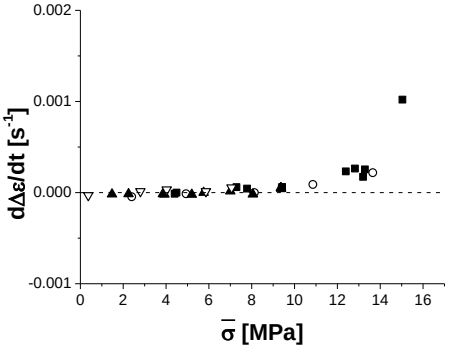

(e): 100 s

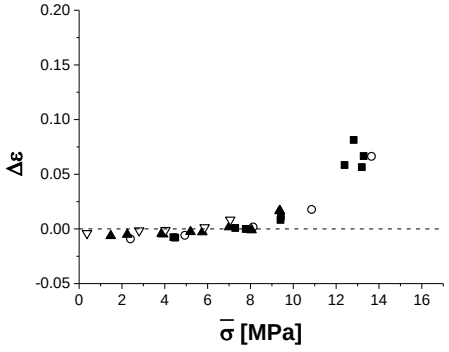

(c): 300 s

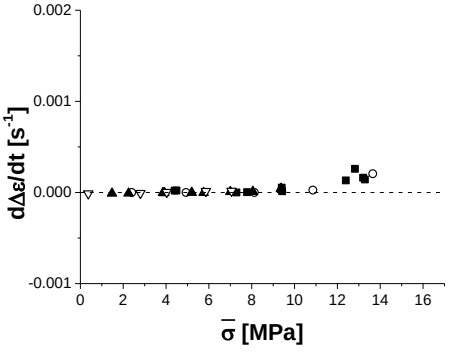

(f): 300 s

Figure 4.23 – (a,b,c) Isochronous $\Delta\varepsilon$ vs. $\bar{\sigma}$ and (d,e,f) $d\Delta\varepsilon/dt$ vs. $\bar{\sigma}$ plots for the tests performed at 23°C.

The Effect of temperature was evaluated adopting the same data reduction scheme: $\Delta\varepsilon$ vs. $\bar{\sigma}$ and the relevant $d\Delta\varepsilon/dt$ curves are reported in Figure 4.24 (a,b,c) and (d,e,f), respectively. It is possible to observe that for all the considered times the curves not overlap at high $\bar{\sigma}$. This fact can be explained considering that, as expected, with increasing temperature the deformation phenomena will occur faster or, in other words, that, at a certain time, the same sample elongation will be reached for a lower value of the constant applied stress. Also in this case, for all the curves, the stress $\bar{\sigma}$ at which $d\Delta\varepsilon/dt$ equals zero decreases with increasing time meaning that sample elongation will occur provided that the hold phase lasts for a sufficient amount of time, irrespective of the considered temperature.

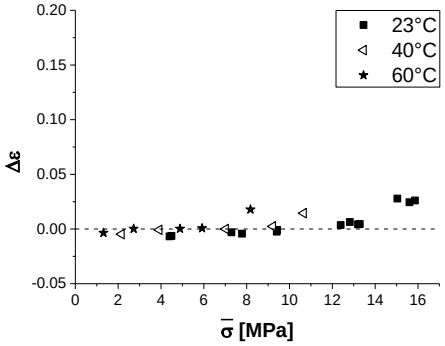

(a): 10 s

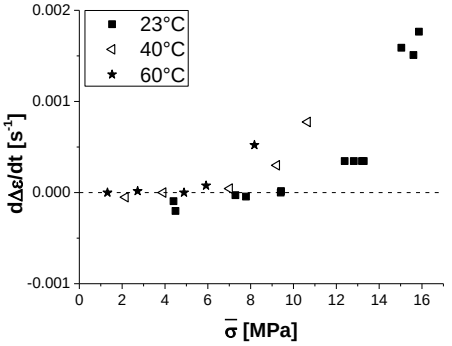

(d): 10 s

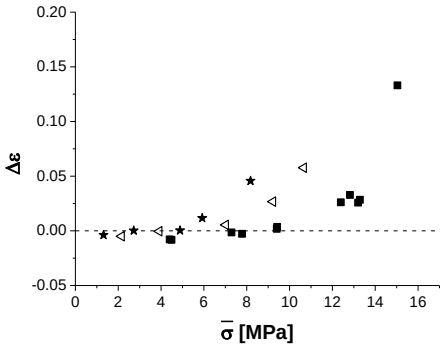

(b): 100 s

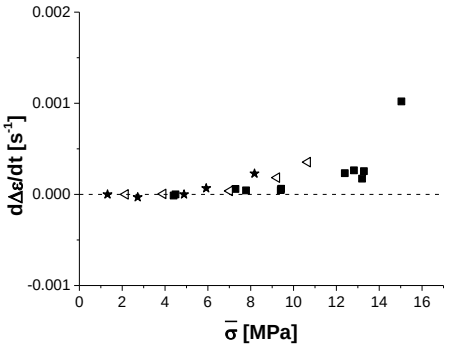

(e): 100 s

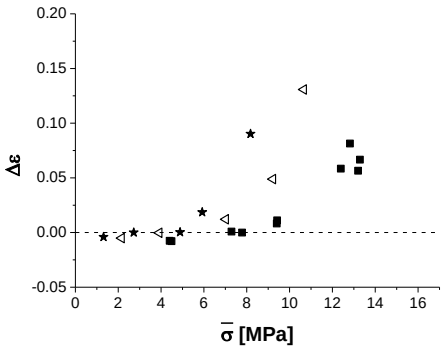

(c): 300 s

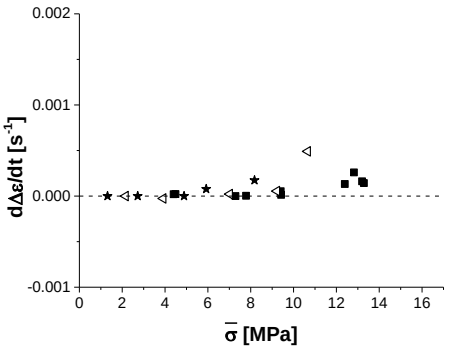

(f): 300 s

Figure 4.24 - (a,b,c) Isochronous $\Delta\varepsilon$ vs. $\bar{\sigma}$ and (d,e,f) $d\Delta\varepsilon/dt$ vs. $\bar{\sigma}$ plots for the tests performed with the loading and unloading at the strain rate of 10^{-2} s^{-1}.

The results obtained during this analysis clearly show that the material response during the hold phase is a complex combination of the previous loading history to which the material is subjected. This fact, together with the effects of

temperature, applied strain rate and maximum strain, suggests that viscoelasticity plays a key role in the rate reversal phenomenon and that a pseudo-linear approach based on the Boltzmann's superposition principle could be adequate to predict the material response to this kind of complex loading history. However, in the literature, the latter has so far been described using viscoplastic theories: a comparison between these different approaches will be presented in the next two Sections.

4.3.4.2 Viscoplastic approach to modelling

To represent the material response to the complex loading history described in the previous section, a phenomenological model based on the viscoplasticity theory based on overstress (VBO) was used; the model was originally proposed by Khan and Yeakle in [160]. This approach had been originally developed for metals and subsequently adapted for the description of polymer behaviour in [159, 162], to quantitatively predict the effect of different loading histories as well as temperature effects.

In the original version of this model the material can be represented with a modified Zener model as reported in Figure 4.25.

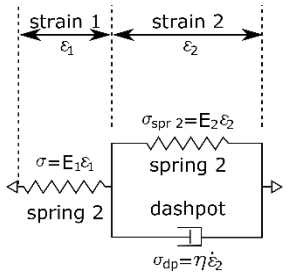

Figure 4.25 – Modified Zener model used for the original formulation of VBO theory. Adapted from [159]

The first spring is linear while the one in the Kelvin-Voigt element is non-linear and hysteretic; the dashpot is also nonlinear and its response depends on the overstress $(\sigma - g)$. The latter, as sketched in Figure 4.26, is defined as the difference between the actual stress σ and the "equilibrium stress" g, which represents the thresholds above which inelastic flow can occur. The model was hence completed with the introduction of the "kinematic stress" f which, if subtracted form g, defines the isotropic stress A, originally introduced in the model to predict cyclic hardening or softening.

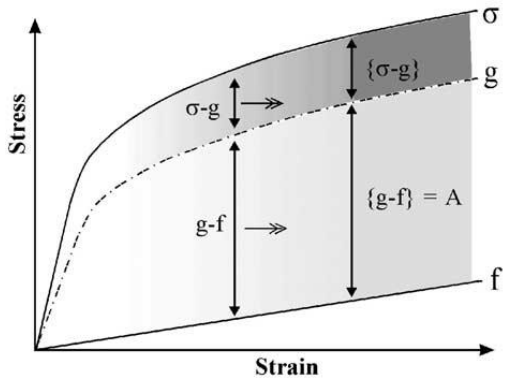

Figure 4.26 - Stress contribution in standard VBO model: σ is the stress, g is the equilibrium stress and f is the isotropic stress. [163]

σ, g and f are linked by the following set of first order, coupled, nonlinear differential equations:

$$\begin{cases} \dot{\varepsilon} = \dfrac{\dot{\sigma}}{E} + \dfrac{\sigma - g}{E \cdot k} \\ \dot{g} = \theta \dfrac{\dot{\sigma}}{E} + \theta \left(\dfrac{\sigma - g}{E \cdot k} - \dfrac{(g - f) \cdot |\sigma - g|}{A \cdot E \cdot k} \right) + \left(1 - \dfrac{\theta}{E} \right) \dot{f} \\ \dot{f} = E_t \dfrac{\sigma - g}{E \cdot k} \end{cases} \tag{4.17}$$

in which k is a viscosity function, θ is a shape function that modulates the transition from quasi-linear elastic behaviour to inelastic flow, E is the Young's modulus and E_t is the final tangent modulus, for a total of eight modelling

parameters (E, E_t, A, three parameters coming from k and two parameters coming from θ). The system in Equation (4.17) can be solved enforcing suitable boundary conditions such as, for example, a constant strain rate or a constant stress; by knowing the constitutive parameters of the material of interest, its behaviour can be predicted for any mechanical history. In particular, if a loading-unloading history is considered, as sketched in Figure 4.27, it is possible to notice that in the whole loading curve and the part of the unloading curve at higher stresses the overstress is positive while in the final part of the unloading curve it is negative. Depending on the sign of the overstress, strains will increase or decrease during a constant load step introduced during unloading.

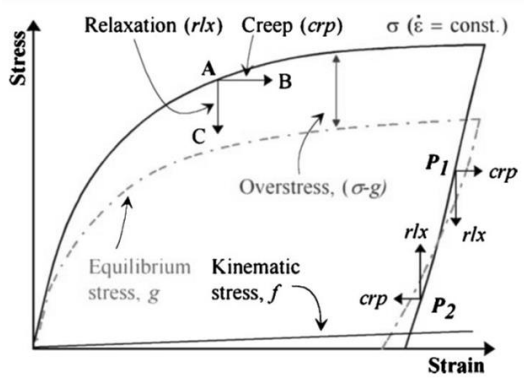

Figure 4.27 – Sketch of the working principle of the original VBO theory.

Even if the original VBO model is able to predict sample elongation and strain recovery during the unloading phase, it is inadequate for the representation of the rate reversal phenomenon described in the previous section. To overcome this limit Khan proposed in [159] a modified version of the VBO theory by inserting a second Kelvin-Voigt element in the analog spring dashpot model and, consequently adding two more differential equations, corresponding to a second equilibrium stress and a second kinematic stress, to the system reported in Equation (4.17).

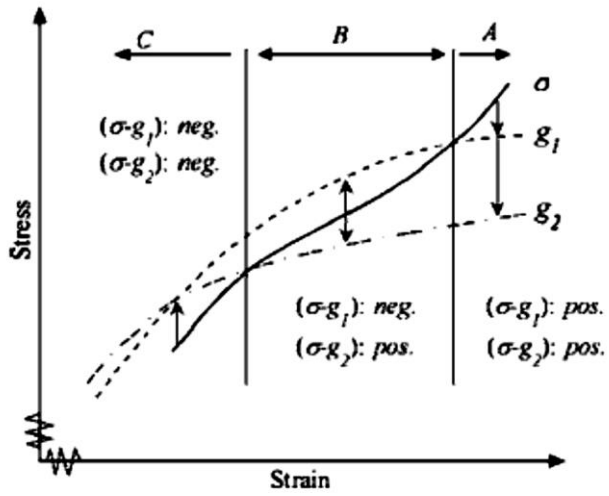

Figure 4.28 - Sketch of the working principle of the modified VBO theory. Region A: sample elongation; region C: strain recovery; region B: strain recovery followed by sample elongation (rate reversal). [159]

This version of the model was used for the first time by Khan and Yeakle in [160] who introduced the two extra aforementioned differential equations and modified the strain rate equation in the system with Equation (4.18)

$$\dot{\varepsilon} = \frac{\dot{\sigma}}{E \cdot w_1(A_1, g, f_1)} + \frac{\sigma - g}{E \cdot k_1} + \frac{\dot{\sigma}}{E \cdot w_2(A_2, h, f_2)} + \frac{\sigma - h}{E \cdot k_2} \tag{4.18}$$

where h is the second equilibrium stress, k_i is the viscosity function of the dashpot i, and w_i is an additional term introduced to capture the curved unloading behaviour. The total number of modelling parameters required for this version of the VBO theory is equal to seventeen.

Using the modified version of the VBO model an attempt to model the experimental results reported in the previous section was done: considering the load curves at 23°C reported in Figure 4.29, the modelling parameters were calibrated for the curve obtained at the strain rate equal to 10^{-2} s^{-1}. Using the same set of parameters to represent the strain rate sensitivity of the material, however,

a first strong limitation of this model can be clearly observed: even if the expected order of the curves was respected, in fact, the theoretical curves do not describe properly the experimental results obtained at the different strain rates.

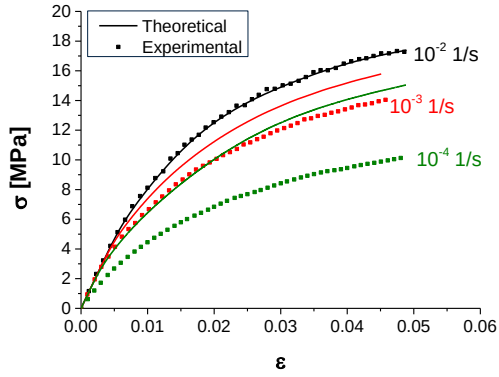

Figure 4.29 – Experimental and VBO theory curves for blow moulded HDPE-1 tested at 23°C and three strain rates. The modelling parameters were calibrated on the curve at the higher strain rate.

Even if the previous results were unsatisfactory, a further analysis was conducted for the data obtained at 23°C and at the strain rate of 10^{-3} s^{-1} to evaluate the prediction capability of the unloading and of the constant stress phases. The modelling parameters were hence recalibrated for the strain rate of interest and using the parameter w_i, introduced in Equation (4.18) the experimental loading-unloading curve in Figure 4.30 was adequately described with the modified VBO theory.

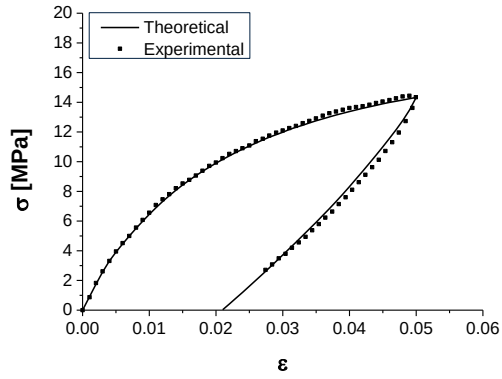

Figure 4.30 - Experimental and VBO theory load unload curves for blow moulded HDPE-1 tested at 23°C and at the strain rate of 10^{-3} s^{-1}.

Considering the constant stress phase, instead, the same set of parameters optimized with the previous loading-unloading curve was used and the results were expressed in terms of $\Delta\varepsilon$ vs. t graphs as shown in Figure 4.31. Also in this case, even if the order of the experimental curves is respected by the model, the theoretical curves do not agree with the obtained experimental data, showing a second strong limitation of the VBO theory.

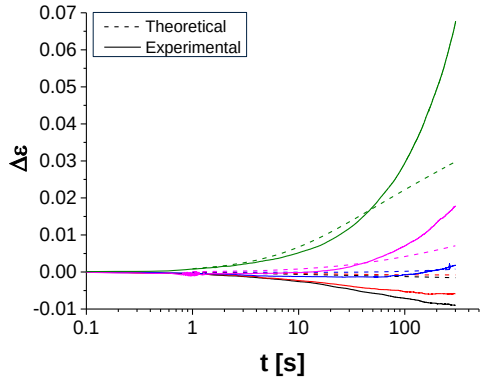

Figure 4.31 - Experimental and VBO theory $\Delta\varepsilon$ vs. t curves for blow moulded HDPE-1 tested at 23°C and with the loading and unloading stages performed at the strain rate of 10^{-3} s^{-1}.

Since most of the modelling parameters have no physical meaning, they cannot be determined with different test procedures and only a least square method can be used to optimize them. However, several minima could be present for each curve and the identification of the most appropriate one, adopting a trial and error approach, is for sure an extremely time consuming procedure.

To summarize, the results obtained from modelling based on a viscoplastic approach do not represent quantitatively the behaviour of blow moulded HDPE-1. The inadequacy of this approach could be related to the fact that, even if the yielding of the material cannot be excluded without further specific analysis, it has to be considered that, as reported in Section 4.3.1, at least at 23°C and at a strain rate of $4.5 \cdot 10^{-3}$ s^{-1}, the yield stress is higher than the maximum stress reached during the tests presented in this section at the same temperature and at a strain rate of 10^{-3} s^{-1}. Therefore it can be assumed that the material is mainly viscoelastically deformed and the use of a viscoplastic theory for the representation of this kind of behaviour is, at least, inappropriate. For these reasons a different approach to predict the behaviour of the materials under study should be used: in the next section some results based on the experimental characterization conducted during this work and on a viscoelastic interpretation of the phenomenon are presented for compression moulded HDPE-1.

4.3.4.3 Viscoelastic approach to modelling

Since, as described in Section 4.3.2, HDPE is a nonlinear viscoelastic material, the evolution of the relaxation modulus must be properly defined to represent the stress-strain behaviour of this material. In fact, if the material is considered as linear viscoelastic and the stress during a tensile test at a certain constant strain rate $\dot{\varepsilon}$ is evaluated starting from Equation (4.3) as

$$\sigma(t) = \int_0^t E(t-\tau)\frac{\partial \varepsilon}{\partial \tau}d\tau = \dot{\varepsilon}\int_0^t E(t-\tau)d\tau \tag{4.19}$$

the result will not represent the experimental data, as shown in Figure 4.32 where the stress-strain curve at 23°C and 100 mm/mm (equal to $4.5 \cdot 10^{-2}$ s^{-1}) is reported together with the two curves obtained using of Equation (4.19) (LVE model), in which the experimental values at $\bar{\varepsilon} =$ 0.002 and 0.042 were considered, respectively, for the relaxation modulus E(t) (evaluated using the power law reported in Equation (4.9) with the relevant slope and intercept).

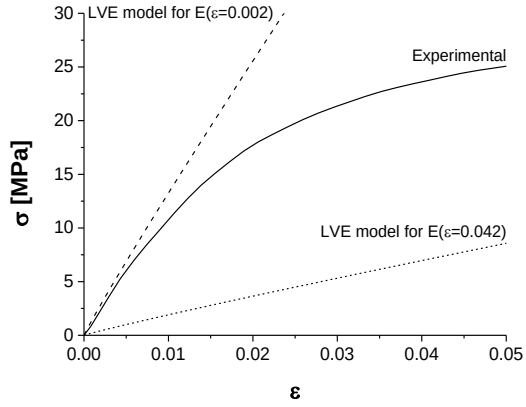

Figure 4.32 – Experimental and LVE load curves for compression moulded HDPE-1 tested at 23°C and at constant displacement rate of 100 mm/min.

To take into account the nonlinear viscoelastic behaviour of HDPE and hence the strain dependence of the relaxation modulus, Equation (4.12) was rewritten in a more general form as

$$Log\big(E(t,\varepsilon)\big) = \left\{C_1 + (C_2 - C_1)\cdot\left[\frac{C_3}{1+10^{(C_4-\varepsilon)\cdot C_5}} + \frac{1-C_3}{1+10^{(C_6-\varepsilon)\cdot C_7}}\right]\right\}\cdot Log(t) + \alpha\cdot\varepsilon + \beta \tag{4.20}$$

Moreover, since for a constant strain rate $\dot{\varepsilon}$, ε can be expressed as the product between the strain rate itself and the time t, Equation (4.20) can be further rearranged giving an expression of $Log(E)$ having t as only variable:

$$Log\big(E(t)\big) = \left\{C_1 + (C_2 - C_1) \cdot \left[\frac{C_3}{1 + 10^{(C_4 - \dot{\varepsilon} \cdot t) \cdot C_5}} + \frac{1 - C_3}{1 + 10^{(C_6 - \dot{\varepsilon} \cdot t) \cdot C_7}}\right]\right\} \cdot Log(t) + \alpha \cdot \dot{\varepsilon} \cdot t + \beta \qquad (4.21)$$

Equation (4.21) was hence used to evaluate a fictitious relaxation modulus using the fitting parameters of compression moulded HDPE-1 reported in Table 4.1 and Table 4.2. Introducing the obtained result in Equation (4.19) and considering the strain rates of $4.5 \cdot 10^{-2}$ s^{-1}, $1.8 \cdot 10^{-2}$ s^{-1}, $4.5 \cdot 10^{-3}$ s^{-1} and $4.5 \cdot 10^{-4}$ s^{-1} (corresponding to displacement rates of 100, 50, 10 and 1 mm/min) the stress-strain curve of the material can be evaluated as reported in Figure 4.33. Comparing the results obtained with this analysis (NLVE model) with the experimental data a fair agreement of the curves can be noticed for every strain rate, meaning that the proposed data reduction scheme is able to capture the strain-rate dependence of compression moulded HDPE-1.

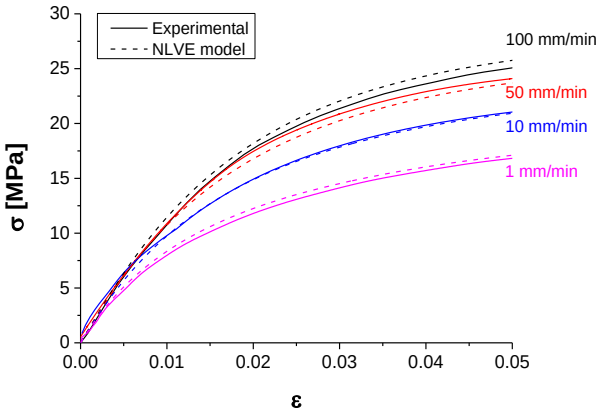

Figure 4.33 - Experimental and NLVE load curves for compression moulded HDPE-1 tested at 23°C and at various constant displacement rates.

However, even if the results shown in Figure 4.33 seem to be promising, one can criticize the fact that the relaxation moduli used to evaluate the fictitious ones were obtained from the load curves themselves and, consequently that the agreement between the NLVE model here proposed and the experimental data can be somehow expected a priori. Hence, to further test the prediction capability of this method a loading-unloading history, performed at the constant displacement rate of 5 mm/min and at the temperature of 50°C was considered. At first, taking advantage of Equation (4.15), the relaxation modulus master curves were evaluated at the temperature of interest. Since this procedure was done applying the time-temperature superposition principle the curve were horizontally shifted: the fitting parameters related to the slope n remained equal to those evaluated at 23°C while those regarding the intercept q changed as shown in Figure 4.34. At this temperature the correlation between q and ε is no more linear and a three-term Prony's series was used to fit the data and Equation (4.21) was rewritten as:

$$Log\big(E(t)\big) = \left\{C_1 + (C_2 - C_1) \cdot \left[\frac{C_3}{1 + 10^{(C_4 - \dot{\varepsilon} \cdot t) \cdot C_5}} + \frac{1 - C_3}{1 + 10^{(C_6 - \dot{\varepsilon} \cdot t) \cdot C_7}}\right]\right\} \cdot Log(t) + q_1 \cdot exp\left(-\frac{\dot{\varepsilon} \cdot t}{\varepsilon_{q1}}\right) + q_2 \cdot exp\left(-\frac{\dot{\varepsilon} \cdot t}{\varepsilon_{q2}}\right) + q_3 \cdot exp\left(-\frac{\dot{\varepsilon} \cdot t}{\varepsilon_{q3}}\right) + q_0 \tag{4.22}$$

being q_0, q_1, q_2, q_3, ε_{q1}, ε_{q2}, ε_{q3} the fitting parameters of the Prony's series as reported in Table 4.5.

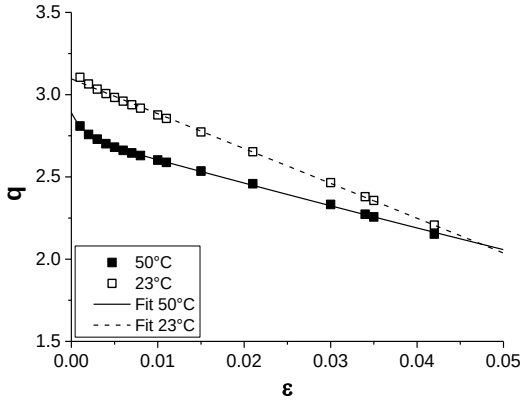

Figure 4.34 - Intercept of the $Log(E)$ vs. $Log(t)$ curve as a function of the strain for HDPE-1 at 23°C and 50°C.

Table 4.5 - Fitting parameters of the relationship between q and ε for compression moulded HDPE-1 at 50°C.

Parameter	HDPE-1
q_0	-3.60
q_1	3.17
ε_{q1}	0.43
q_2	3.18
ε_{q2}	0.44
q_3	0.14
ε_{q3}	0.0016

The two phases of the loading history were considered separately and, taking advantage of Boltzmann's superposition principle, the global behaviour of the material was evaluated. As shown in Figure 4.35, in fact, the strain in the unloading phase can be considered as the sum of the strain reached during the loading phase, conducted at the strain rate of approximately $1.5 \cdot 10^{-3}$ s^{-1}, and of the strain reached during a fictitious compression phase at a double strain rate

with respect to the first one. If Boltzmann's superposition principle holds true, the sum of stress in this two stages should be equal to the actual stress during the unloading phase.

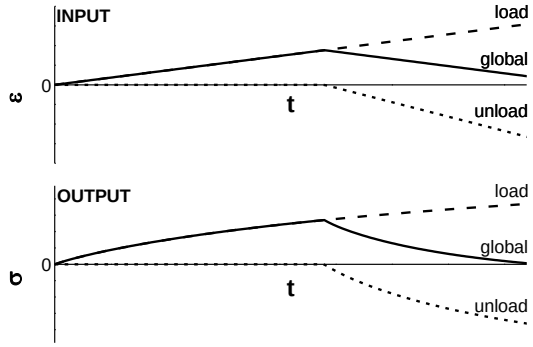

Figure 4.35 - Decomposition of the global loading history to apply Boltzmann's superposition principle.

By applying this method, however, it has to be considered that when the load curve reaches strains higher than those considered for the relaxation modulus master curve the curve obtained from the NLVE model could be inaccurate affecting, obviously, also the global unloading curve. Hence, a maximum displacement of 1 mm, corresponding to a maximum strain of 0.018, was reached during the loading phase after which the sample was completely unloaded: using this loading history the strain in the fictitious load curve does not exceed the maximum strain considered for the relaxation modulus master curves as can be observed in Figure 4.36.

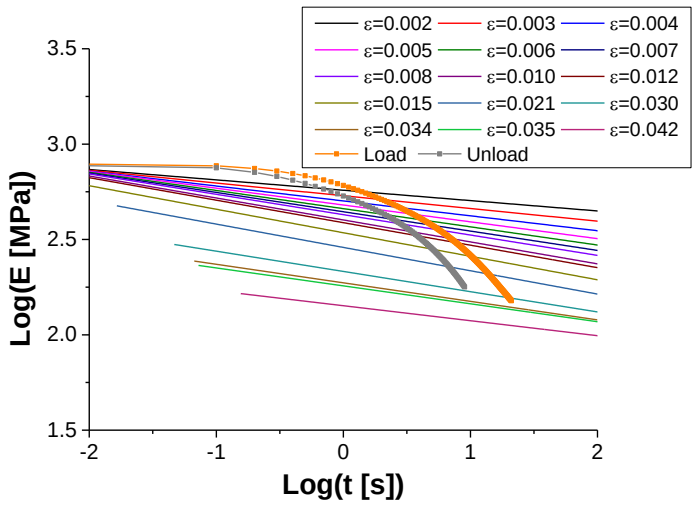

Figure 4.36 – Power law fittings of the relaxation modulus at various strain at 50°C (lines) and fictitious moduli for the load and unload curves defined for Boltzmann's superposition principle (dots).

Using the two fictitious moduli the loading-unloading behaviour of compression moulded HDPE-1 was hence evaluated using the procedure previously described for the tests at 23°C and at different strain rates. The results are reported in term of ε and σ vs. t and σ vs. ε curves in Figure 4.37 (a) and (b) respectively. The NLVE model is in good agreement with the experimental data even if, as can be clearly observed from the stress-strain curve there is a slight discrepancy of the two curves in the final part of the unloading phase which can lead to an underestimation of the residual strain.

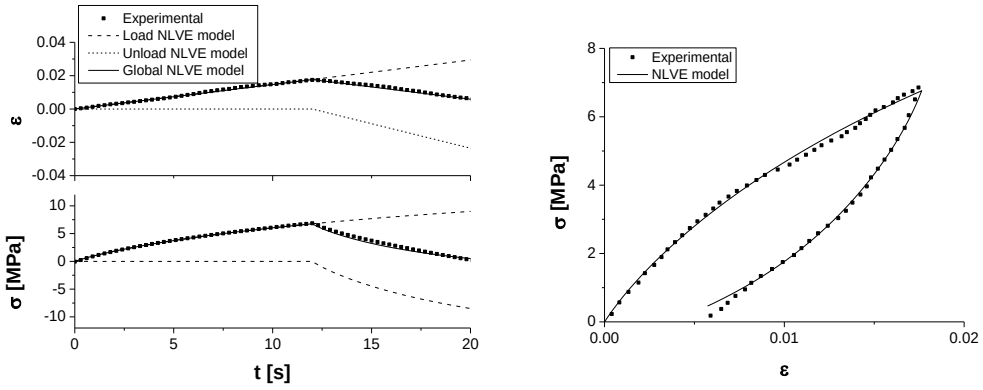

(a) (b)

Figure 4.37 – Comparison between the experimental results and the NLVE for the load unload experiment performed on compression moulded HDPE-1 at 50°C and at a constant displacement rate of 5 mm/min. (a) ε and σ vs. t curves; (b) σ vs. ε curve.

At this point it should be possible to investigate the behaviour of the material during a phase of constant stress after a partial unloading, as shown in the previous Section. To do this one can approximate the material creep compliance $D(t)$ with the expression:

$$D(t) = \frac{1}{E(t)} \tag{4.23}$$

or using similar equations as proposed, for example, by Ferry [164] or Christensen [165]. This approach, however does not take into account the material nonlinearity and, consequently, no indication about the stress dependence of the creep compliance would be obtained in this case. On the other hand, one can use the creep compliance obtained from constant load tests on the blunt notched samples used during the fracture characterization (see next Chapter). However, as reported in [156] the creep compliance evaluated in this way does not correspond to the creep compliance of unnotched samples, since a plastic zone will be always present at the crack tip, affecting somehow the result. Hence the only way to obtain useful information for the modelling of the

constant stress phase is to perform an extensive mechanical characterization which, nevertheless, is out of the main scope of this work. As stated at the beginning of this Chapter, in fact this aspect of the analysis is still an open question and further work has to be done to complete this research.

4.4 Conclusions

The tensile tests conducted during this work have been used to investigate different aspects of the material mechanical behaviour.

At first, the comparison of the results obtained from samples cut in different directions of the compression moulded plates confirmed that the material is not oriented during this production process. Similarly, it has been shown that the properties measured in the longitudinal and in the transversal direction of the central part of the bottle are comparable, meaning that probably also in this case there is no material orientation or that the material is equally bi-oriented in these two directions.

Subsequently, the relaxation modulus was evaluated. It turned out that the mechanical behaviour of the considered material was highly nonlinear. An empirical reduction scheme was defined to analytically describe this aspect. The yield stress vs. time to yield curves were also defined: the Eyring equation properly describes the experimental data.

Finally, the material response to complex loading histories was studied both from an experimental and from a modelling point of view. From this analysis it turned out that the viscoelasticity of the material has a key role on the behaviour of the considered samples and encouraging results were obtained with a nonlinear viscoelastic data reduction scheme developed during this work as opposed to viscoplasticity theory based on overstress. As previously outlined

during this Chapter, a more complete experimental characterization, based on simpler mechanical histories, is required to fully understand the deformation behaviour of the two HDPEs and to adequately model the material response.

5 Fracture behaviour

5.1 Aims of the study

In this Chapter the fracture behaviour of the materials under study was defined as a reference for the ESC behaviour which will be discussed from Chapter 7 to Chapter 9.

As highlighted in the literature review of Chapter 2, LEFM theory was considered in view of its application to ESC. Notched specimens, having adequate dimensions to guarantee that both materials were under plane strain conditions during the tests, were produced via compression moulding; the adequacy of the stress intensity factor K and of the energy release rate G as critical fracture parameters for the two HDPEs under study was evaluated.

Moreover, since one of the main objective of this work was to evaluate the fracture and ESC resistance of the bleach bottles, specimens were also obtained from the containers themselves. In this case, however, due to the reduced bottle wall thickness, the material is mainly under plane stress conditions and extensive plastic deformations develop before and during crack propagation; a J-integral approach was thus used to analyse the obtained data.

5.2 Experimental details

5.2.1 Plane strain tests

To properly define the sample dimensions required for validity of LEFM theory, a study on size effects was conducted. Single Edge Notched Bending (SENB) and Double Cantilever Beam (DCB) specimens, having the geometry reported in Figure 5.1, were obtained from 11 mm thick compression moulded plates via saw cutting and subsequent finishing with a milling machine; to evaluate the

thickness effect a set of 6 mm thick plates was also produced. Specimens were grooved with a V-profile on both sides in order to guide crack propagation in the notch plane. Notches were made via automated "chisel-wise" cutting, obtaining a final notch root radius lower than 10 μm. Blunt notched specimens were also produced with a circular profile blade with 1 mm radius; these specimens were used during constant load experiments described in the following.

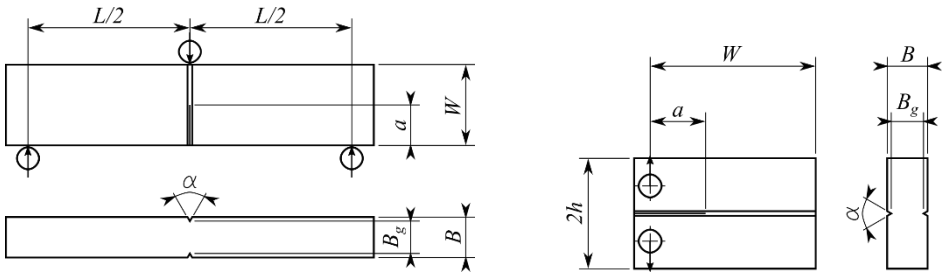

SENB (a)		DCB (b)	
W[mm]	22; 44	W[mm]	42-76
a/W	0.5	a/W	0.16-0.5
L [mm]	4 W	$2h$ [mm]	30
B[mm]	6; 11	B[mm]	11
B_g [mm]	0.8 B	B_g [mm]	0.8B
α	60°	α	60°

Figure 5.1 – (a) Single Edge Notched Bending and (b) Double Cantilever Beam specimens used for the study of the size effects.

Tests were performed using an Instron 1185R5800 electro-mechanical dynamometer (equipped with a 10 kN load cell) at 23°C and at a constant displacement rate of 10 mm/min, as prescribed in [166]. The specimen deflection was measured directly from the crosshead displacement and tests were video recorded using a 10 MPixel uEye UI 5490 SE camera to determine crack initiation by visual means. Nevertheless, the formation of rim films near the crack tip during SENB tests prevented in most cases a reliable determination of this point (see Figure 5.2); in those instances in which detection could be performed, crack initiation was found to occur very close to the maximum of the

load-time curve. The latter was therefore taken as a more objective criterion to identify crack initiation during SENB tests while for DCB tests no rim film was observed at the crack tip, allowing a visual determination of crack initiation.

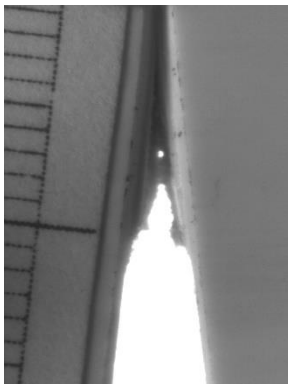

Figure 5.2 - Video frame recorded during a SENB test. The formation and evolution of the rim film prevents visual determination of crack length with sufficient accuracy.

For SENB samples tested in three-point bending configuration, the stress intensity factor K was calculated as reported in [131]:

$$K = Y\frac{P}{B_g\sqrt{W}} \tag{5.1}$$

where P is the load, W and B_g are the specimen width and the thickness of its grooved section, respectively, and Y is the shape factor for the considered test configuration:

$$Y = \frac{3\frac{L}{W}\sqrt{\frac{a}{W}}}{2\left(1+2\frac{a}{W}\right)\left(1-\frac{a}{W}\right)^{\frac{3}{2}}}\left\{1.99-\frac{a}{W}\left(1-\frac{a}{W}\right)\left[2.15-3.93\frac{a}{W}+2.7\left(\frac{a}{W}\right)^2\right]\right\} \tag{5.2}$$

in which L is the span between the lower pins and a is the crack length.

For DCB samples, instead, the Kanninen solution proposed in [167] was used for the evaluation of the stress intensity factor:

$$K = 2\sqrt{3}\frac{Pa}{B^* h^{3/2}}\left(1 + 0.64\frac{h}{a}\right) \tag{5.3}$$

in which B^* is the effective thickness that, in case of DCB samples, can be calculated using the formula proposed in [168]:

$$B^* = \sqrt{B \cdot B_g} \tag{5.4}$$

where B is the thickness of the specimen outside the grooved region. The effect of the ligament length $W - a$ and of the specimen thickness B on the fracture toughness K_{IC}, determined at crack initiation, is reported in Figure 5.3 and Figure 5.4 respectively.

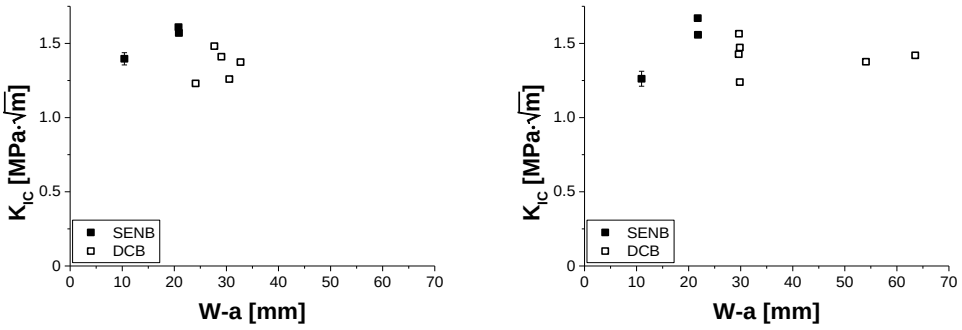

Figure 5.3 – Effect of ligament length on the fracture toughness of (a) HDPE-1 and (b) HDPE-2. For specimens having nominal dimensions of W = 22 mm ($W - a$= 11 mm), average values are reported with error bars representing standard deviation over at least 5 samples.

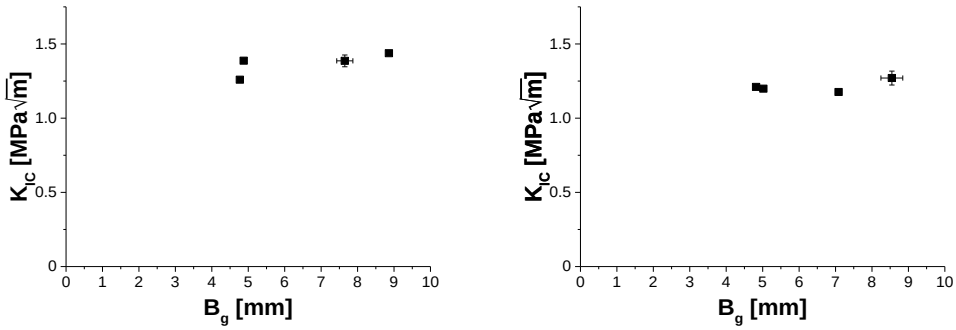

Figure 5.4 - Effect of specimen thickness on the fracture toughness of (a) HDPE-1 and (b) HDPE-2. For specimens having nominal B_g equal to 8.8, average values are reported with error bars representing standard deviation over at least 5 samples.

For both materials K_{IC} turned out to be independent of sample dimensions in the range of thickness and ligament length examined: SENB specimens with W= 22 mm, B= 11 mm, B_g= 0.8B and with an initial crack length a_0 = 11 mm were adopted to study the fracture and ESC behaviour under plane strain conditions. These samples were tested at five temperatures (23, 31, 40, 50 and 60°C) applying two different loading histories: constant displacement rate (from 0.001 up to 200 mm/min) and constant load at varying levels (creep) adopting three- and four-point bending configuration as shown in Figure 5.5. These two loading histories were applied using an Instron 1185R5800 dynamometer and dedicated custom-built creep machines, thus allowing the exploration of different time ranges (longer in the case of creep). As already pointed out in Chapter 2, previous works on polyethylene [74] and high impact polystyrene [22] demonstrated that results are independent on the applied loading history and test configuration, supporting this approach for the extension of the available experimental window.

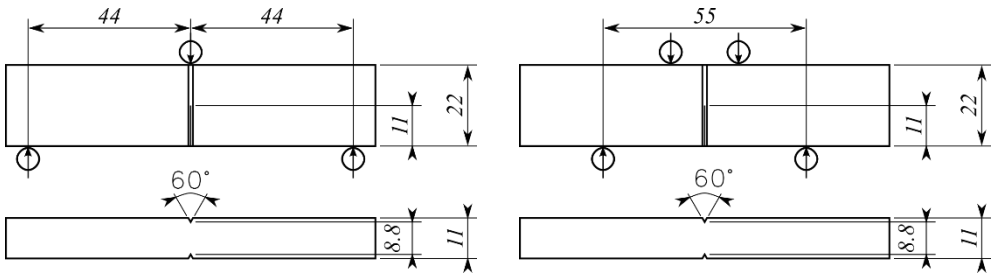

Figure 5.5 – Sample geometry for the evaluation of the fracture and ESC behaviour of the two HDPEs under plane strain conditions: (a) three-point bending (constant displacement rate) and (b) four-point bending (constant load).

In the creep machines the two lower pins are fixed and the load can be applied via the top ones which are connected to a pneumatic device able to release a dead weight in a controlled fashion within a few seconds. In this case specimen deflection at the load pins was measured by a Linear Variable Displacement Transducer (LVDT).

In accordance with [169], the stress intensity factor K was evaluated as:

$$K = Y\frac{PL\sqrt{\pi a}}{B^{*}W^{2}} \tag{5.5}$$

in which the shape factor Y is valid up to $\frac{a}{W} = 0.6$ and it can be expressed as:

$$Y = 1.12 - 1.39\left(\frac{a}{W}\right) + 7.32\left(\frac{a}{W}\right)^{2} - 13.1\left(\frac{a}{W}\right)^{3} + 14.0\left(\frac{a}{W}\right)^{4} \tag{5.6}$$

In this case, in accordance with [22], the effective thickness B^{*} was evaluated as:

$$B^{*} = B^{0.263}B_{g}^{0.737} \tag{5.7}$$

Visual observation of the specimens during the tests was not possible due to the design of these testing machines and consequently, a compliance calibration method was adopted to detect crack initiation and to obtain information regarding the crack growth rate. This method has been already used, for the four-point bending configuration, in [7, 22, 74] and it is based on the assumption

that an increase of the sample compliance C can be expressed in term of separate viscoelastic creep and crack growth contributions as shown in Figure 5.6.

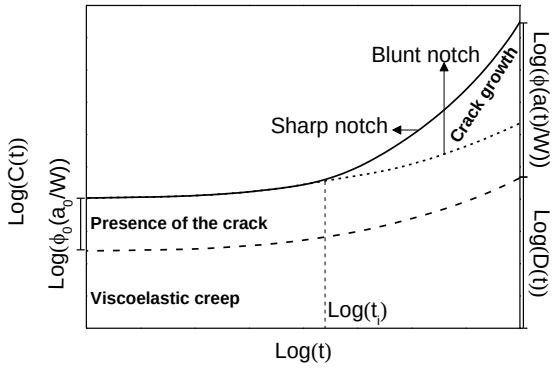

Figure 5.6 - Sample compliance during a creep test as sum of viscoelastic creep and crack growth contributions.

For the four-point bending configuration C can be defined as:

$$C\left(\frac{a}{W},t\right) = D(t)\frac{L}{BW}\left[\frac{15}{81}\left(\frac{L}{W}\right)^2 + \frac{3}{8}(2+\nu) + \frac{2\pi L}{W}\int_0^{a/W}\frac{a}{W}Y^2 d\left(\frac{a}{W}\right)\right] \tag{5.8}$$

where $D(t)$ and ν are the material creep compliance and the Poisson's ratio, respectively. Considering that, for a given specimen, the only two parameters varying during a test are $D(t)$ and $\frac{a}{W}$, Equation (5.8) can be rewritten as:

$$C\left(\frac{a}{W},t\right) = D(t)\phi\left(\frac{a}{W}\right) \tag{5.9}$$

in which $\phi\left(\frac{a}{W}\right)$ is a geometry calibration factor. Moreover, if a creep test is conducted on a sample having a blunt notch of length a_0, the crack would not initiate and the only quantity varying during the test would be the material creep compliance; Equation (5.9) would therefore assume the following form:

$$C_b\left(\frac{a_0}{W},t\right) = D(t)\phi_0\left(\frac{a_0}{W}\right) \tag{5.10}$$

Equations (5.9) and (5.10) can be combined to identify crack initiation:

$$\frac{C}{C_b} = \frac{\phi}{\phi_0} \tag{5.11}$$

Since for identical sharp and blunt notch length ϕ is equal to ϕ_0 (up to crack initiation) the ratio in Equation (5.11) is equal to 1 up to this point; afterwards it starts increasing because of crack growth. Crack initaition can be hence detected when $\frac{C}{C_b}$ exceeds a pre-set threshold value which in this work was set at 1.01. Furthermore, during the propagation phase the crack length can be calculated; combining Equations (5.8) and (5.11), it is possible to write:

$$\phi_0 \frac{C}{C_b} = \phi = \frac{L}{BW}\left[\frac{15}{81}\left(\frac{L}{W}\right)^2 + \frac{3}{8}(2+\nu) + \frac{2\pi L}{W}\int_0^{a/W} \frac{a}{W} Y^2 d\left(\frac{a}{W}\right)\right] \tag{5.12}$$

This operation was performed taking advantage of a purposedly made Matlab® script while the analitical derivation of the geometry calibration factor for the four-point bending configuration is reported in ANNEX A.1 .

The creep compliance of HDPE-1 at 40°C, measured from notched samples tested at different loads and therefore different initial stress intensity factor K_0, is reported in Figure 5.7; these value were computed both from a blunt notched sample and from sharp notched ones for which crack initiation had not taken place yet. Despite the nonlinear behaviour described in the previous Chapter, it is possible to observe that the various curves are practically coincident before crack initiation and consequently, for each temperature and material, a unique creep compliance curve was used to evaluate crack initiatiation and propagation using the equations aforementioned.

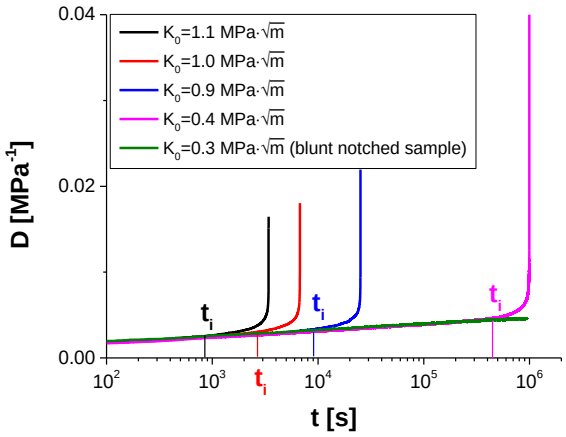

Figure 5.7 - Creep compliance of compression moulded HDPE-1 samples loaded at 40°C with different initial stress intensity factor K_0. For sharp notched samples after crack initiation t_i the curve contains the compliance contribution related to the crack growth and, consequently, they represent the creep compliance only before this point.

The crack initiation behaviour was characterized in term of $Log(K)$ vs. $Log(t_i)$ curves, t_i being the crack initiation time, while the propagation behaviour was expressed in terms of $Log(K)$ vs. $Log(\dot{a})$ curves in which $\dot{a}$ is the crack propagation speed. Due to high data scatter, which can be related to noise during the displacement measurement and during the evaluation of the numerical derivative of the crack length a, only average values for each specimen were considered for the propagation phase as shown in Figure 5.8.

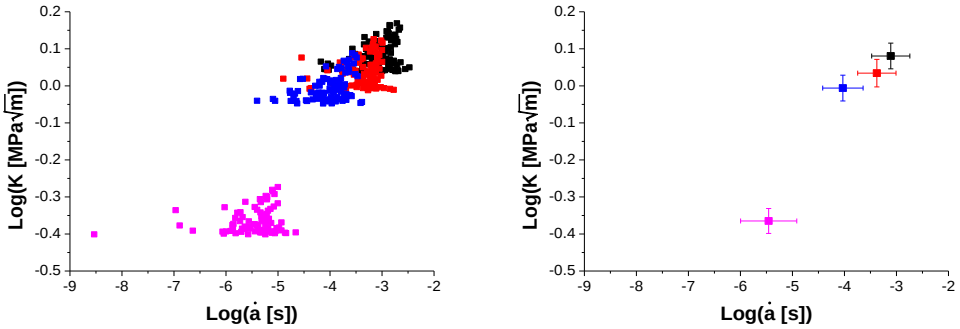

Figure 5.8 – $Log(K)$ vs. $Log(\dot{a})$ curves for HDPE-1 at 40°C. (a) instantaneous values; (b) average values.

The fracture behaviour of the two HDPEs was characterized also in terms of the energy release rate using $Log(G)$ vs. $Log(t_i)$ and $Log(G)$ vs. $Log(\dot{a})$ curves for crack initiation and propagation, as done for the stress intensity factor analysis. In particular, the energy release rate was evaluated as:

$$G = \frac{U}{BW} \cdot \frac{1}{\psi\left(\frac{a}{W}\right)} \tag{5.13}$$

in which U is the energy accumulated by the sample and $\psi\left(\frac{a}{W}\right)$ is the energy calibration factor for the considered test configuration (the notation $\phi\left(\frac{a}{W}\right)$ adopted in [92] is not applied in this work for the sake of clarity since this symbol already represents the geometry calibration factor introduced in Equation (5.9)). Due to the difficulties related to the identification of the initiation point during the three-point bending tests at constant displacement rate, the data obtained from this characterization were not considered for the determination of G since a small error in the crack initiation time would lead to a significant variation of this fracture parameter. For the four-point bending constant load tests, instead, U was evaluated as the product of the applied load P and of the sample displacement u. The energy calibration for the four-point bending configuration

was computed starting from the expression of the sample compliance of Equation (5.9) as shown in ANNEX A.2.

For both approaches (i.e. stress intensity factor and energy release rate) a time-temperature reduction scheme was applied to further extend the available experimental window. From the data obtained at the five different temperatures aforementioned (23, 31, 40, 50 and 60°C) the relevant shift factors were evaluated using the procedure already described for the relaxation modulus and the yield stress in Section 4.2 and the initiation and propagation master curves were built for the two materials.

5.2.2 Plane stress tests

To study the fracture behavior of the bottle of HDPE-1, tests were performed at 23°C on Single Edge Notched Tension samples obtained longitudinally and transversally with respect to the bottle symmetry axis and having the geometry shown in Figure 5.9. In this case the notch was introduced via razor blade sliding on the edge of the sample, using a die to guarantee the orthogonality between the notch and the edge. Since, as reported in Figure 5.10, no significant differences were observed in the behavior of the two kind of samples, it was confirmed that, as previously observed from the tensile test of Section 4.3.1, the material in the central region of the bottle is not oriented (or at least it is equally bi-oriented in the two considered directions). No further investigation was hence conducted on the orientation of the polymer in the bottle and the specimens were obtained longitudinally with respect to the symmetry axis, because in this direction a higher number of specimen per bottle could be obtained.

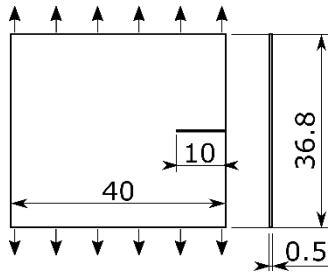

Figure 5.9 - Single Edge Notched Tension sample geometry. 36.8 mm corresponds to the effective height of the sample without considering the region in the grips.

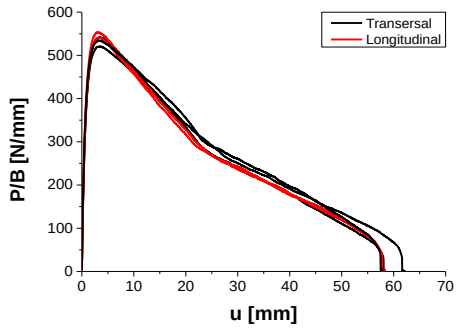

Figure 5.10 – Load/thickness vs. displacement curves obtained from SENT samples in longitudinal and transversal direction with respect to the bottle symmetry axis.

Moreover, to avoid sample rotations observed during preliminary SENT tests, a change of sample geometry was adopted and Double Edge Notched Tension (DENT) samples having the geometry shown in Figure 5.11 were obtained from the bottles and from 1 mm thick compression moulded plates of HDPE-1. Also in this case the notches were introduced via die-assisted razor blade sliding.

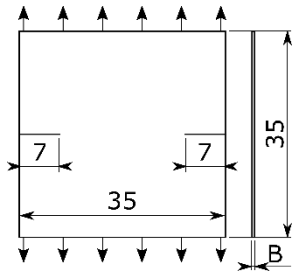

Figure 5.11 - Double Edge Notched Tension sample geometry. 35 mm corresponds to the effective height of the sample without considering the gripped region and B is the thickness, equal to 0.5 mm for the bottles and 1 mm for compression moulded plates.

Due to the reduced thickness of the considered samples, in this case the material was tested under plane stress conditions observing extensive plastic deformations in the ligament region, as shown in Figure 5.12. For this reason, a nonlinear elastic fracture mechanics approach, based on the *J*-integral, was considered more adequate to describe the fracture behaviour of the material in this stress state. Tests were conducted using an Instron 1185R5800 at various constant displacement rates at 60°C and a J vs. t_i curve was built for these test conditions; the propagation behaviour was not considered.

Figure 5.12 - Plastic zone ahead of the crack tips during a test on 0.5 mm thick DENT sample obtained from a bottle.

The J-integral was evaluated as:

$$J = J_{el} + J_{pl} = \eta_{el} \frac{U_{el}}{B(W-a)} + \eta_{pl} \frac{U_{pl}}{B(W-a)} \tag{5.14}$$

in which B is the thickness, $W - a$ is the ligament length, U_{el} and U_{pl} are the elastic and plastic components of the total energy absorbed by the specimen and η_{el} and η_{pl} are the elastic and plastic shape factors. The elastic and plastic components of the total energy were evaluated integrating up to crack initiation the area under the load vs. elastic displacement (P vs. u_{el}) and the load vs. plastic displacement (P vs. u_{pl}), respectively. To build these curves from load vs. displacement data, the measured displacement u was taken as the sum of a plastic component u_{pl} and of an elastic component u_{el}; the latter was evaluated according to Equation (5.15):

$$u_{el} = P \cdot C_0 \tag{5.15}$$

where C_0 is the initial compliance of the specimen, evaluated directly from the load displacement curve.

The elastic and plastic shape factors η_{el} and η_{pl} were determined with a numerical and experimental analysis, respectively. Starting from the elastic shape factor a finite element model of the DENT sample was implemented in Abaqus® and the compliance of the sample for different crack lengths was determined; this procedure allowed the evaluation of the energy calibration factor ψ for the considered configuration, as reported in Figure 5.13. In the case of a linear elastic material J-integral and the energy release rate are equivalent and thus:

$$J_{el} = G = \frac{U_{el}}{BW\psi} = \frac{(W-a)}{W\psi} \cdot \frac{U_{el}}{B(W-a)} = \frac{1-\frac{a}{W}}{\psi} \cdot \frac{U_{el}}{B(W-a)} \tag{5.16}$$

which, if compared with Equation (5.14) allows to define η_{el} as:

$$\eta_{el} = \frac{1 - \frac{a}{W}}{\psi} \tag{5.17}$$

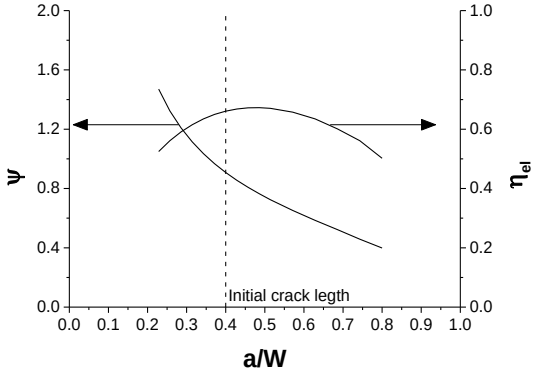

Figure 5.13 - Energy calibration factor ψ and elastic shape factor η_{el} for DENT.

To evaluate the plastic shape factor η_{pl}, instead, the method based on the load separation criterion proposed by Sharobeam and Landes in [138] and described in Section 2.5.3 was adopted. Tests at a constant displacement rate of 10 mm/min and at 60°C were performed on blunt notched DENT specimens having different ligament lengths; as mentioned in the previous Section (for SENB specimens) blunt notches were introduced with a circular profile blade having 1 mm radius. Since the considered samples had not exactly the same thickness, the load was normalized for the thickness itself and the normalized load vs. plastic displacement curve was built as shown in Figure 5.14 (a). Starting from this curve the separation parameter was evaluated taking into account the normalization made for the thickness:

$$\left.\frac{P(a_i)/B_i}{P(a_j)/B_j}\right|_{u_{pl}} = S_{i,j} \cdot \frac{B_j}{B_i} \tag{5.18}$$

As can be observed in Figure 5.14, in which the sample with ligament length equal to 25 mm was considered as the reference one to compute the normalized separation parameter, an extended unseparable region is present with variable $S_{i,j}$. This is probably related to the slightly different behaviour displayed by the samples before complete ligament yielding which, moreover, is reached at different plastic displacements. This fact can be observed from the position of the change of the slope after the maximum of the load vs. plastic displacement curves of Figure 5.14; due to this fact the application of Equation (5.18) gives peculiar "fin" shape. Beyond this unseparable region, however, a constant normalized separation parameter can be clearly observed and the value of this factor obtained from the various curves were used to evaluate η_{pl}.

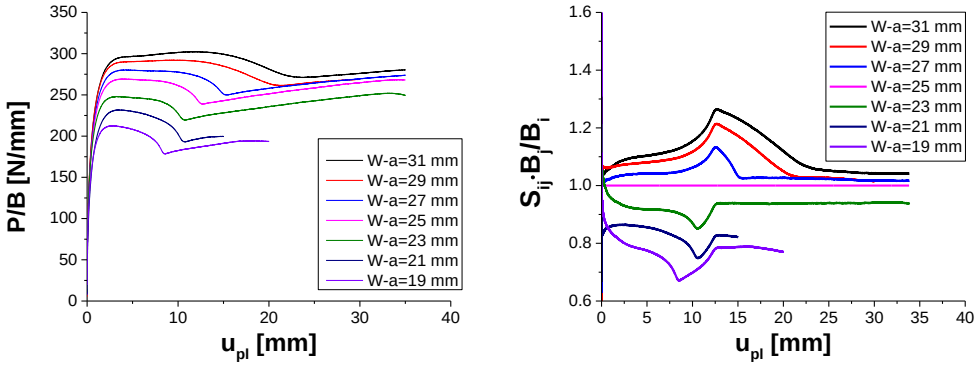

Figure 5.14 – (a) normalized load vs. plastic displacement curves for blunt notched DENT samples with different ligament length; (b) relevant normalized separation parameter vs. plastic displacement curves.

If the value of $S_{i,j} \cdot \frac{B_j}{B_i}$ is expressed as a function of the ligament length to specimen width ratio and logarithmic scales are adopted, as shown in Figure 5.15, it is possible to observe that a power law gives a good approximation of the obtained data and, consequently, the plastic shape factor can be determined directly from the slope of the fitted curve. The separation parameter was

evaluated taking also different samples as reference and η_{pl} was evaluated as the average of the slopes of the obtained $S_{i,j} \cdot \frac{B_j}{B_i}$ vs. $\frac{W-a}{W}$ curves, equal to 0.680 ±0.091.

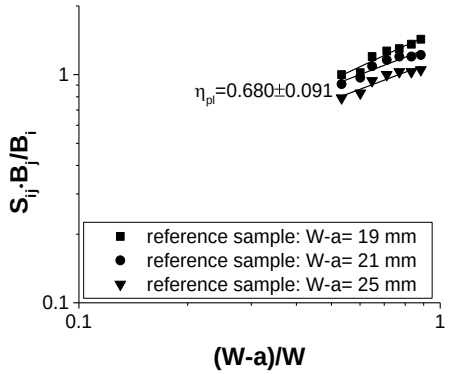

Figure 5.15 - Normalized separation parameter vs. ligament to width ratio curves.

As previously mentioned, only the initiation behaviour of blow and compression moulded HDPE-1 was evaluated in this part of the work. Due to extensive crack tip blunting, however, the detection of crack initiatin by visual means would have introduced an extremely high uncertainty on the analysis. Therefore, an alternative method had to be considered to determine t_i and hence the relevant value of J. A first attempt was conducted with the load separation criterion already considered for the determination of η_{pl}. Even if, in accordance with [139], the crack initiation time could be determined, for most of the tested samples, from the plastic displacement at which the separation parameter starts to decrease after the separable region, this method appeared to be inadequate for the determination of a well defined J vs. t_i curve. As can be observed in Figure 5.16, in fact, if two different blunt notched samples are used for the evaluation of the separation parameter of the same sharp notched specimen, considerably different results in term of crack initiation time, and therefore in term of nonlinear energy release rate, can be obtained; this fact introduces an

excessive degree of uncertainty. Considering that tests at several constant displacement rate had to be performed to define the relationship between J and t_i, it turned out that, to obtain a reduced scatter of the data and therefore to properly define the initiation behaviour under plane stress conditions, a different method had to be considered to identify crack initiation time.

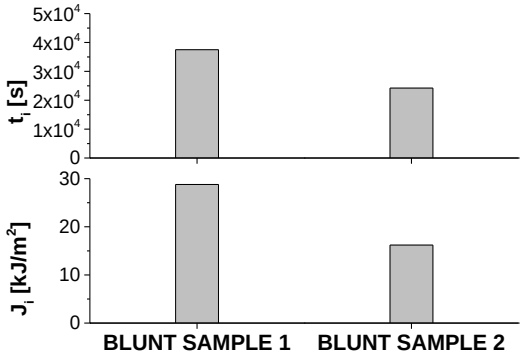

Figure 5.16 – Crack initiation time and relevant nonlinear energy release rate of a blow moulded HDPE-1 sample determined with the load separation criterion using two different blunt notched samples as reference for the separation parameter.

Most of the tests were hence video recorded with a 10 MPixel uEye UI 5490 SE camera and, for each frame of the video, the ligament length was measured using the ImageJ® macro already adopted for the determination of the strains during the tensile tests. The ligament length was hence represented as a function of time as shown in Figure 5.17 and it was observed that, as expected, in the first part of the curve the apparent ligament length decreases with a moderate rate due to crack tip blunting; during propagation the rate was considerably higher. The first part of the curve was extrapolated to the whole timescale of the test and the ratio between the experimental data and this blunting line was evaluated: crack initiation was considered to occur when the value of this parameter reached 0.99 (i.e. when a difference of 1% was present between the experimental

data and the blunting line). Even if this value was defined quite arbitrarily, this approach gives reasonable results in term of energy release rate for all the video recorded samples and reduces data scatter; this method was thus adopted to study the initiation behaviour under plane stress conditions.

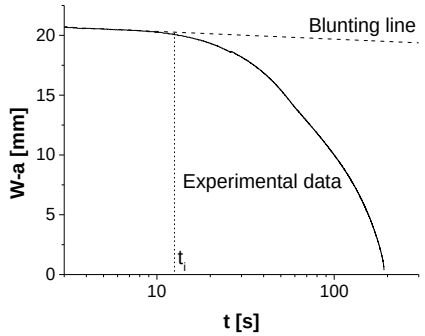

Figure 5.17 - Example of ligament length vs. time curve for a DENT sample.

Considering the results obtained from all the video recorded tests, moreover, it was observed that, as reported in Figure 5.18, crack initiation occurred always at a load P_i close to the 90% of the maximum load P_{max} for blow moulded samples and at about the 96% of P_{max} for compression moulded ones, irrespectively of the displacement rate applied during the tests. These values were considered as an alternative initiation criterion for some of the inital tests during which videos had not been recorded.

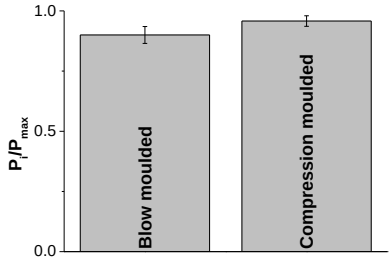

Figure 5.18 - Ratio between the load at initiation and the maximum load measured during tests on sharp notched DENT samples.
The reported values are an average of at least 6 samples.

5.3 Results and discussion

5.3.1 Plane strain behaviour

5.3.1.1 Stress intensity factor approach

Figure 5.19 and Figure 5.20 show the results obtained from the analysis of crack initiation at the various considered temperatures for compression moulded HDPE-1 and HDPE-2 respectively.

It can be seen that data obtained from constant displacement rate and creep tests fall on a single curve, indicating that the $Log(K)$ vs. $Log(t_i)$ correlation does not depend on the loading history as previously reported in [22, 74] and further confirming that the different loading histories can be used to extend the available experimental window. For all the temperatures and for both materials the data follow a power law and crack initiates at longer times for decreasing values of the stress intensity factor. As expected, for a given value of the stress intensity factor the initiation time decreases with increasing temperature while the slope of the various curves can be considered practically independent of the temperature itself. Moreover, in the curve at 23°C of HDPE-1 and in those at 23°C, 40°C and 60°C of HDPE-2 a pronounced change of the slope is visible at a value of K of about 2.5 MPa·m$^{1/2}$ for HDPE-1 and of about 2 MPa·m$^{1/2}$ for HDPE-2

(corresponding to $Log(K)$ equal to 0.4 and 0.3 respectively). As shown in Figure 5.21, this variation can be related to a ductile to brittle transition typical of polyolefines and specifically of polyethylene as reported , for example, in [43, 46, 100, 132, 170].

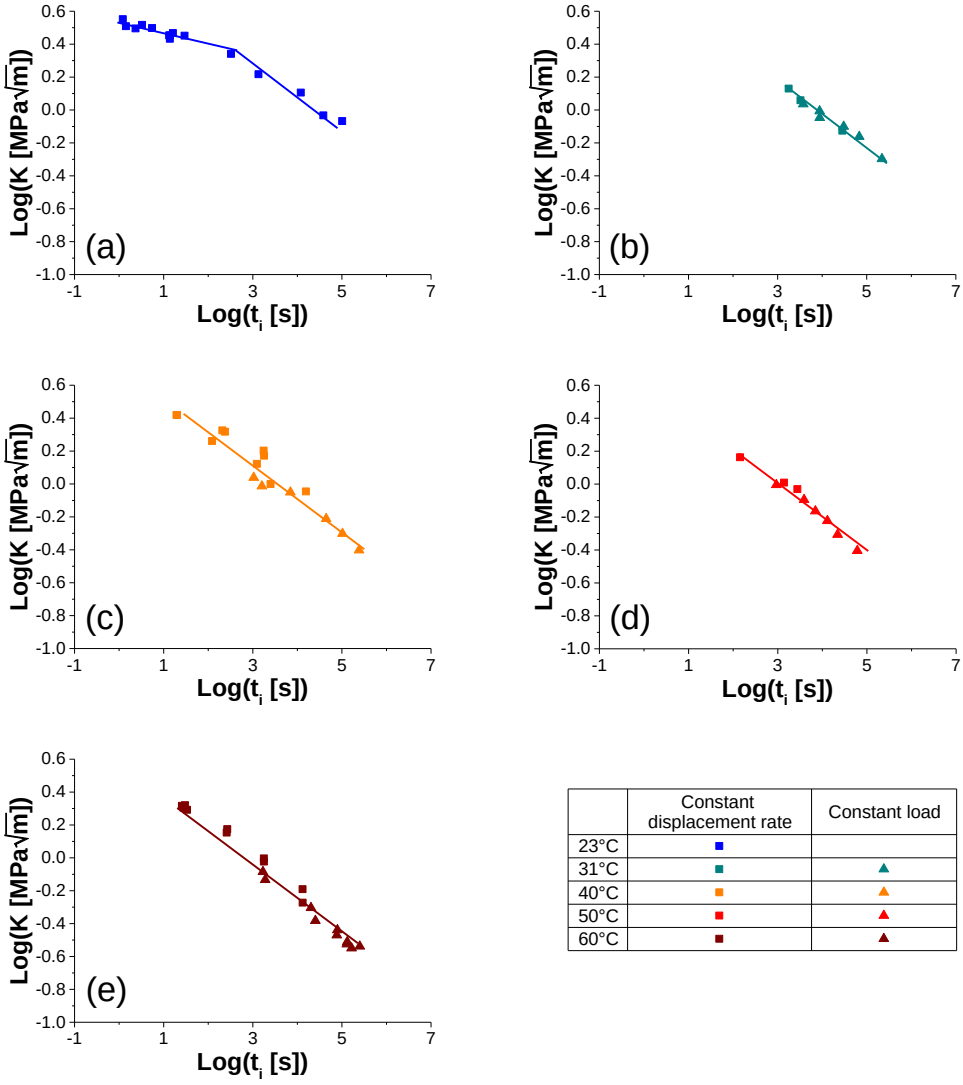

Figure 5.19 - $Log(K)$ vs. $Log(t_i)$ curves of HDPE-1.
(a) 23°C; (b) 31°C; (c) 40°C; (d) 50°C; (e) 60°C.

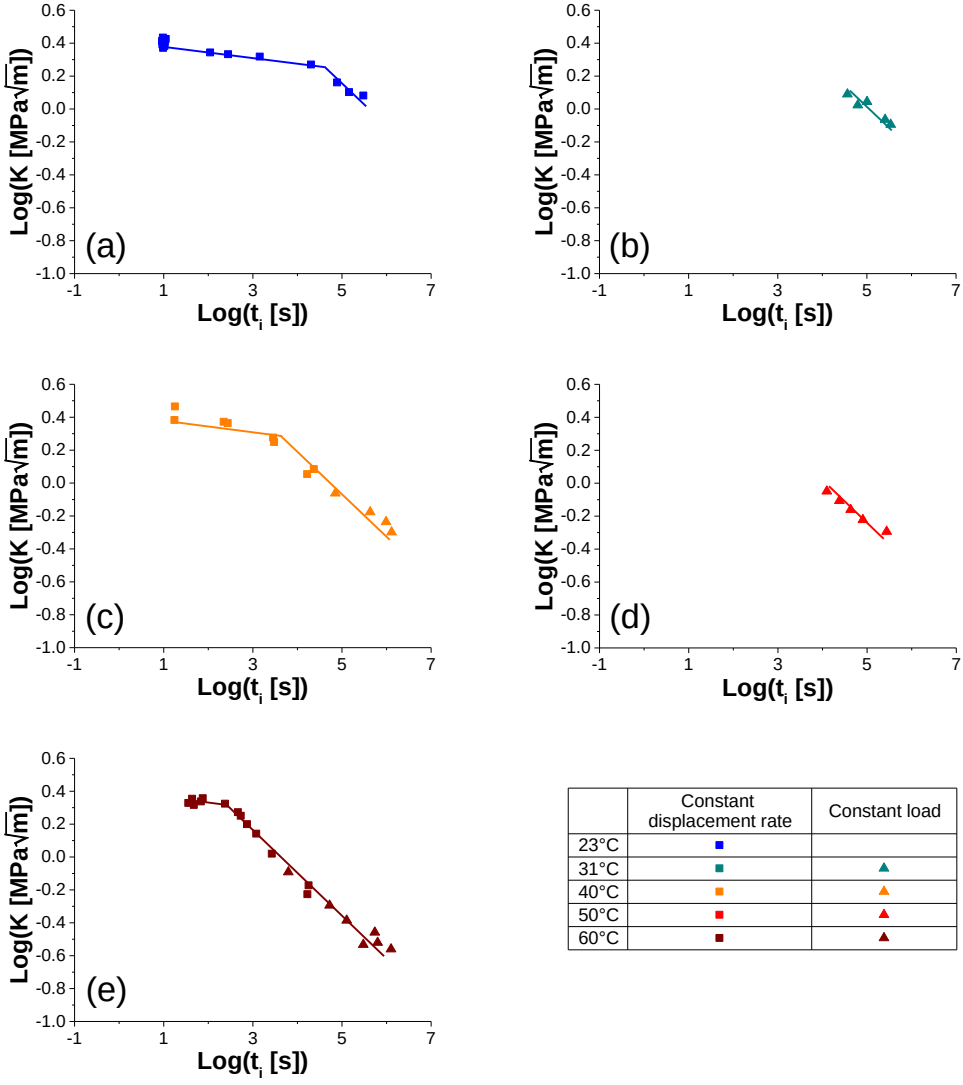

Figure 5.20 - $Log(K)$ vs. $Log(t_i)$ curves of HDPE-2.
(a) 23°C; (b) 31°C; (c) 40°C; (d) 50°C; (e) 60°C.

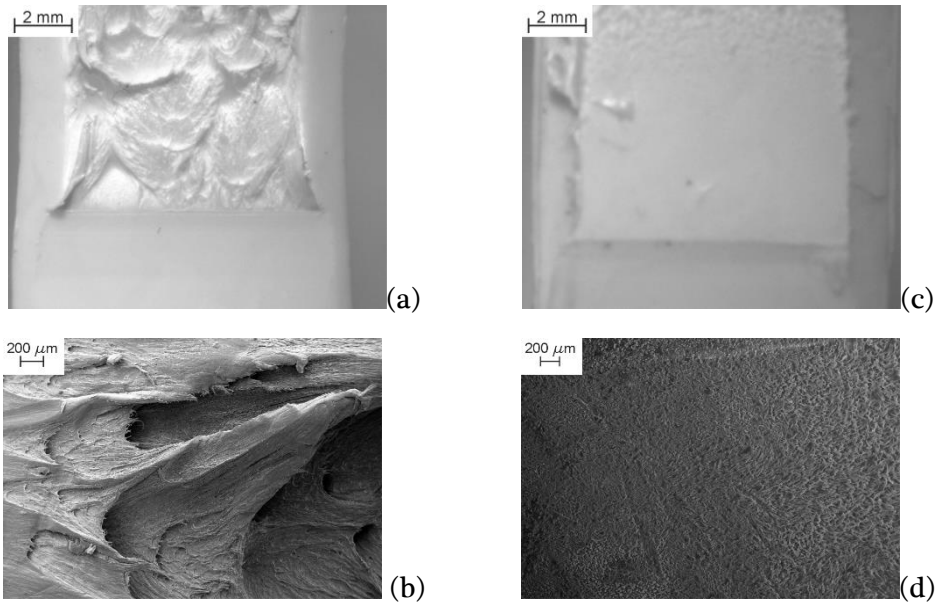

Figure 5.21 – (a) optical and (b) scanning electron micrograph of HDPE-2 tested at 60°C in the region of stress intensity factor above 2 MPa·m$^{1/2}$.
(c) optical and (d) scanning electron micrograph of HDPE-2 tested at 60°C in the region of stress intensity factor below 2 MPa·m$^{1/2}$

The propagation behaviour, expressed in terms of $Log(K)$ vs. $Log(\dot{a})$ curves is reported in Figure 5.22 and Figure 5.23 for HDPE-1 and HDPE-2 respectively. As reported in Section 5.2.1, propagation data were obtained only from the constant load tests. Due to this fact, data at 23°C are not available since no test was conducted at this temperature (due to the excessive time required for its completion) and the ductile to brittle transition cannot be identified from these graphs since the stress intensity factor level at which this transition occurs for the two materials cannot be reached with the constant load machines used for this work. Nevertheless, it can be observed that the obtained data follow a power law, with crack propagation rate increasing with K and that, for a certain value of this fracture parameter, an increase of the temperature causes an increase of

the propagation rate. Finally, as already noticed for the initiation behaviour, the slope of the curves does not depend on the test temperature.

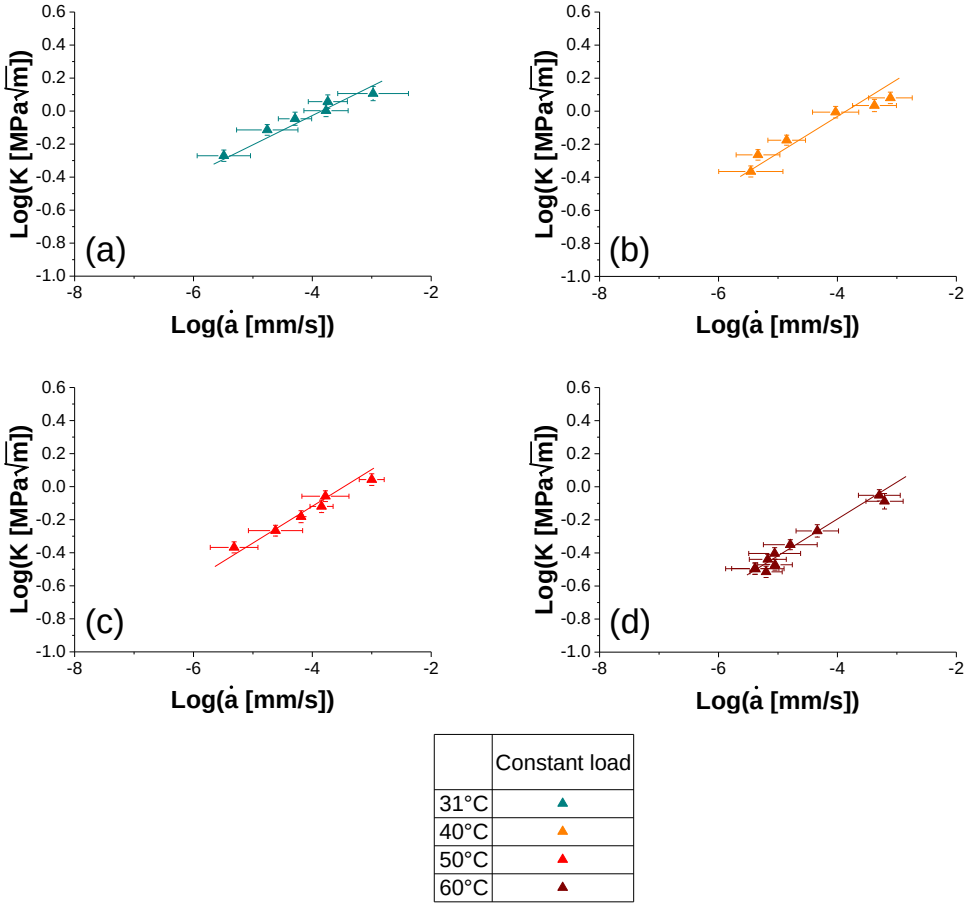

Figure 5.22 - $Log(K)$ vs. $Log(\dot{a})$ of HDPE-1.
(a) 31°C; (b) 40°C; (c) 50°C; (d) 60°C.

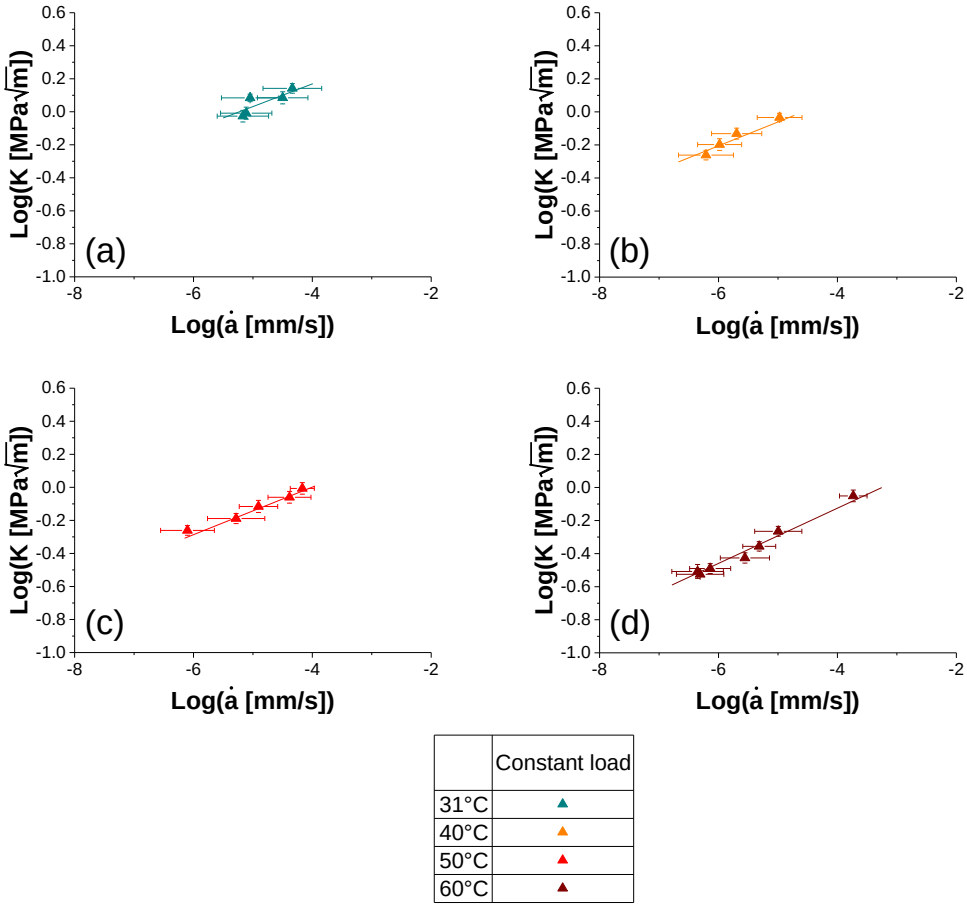

Figure 5.23 - $Log(K)$ vs. $Log(\dot{a})$ curves of HDPE-2.
(a) 31°C; (b) 40°C; (c) 50°C; (d) 60°C.

For each material, taking into account the typical experimental error of fracture tests, the shape of the initiation and propagation curves and the stress intensity factor level at which the ductile to brittle transition occurs at the various temperatures are practically coincident, meaning that a time temperature superposition reduction scheme can be applied to extend the available experimental window. The procedure described in Section 4.2 was hence applied

to identify the shift factors for both propagation and initiation. In the latter case the slope of the brittle branch was considered to evaluate $Log\left(a_T^{60°C}\right)$.

The shift factors for the two materials, evaluated considering the temperature of 60°C as the reference one, are reported in Figure 5.24, where they can be seen to follow an Arrhenius law. While shift factors for the two polymers differ slightly, for each one the shift factors obtained separately on the initiation and propagation curves show a good agreement, within the uncertainty related to their evaluation.

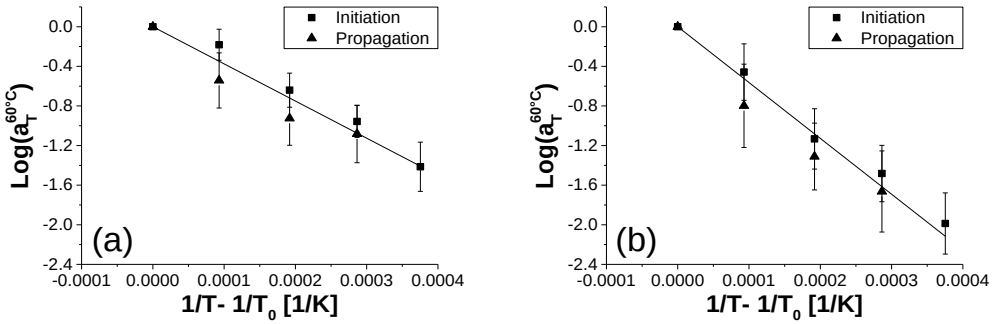

Figure 5.24 –Shift factors for (a) HDPE-1 and (b) HDPE-2. Reference temperature: 60°C.

Averaged shift factors were hence used to build the initiation and propagation master curves reported in Figure 5.25 for the temperature of 23°C and the fracture behaviour of the two polyethylenes was thus compared.

The two initiation master curves have essentially the same shape, characterized by identical slopes in the two branches and the ductile to brittle transition occurs at longer times for HDPE-2. This result can be explained considering that HDPE-2 possesses a significantly larger fraction of long polymeric chains. As reported in [43], in fact, the brittle failure of a semicrystalline polymer is related to fracture of the tie-molecules, connecting the various crystallites. In the brittle

failure region tie-molecules have enough time to untangle while relaxing and they can reach their full extension before failure. In the case of HDPE-2, a longer time is required for this phenomenon to occur because of the high length tail in the molecular weight distribution. At higher stress, instead, fracture occurs before tie molecules can disentangle; since at the time of failure a great number of them are still acting as a bridge between the crystalline domains, the lamellae break up in "mosaic blocks" generating the typical rough fracture surface observed for ductile failure. In this regime, the difference in MWD does not play an important role and the response is governed by the crystalline phase, whose fraction is approximately the same for the two material as reported in Chapter 3.

On the other hand, considering the propagation behaviour it is possible to observe that the slope of the curves obtained for the two materials is again approximately the same. In this case, due to the high length tail in the molecular weight distribution of HDPE-2, the curve representing the behaviour of this material is shifted towards lower propagation rates.

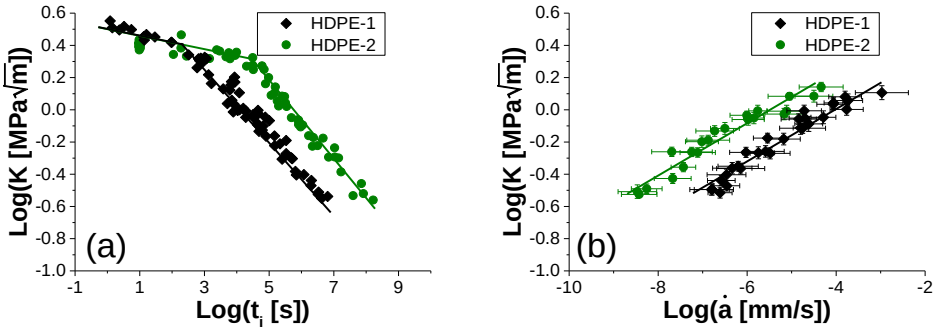

Figure 5.25 - (a) initiation and (b) propagation master curves at 23°C for the two materials.

5.3.1.2 Energy release rate approach

The initiation and propagation behaviour of HDPE-1 and HDPE-2 obtained from the elaboration of the creep data according to the energy release rate approach described in Section 5.2.1 is reported for the four considered temperatures (31°C, 40°C 50°C and 60°C) from Figure 5.26 to Figure 5.29 in terms of Log(G) vs. Log(t_i) and Log(G) vs. Log($\dot{a}$) curves. Of course, as already observed from the stress intensity factor analysis, the crack initiation time increases decreasing the value of G or decreasing the temperature while the opposite is true for the crack growth rate.

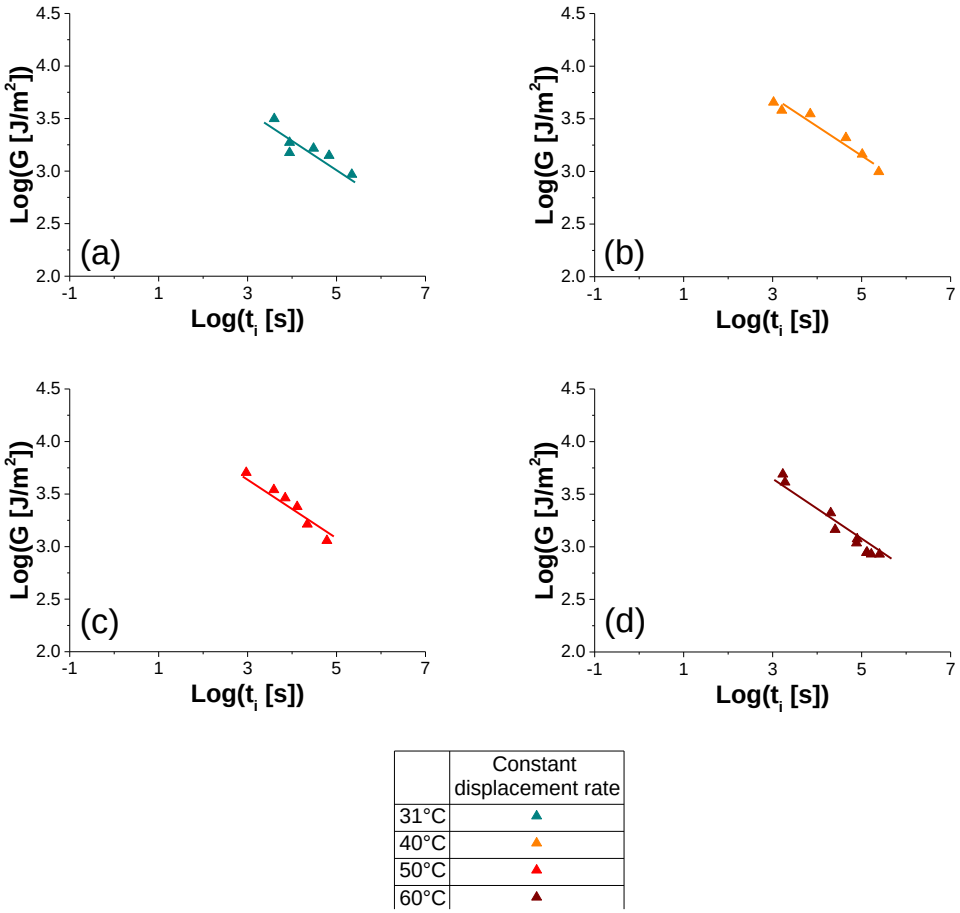

Figure 5.26 - Log(G) vs. Log(t_i) of HDPE-1. (a) 31°C; (b) 40°C; (c) 50°C; (d) 60°C.

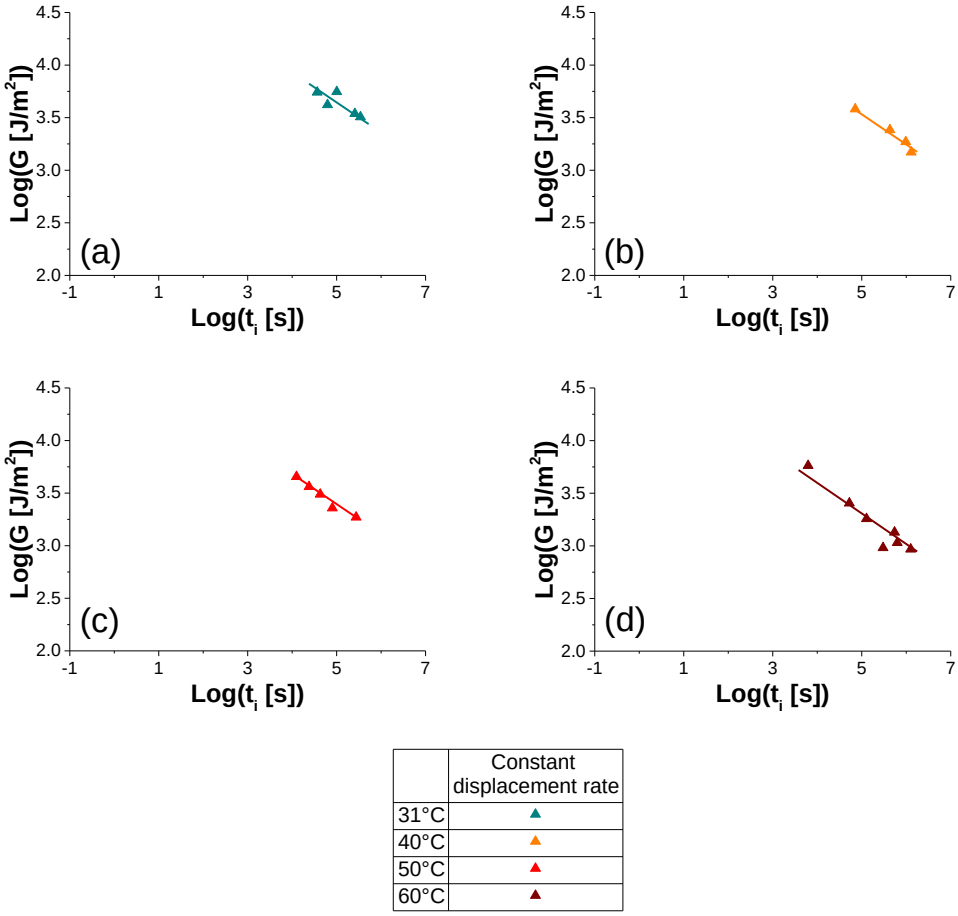

Figure 5.27 - $Log(G)$ vs. $Log(t_i)$ of HDPE-2. (a) 31°C; (b) 40°C; (c) 50°C; (d) 60°C.

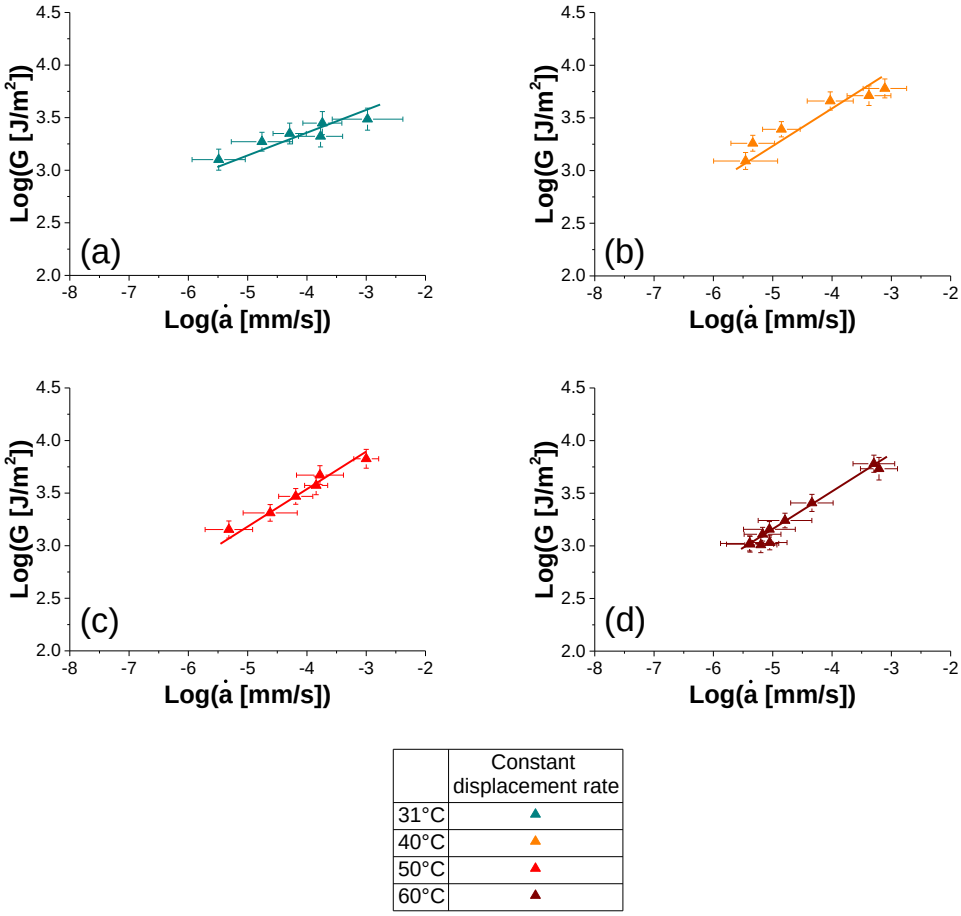

Figure 5.28 - $Log(G)$ vs. $Log(\dot{a})$ of HDPE-1. (a) 31°C; (b) 40°C; (c) 50°C; (d) 60°C.

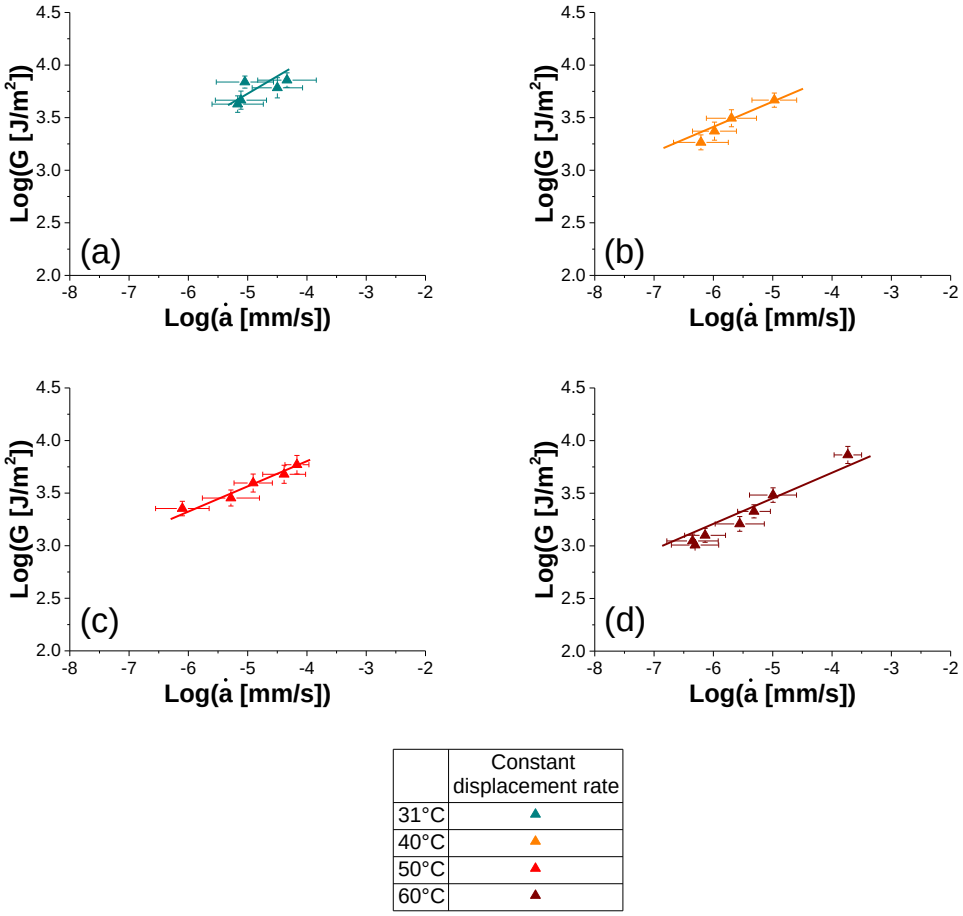

Figure 5.29 - $Log(G)$ vs. $Log(\dot{a})$ of HDPE-2. (a) 31°C; (b) 40°C; (c) 50°C; (d) 60°C.

As can be observed from the previous graphs, with the exception of the data at 31°C for which a different slope was measured, all the other obtained curves can be overlapped with a simple horizontal translation meaning that the equivalence condition required for the applicability of the time temperature superposition principle seems to be fulfilled also in this case. The discrepancy of the data obtained at 31°C may be related to a different procedure for the calibration of the LVDT, which had been used only for this data: this fact could have introduced an error in the determination of the sample displacement during the test. This

procedure is more critical for the energy based approach since, as mentioned in Section 5.2 a wrong estimation of the initiation point (and of the crack length for the propagation behaviour) would introduce a significant error in the evaluation of G but only limited variations in the case of K. Due to this fact the data obtained at this temperature were not considered for further analyses.

The shift factors shown in Figure 5.30, required to overlap the various curves, were evaluated considering 60°C as the reference temperature. Comparing these results with those obtained from the analysis done in Section 5.3.1.1, it is possible to observe that different trends can be defined between the two series of data while also in this case only minor differences can be observed between the shift factor evaluated from the initiation and the propagation data. In considering this difference, however, it has to be considered that the number of data available from the analysis of G is considerably lower than those available from the stress intensity factor and, therefore, a higher level of uncertainty is present in the determination of the slope of the Log(G) vs. Log(t_i) and of the Log(G) vs. Log(ȧ) curves, as revealed by the larger error bars.

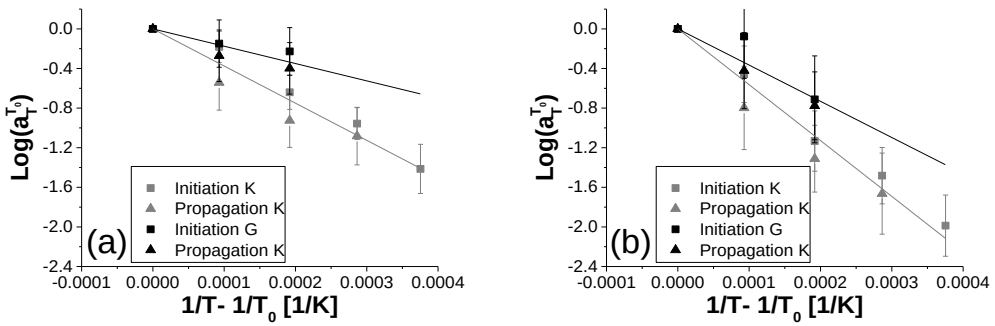

Figure 5.30 - Shift factors for (a) HDPE-1 and (b) HDPE-2. Reference temperature: 60°C.

Using an average shift factor calculated from the initiation and propagation ones, the master curves of Figure 5.31 were built at the temperature of 23°C; obviously, the comparison of the two materials gives the same information deduced from the stress intensity factor analysis of the previous Section (see Figure 5.25). Due to all the uncertainty related to the determination of G and its relevant shift factors it has to be noticed that these master curves are less accurate than K-based ones.

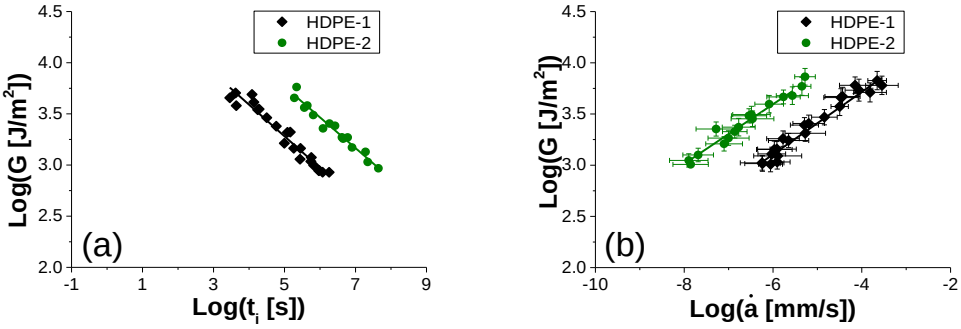

Figure 5.31 - (a) initiation and (b) propagation master curves at 23°C for the two materials.

Since, as clearly demonstrated in Section 4.3.2, HDPE exhibits nonlinear behaviour even for very low strain levels, a theory based on the linear viscoelasticity as the one proposed by Williams in [92] is not suitable to describe the fracture behaviour of this material.

On the other hand, considering the so called pseudo-elastic approach, the energy release rate and the stress intensity factor are linked, for a linear elastic material, with the following equation:

$$G = \frac{K^2(1-\nu^2)}{E(t)} \tag{5.19}$$

in which $E(t)$ is the relaxation modulus at a relevant time t. If Equation 5.19 holds it could be used to evaluate one of the two fracture parameters starting from the other. Nevertheless, for a nonlinear material the dependence of the relaxation modulus on the strain level has to be somehow considered.

To further develop this point, an effective relaxation modulus was evaluated using Equation (5.19). For each sample, two pairs of K and G values were used, one at fracture initiation, in which the time was the initiation time, and one for crack growth, in which an average time during propagation was considered.

Figure 5.32 shows the results obtained, at 40, 50 and 60°C, for HDPE-1 and HDPE-2. It can be noticed that, irrespectively from the fracture phase, at each single temperature all the obtained data seem to fall on the same curve which can be compared against the relevant relaxation modulus at the strains reached during the fracture process.

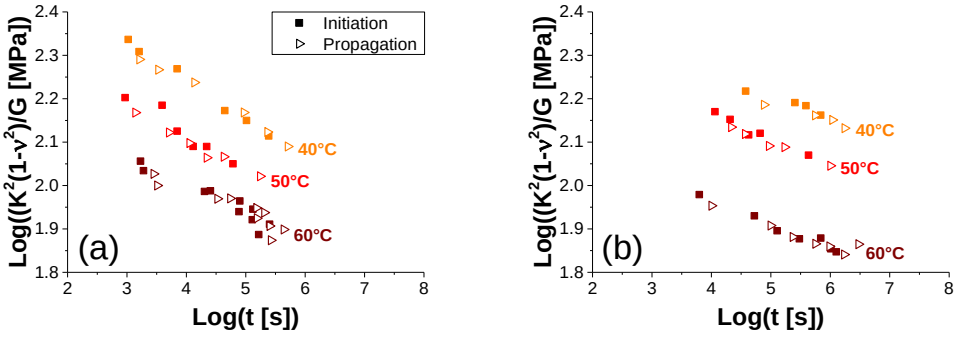

Figure 5.32 - Effective moduli of (a) HDPE-1 and (b) HDPE-2.

Since the strain field around the crack tip was not measured during the tests, beam theory was used to estimate it. The maximum strain of a beam in four-point bending configuration can be evaluated as:

$$\varepsilon = 4.36 \cdot u \cdot \frac{H}{L^2} \tag{5.20}$$

where H is the specimen width, L is the span length and u is the measured mid-span displacement. To take into account the presence of the initial defect, H was taken equal to the ligament length $W - a$, making possible the evaluation of the local strain close to the crack tip. For each sample the strain at initiation (a/W=0.5) and at the end of the analysed propagation phase (a/W=0.6) were computed; for each temperature the lower and the higher strains, ε_{min}^{T} and ε_{max}^{T} respectively, were considered as reference values. The values obtained are reported in Table 5.1. Since the maximum and minimum load applied at the different temperatures, to which the mid-span deflections are intrinsically linked to, were not the same in all cases, a direct comparison of the results for the different temperatures cannot be made. Comparing these values and the results shown in Section 4.3.2, it is possible to observe that, even at the lower strain evaluated with this procedure, the material behavior is nonlinear.

Table 5.1 – Maximum and minimum value of the strain during fracture tests evaluated as per Equation (5.20).

T [°C]	HDPE-1		HDPE-2	
	ε_{min}^{T}	ε_{max}^{T}	ε_{min}^{T}	ε_{max}^{T}
40	0.007	0.021	0.008	0.019
50	0.008	0.03	0.008	0.026
60	0.005	0.034	0.006	0.042

These are the limiting values of strain to which any given group of samples is subjected to during the fracture tests. The relevant relaxation modulus, after being shifted to the temperature of interest (see Section 4.3.2), was compared with the effective relaxation modulus from Equation (5.19) as shown in Figure 5.33 and Figure 5.34 for HDPE-1 and HDPE-2, respectively. From these graphs, it is possible to observe that, for both materials and at any temperature, the values derived from fracture tests lie between those of the relaxation

modulus at the limiting maximum and minimum strain. The slopes of these two relaxation moduli were compared with that of the effective modulus curve: the fair agreement found suggests that the latter represents the relaxation modulus curve at an effective strain level which is relevant for the fracture process. This strain level seems to be the same for all the tested specimens, irrespective of the applied stress intensity factor: this result is in agreement with the unique creep compliance curve previously found and shown in Figure 5.7. Therefore if the effective strain during a fracture test is known, Equation (5.19) could be used to evaluate G from K or vice versa.

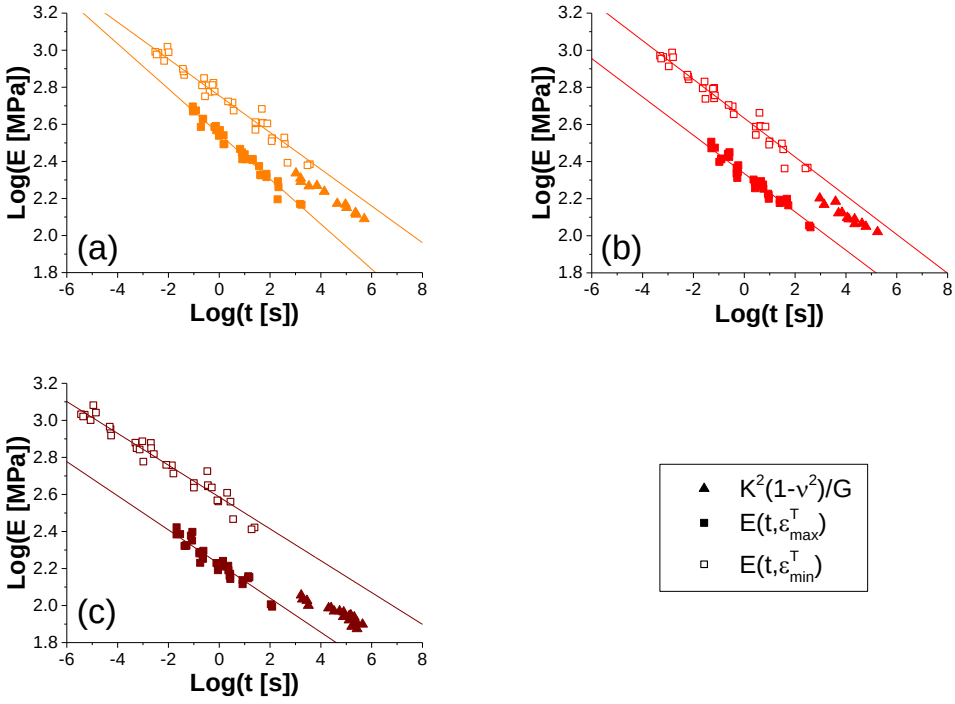

Figure 5.33 –Comparison between the effective relaxation modulus and the relaxation modulus at the maximum and minimum strain evaluated as per Equation (5.20) for HDPE-1. (a) 40°C; (b) 50°C; (c) 60°C.

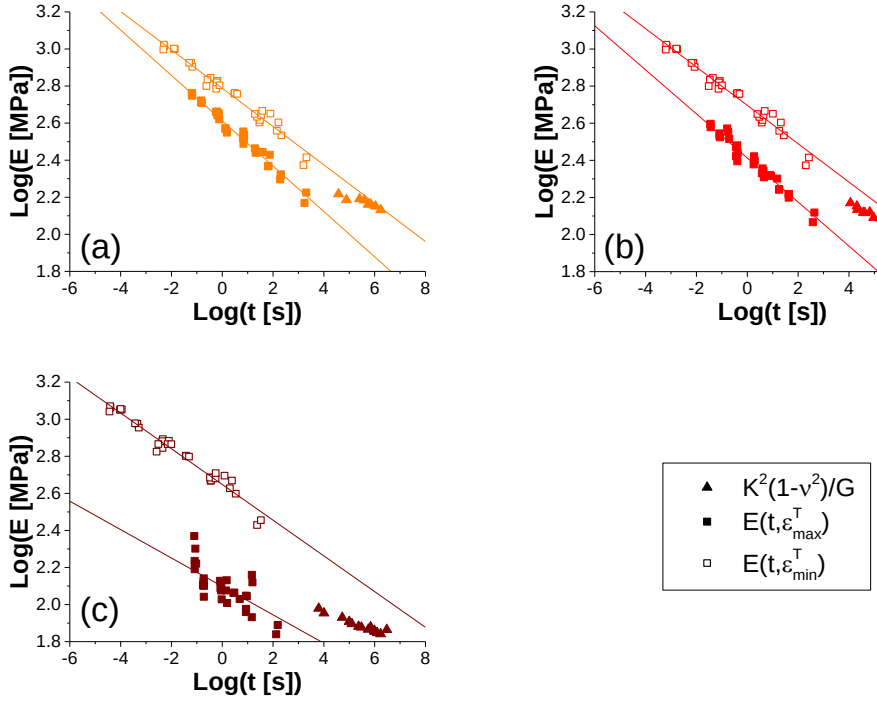

Figure 5.34 - Comparison between the effective relaxation modulus and the relaxation modulus at the maximum and minimum strain evaluated as per Equation (5.20) for HDPE-2. (a) 40°C; (b) 50°C; (c) 60°C.

5.3.2 Plane stress behaviour

The effect of stress state on the initiation behaviour of compression moulded HDPE-1 is shown in Figure 5.35: in this graph the results of the tests on DENT samples are presented together with the G master curve under plane strain condition at the temperature of 60°C. For the latter, in particular, the assumption $J = G$ was used since, as discussed in the previous Section, the LEFM theory is considered to be valid and, therefore, the equivalence of the two fracture parameters should hold true. Also in the case of plane stress condition a power law correlation between the nonlinear energy release rate and the crack initiation time gives a good description of the obtained data. However, the slope

of this curve is considerably lower with respect to the one describing the plane strain behaviour, highlighting a lower rate sensitivity of the thin samples. These different slopes could be related to the deformational behaviour of the material in the different stress states. As described in Section 5.2.2, in fact, extensive plastic deformations occur highlighting the ductile behaviour of the material during the tests under plane stress conditions. In this case a lower slope of the initiation curve can be expected as already observed considering the differences between the ductile and brittle branches of the *K*-based initiation curve. On the other hand, data used for the G-based initiation master curve represents only the brittle branch of the initiation curves were a higher slope is expected.

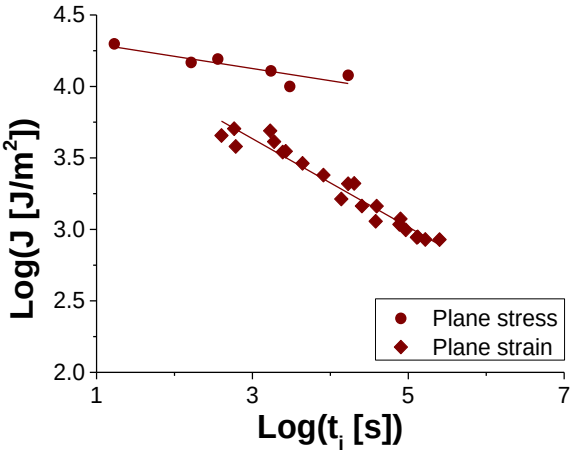

Figure 5.35 – Effect of stress state on the initiation behaviour at 60°C of compression moulded HDPE-1.

The effect of the production process was evaluated as well. Observing Figure 5.36 is it possible to see that the curve obtained from the specimen produced via compression moulding lies at a higher value of nonlinear energy release rate with respect to the one representing the behaviour of the bottles produced via extrusion blow moulding. This fact is of course related to the higher degree of

crystallinity of the compression moulded material which, as already observed for tensile properties, causes an increase in the mechanical properties in air.

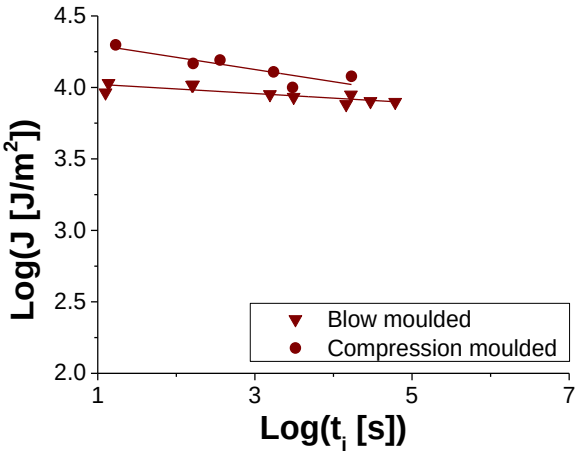

Figure 5.36 – Initiation behaviour at 60°C of blow moulded and compression moulded HDPE-1 under plane stress conditions.

5.4 Conclusions

In this Chapter the fracture behaviour in air of HDPE has been described under both plane strain and plane stress conditions.

Starting from the behaviour of the thick samples, tested in plane strain, both the initiation and propagation phases of fracture have been analysed adopting a pseudo-elastic approach based on the LEFM theory. For both materials a ductile to brittle transition was reported. Moreover, a very similar shape of the initiation and propagation curves has been observed for different testing temperatures and relevant master curves were hence built.

The effective modulus was evaluated starting from the stress intensity factor and the energy release rate. It turned out that a unique curve could be defined: it was hence concluded that fracture of HDPE occurred at the same strain irrespective of the applied stress intensity factor and fracture phase. If this strain

is evaluated during the test, the relevant relaxation modulus can be determined and the pseudo-elastic approach can be used to evaluate the stress intensity factor from the energy release rate or vice versa.

For what concerns the tests conducted in plane stress, instead, a different approach, based on the *J*-integral, has been used for the reduction of the data. In this stress state extensive plastic deformations occurred during the test. Comparing the results obtained from thick and thin compression moulded samples showed that the latter are less rate sensitive since a more flat initiation curve was obtained from plane stress tests. The effect of the production process, and in particular of the degree of crystallinity, was determined measuring a higher resistance of the more crystalline compression moulded specimens with respect to blow moulded ones.

6 Evaluation of the chemical interaction

6.1 Aim of the study

Due to the different chemical nature of the contained ingredients, it was investigated whether bleach, or one of its components, can chemically interact with the two HDPEs considered during this work. This process, in fact, could lead to a pronounced variation of the mechanical behaviour of polymeric materials and had to be considered as one of the possible reasons for a premature failure of a container for household products.

6.2 Experimental details

Type 5 dumb-bell specimens [155] were obtained via die cutting from 1 mm thick compression moulded plates for both HDPE-1 and HDPE-2, as already described in Chapter 4.

At least three of these specimens, together with some of the scraps coming from the plates, were soaked in the eight solutions described in Chapter 3 for various amount of time ranging from 1 week to 6 months (a time comparable with the service life of a bottle). It is hereby remembered that the various components are abbreviated as capital letters: H stands for sodium hypochlorite, A for the alkaline base composed by sodium hydroxide and sodium carbonate, S for surfactant, and P for perfume. A system to prevent specimens to get in contact one with the other during the soaking test was developed using expanded PE supports (see Figure 6.1).

At the end of the soaking phase, some of the properties of the two materials, described below, were evaluated to determine their evolution with the ageing time and to establish if chemical interaction occurred.

(a) (b)

Figure 6.1 – Setup for the soaking experiments.
(a) specimens in an expanded PE support;
(b) specimens and support in a glass vessel containing one of the eight solution of interest.

6.2.1 Relative mass variation

Periodical weighing was scheduled using a RADWAG AS 310.R2 precision balance, with a sensitivity of 0.1 mg. For each set of conditions the average relative mass variation Δm of the three samples and its relative standard deviation was computed. The evolution of this parameter was investigated to detect absorption by the material (giving a mass increase) or chain scission in the amorphous phase, typical of the chemical degradation of polyolefins, which in turn would lead to a decrease of the sample weight.

6.2.2 Tensile properties

Tensile tests were conducted on an Instron 1185R5800 electro-mechanical dynamometer, equipped with a 10 kN load cell, at a constant displacement rate of 10 mm/min and in standard environmental conditions (23°C and 50% RH). The elastic modulus E and the yield stress σ_y were measured as described in Chapter 4. These two properties were selected to evaluate the influence of the ageing time on the bulk mechanical properties of the two HDPEs.

6.2.3 Scratch resistance

To evaluate the evolution of the surface properties with the ageing time, scratch tests were performed on the samples immersed in the solutions described in Chapter 3. A normal force F_n was applied to a conical indenter at a constant speed v of 5 mm/min as sketched in Figure 6.2. Since no particular sample geometry is required for the samples used in this test (besides having a flat surface), scraps coming from the 1 mm plates, glued on a glass fibre reinforced support, were used. The instrument used during this work was a CSM Microscratch tester equipped with conical diamond tip indenters with a tip radius of 200 μm and an angle φ of 120° or 90°. During the tests, which were conducted at 23°C, the penetration depth P_d, the residual depth R_d (related to recovery phenomena), the tangential force F_t and the acoustic emission during the scratch were continuously measured.

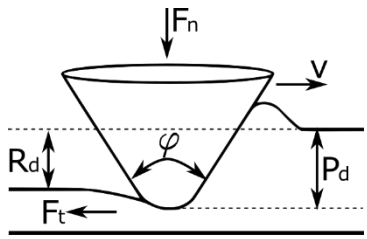

Figure 6.2 – Sketch of the scratch test: a normal force F_n is applied to the indenter which scratches the surface at a constant speed v.

To select the proper setup and to identify the most significant parameters to evaluate the chemical ageing, some preliminary tests were performed measuring the reference behaviour of unaged specimens and confirming that no orientation in compression moulded plates was present as reported in [30]. At the end of this preliminary analysis it was decided to perform scratches applying four different values of constant normal force F_n (1.20 N, 2.50 N, 6.25 N, 17.50 N) to analyse different P_d ranges. Three scratches having a length of 4 mm were

performed for each condition. Before and after the actual test surface profile of the various specimens was measured: this operation allowed the correct evaluation of P_d and R_d respectively.

An example of P_d and R_d data measured during a scratch test is shown in Figure 6.3. Raw data were elaborated considering only the central part of the graph were all the transient effect can be neglected; average values were computed for the three measures repeated for each test condition. As shown in [30], the penetration depth P_d was considered to be a meaningful parameter for the comparison between aged and unaged samples; since a detailed evaluation of the scratch resistance of the HDPEs constituting the bottles was out of the scope of this work, no other parameter was considered (e.g. scratch hardness). A similar test procedure was proposed in [171] to evaluate the change of surface mechanical properties of several polymers after the application of an artificial photo-oxidative ageing protocol. It was found that this kind of approach is a very effective tool for the evaluation of the occurrence of oxidative phenomena at the polymer surface since a clear variation of the penetration depth and of the scratch morphology occurred due to this process.

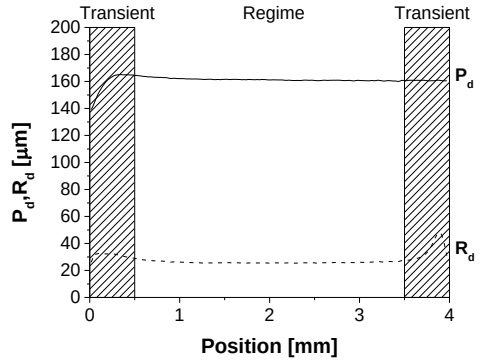

Figure 6.3 – Raw data obtained from a scratch test on HDPE-1. F_n=17.5 N, φ=120°

6.2.4 Chemical ageing of blow moulded materials

A more concise characterization campaign was also conducted on the blow moulded materials obtained from the bottles to verify if the results obtained from compression moulding samples were representative of the behaviour of the final product. In this case only two solutions (H+A+P+S and A+P+S) were considered as active environments.

The relative mass variation and the tensile properties of dumb-bell specimens obtained along the longitudinal axis of the bottle were measured. The maximum ageing time considered was about 9 months and the variation of E and σ_y after 7 and 9 months was considered.

In addition to these tests, IR analyses were conducted on samples both unaged and exposed for 4 month the two solutions. The instrument used for these tests was a silicon single bound Nicolet Nexus equipped with a diamond tip.

6.3 Results and discussion

6.3.1 Relative mass variation

6.3.1.1 Compression moulded samples

The results obtained from the relative mass variation tests on compression moulded samples of HDPE-1 and HDPE-2 are shown in Figure 6.4 and Figure 6.5 respectively. For both materials and for most of the solutions there was an almost negligible increase of the relative mass after six month of exposure. The behaviour of samples soaked in the solutions H+A+P+S and A+P+S was significantly different: a faster mass increase was observed during the first three months of soaking, after which an almost constant value of 0.35% was reached. This behaviour suggested that the affinity of these solutions with the HDPEs was higher with respect to the other environments and that the simultaneous

presence of the perfume and surfactant led to an easier absorption of the solutions into the polymers.

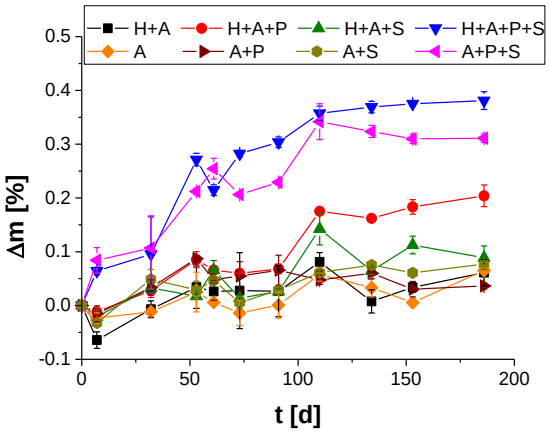

Figure 6.4 – Results of the relative mass variation tests for compression moulded HDPE-1

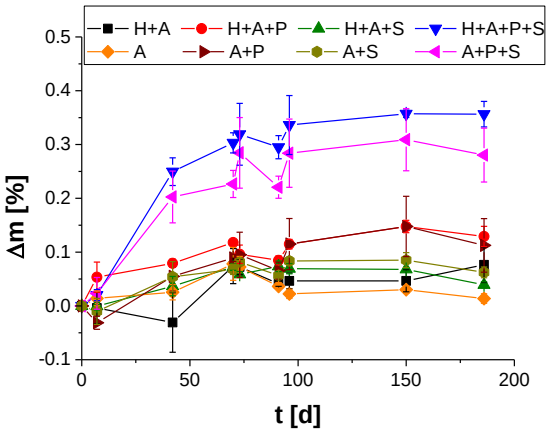

Figure 6.5 – Results of the relative mass variation tests for compression moulded HDPE-2

The fact that no significant differences were detected in the behaviour of the specimens exposed to the various solutions, regardless to the presence of sodium hypochlorite, seemed to be a first hint of the fact that this substance does not

influence the material behaviour from a weight variation point of view, at least within the considered experimental window.

6.3.1.2 Blow moulded samples

As can be observed in Figure 6.6 and Figure 6.7, also in the case of the samples obtained from the bottles the solutions H+A+P+S and A+P+S were absorbed in the two HDPEs. Moreover, comparing these results with those obtained from compression moulded samples, a quantitative agreement of the curves can be noticed suggesting that, probably, the kinetics of the absorption phenomena were the same in the two cases, irrespectively of the different degree of crystallinity of the materials produced with the two processes (see Chapter 3).

Also in this case, no significant effect of sodium hypochlorite was detected.

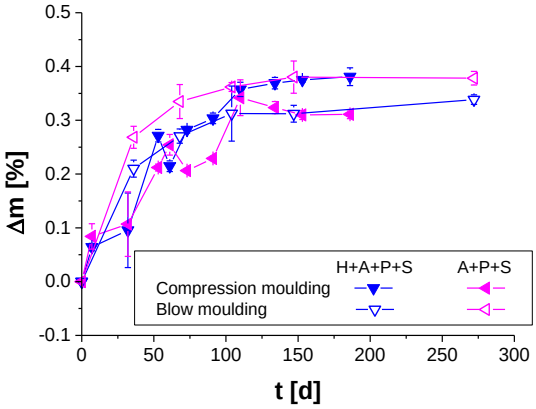

Figure 6.6 – Comparison of the results obtained from relative mass variation experiments on compression moulded and blow moulded HDPE-1 soaked on H+A+P+S and A+P+S.

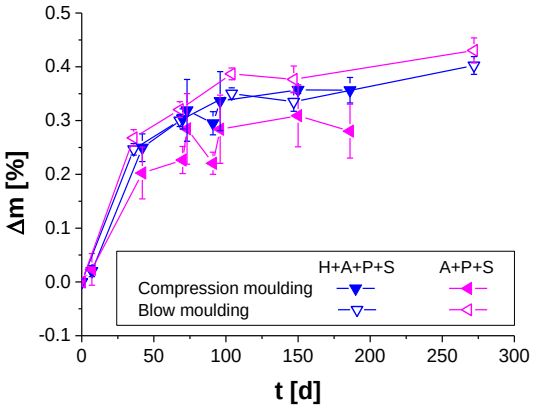

Figure 6.7 – Comparison of the results obtained from relative mass variation experiments on compression moulded and blow moulded HDPE-2 soaked on H+A+P+S and A+P+S.

6.3.2 Tensile properties

The elastic modulus and yield stress of the two HDPEs in the compression moulded and blow moulded forms are reported from Figure 6.8 to Figure 6.11. The influence of the production process on the tensile properties of the materials has been already described in Chapter 4 and no further comment will be added here; in this Section the evolution of these properties with respect to the ageing time (considered as the time samples were kept immersed in the different solutions) was investigated for the four groups of samples.

For all the groups, some oscillations of E were measured; however, since no clear trend was observed with increasing soaking time, these variations were ascribed to experimental uncertainties in the determination of this property and not to a real ageing effect. This hypothesis was further confirmed by the fact that no clear distinction could be made between the effects of the various environments (i.e. of the various bleach ingredients) on the elastic modulus of the four groups of samples. For what concerns σ_y, instead, it could be determined with better accuracy and a constant value was observed in all cases.

Even if chemical interaction cannot be completely ruled out from these tests, these results show that its effect on bulk mechanical properties of HDPE is negligible.

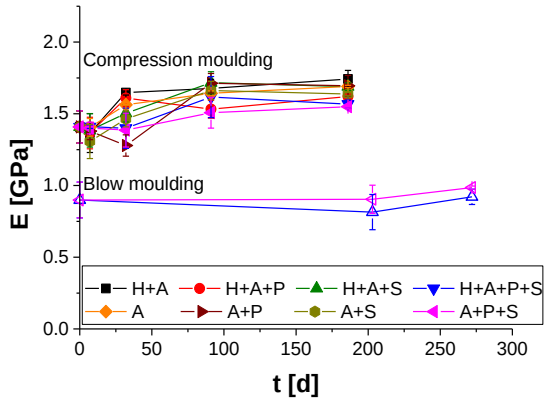

Figure 6.8 – Evolution of the elastic modulus of HDPE-1 with soaking time.

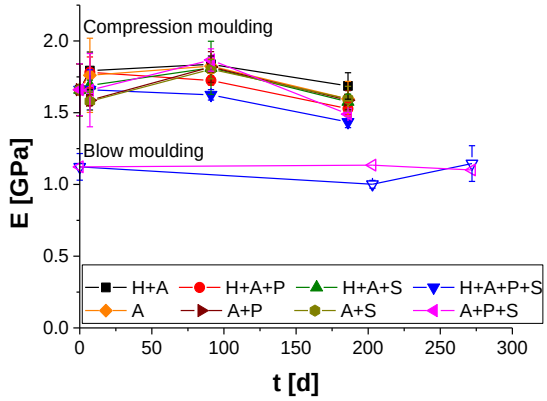

Figure 6.9 – Evolution of the elastic modulus of HDPE-2 with soaking time.

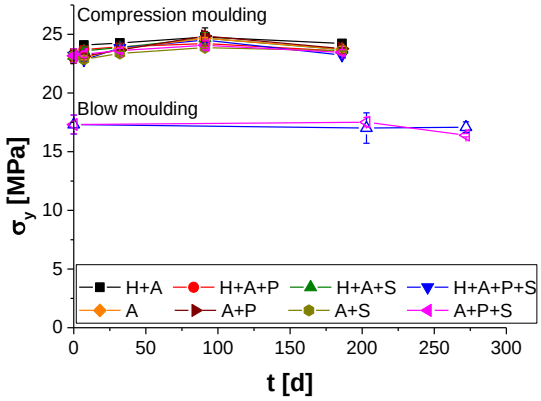

Figure 6.10 – Evolution of the yield stress of HDPE-1 with soaking time.

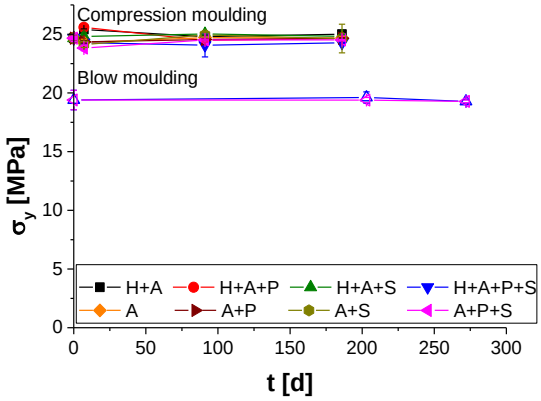

Figure 6.11 – Evolution of the yield stress of HDPE-2 with soaking time.

6.3.3 Scratch tests

Scratch tests were performed at the end of the experimental campaign described in this Chapter; at this stage, it was already clear that probably chemical aging had negligible effects on the behaviour of the HDPEs. Therefore, only compression moulded samples aged in three solutions (H+A, H+A+P+S and A+P+S) were selected to analyse the surface properties as a function of soaking time; moreover, contrary to what done during the tensile tests presented in the previous Section, only large ageing times were considered. Solution H+A was

used as a control to check whether surfactants and perfumes had some effects on the scratch resistance of the two polymers.

The penetration depths measured during the tests conducted with the 120° conical indenter are shown in Figure 6.12 and Figure 6.13 for HDPE-1 and HDPE-2 respectively. For both materials, a general increase of the penetration depth with soaking time was measured. Moreover, the equality of the results obtained from the samples exposed to the three environments suggests that the observed behaviour is not related to the composition of the environments. Observing the results obtained for different applied normal forces, it is possible to notice that the various curves have approximately the same slope, suggesting that very slight interaction between the material and the environment occurred homogeneously within a material layer whose thickness was about 200 μm from the sample surface.

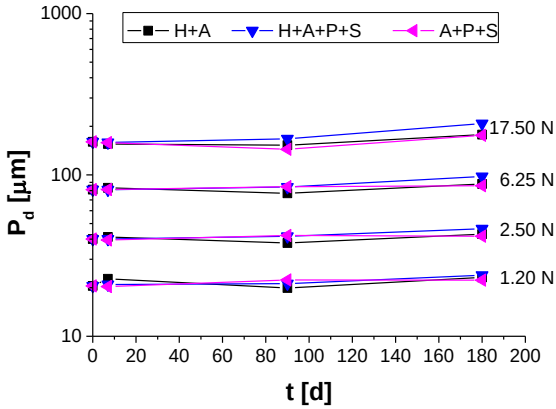

Figure 6.12 – Penetration depth as a function of soaking time for HDPE-1. Four normal forces were applied to the conical indenter with φ=120°.

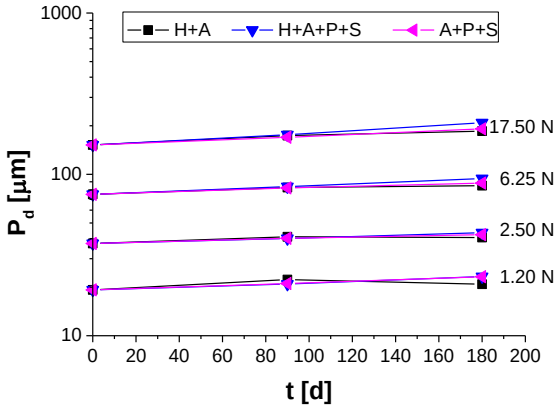

Figure 6.13 – Penetration depth as a function of soaking time for HDPE-2. Four normal forces were applied to the conical indenter with φ=120°.

To clarify the nature of the interaction between the solution and the polymers a second series of test with the 90° indenter was conducted. The different attack angle produces higher strains in the material region close to the indenter tip. In this case, as depicted in Figure 6.14 and Figure 6.15, slightly higher penetration depths but the same trends observed for the 120° indenter were observed.

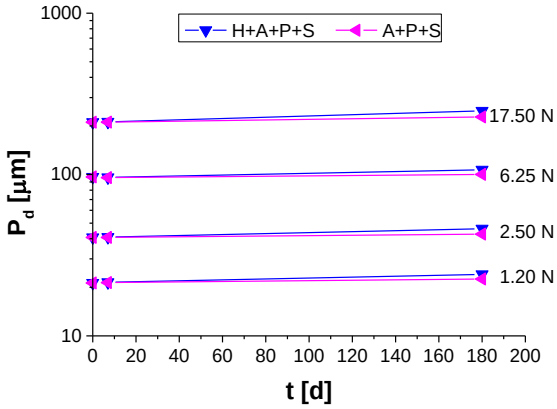

Figure 6.14 – Penetration depth as a function of soaking time for HDPE-1. Four normal forces were applied to the conical indenter with φ=90°.

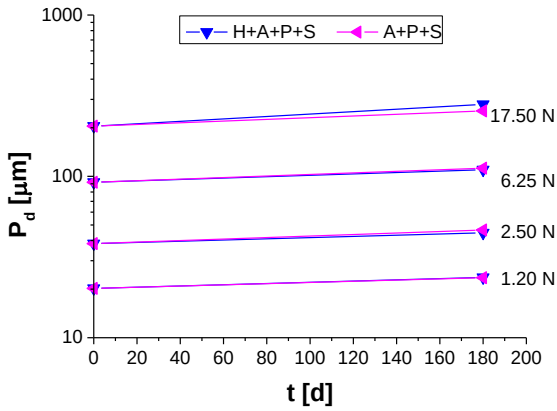

Figure 6.15 – Penetration depth as a function of soaking time for HDPE-2. Four normal forces were applied to the conical indenter with φ=90°.

The main reason to use the 90° indenter was to promote the evolution of critical surface failures via the formation of brittle cracks along the scratch path. Hence, an analysis of the samples after the scratch was conducted using a metallographic microscope Olympus BX60. Unaged samples and specimens exposed for 6 months to solution H+A+P+S were considered for this purpose and the scratches done at a normal force of 17.50 N were selected since, in these severe conditions, the appearance of cracks should be more likely. However, as can be noticed from Figure 6.16, no signs of cracks or brittle failures were detected and no appreciable differences were observed between unaged and aged samples, nor between the different materials.

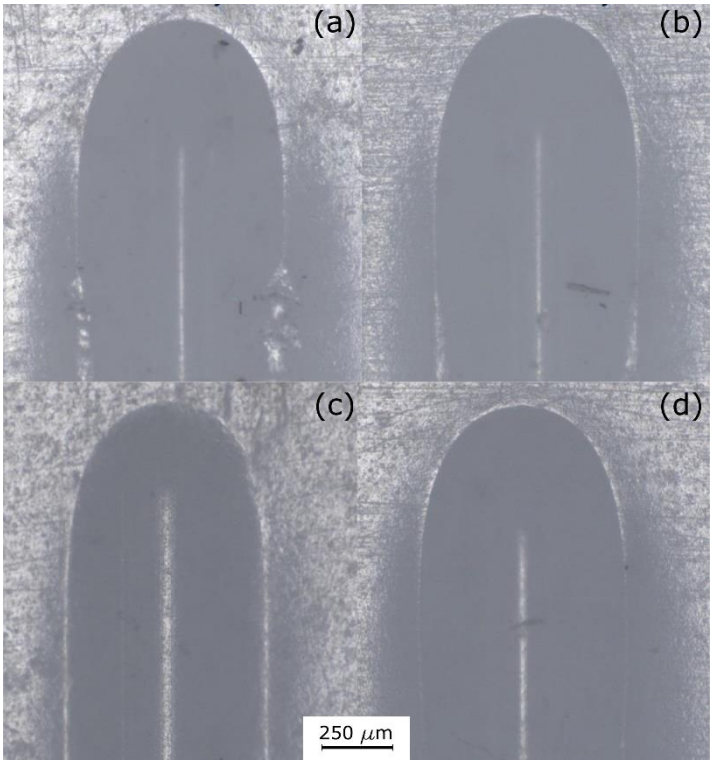

Figure 6.16 – Scratch paths obtained from tests at F_n=17.50 N with the 90° conical indenter. (a) unaged HDPE-1; (b) HDPE-1 exposed for 6 month to H+A+P+S; (c) unaged HDPE-2; (b) HDPE-2 exposed for 6 month to H+A+P+S. Original magnification: 50X.

A possible explanation for the results observed in this section is that the various solutions were absorbed in a certain surface layer of the two HDPEs, having a thickness of at least 200 μm as shown by the tests with the 90° indenter; this absorption led to a decrease of the scratch resistance of the HDPEs. This explanation is validated by the results obtained by the samples aged in H+A, which showed the lower mass increase after soaking, as reported in Section 6.3.1, but the same penetration depth of specimens aged in the other considered solutions. On the other hand, the absence of brittle cracks along the scratch path suggest that the occurrence of a chemical degradation of the HDPEs due to the

exposure to bleach, for an amount of time comparable to the bottle service life, has negligible effect on material surface properties.

6.3.4 IR analysis

To definitively confirm the assumption of no or negligible chemical degradation of the aged materials some IR analysis was conducted on blow moulded samples exposed for 4 months to solutions H+A+P+S and A+P+S which results are reported in Figure 6.17 and Figure 6.18 for HDPE-1 and HDPE-2 respectively. The absence of peaks at frequencies of 3600 cm^{-1}, 3300 cm^{-1}, 1660 cm^{-1}, 1500 cm^{-1} (typical of the OH group), 1000 cm^{-1}, 1200 cm^{-1} (typical of the C-O-C group) and 887 cm^{-1} (typical of the $C=CH_2$ group) [4] indicates that the HDPEs were not oxidized after exposure to the two considered environments.

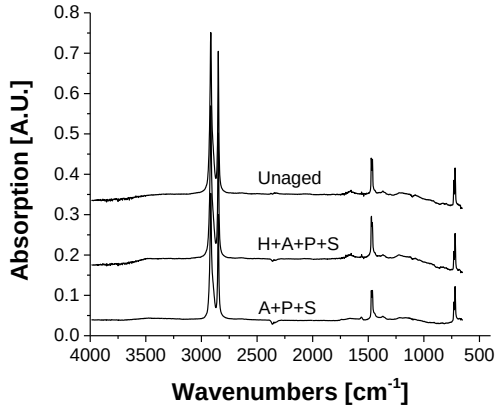

Figure 6.17 – IR spectra of unaged and 4 month aged HDPE-1.

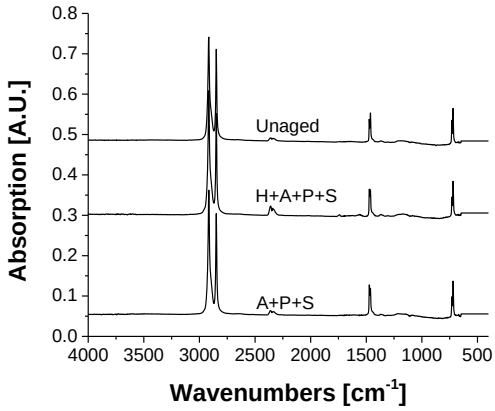

Figure 6.18 - IR spectra of unaged and 4 month aged HDPE-2.

6.4 Conclusions

The results shown in this Chapter indicate that the exposure of the two HDPEs to the various solutions, for an amount of time comparable to the typical service life of a bleach bottle, leads to negligible variations of the considered properties.

The most important consequence for this work is that, in light of this evidence, the Environmental Stress Cracking problem could be considered separately from the chemical interaction one, highlighted, for example, in [1, 2, 4, 51–55]. Hence, since no variation of the mechanical properties was observed from the tests described in this Chapter, the samples were exposed to the aggressive solutions only during the actual fracture tests, with no previous ageing performed.

Finally, from the mass variation tests (Section 6.3.1) it was evident that the absorption of the solutions H+A+P+S and A+P+S within the two HDPEs was higher with respect to the other considered environments. This result pointed out that the simultaneous presence of perfume and surfactant increased the affinity of the solution with the polymers; this fact was considered important and interesting in view of the ESC study. Consequently, as can be noticed in the next Chapters, most of the fracture tests conducted to evaluate the Environmental

Stress Cracking Resistance of the two polymers were carried out in these two solutions.

7 Environmental Stress Cracking under plane strain conditions

7.1 Aims of the study

In this Chapter the plane strain fracture behaviour of the two HDPEs in presence of the same solutions used during the chemical interaction tests (whose composition is reported in Section 3.1) is described.

As previously done in air (Chapter 5), a fracture mechanics approach was used to analyse the Environmental Stress Cracking Resistance (ESCR) of the two materials; the stress intensity factor was considered as a more reliable fracture parameter to evaluate their fracture behaviour.

7.2 Experimental details

SENB samples, having the same dimensions shown in Figure 5.5, were tested at 60°C in three- and four-point bending configurations by applying various constant displacement rates and constant loads, respectively; the testing procedure was the same adopted to conduct tests in air. Since, as shown in Chapter 5, the loading history gives no influence on the material fracture behaviour, no distinction will be made in the following between the data obtained from the two testing configurations.

As shown in Figure 7.1, to study the effect of the different solutions on the fracture resistance of the two polymers, the samples were put inside hermetically closed, flexible polyethylene bags filled with the solution of interest, without any previous exposure of the material to the chemical agent. The active environment was injected in the bag by means of a hypodermic syringe, which was also used to evacuate excess air; the syringe hole was then sealed with a butyl-based tape, of a type generally used to seal vacuum bags for composite lamination. A second

layer of polyethylene film was sealed around the bag containing the solution and the specimen to avoid damage to the testing equipment in case of fluid leakage.

Figure 7.1 – Flexible polyethylene bag used for fracture tests in active environment.

To evaluate the separate influence of the various constituents of the bleach the following solutions were considered: A, A+P, A+S, A+P+S, H+A+P+S. To further evaluate the influence of sodium hypochlorite on the mechanical behavior of the two polymers, moreover, two additional solutions with higher content of NaClO (with respect to H+A+P+S) were considered. These two environments will be named MF and SL in the following; an higher content of NaClO was present in MF while SL was characterized by intermediate sodium hypochlorite content in comparison to MF and H+A+P+S.

The crack initiation time, the propagation rate and the stress intensity factor for the two tests configurations were evaluated following the same procedure and analysis adopted for the determination of the plane strain fracture behaviour in air: please refer to Section 5.2.1 for further details.

$Log(K)$ vs. $Log(t_i)$ and $Log(K)$ vs. $Log(\dot{a})$ master curves representing the in air behaviour of the two materials at 60°C were compared to the relevant curves obtained in the environment.

7.3 Results and discussion

As reported in Section 7.1, the main purpose of this series of tests was to determine the influence of the various ingredients of the commercial blech solutions on the fracture resistance of the two considered materials. Since as reported, for example, in [172, 173] localized chemical aging at crack tip could occur during fracture tests even in the presence of distilled water, the effect of the most oxidative chemical contained in bleach, i.e. NaClO, was analysed first. Three solutions, H+A+P+S, SL and MF, having increasing content of sodium hypochlorite were considered together with A+P+S, which is equivalent to the first one but with no NaClO.

Figure 7.2 reports the behaviour at fracture initiation and during crack propagation for the two materials in the presence of the four solutions compared with that in air: all the environments have a deleterious effect on the fracture resistance of the two HDPEs therefore suggesting the occurrence of Environmental Stress Cracking.

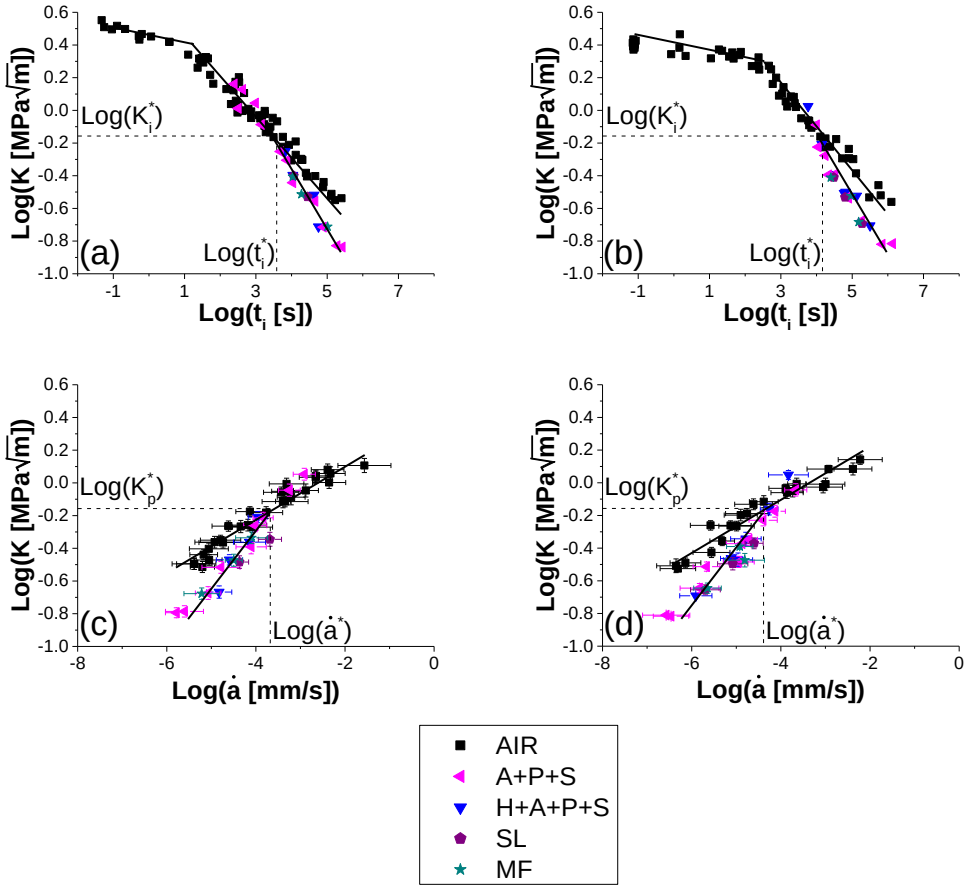

Figure 7.2 – Fracture behaviour in the presence of H+A+P+S, A+P+S, SL and MF. (a) initiation of HDPE-1; (b) initiation of HDPE-2; (c) propagation of HDPE-1; (d) propagation of HDPE-2.

Considering a certain value of the stress intensity factor it is possible to observe that, for both materials, the fracture initiates in a shorter time and it propagates faster in the presence of the active environments. Furthermore, in accordance with [7, 22, 24, 87], it is possible to define a critical interaction time t_i^*, a critical propagation rate $\dot{a}^*$, and the relevant critical stress intensity factors for initiation and propagation, K_i^* and K_p^* respectively, required to observe the effect of the environment on the material fracture resistance. Analysing with more attention these parameters it is possible to observe that, considering the typical data

dispersion obtained from fracture tests, for both materials and for both phases of the fracture process the same value of critical stress intensity factor K^*, equal to about 0.7 MPa·m$^{1/2}$ ($Log(K^*)$ = -0.15), can be identified. This means that, for the considered materials and environments, the magnitude of the applied K is a critical parameter that determines whether ESC occurs or not. Also in the presence of the active environments the slopes of the initiation and propagation curves of the two materials are very similar suggesting that even when Environmental Stress Cracking occurs, the same failure mechanisms are active in the two materials. Since K^* is included in the range of stress intensity factors in which brittle failure was observed in air it is possible to conclude that the disentanglement of the tie molecules should be the dominant phenomenon and that the active environments acts by increasing the rate at which it occurs promoting, therefore, the premature failure of the materials. This observation is in agreement with the higher ESC resistance of HDPE-2 which, as previously mentioned, possesses a significant larger amount of long polymeric chains with respect to HDPE-1.

Since the data obtained in A+P+S fall on the same curve defined by those obtained in the presence H+A+P+S, it should be argued that, in this case, sodium hypochlorite has no effect on the interaction between the commercial bleach solution and HDPE. To further confirm this hypothesis data obtained in these two environments were compared to those obtained in SL and MF: should local oxidation occur during the fracture test, the reduction of the fracture resistance of the material in presence of the active environments would show a correlation with the effective NaClO content. Yet, as can be observed from Figure 7.2, for both HDPEs, the results obtained in the presence of the four solutions fall on the same curve both for initiation and propagation of fracture. This fact can be

explained considering that, in this case, the decomposition of sodium hypochlorite into more aggressive species which can lead to extensive oxidation of HDPE is prevented by NaOH and Na_2CO_3 which, as reported in Chapter 3, are added to the considered solutions precisely to stabilize NaClO.

Since it appears that sodium hypochlorite has no effect on the ESCR of the two materials, the data obtained from the four solutions previously analysed were considered together in the following. The effect of the other bleach ingredients was studied using NaClO-free environments in order to prevent problems related to the corrosion of the metallic grips of the dynamometer or of the creep machines. In particular, as shown in Figure 7.3, A, A+P and A+S were considered to define which of the chemical species contained in a commercial bleach had the greater influence on the fracture behaviour of the two polymers.

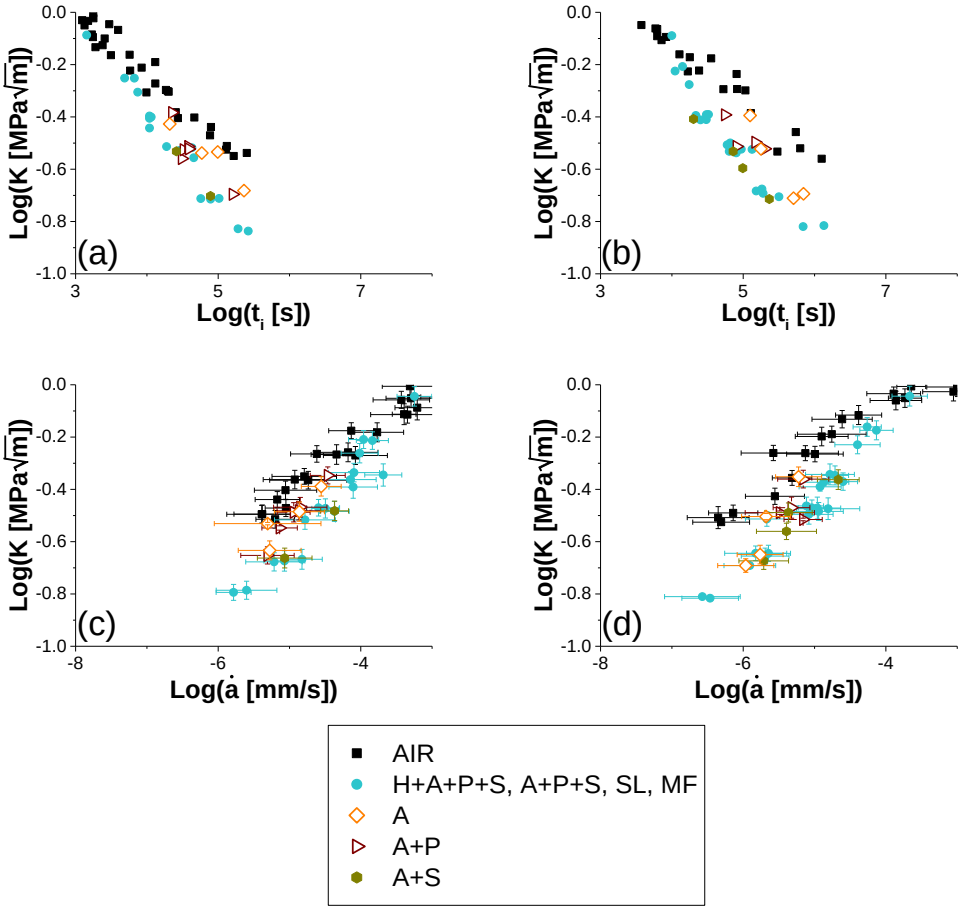

Figure 7.3 - Fracture behaviour in the presence of A, A+P and A+S.
(a) initiation of HDPE-1; (b) initiation of HDPE-2;
(c) propagation of HDPE-1; (d) propagation of HDPE-2.

As can be observed from these graphs it turned out that the data obtained in presence of A+S fall on the same curves previously defined for the other environments meaning that, probably also the perfume (not included in this formulation) has only a marginal role in the Environmental Stress Cracking of HDPE-1 and HDPE-2. This fact is partially confirmed from the data obtained in A+P which fall between the curves defined by the five environments considered up to now (H+A+P+S, A+P+S, MF, SL and A+S) and the master curve in air.

However, it has to be considered that, as reported in Chapter 3, A+P contains a small amount of surfactant and, even if its content in this solution is two orders of magnitude lower with respect to the other environments, this species has a strong effect on the fracture resistance of HDPE (as also reported in [5, 6, 7, 18, 19, 21, 23, 44, 46, 62–82]). Since the data obtained on A, which contains only NaOH and Na_2CO_3, seem to be practically coincident with those of A+P this means that if the surfactant is contained in such a small quantity, its effect can be practically neglected. The reported influence of A on the fracture resistance of the two polymers under study is partially in disagreement with previous findings by Tonyiali, Rogers and Brown in [21], according to which ESC was not influenced by sodium hydroxide.

To definitely understand the influence of all the ingredients composing a commercial bleach more tests and more solutions would be probably required. In light of the results presented in this Section, however, it is possible to conclude that sodium hypochlorite does not have a significant role in the Environmental Stress Cracking of HDPE-1 and HDPE-2, which is instead caused by the presence of a minimum quantity of surfactant. Since H+A+P+S, A+P+S, MF, SL and A+S have the more pronounced effect (if compared with A and A+P) on the considered phenomenon these solutions represents a conservative choice to characterize the ESCR for this specific application. In particular, in the following only the data obtained in the presence of H+A+P+S and A+P+S will be considered since the majority of the tests was conducted in these two environments.

7.3.1 Evaluation of the sensitivity to the environment

To quantify the sensitivity to the environment different approaches can be adopted. One strategy can be to evaluate the parameter λ, proposed by Kamaludin in [24], which, as described in Section 2.5.4, is defined as:

$$\lambda = \frac{t_i^*}{t_{i,max}} \cdot \frac{\dot{a}_{min}}{\dot{a}^*} \tag{7.1}$$

where t_i^* and $\dot{a}^*$ are the critical interaction time and the critical crack growth rate, respectively, while $t_{i,max}$ and $\dot{a}_{min}$ are the maximum value of crack initiation time and the minimum crack growth rate measured, respectively. In the original work the author did not specified if $t_{i,max}$ and $\dot{a}_{min}$ have to be obtained from the tests conducted in air or in active environment; during this analysis the values obtained from tests in environment were considered.

Two possible choices can be made to compare the behaviour of the two materials. In fact, one can select the highest $t_{i,max}$ and the lowest $\dot{a}_{min}$ between those obtained from the two materials and evaluate λ using these values for both polymers, as shown in Figure 7.4 (a). It is possible to observe that for HDPE-1 λ is considerably lower than for HDPE-2 suggesting that a higher ESC sensitivity of this material. However, considering the graphs reported in the previous section it can be observed that the reduction of fracture resistance caused by ESC, or in other words the sensitivity to the environment of the two polymers, is similar and that HDPE-2 is characterized by a higher Slow Crack Growth resistance being the initiation and propagation curves of this material shifted towards higher times and lower propagation rates, respectively.

On the other hand, one can evaluate λ considering for each material the relevant maximum initiation time and minimum propagation rate, as originally proposed

in [24]. The results obtained from this analysis are shown in Figure 7.4 (b) from which a similar sensitivity to the active environment can be observed for the two materials. Yet, it has to be considered that λ is defined starting from the minimum crack growth rate and the maximum initiation time observed during the tests which, of course, are related to the minimum applied stress intensity factor.

From the aforementioned considerations, it appears that a further refining of the λ parameter is necessary to make it suitable for an unequivocal evaluation of the material sensitivity to the environment.

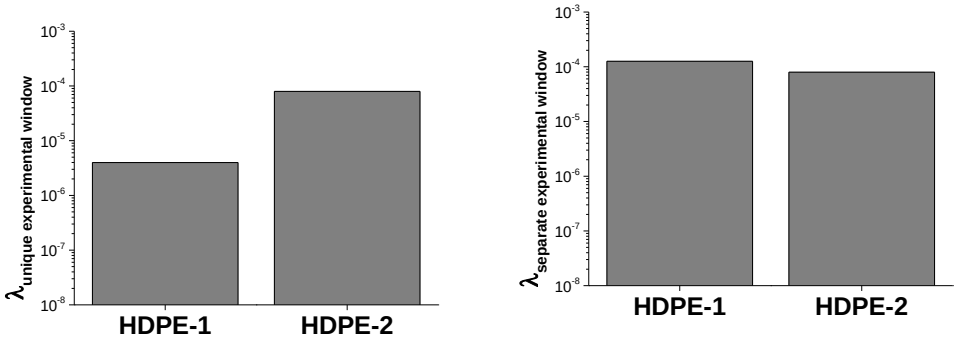

Figure 7.4 - Parameter λ for the two HDPEs. (a) parameter evaluated considering the highest $t_{i,max}$ and the lower $\dot{a}_{min}$ for the two materials; (b) parameter evaluated considering for each material the relevant $t_{i,max}$ and $\dot{a}_{min}$.

A different approach to determine the sensitivity of the materials to the environment could be the evaluation of the plasticisation factor β defined by Chan in [151] could be used to evaluate the effect of the environment. This parameter is defined, only for the propagation phase, as:

$$\beta = \frac{K_{environment}}{K_{air}} \tag{7.2}$$

As described in Section 2.5.4, this parameter is suitable at low propagation rates when the curve in air and in environment are parallel. However, in the experimental window considered during this work this is not true: β will therefore depend on the propagation rate considered for its evaluation. To overcome this limitation and to evaluate the effect of the environment on both phases of fracture, modified plasticisation factors β_m were defined for initiation and propagation as per Equations (7.3) and (7.4), respectively:

$$\beta_{m,i} = \frac{\left(dLog(K)/dLog(t_i)\right)_{environment}}{\left(dLog(K)/dLog(t_i)\right)_{air}} \tag{7.3}$$

$$\beta_{m,p} = \frac{\left(dLog(K)/dLog(\dot{a})\right)_{environment}}{\left(dLog(K)/dLog(\dot{a})\right)_{air}} \tag{7.4}$$

These parameters can be easily determined from the slope of the relevant fracture curves. Since, in contrast in contrast to what reported [5, 18] and shown in Figure 2.34, for the considered materials the slope of the $Log(K)$ vs. $Log(\dot{a})$ in environment is not equal to 0.5 (it is 0.38±0.04 for HDPE-1 and 0.29±0.02 for HDPE-2), $\beta_{m,p}$ does not constitute a redundant information.

The modified plasticisation factors for the two materials are shown in Figure 7.5. Considering the error related to the evaluation of this parameter it is possible to observe that the four parameters are practically coincident, meaning that the active environments causes the same variation of slope on the $Log(K)$ vs. $Log(t_i)$ and $Log(K)$ vs. $Log(\dot{a})$ curves of the two materials. In other words, this result demonstrates that the active environment has quantitatively the same detrimental effect on both phases of fracture and on both materials.

In using this parameters, however, it has to be noticed that they are valid only if there are not variation in the slope of the in air and in environment fracture curves in the considered range. If this is not true, a different parameter must be used (or defined) to determine the ESC sensitivity of the considered polymer. Moreover, the modified plasticisation parameter does not highlight the different critical interaction time t_i^* and critical crack growth rate $\dot{a}^*$ of HDPE-1 and HDPE-2 and the relevant critical stress intensity factor K^*: these parameters must be considered together with β_m to obtain a complete indication of the environmental stress cracking resistance of the considered polymers.

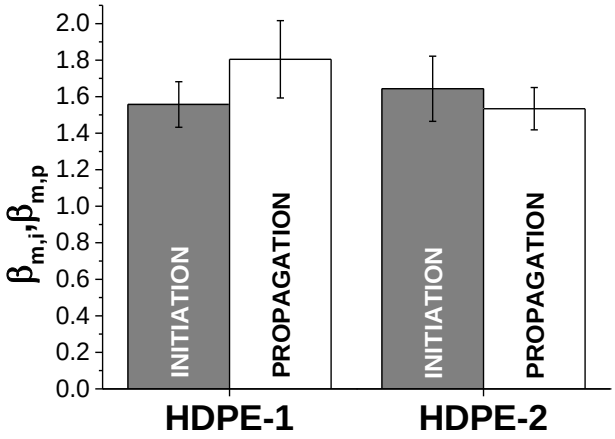

Figure 7.5 - Modified plasticisation factor for HDPE-1 and HDPE-2.

7.4 Conclusions

In this Chapter the Environmental Stress Cracking of the two HDPEs under study was analysed under plane strain conditions.

It was discovered that sodium hypochlorite, the bleaching agent in the considered commercial bleaches, has no influence in the fracture behaviour of the two materials and it was confirmed that, as expected, the surfactants play a

major role on the phenomenon of the Environmental Stress Cracking of polyethylene.

The solutions influence the behaviour of the two polymers in the brittle branches of the initiation and propagation curves therefore the environments act by favouring the disentanglement of the tie molecules as proposed in [42, 43]. Since the same mechanism are activated by the environment in the two HDPEs, a similar reduction of the fracture resistance is caused by the latter and the polymers have a comparable sensitivity to the considered active environments. However, since HDPE-2 has a significantly larger amount of long polymeric chains, its Slow Crack Growth resistance is higher and, therefore, for this material, a longer critical interaction time and a lower critical crack growth rate are required to observe Environmental Stress Cracking.

8 Effect of temperature on Environmental Stress Cracking Resistance

8.1 Aim of the work

It is common, as shown in the previous Chapter, to carry out ESC tests at high temperatures to accelerate the fracture phenomena. However, to the author's knowledge, in case of ESC a quantitative evaluation of the accelerating effect of the temperature has never been reported in the relevant scientific literature and the applicability of a time-temperature reduction scheme has never been verified.

From a theoretical point of view two situations can occur:

- if the temperature dependence is only due to material viscoelasticity, curves having the same shape (in *Log* scale) at different temperatures would be obtained and a time temperature reduction scheme could be suitable to extend the available experimental window
- if the interaction with the fluid displays its own temperature dependence, instead, the different interaction of the active environment would negate the applicability of a time-temperature reduction scheme

In considering these two possible scenarios, it is noteworthy that, of course, relevant properties of the active environment (diffusion coefficient of the surfactants, viscosity, chemical activity…) may change with the temperature as well as those of the polymer (fracture resistance, extension of the craze…). However, the way in which the properties of the fluid and its interaction with the polymer vary with temperature with respect of those of the polymer itself is not easily predictable; this is a key factor in determining whether the temperature

dependence of the fracture behaviour remains the same which had been observed during the tests in air, or is modified by the presence of the active environment itself.

During this Chapter the applicability of the time temperature equivalence as an instrument for long term prediction of the behaviour of the considered HDPEs in the presence of the commercial bleach solution (or of its NaClO-free counterpart) will be evaluated. If applicable, this approach could represent a valuable engineering tool for the prediction of ESCR of polymeric components.

8.2 Experimental details

SENB samples were used for the evaluation of the ESCR of the two compression moulded HDPEs as previously done in Chapter 7. Tests were conducted in the presence of A+P+S in three-point bending / constant displacement rate and four-point bending / constant load configuration at 40°C and 50°C. The relevant results were compared to those obtained at 60°C in the presence of H+A+P+S and A+P+S, which, as shown in the previous Chapter, have quantitatively the same effect on the fracture resistance of the two polymers. Also for these tests, specimens were put in polyethylene bags filled with the active environment.

Fracture initiation time, crack propagation rate and the stress intensity factor for the two tests configurations were evaluated according to the methods previously adopted for the characterization of the plane strain fracture behaviour, while the relevant shift factors were computed according to the procedure described in Section 4.2.

Also in this case the $Log(K)$ vs. $Log(t_i)$ and $Log(K)$ vs. $Log(\dot{a})$ master curves in air were taken as a reference. Moreover, the energy release rate approach was

also adopted to define master curves which will be further considered in Chapter 9.

8.3 Results and discussion

Initiation and propagation data obtained at 40°C, 50°C and 60°C on HDPE-1 and HDPE-2 in presence of the active environment are reported, together with the relevant master curves in air, in Figure 8.1 to Figure 8.4.

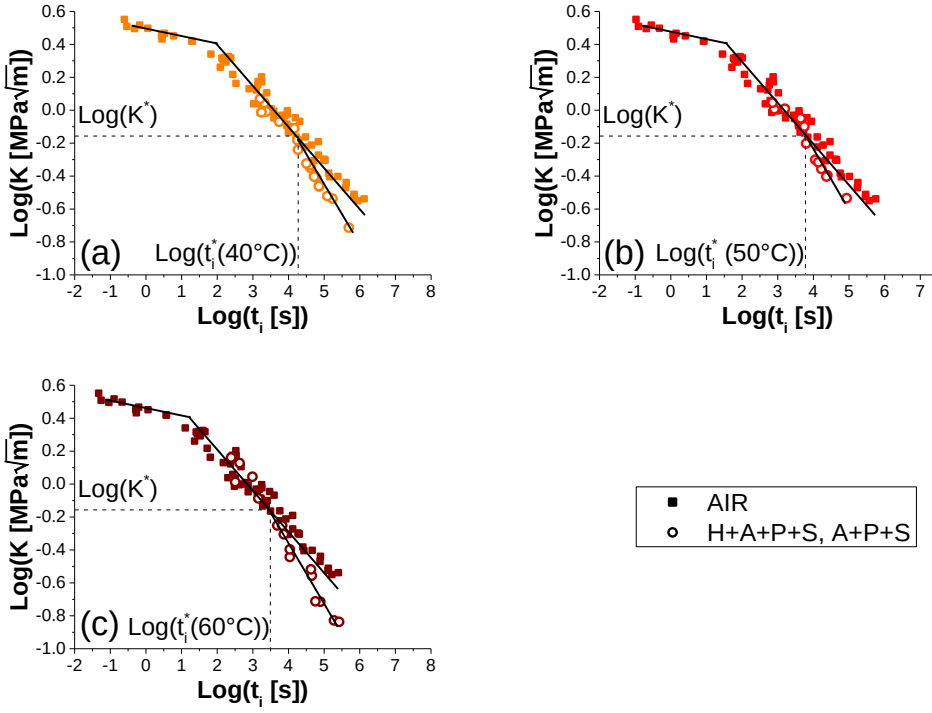

Figure 8.1 – Crack initiation behaviour of HDPE-1 in the presence of H+A+P+S and A+P+S at different temperatures: (a) 40°C; (b) 50°C; (c) 60°C.

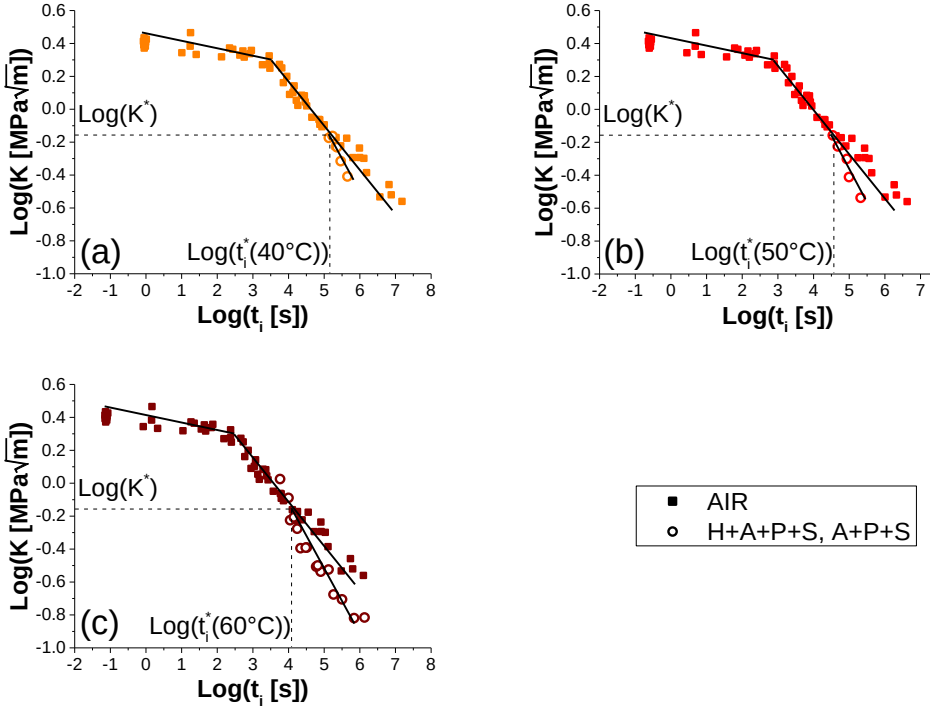

Figure 8.2 - Crack initiation behaviour of HDPE-2 in the presence of H+A+P+S and A+P+S at different temperatures: (a) 40°C; (b) 50°C; (c) 60°C.

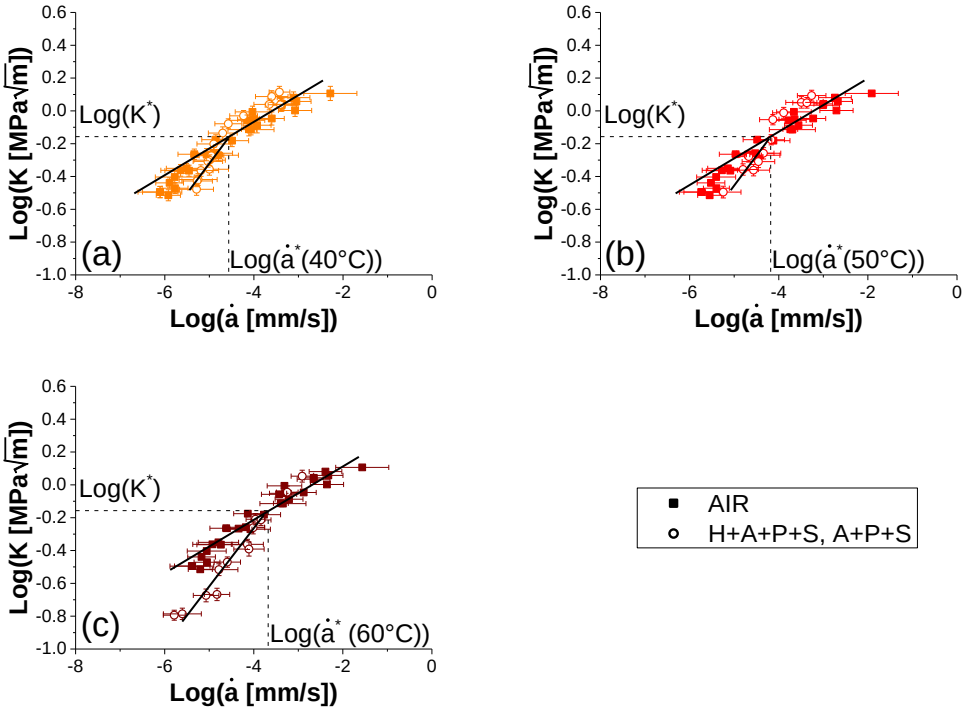

Figure 8.3 - Crack propagation behaviour of HDPE-1 in the presence of H+A+P+S and A+P+S at different temperatures: (a) 40°C; (b) 50°C; (c) 60°C.

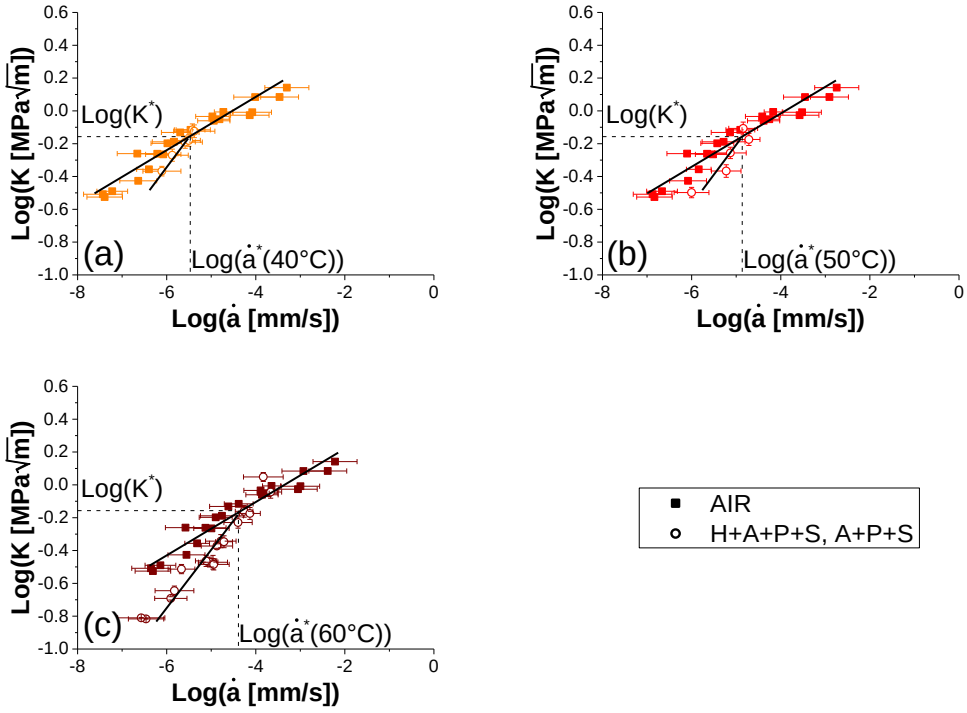

Figure 8.4 - Crack propagation behaviour of HDPE-2 in the presence of H+A+P+S and A+P+S at different temperatures: (a) 40°C; (b) 50°C; (c) 60°C.

As already observed for the fracture behaviour in air, also the data obtained in the presence of the active environment can be described using power laws having the same slope at the different temperatures as could be expected by purely viscoelastic effects [125, 132, 153, 154]. Therefore, also in environment, relevant fracture mechanisms are not affected by temperature except for their kinetics.

An extremely valuable consequence is that, as already done for the relaxation modulus, for the yield stress and for the fracture in air, also in this case the data can be shifted along the logarithmic time / crack growth rate axis and overlapped extending the available experimental window. This is an evidence that, at least in the considered range, time-temperature equivalence is applicable also in presence of the active environment. As shown in Figure 8.5, the same shift factors

are required to overlap data obtained in air and in the environment: this fact implies that the accelerating effect of temperature and environment are independent from each other. Therefore, it is possible to conclude that, in the considered range of temperatures, the solutions investigated do not influence the temperature-dependence of the fracture behaviour, which depends only on the material viscoelasticity.

Since the curves for all temperatures have identical slopes in all three branches (ductile, brittle-air and brittle-environment), it turns out that the critical stress intensity factor K^*, which, as shown in the previous Chapter, is equal for the two material and for both phases of fracture, does not depend on the temperature either, at least in the considered range. This means that the magnitude of the applied K alone determines whether ESC occurs or not and temperature only determines the time needed for this phenomenon to occur: with increasing temperature, the critical interaction time t_i^* decreases while the $\dot{a}^*$ critical crack growth rate increases and these two quantities share the same temperature dependency with the whole relevant fracture curve.

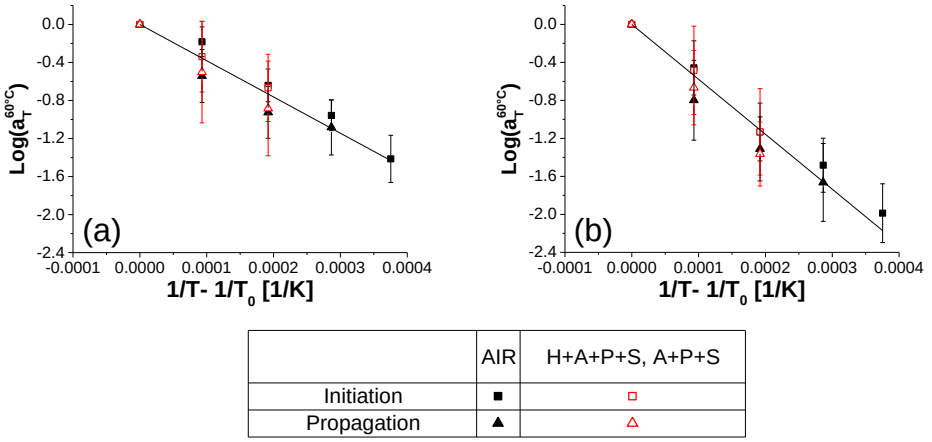

Figure 8.5 - Shift factors for (a) HDPE-1 and (b) HDPE-2 in air and in the presence of H+A+P+S and A+P+S. Reference temperature: 60°C.

Therefore, assuming that time-temperature superposition in presence of the environment remains applicable down to 23°C, the behaviour of the material at room temperature can be predicted. The initiation and propagation master curves of HDPE-1 and HDPE-2 at 23°C are reported in Figure 8.6; these were built using, for each material, the average shift factor evaluated from the data of Figure 8.5. As previously observed in Chapters 5 and 7, from the initiation and propagation master curves the longer critical interaction time, the lower critical crack growth rate and ultimately the higher overall fracture resistance of HDPE-2 can be demonstrated.

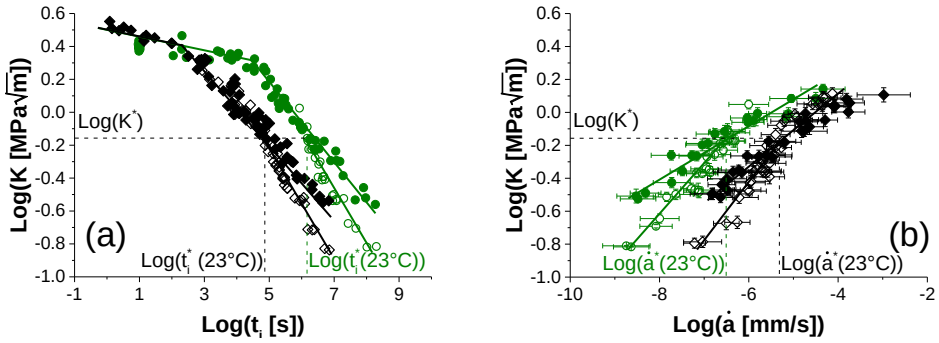

	AIR	H+A+P+S, A+P+S
HDPE-1	◆	◇
HDPE-2	●	○

Figure 8.6 – (a) initiation and (b) propagation master curves at 23°C for the two materials in air and in the presence of H+A+P+S and A+P+S.

The data obtained in environment at the different temperatures were analysed also with the energy release rate approach, as done for the fracture behaviour in air during Chapter 5. It turned out that, as expected, also in this case time-temperature superposition principle remains applicable even in presence of

ESC and, therefore, the shift factors of Figure 8.7 were evaluated and the relevant initiation and propagation master curves were built as shown in Figure 8.8.

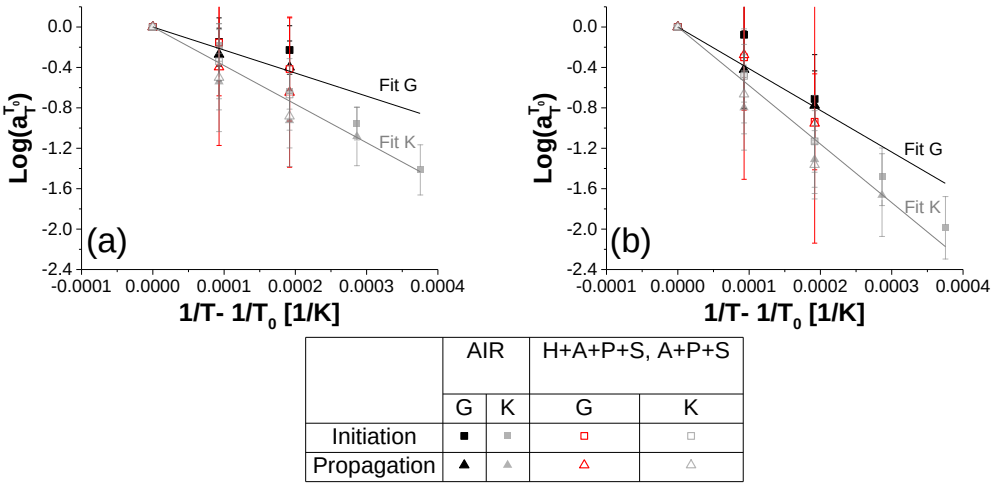

Figure 8.7 – Comparison of the shift factors for (a) HDPE-1 and (b) HDPE-2 evaluated from the stress intensity factor and the energy release rate approaches. Reference temperature: 60°C.

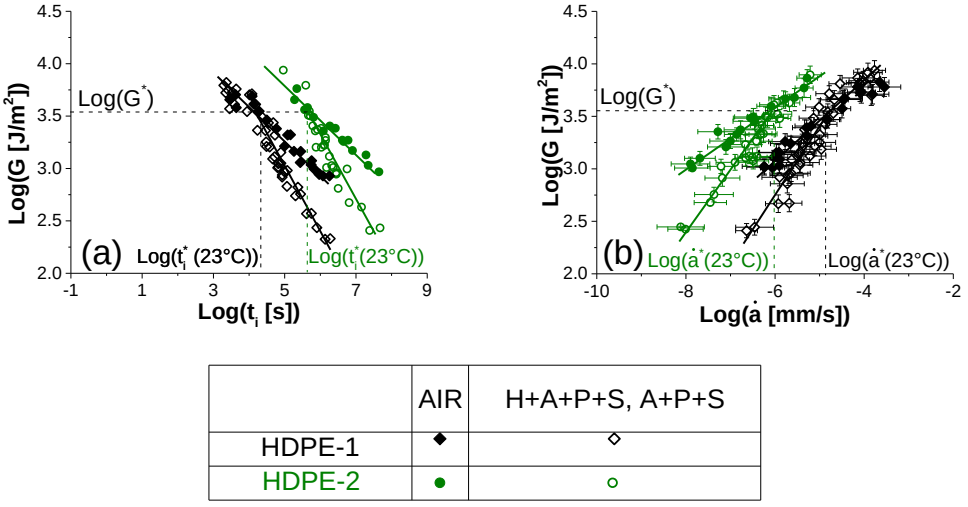

Figure 8.8 - (a) initiation and (b) propagation master curves at 23°C for the two materials in air and in the presence of H+A+P+S and A+P+S in terms of the energy release rate G.

Moreover, since, as demonstrated in Chapter 5, K and G are equivalent fracture parameters for HDPE and since time-temperature superposition principle can be applied using both approaches, the effective modulus evaluated from Equation (5.19) in the presence of the active environment results coincident with the one from fracture tests in air as shown in Figure 8.9 and Figure 8.10. This fact can be explained considering that the active environment significantly interacts with HDPE only in the region of the forming craze, by penetrating into it: therefore there should be no reason for a material bulk property such as the relaxation modulus to be influenced by the presence of the active environment itself.

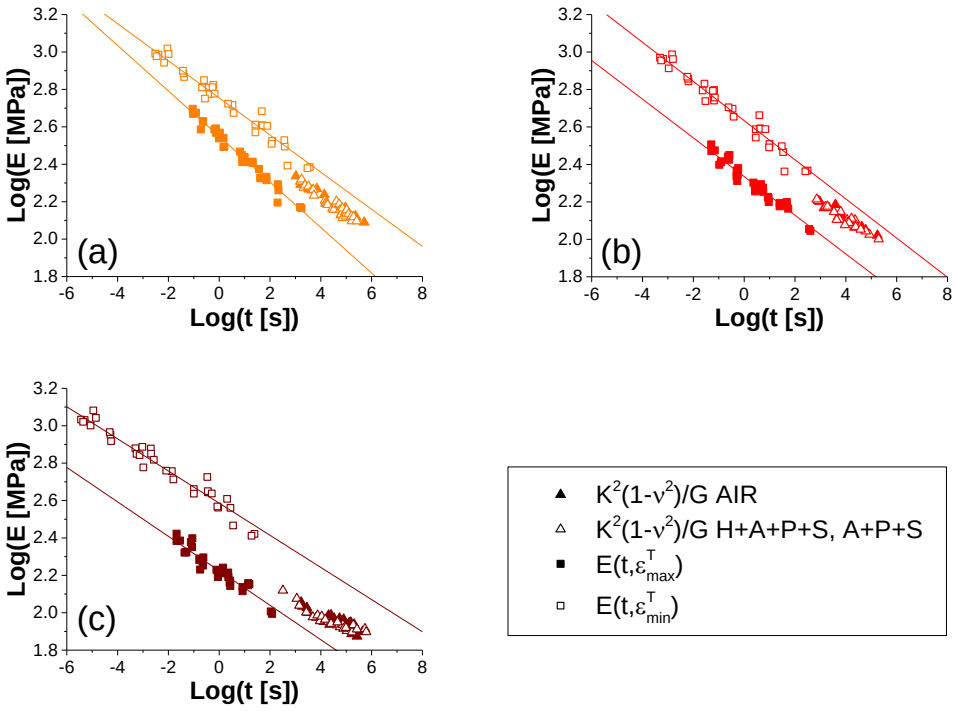

Figure 8.9 - Comparison between the effective relaxation modulus and the relaxation modulus at the maximum and minimum crack tip strain for HDPE-1 in air and in environment. (a) 40°C; (b) 50°C; (c) 60°C.

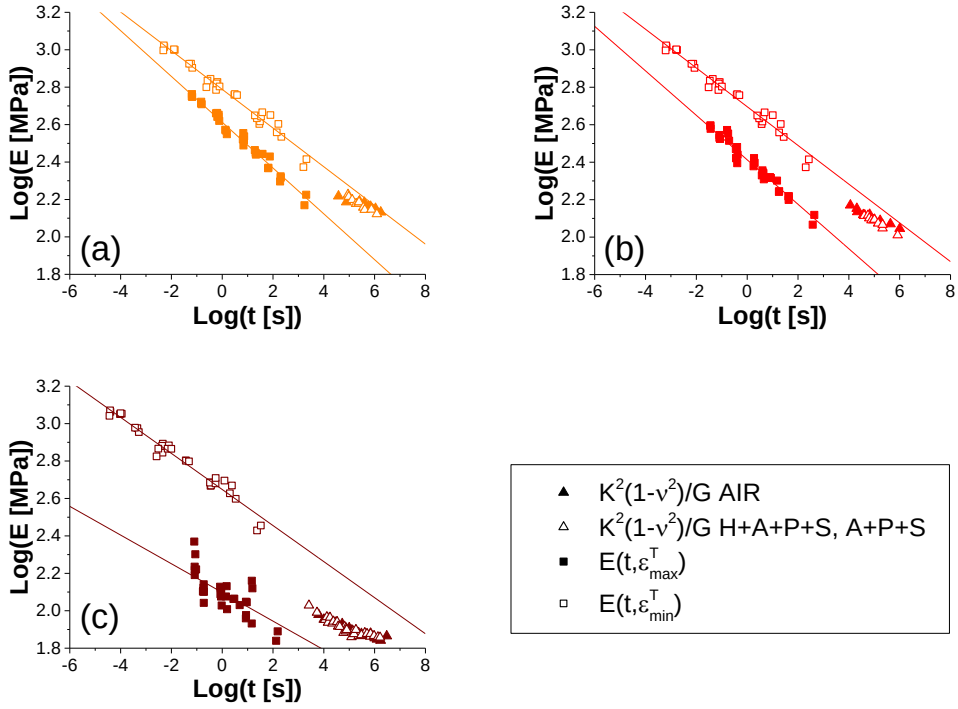

Figure 8.10 - Comparison between the effective relaxation modulus and the relaxation modulus at the maximum and minimum crack tip strain for HDPE-2 in air and in environment. (a) 40°C; (b) 50°C; (c) 60°C.

To verify the latter assumption tensile tests on 1mm thick type 5 dumb-bell specimens of compression moulded HDPE-1 were performed in air and in the presence of A+P+S, thanks to a custom-designed chamber for environmental tests (described in details in Section 9.2). These tests were conducted at 50°C and at a constant displacement rate of 1 mm/min; due to the presence of the active environment the optical measurement of the strains was not possible and neither was the use of a mechanical extensometer: in this case the displacement, measured directly from the crosshead, was considered. The results of this tests are shown in Figure 8.11 from which it is possible to observe that the two stress-displacement curves perfectly overlap up to almost the maximum stress.

This difference, comparable to those observed in Chapter 4, could be related to some irregularities in the specimens which could cause a slightly different post yielding behaviour. In any case, the two curves have practically an identical shape and the same material behaviour was observed during the test, irrespective of the presence of the active environment. Therefore, it is confirmed that the latter plays a significant role only locally at the tip of a crack or notch.

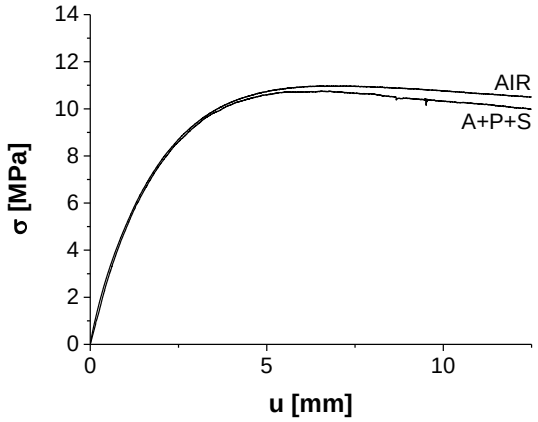

Figure 8.11 – Stress-displacement curves of 1mm thick type 5 dumb-bell specimens of compression moulded HDPE-1 in air and in the presence of A+P+S. Tests were conducted at 50°C and 1mm/min.

8.4 Conclusions

Fracture data presented in this Chapter revealed that the temperature has the same accelerating effect both in air and in presence of the active environment, at least in the considered experimental range. Therefore, relevant initiation and propagation curves can be superimposed using the same shift factor found in air. Critical interaction times and critical crack speeds previously identified for both polymers at 60°C depend on temperature with the same dependency observed for the relevant fracture curves; they all correspond to the same critical stress intensity factor K^*, which instead does not vary with temperature, material and

fracture phase. These results are an indication of the fact that, in the considered range, the temperature only acts by modifying the kinetics of the fracture process, according to the material inherent viscoelasticity.

The applicability of time-temperature equivalence in the case of ESC is very important: if verified for several polymer-environment systems, this result can lead to the use of fracture mechanics data for the prediction of the long-term behaviour of polymeric products also in presence of aggressive environments.

Moreover, comparing the stress intensity factor and the energy release rate approaches for the study of ESC it was further demonstrated that LEFM can be used to properly describe also the behaviour of nonlinear viscoelastic materials as the two HDPEs under study.

Finally, the effective relaxation moduli, evaluated from K and G, fall on the same curves defined by the data in air showing the independence of bulk mechanical properties from the presence of the fluid, as further demonstrated by tensile tests at high temperature performed in air and in presence of the active environment.

9 Environmental Stress Cracking under plane stress conditions

9.1 Aim of the work

In this Chapter ESC under plane stress conditions was investigated.

During the first preliminary tests, conducted to properly define the experimental procedure, an old A+P+S solution, prepared at the beginning of the research activity, was used: once the protocol was developed, the effect of a more aggressive active environment and of sodium hypochlorite was evaluated performing tests in the presence of fresh A+P+S and H+A+P+S which had become available.

The effect of the production process on ESCR was studied as well, performing tests on blow moulded and compression moulded samples of similar thickness. In this case, moreover, the elastic and plastic contribution of the energy release rate were considered separately to better understand the mechanisms influenced by the presence of the considered solutions.

Finally, the effect of the stress state was evaluated by comparing the G-based initiation master curve of HDPE-1 defined in the previous Chapter and the data obtained from the thin compression moulding samples presented in the following.

9.2 Experimental details

Double Edge Notched Tension (DENT) samples of HDPE-1, obtained from the bottles or produced via compression moulding, were used to evaluate the effect of the production process (see Figure 5.11 for specimen geometry). Tests were conducted at 60°C and at various displacement rates (ranging from 0.1 to 0.0007 mm/min) using an Instron 1185R5800 dynamometer.

An environmental chamber, having capacity of about 5 l and designed for a previous study [22], was connected to the lower moving crosshead of the dynamometer. As shown in Figure 9.1, the chamber is composed of three fixed walls, a door and a flange to mechanically connect the clamping system. All the components used during this characterisation (chamber, clamping system and extension bars) were made of stainless steel to avoid corrosion of the equipment; the only exceptions are two glass windows, in the door and in the opposite wall, which, in case of transparent solutions, allow video recording of the test.

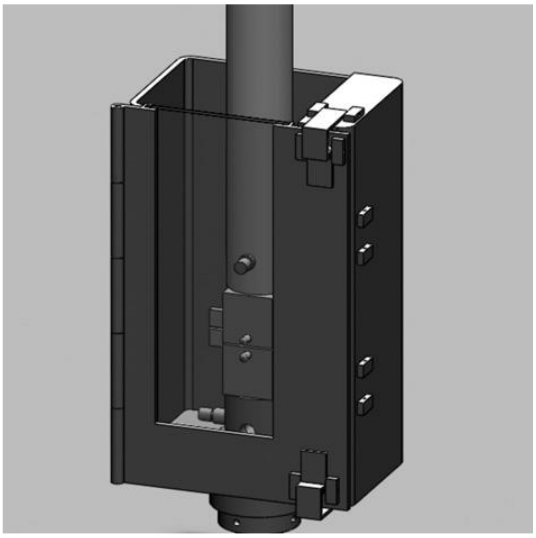

Figure 9.1 – Sketch of the chamber used during tests on DENT samples. [22]

A+P+S was principally used as active environment and the effect of sodium hypochlorite was further investigated performing some tests in the presence of H+A+P+S. Due to the relatively high capacity of the chamber (in comparison with the bags used during plane strain experiments), during the first tests on blow moulded samples, the same solution was reused to define the time required to condition at 60°C the whole system (chamber, clamping system, solution, specimen…) and to properly define the experimental procedure. After this

preliminary analysis, it was established that at least 3 hours were required to reach the thermal equilibrium and that tests had to be performed at rates lower than 0.01 mm/min to observe a significant effect of the active environment.

After the definition of the experimental protocol, tests were conducted on new specimens using every time a fresh solution. The effect of the ageing of the active environment was evaluated by comparing the results obtained from these tests and from the preliminary ones.

Due to the colour of the solutions (see Figure 6.1), video recording of the tests was not possible. However, after carrying out the tests in the presence of a colourless solution equivalent to A+P+S, which made possible the analysis of the ligament length, it was found that, as observed during tests in air, also in these tests initiation occurred at a load P_i close to the 90% of the maximum load P_{max} for blow moulded samples and at about the 96% of P_{max} for compression moulded ones. These two criteria were hence applied to determine fracture initiation during all the tests conducted in environment and the nonlinear energy release rate at initiation was evaluated according to the equations introduced in Section 5.2.2. $Log(J)$ vs. $Log(t_i)$ curves were hence obtained and compared to the relevant behaviour in air.

Even if the analysis of propagation was not possible, a huge difference between the specific load vs. displacement curves and the ligament of the samples after the test was observed, due to the presence of the active environment, as reported in Figure 9.2 and Figure 9.3, respectively. To better understand the mechanisms acting during the ESC in this stress state, therefore, initiation data were further analysed and the elastic and plastic contributions to the nonlinear energy release rate, J_{el} and J_{pl} respectively, were considered separately.

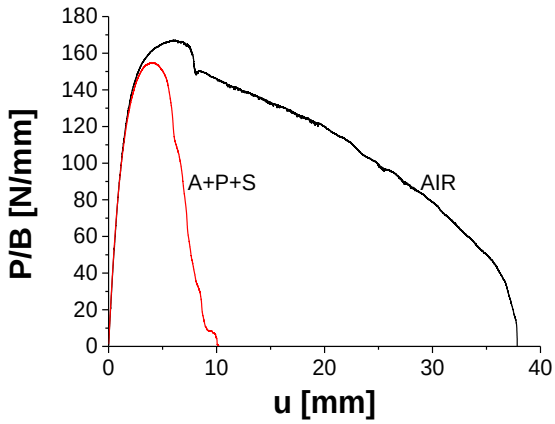

Figure 9.2 – Specific load vs. displacement curve obtained from DENT tests conducted in air and in active environment.

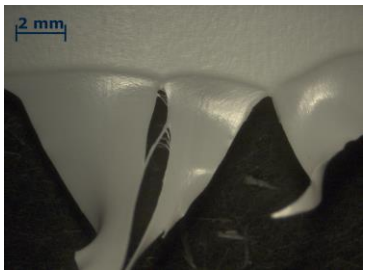

(a)

(b)

Figure 9.3 - Ligament of two samples after a fracture test (a) in air and (b) in A+P+S.

9.3 Results and discussion

The $Log(J)$ vs. $Log(t_i)$ curve of blow moulded HDPE-1 obtained in the presence the old solution is reported in Figure 9.4, together with the data obtained in air and in presence of fresh A+P+S and H+A+P+S. As can be observed from this graph the data obtained in the old environment fall to the right of those obtained in fresh solutions and this two curves are parallel. As expected, and previously reported in [70], fresh solutions are more aggressive: a lower critical interaction time t_i^* can be determined in this case, even if practically no differences are present in the critical nonlinear energy release rate at initiation J_i^* due to the very

low slope of the in air curve. On the other hand data obtained in the presence of fresh H+A+P+S fall exactly on the same curve defined in the presence of fresh A+P+S, further demonstrating that sodium hypochlorite has no effect on the environmental stress cracking of the considered materials. In light of these results, in the following no distinction will be made between the data obtained in the two fresh environments while preliminary ones obtained from the aged environment will be no longer considered.

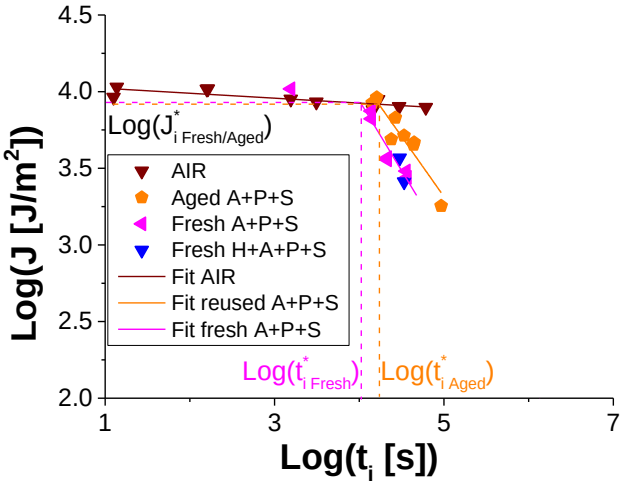

Figure 9.4 - $Log(J)$ vs. $Log(t_i)$ of blow moulded HDPE-1 tested in air, in aged and fresh A+P +S and in fresh H+A+P+S. Temperature: 60°C.

The effect of the production process on the Environmental Stress Cracking Resistance of HDPE-1 was also studied, comparing the results obtained from blow moulded (BM) and compression moulded (CM) samples, as shown in Figure 9.5.

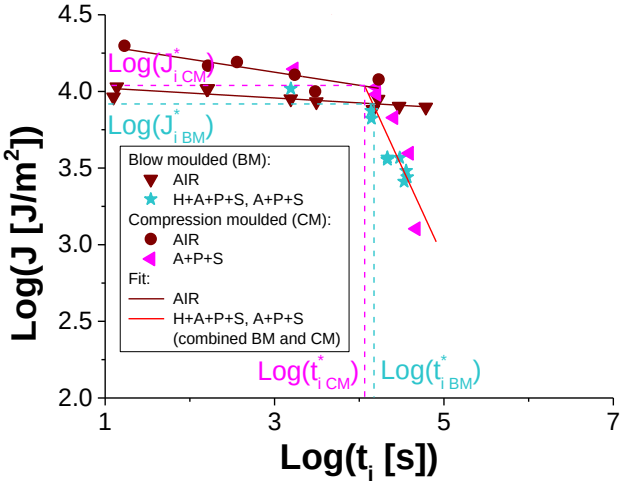

Figure 9.5 - $Log(J)$ vs. $Log(t_i)$ of blow moulded and compression moulded HDPE-1 tested in air and in fresh active environments. Temperature: 60°C.

Despite the different behaviour in air, which, as described in Chapter 5, can be related to the different crystalline content of the two kinds of samples (higher for CM), the data obtained in the active environment seem to fall on the same curve. This result can be explained considering that, as described in Chapter 2 and further discussed during the evaluation of the ESC resistance of HDPE-1 and HDPE-2 under plane strain conditions, the active environment mainly acts by favouring the disentanglement of the amorphous polymeric chains connecting the different crystalline domains. Since in this case the starting material is the same, the length of the polymeric chains is identical in BM and CM samples and, therefore, it is reasonable to expect that the same amount of energy will be required to disentangle them and promote ESC. This finding constitutes an important result during the material ranking and selection: it is possible to evaluate the ESCR of a given HDPE grade from compression moulded plates, with no need to manufacture the bottles and,

therefore, without interfering with the production line. This fact can lead to significant savings of time and money.

Due to the different behaviour in air of BM and CM samples, however, it has to be noticed that a difference in t_i^* and J_i^* exists: a higher critical interaction time and a lower critical energy release rate were measured for blow moulded HDPE-1. In this case, the difference is limited; it is reasonable to expect that it would be small also for other HDPE grades but the same could not be true for different polymers or polymer-environment systems. Therefore, without further analyses, it is suggested to use this procedure to evaluate the ESCR of HDPE grades in a range of J far enough from the critical J_i^*.

To define the deformation mechanisms mainly influenced by the presence of the active environment, the elastic and plastic contribution to the nonlinear energy release rate, respectively J_{el} and J_{pl}, were considered separately. As reported in Figure 9.6, considering the behaviour of BM and CM samples in air it is possible to observe that the elastic contribution to J is practically coincident in the two cases and that the plastic contribution is almost 3 times higher in the case of blow moulded samples and from 4 to 6 times higher for compression moulded ones.

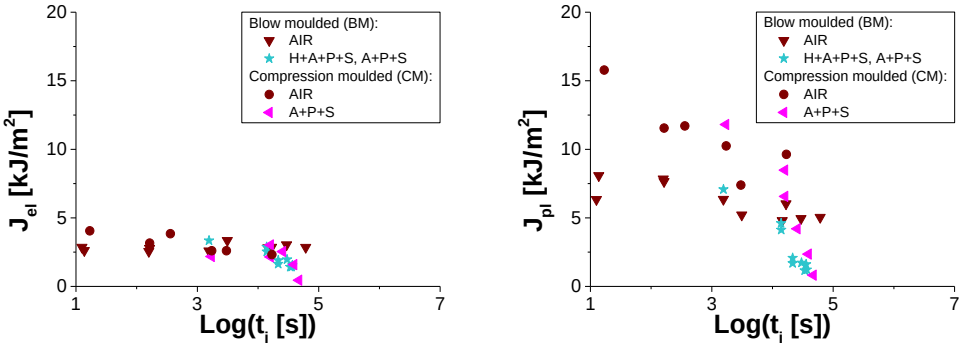

(a) (b)

Figure 9.6 – (a) elastic and (b) plastic contributions to the nonlinear energy release rate. Temperature: 60°C.

This result can be explained considering the higher crystallinity of compression moulding samples: since the ductile failure observed in air can be correlated to the fragmentation of the crystalline domains [42, 43], it is reasonable to expect that a higher energy should be required to plastically deform and break a higher amount of crystallites. On the other hand, considering the same two contributions in the environment, it is possible to notice that, for both BM and CM samples, J_{pl} considerably decreases while only minor variations are detected for what concerns J_{el}. In this case, since, as previously mentioned, the disentanglement of the tie molecules in the amorphous phase should be favoured, this mechanism should occur preferentially leading to accelerated fracture initiation with reduced deformation of the crystalline phase and, therefore, with lower required energy. Again, since the length of the polymeric chains is equal in the two cases, data obtained from CM and BM samples tested in the active environment seem to fall on the same curve both for the elastic and plastic contribution of J.

Even if the appearance of the ligament after the test should be related to propagation phenomena, the pictures previously showed in Figure 9.3 somehow validate this analysis. Specimens tested in air, in fact, display a greater extent of plastic deformation with respect to those tested in the active environments for which plastic deformation of the ligament was largely suppressed leading to a more brittle failure.

9.3.1 Effect of the stress state

The effect of the stress state was also evaluated by comparing the G-based initiation master curve of HDPE-1, introduced in Chapter 8, and the data reported in the previous Section; the assumption $J = \mathrm{G}$ was used for plane strain data since the LEFM theory is considered to be valid and, therefore, the equivalence of the two fracture parameters should hold true. In the case of plane stress fracture, to compare materials having the same degree of crystallinity, data obtained from compression moulded samples were considered to describe the behaviour in air while for the ESC curve both CM and BM data were considered since, as previously shown, they fall on the same line. The results are expressed in term of $Log(J)$ vs. $Log(t_i)$ curves in Figure 9.7 (a): from this graph, it is possible to observe that higher critical interaction time and critical energy release rate at initiation can be defined for HDPE-1 under plane stress conditions. The higher value of J_i^* measured from thin samples can be explained considering that more extensive plastic deformations can occur in this case and, as previously described in Chapter 5, fracture initiation in air will require an higher amount of energy with the relevant curve in air lying at higher J values. On the other hand, to explain the higher t_i^* one can argue that, the material is more plastically deformed under plane stress conditions leading to a more compact structure in which the active environment can diffuse more slowly.

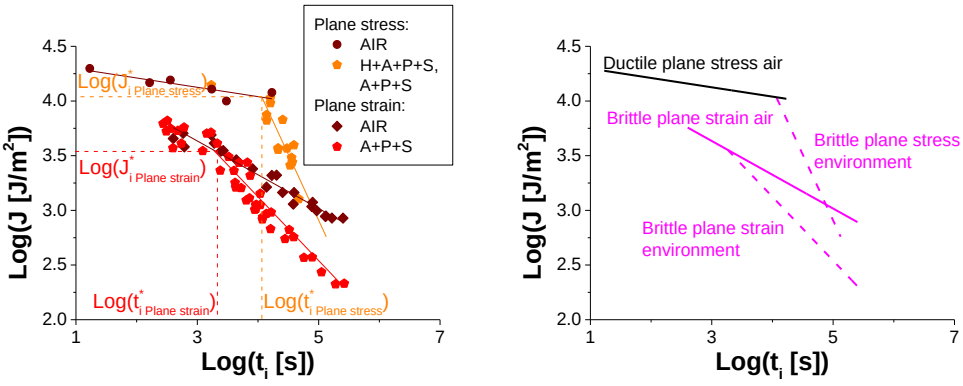

Figure 9.7 – (a) Initiation curves at 60°C of HDPE-1 in different stress states; (b) relevant failure type.

When the active environment influences the initiation behaviour of HDPE-1, however, it can be observed that the slope of the curve under plane stress condition is higher than that in plane strain meaning that the solution has a more severe effect in the first case. This fact becomes even more evident if the modified plasticisation factor $\beta_{m,i}$, defined in Section 7.3.1, is evaluated from the curves of Figure 9.7, as shown in Figure 9.8. This result can be explained considering that, under plane strain conditions, as described in Chapters 7 and 8 and highlighted in Figure 9.7 (b), the active environment starts to have an influence when the disentanglement of tie molecules is already the dominant mechanism, while in plane stress the occurrence of this mechanism prevents the complete fragmentation of the crystalline domains occurring during the fracture in air at the same rates. Therefore, in the first case the effect of the active environment is to accelerate an already occurring phenomenon, while in the latter it is the active environment itself which leads to a change in the fracture mechanism and causes a considerably more brittle failure.

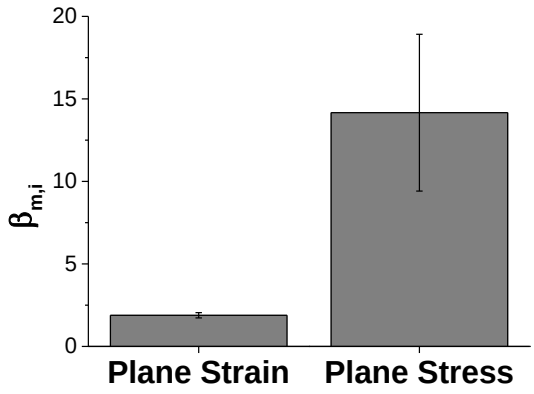

Figure 9.8 – Ratio between the slope of the initiation curve in environment and in air for the two stress state.

9.4 Conclusions

The ESC of HDPE-1 under plane stress condition has been studied and the effect of solution ageing, production process and stress state were evaluated.

Aged solutions turned out to be less aggressive than fresh ones, in accordance with [70], and, as already revealed by plane strain tests, it was further confirmed that, for this specific application, sodium hypochlorite does not influence the ESC resistance of the considered material.

Despite the different initiation behaviour in air, described in Chapter 5, environmental data obtained from samples produced via blow moulding and via compression moulding seemed to fall on the same line suggesting that the same mechanism is activated in the two cases. Considering the model proposed in [42, 43], the disentanglement of the tie molecules in the amorphous phases is the dominant phenomenon occurring during brittle failure of HDPE. Since in the two cases the base material is the same, it is reasonable to expect that, in the presence of the active environment, the same amount of energy is required to

activate this mechanism which occurs instead of a ductile failure, observed in air, governed by deformation and fragmentation of crystalline domains.

Finally, the effect of the stress state has been evaluated by comparing the results described in the previous Chapters, obtained under plane strain conditions, with those obtained in plane stress for a fixed degree of crystallinity equal to 70%. It turned out that a higher critical interaction time and critical nonlinear energy release rate were required in case of plane stress conditions. However, when ESC occurs, a higher slope of the initiation curve was observed in the latter situation meaning that, in this case, the active environment had a more severe effect. This fact can be explained considering that a relatively brittle behaviour was observed in presence of the active environment under both stress states while a ductile and a relatively brittle failure were observed in air under plain stress and plane strain condition, respectively. Therefore it can be concluded that under plane stress conditions the active environment causes a change in the fracture mechanism.

10 Concluding remarks

During this thesis the fracture behaviour of two high density polyethylene and their interaction with several aqueous solutions containing the main ingredients of a commercial bleach have been studied extensively.

The main conclusions of this work, already reported with more details in the previous Chapters, are here summarized:

- **Interaction between the commercial bleach solutions and the HDPEs:**
  - Negligible chemical interaction occurred after nine months of exposure of the two polymers to the various environments.
  - Environmental Stress Cracking (ESC) occurred mainly due to the presence of surfactants, while other bleach ingredients (sodium hypochlorite, sodium hydroxide, sodium carbonate and perfumes) had only minor or no effects on the fracture resistance of the two polymers.
- **Fracture behaviour and Environmental Stress Cracking under plane strain conditions:**
  - Despite the nonlinear behaviour revealed by tensile tests, Linear Elastic Fracture Mechanics theory seemed to be adequate to describe the behaviour of compression moulded materials under plane strain conditions. Relevant size effects were evaluated comparing the results, expressed in terms of the stress intensity factor K, from samples tested in different stress configuration and having different ligament length and thickness, finding that in the considered experimental range the measured K did not

depend on sample dimensions. The energy calibration function for the four point bending configuration was evaluated analytically and the fracture data were analysed also in terms of the energy release rate G which was computed independently from the stress intensity factor K.

- A pseudo-elastic approach was adopted to evaluate the effective modulus from the stress intensity factor and the energy release rate. For a certain temperature all the data fell on the same curve, corresponding to a unique strain level, irrespective of the applied stress intensity factor, of the fracture phase (i.e. initiation and propagation) and of the presence of the active environment. This fact implies that, for a given temperature, fracture occurred at a constant strain and that, by taking into account the strain dependence of the relaxation modulus and knowing the strain field during fracture, it should be possible to evaluate G from K or vice versa.

- The effect of temperature on fracture behaviour in air and in environment was studied: it was observed that, in both cases, a temperature change only caused a horizontal translation along the logarithmic time or crack rate axes, meaning that the equivalence condition required for the applicability of a time-temperature superposition reduction scheme was fulfilled. Fracture master curves were hence built after the evaluation of the relevant shift factors which, for each polymer, turned out to be the same irrespective of the considered propagation phase and

of the presence of the active environment: in the considered case, temperature only acted by modifying the kinetics of the fracture process, according to the material inherent viscoelasticity. This finding constitutes one of the most important results of this thesis work since, to the author's knowledge, no previous work on the applicability of the time-temperature equivalence to fracture in presence of an active environment had been reported in the relevant scientific literature. This approach could be used to extend the available experimental window and to predict the material behaviour at temperatures other than those typically adopted during Environmental Stress Cracking measurements; moreover, if verified for different polymer-environment couples, this procedure could become a valuable engineering tool during the design phase of other products.

- Using these master curves the fracture behaviour of the two polymers was compared: considering the behaviour in air, a ductile to brittle transition was observed and a change in the controlling failure mechanisms could be the reason for this transition. In accordance with the specific existing literature, for high stresses (or stress intensity factors) fracture should be governed by the fragmentation of the crystalline domains in the polymer, while at lower stresses the disentanglement of the tie molecules connecting the crystalline domains should occur leading to a more brittle failure. In presence of solutions containing surfactants, after a critical interaction time and below a critical crack growth rate, a clear reduction of the fracture

initiation time and an increase of the propagation rate was measured. Since the critical values lay in the region in which brittle initiation and propagation occurred, it was concluded that the plasticization effect of the solutions led to an acceleration of tie molecule disentanglement. Even if the sensitivity of the two materials to the environment is similar (as revealed by the variation of fracture resistance of the two materials in presence of the environment) the longer polymeric chains of HDPE-2 confers intrinsically higher fracture and environmental stress cracking resistance. For this material the critical interaction time is higher, the critical crack growth rate is lower and the ductile-brittle transition observed in air occurs at a higher time with respect to HDPE-1. A unique critical stress intensity factor was measured at the critical interaction time (or critical propagation rate) for all the temperatures and for both materials. The fracture behaviour of the two materials was evaluated also in term of the energy release rate even if in this case only the data belonging to the brittle branches of the fracture curves were considered. Also in this case it was possible to build the in air and in environment initiation and propagation master curves: a fair quantitative agreement with results obtained from the stress intensity factor analysis was found.

- **Fracture behaviour and Environmental Stress Cracking under plane stress conditions:**
  - A *J*-integral approach was adopted to describe the fracture behaviour of thin compression moulded and blow moulded samples of HDPE-1 since extensive plastic deformation was observed during these tests conducted at 60°C. This part of the analysis was limited only to the initiation phase which, for in air tests conducted at various constant displacement rates, was evaluated by measuring the uncracked ligament length from video recordings. From the relevant ligament length vs. time curves the initiation time was defined at the end of the crack blunting region: it turned out that initiation occurred at a fixed fraction of the maximum load reached during the test, irrespective of the applied displacement rate. After its validation for in environment tests, this load criterion was adopted also for the determination of initiation time in presence of the aggressive solution.
  - The behaviour in air of the material produced with the two production processes is different: the initiation curve of compression moulded samples lies at higher values of *J*. This fact can be explained considering that the compression moulding process is characterized by lower cooling rates, and therefore higher degree of crystallinity, with respect to blow moulding.
  - After a critical interaction time, when Environmental Stress Cracking occurred, a brittle failure of the material was observed.

This change in the fracture behaviour was explained considering that, as described for plane strain tests, the disentanglement of the tie molecules should be favoured by the presence of the active environment, thus preventing the complete fragmentation of the crystalline domains, typical of ductile failure in air. This explanation found an experimental validation since data obtained from compression moulded and blow moulded materials lied on the same curve meaning that the same mechanism acted during the fracture process. Since the base material is the same, the length of the polymeric chains in the two kinds of specimens and the energy required to disentangle them should be exactly the same.

- **Effect of the stress state:**
  - The fracture behaviour and the environmental stress cracking resistance under plane stress and plane strain conditions at 60°C were compared using the J-integral and the energy release rate results obtained during the previous analyses. In particular, for plane strain the equivalence between J and G was considered valid.
  - As expected, the fracture behaviour in air of compression moulded material under plane stress conditions is characterized by a higher amount of energy required for fracture initiation and a lower rate sensitivity. These facts were explained considering that extensive plastic deformation occurred under plane stress conditions, in contrast with what had been observed from the

considered plane strain data belonging to the brittle branch of the initiation curve.

- A higher critical interaction time, required to observe Environmental Stress Cracking, was measured under plane stress conditions. However, the slope of the initiation curves is higher in this case meaning that the active environment had a more severe effect. This fact was explained considering that, as previously described, under plane strain conditions the active environment only accelerated the disentanglement of the tie molecules while under plane stress conditions this mechanism was induced by the active environment itself.

The results obtained during this work demonstrate that the employed approaches provide more information with respect to the standardized ones currently adopted in the industry. Therefore, in the future, the experimental techniques here adopted could be implemented within an experimental protocol to evaluate the Environmental Stress Cracking Resistance of different high density polyethylene grades, used for the production of bleach bottles. This protocol could be used not only for ranking purposes, as with the methods employed nowadays, but also to obtain useful information for the design phase of the containers and of the contained products. Plane strain tests could be used to evaluate more precisely which ingredients are more critical for the polymer constituting the bottles or, for a certain composition of the cleaning product, to detect which grade (or polymer) is more resistant to the Environmental Stress Cracking. On the other hand, tests under plane stress conditions could be used to obtain information regarding the behaviour of the material operating in a

stress state similar to that of the final product. To complete this work, anyway, some further analyses are required especially to define the temperature dependence of the fracture behaviour under plane stress conditions and to evaluate the effect of different compositions of cleaning products (e.g. surfactant type and concentration) on the fracture behaviour of the two HDPEs here considered. Once completed these analyses, the results obtained during this work could constitute the basis of a numerical model which could be used as an extremely valuable design tool to predict the service life of a container knowing the in air and relevant environment mechanical behaviour of the polymer and the loading conditions.

On a side note, a first step towards modelling of the material deformation during complex loading histories was done during this work. The results here obtained could be used as a basis for further analyses which are required to fully understand the material deformation behaviour.

References

[1] Hassinen, J.: Deterioration of polyethylene pipes exposed to chlorinated water. *Polymer Degradation and Stability*, vol. 84, pp. 261–267, 2004.

[2] Choi, B.H., Zhou, Z., Chudnovsky, A., Stivala, S.S., Sehanobish, K., Bosnyak, C.P.: Fracture initiation associated with chemical degradation: Observation and modeling. *International Journal of Solids and Structures*, vol. 42, no. 2, pp. 681–695, 2005.

[3] Beholz, L.G., Aronson, C.L., Zand, A.: Adhesion modification of polyolefin surfaces with sodium hypochlorite in acidic media. *Polymer*, vol. 46, pp. 4604–4613, 2005.

[4] Castillo Montes, J., Cadoux, D., Creus, J., Touzain, S., Gaudichet-Maurin, E., Correc, O.: Ageing of polyethylene at raised temperature in contact with chlorinated sanitary hot water. Part I - Chemical aspects. *Polymer Degradation and Stability*, vol. 97, no. 2, pp. 149–157, 2012.

[5] Chan, M.K. V, Williams, J.G.: Slow stable crack growth in high density polyethylenes. *Polymer*, vol. 24, no. 2, pp. 234–244, 1983.

[6] Tonyali, K., Brown, H.R.: Effects of detergent concentration and ethylene oxide chain length of the detergent molecule on stress-cracking of low-density polyethylene. *Journal of Materials Science*, vol. 22, no. 9, pp. 3287–3292, 1987.

[7] Rink, M., Frassine, R., Mariani, P., Carianni, G.: *Effects of detergent on crack initiation and propagation in polyethylenes*. In: Fracture of Polymers, Composites and Adhesives II (Editors: B. R. K. Blackman et al.). Elsevier, 2003, pp. 103–114.

[8] *ISO 22088-2: Plastics — Determination of resistance to environmental stress cracking (ESC) — Part 2: Constant tensile load method*. 2006.

[9] *ISO 22088-3: Plastics — Determination of resistance to environmental stress cracking (ESC) — Part 3: Bent strip method*. 2006.

[10] *ISO 22088-4: Plastics — Determination of resistance to environmental stress cracking (ESC) — Part 4: Ball or pin impression method*. 2006.

[11] *ISO 22088-5: Plastics — Determination of resistance to environmental stress cracking (ESC) — Part 5: Constant tensile deformation method*. 2006.

[12] *ISO 22088-6: Plastics — Determination of resistance to environmental stress cracking (ESC) — Part 6: Slow strain rate method*. 2006.

[13] *ISO 16770: Plastics — Determination of environmental stress cracking (ESC) of polyethylene — Full-notch creep test (FNCT) P*. 2004.

[14] *IEC 60811-4-1: Insulating and sheathing materials of electric and optical cables – Common test methods – Part 4-1: Methods specific to polyethylene and polypropylene compounds – Resistance to environmental stress cracking – Measurement of the melt flow in*. 2004.

[15] *ASTM D2561-95: Standard test method for environmental stress-crack resistance of blow-molded polyethylene containers*. 2001.

[16] *ASTM D1693-15: Standard test method for environmental stress-cracking of ethylene plastics*. 2015.

[17] *ASTM F2136-08: Standard test method for notched , constant ligament-stress (NCLS) test to determine slow-crack-growth resistance of HDPE resins or HDPE corrugated pipe*. 2015.

[18] Williams, J.G., Marshall, G.P.: Environmental crack and craze growth phenomena in polymers. *Proceedings of the Royal Society of London. Series A, Mathematical and Physical Sciences*, vol. 342, no. 1628, pp. 55–77, 1975.

[19] Tonyali, K., Brown, H.R.: On the applicability of linear elastic fracture mechanics to environmental stress cracking of low-density polyethylene. *Journal of Materials Science*, vol. 21, no. 9, pp. 3116–3124, 1986.

[20] Moskala, E.J.: A fracture mechanics approach to environmental stress cracking in poly(ethyleneterephthalate). *Polymer*, vol. 39, no. 3, pp. 675–680, 1998.

[21] Tonyali, K., Rogers, C.E., Brown, H.R.: Stress-cracking of polyethylene in organic liquids. *Polymer*, vol. 28, no. 9, pp. 1472–1477, 1987.

[22] Andena, L., Castellani, L., Castiglioni, A., Mendogni, A., Rink, M., Sacchetti, F.: Determination of environmental stress cracking resistance of polymers: Effects of loading history and testing configuration. *Engineering Fracture Mechanics*, vol. 101, pp. 33–46, 2013.

[23] Kamaludin, M.A., Patel, Y., Blackman, B.R.K., Williams, J.G.: Fracture mechanics testing for environmental stress cracking in thermoplastics. *Procedia Structural Integrity*, vol. 2, pp. 227–234, 2016.

[24] Kamaludin, M.A.: *Characterising the environmental stress cracking behaviour of thermoplastics: a fracture mechanics approach*. Imperial College London, 2017.

[25] Contino, M., Andena, L., Rink, M., Colombo, A., Marra, G.: Fracture of high-density polyethylene used for bleach bottles. *Procedia Structural Integrity*, vol. 2, pp. 213–220, 2016.

[26] Contino, M., Andena, L., Rink, M., Marra, G., Resta, S.: Time-temperature equivalence in environmental stress cracking of high-density polyethylene. *Engineering Fracture Mechanics*, 2018. https://doi.org/10.1016/j.engfracmech.2018.04.034

[27] Contino, M., Andena, L., Rink, M., Marra, G., Resta, S.: *Environmental stress cracking of thin high density polyethylene samples*. In: DYFP2018 Book of Abstract (Editors: A. J. Crosby and L. E. Govaert). Rolduc Abbey, Kerkrade, the Netherlands, 2018, pp. 271–274.

[28] Contino, M., La Valle, V., Andena, L., Rink, M., Marra, G., Resta, S.: *A comparison between K and G approaches for a viscoelastic material : the case of environmental stress cracking of HDPE.*. In: MTDM2018 Book of Abstracts (Editors: F. Briatico-Vangosa and C. Marano). Politecnico di Milano, Milano, 2018, pp. 25-26.

[29] Maida, S., Moletti, C., Perletti, M., Senna, S., Villa, F.: *Caratterizzazione del comportamento meccanico in aria di HDPE*. Politecnico di Milano, 2016.

[30] Colombo, A.: *Environmental stress cracking of high density polyethylene packages*. Politecnico di Milano, 2015.

[31] La Valle, V.: *Linear elastic fracture mechanics approach to evaluate environmental stress cracking resistance of HDPE*. Politecnico di Milano, 2017.

[32] Reinhardt, G., Borchers, G.: *Application of Bleaching detergent formulations*. In: Handbook of detergents Part E: Applications (Editor: U. Zoller). Boca Raton: CRC Press, 2009, pp. 375–418.

[33] Croud, V.: *Oxygen bleaches*. In: Handbook of detergents Part A: Properties (Editor: G. Broze). Boca Raton: CRC Press, 1999, pp. 597–617.

[34] Smith, W.L.: *Inorganic bleaches: production of hypochlorite*. In: Handbook of detergents Part F: Production (Editor: U. Zoller). Boca Raton: CRC Press, 2009, pp. 435–472.

[35] Church, J.A.: *Hypochlorite bleach*. In: Handbook of detergents Part A: Properties (Editor: G. Broze). Boca Raton: CRC Press, 1999, pp. 619–629.

[36] Bühler-Vidal, J.O.: *The business of polyethylene*. In: Handbook of industrial polyethylene and technology: definitive guide to manufacturing, properties, processing, applications and markets set (Editors: M. A. Spalding and A. Chatterjee). John Wiley & Sons, 2017, pp. 1297–1330.

[37] Klimesch, R., Littmann, D., Mähling, F.-O.: *Polyethylene : high-pressure*. Pergamon, 2001, pp. 7181–7184.

[38] Enderle, H.F.: *Polyethylene: high-density*. Pergamon, 2001, pp. 7172–7181.

[39] Sardashti, A.: *Methodologies for obtaining reliable indicators for the environmental stress cracking resistance of polyethylene*. University of Waterloo, 2014.

[40] Keller, A.: Polymer crystals. *Reports on Progress in Physics*, vol. 31, pp. 623–704, 1968.

[41] Mandelkern, L., Alamo, R.G., Kennedy, M.A.: Interphase thickness of linear polyethylene. *Macromolecules*, vol. 23, no. 21, pp. 4721–4723, 1990.

[42] Lustiger, A., Markham, L.: Importance of tie molecules in preventing polyethylene fracture under long-term loading conditions. *Polymer*, vol. 24, no. 12, pp. 1647–1654, 1983.

[43] Lustiger, A.: *Environmental stress cracking: the phenomenon and its utility*. In: Failure of plastics (Editors: W. Brostow and R. D. Corneliussen). Munich, Vienna, New York: Hanser Publishers, 1986, pp. 305–329.

[44] Cheng, J.J., Polak, M.A., Penlidis, A.: Influence of micromolecular structure on environmental stress cracking resistance of high density polyethylene. *Tunnelling and Underground Space Technology*, vol. 26, no. 4, pp. 582–593, 2011.

[45] Bartczak, Z., Galeski, A.: Plasticity of semicrystalline polymers. *Macromolecular Symposia*, vol. 294, no. 1, pp. 67–90, 2010.

[46] Plummer, C.J.., Goldberg, A., Ghanem, A.: Micromechanisms of slow crack growth in polyethylene under constant tensile loading. *Polymer*, vol. 42, no. 23, pp. 9551–9564, 2001.

[47] Brown, N., Ward, I.M.: The influence of morphology and molecular weight on ductile-brittle transitions in linear polyethylene. *Journal of Materials Science*, vol. 18, no. 5, pp. 1405–1420, 1983.

[48] Huang, Y.-L., Brown, N.: The effect of molecular weight on slow crack growth in linear polyethylene homopolymers. *Journal of Materials Science*, vol. 23, pp. 3648–3655, 1988.

[49] Brown, N., Lu, X., Huang, Y., Harrison, I.P., Ishikawa, N.: The fundamental material parameters that govern slow crack growth in linear polyethylenes. *Plastics Rubber and Composites Processing and Applications*, vol. 17, no. 4, pp. 255–258, 1992.

[50] Huang, Y., Brown, N.: The dependence of butyl branch density on slow crack growth in polyethylene: kinetics. *Journal of Polymer Science Part B: Polymer Physics*, vol. 28, no. 11, pp. 2007–2021, 1990.

[51] Lundbäck, M., Hassinen, J., Andersson, U., Fujiwara, T., Gedde, U.W.: Polybutene-1 pipes exposed to pressurized chlorinated water: Lifetime and antioxidant consumption. *Polymer Degradation and Stability*, vol. 91, no. 4, pp. 842–847, 2006.

[52] Castagnetti, D., Scir Mammano, G., Dragoni, E.: Effect of chlorinated water on the oxidative resistance and the mechanical strength of polyethylene pipes. *Polymer Testing*, vol. 30, no. 3, pp. 277–285, 2011.

[53] X. Colin, J. Verdu, B.R.: Stabilizer Thickness Profiles in Polyethylene Pipes Transporting Drinking Water Disinfected by Bleach. *Polymer Engineering & Science*, vol. 47, pp. 1541–1549, 2011.

[54] Ettori, A., Gaudichet-Maurin, E., Schrotter, J.C., Aimar, P., Causserand, C.: Permeability and chemical analysis of aromatic polyamide based membranes exposed to sodium hypochlorite. *Journal of Membrane Science*, vol. 375, no. 1–2, pp. 220–230, 2011.

[55] Whelton, A.J., Dietrich, A.M., Gallagher, D.L.: Impact of chlorinated water exposure on contaminant transport and surface and bulk properties of high-density polyethylene and cross-linked polyethylene potable water pipes. *Journal of Environmental Engineering*, vol. 137, no. 7, pp. 559–568, 2011.

[56] Valadez-Gonzalez, A., Cervantes-Uc, J.M., Veleva, L.: Mineral filler influence on the photo-oxidation of high density polyethylene: I. Accelerated UV chamber exposure test. *Polymer Degradation and Stability*, vol. 63, no. 2, pp. 253–260, 1999.

[57] Guadagno, L., Naddeo, C., Vittoria, V., Camino, G., Cagnani, C.: Chemical and morphologial modifications of irradiated linear low density polyethylene (LLDPE). *Polymer Degradation and Stability*, vol. 72, pp. 175–186, 2001.

[58] Gulmine, J. V., Janissek, P.R., Heise, H.M., Akcelrud, L.: Degradation profile of polyethylene after artificial accelerated weathering. *Polymer Degradation and Stability*, vol. 79, no. 3, pp. 385–397, 2003.

[59] Mendes, L.C., Rufino, E.S., De Paula, F.O.C., Torres, A.C.: Mechanical, thermal and microstructure evaluation of HDPE after weathering in Rio de Janeiro City. *Polymer Degradation and Stability*, vol. 79, no. 3, pp. 371–383, 2003.

[60] Valadez-González, A., Veleva, L.: Mineral filler influence on the photo-oxidation mechanism degradation of high density polyethylene. Part II: Natural exposure test. *Polymer Degradation and Stability*, vol. 83, no. 1, pp. 139–148, 2004.

[61] Richards, R.B.: The phase equilibria between a crystalline polymer and solvents. *Transactions of the Faraday Society*, vol. 42, pp. 10-28, 1946.

[62] Lustiger, A., Markham, R.L., Epstein, M.M.: Environmental stress crack growth in medium-density polyethylene pipe. *Journal of Applied Polymer Science*, vol. 26, no. 3, pp. 1049–1056, 1981.

[63] Belcher, J.L., Brown, H.R.: Crack branching and arrest in environmental cracking of polyethylene. *Journal of Materials Science*, vol. 21, pp. 717–724, 1986.

[64] Lustiger, A., Corneliussen, R.D.: The role of crazes in the crack growth of polyethylene. *Journal of Materials Science*, vol. 22, no. 7, pp. 2470–2476, 1987.

[65] Chang, P., Donovan, J.A.: Crack size independence of the crack driving force in the buckled plate specimen. *Journal of Materials Science*, vol. 24, no. 3, pp. 816–820, 1989.

[66] Ward, A.L., Lu, X., Huang, Y., Brown, N.: The mechanism of slow crack growth in polyethylene by an environmental stress cracking agent. *Polymer*, vol. 32, no. 12, pp. 2172–2178, 1991.

[67] Lu, X., Zhou, Z., Brown, N.: A Sensitive Mechanical Test for Slow Crack Growth in Polyethylene. *Polymer Engineering & Science*, vol. 37, no. 11, pp. 1896–1900, 1997.

[68] Fleissner, M.: Experience With a Full Notch Creep Test in Determining the Stress Crack Performance of Polyethylenes. *Polymer Engineering & Science*, vol. 38, no. 2, pp. 330–340, 1998.

[69] Ayyer, R., Hiltner, A., Baer, E.: A fatigue-to-creep correlation in air for application to environmental stress cracking of polyethylene. *Journal of Materials Science*, vol. 42, no. 16, pp. 7004–7015, 2007.

[70] Pinter, G., Haager, M., Lang, R.W.: Influence of nonylphenol-polyglycol-ether environments on the results of the full notch creep test. *Polymer Testing*, vol. 26, no. 6, pp. 700–710, 2007.

[71] Ayyer, R., Hiltner, A., Baer, E.: Effect of an environmental stress cracking agent on the mechanism of fatigue and creep in polyethylene. *Journal of Materials Science*, vol. 43, no. 18, pp. 6238–6253, 2008.

[72] Choi, B.-H., Weinhold, J., Reuschle, D., Kapu, M.: Modeling of the Fracture Mechanism of HDPE Subjected to Environmental Stress Crack Resistance Test. *Polymer Engineering and Science*, vol. 49, no. 11, pp. 2085–2091, 2009.

[73] Schilling, M., Niebergall, U., Böhning, M.: Full notch creep test (FNCT) of PE-HD – Characterization and differentiation of brittle and ductile fracture behavior during environmental stress cracking (ESC). *Polymer Testing*, vol. 64, pp. 156–166, 2017.

[74] Andena, L., Castellani, L., Castiglioni, A., Mendogni, A., Rink, M., Sacchetti, F., Adib, A.: *Environmental crack initiation and propagation in polyethylene under different loading conditions*. In: Proceedings of the 15th International Conference on Deformation, Yield and Fracture of Polymers. 2012, pp. 182–185.

[75] A. Sharif, N. Mohammadi, S.R.G.: Model Prediction of the ESCR of Semicrystalline Polyethylene: Effects of Melt Cooling Rate. *Journal of Applied Polymer Science*, vol. 112, no. 6, pp. 3249–3256, 2009.

[76] Lagarón, J.M., Pastor, J.M., Kip, B.J.: Role of an active environment of use in an environmental stress crack resistance (ESCR) test in stretched polyethylene: A vibrational spectroscopy and a SEM study. *Polymer*, vol. 40, no. 7, pp. 1629–1636, 1999.

[77] Lagarón, J.M., Capaccio, G., Rose, L.J., Kip, B.J.: Craze morphology and molecular orientation in the slow crack growth failure of polyethylene. *Journal of Applied Polymer Science*, vol. 77, no. 2, pp. 283–296, 2000.

[78] Kurelec, L., Teeuwen, M., Schoffeleers, H., Deblieck, R.: Strain hardening modulus as a measure of environmental stress crack resistance of high density polyethylene. *Polymer*, vol. 46, no. 17, pp. 6369–6379, 2005.

[79] Men, Y.F., Rieger, J., Enderle, H.F., Lilge, D.: The mobility of the amorphous phase in polyethylene as a determining factor for slow crack growth. *European Physical Journal E*, vol. 15, no. 4, pp. 421–425, 2004.

[80] Munaro, M., Akcelrud, L.: Polyethylene blends: A correlation study between morphology and environmental resistance. *Polymer Degradation and Stability*, vol. 93, no. 1, pp. 43–49, 2008.

[81] Cazenave, J., Sixou, B., Seguela, R.: Structural approaches of polyethylene environmental stress-crack resistance. *Oil & Gas Science and Technology*, vol. 61, no. 6, pp. 735–742, 2006.

[82] Cazenave, J., Seguela, R., Sixou, B., Germain, Y.: Short-term mechanical and structural approaches for the evaluation of polyethylene stress crack resistance. *Polymer*, vol. 47, no. 11, pp. 3904–3914, 2006.

[83] Schoeffl, P.F., Bradler, P.R., Lang, R.W.: Yielding and crack growth testing of polymers under severe liquid media conditions. *Polymer Testing*, vol. 40, pp. 225–233, 2014.

[84] Yarysheva, A.Y., Rukhlya, E.G., Yarysheva, L.M., Bagrov, D. V., Volynskii, A.L., Bakeev, N.F.: The structural evolution of high-density polyethylene during crazing in liquid medium. *European Polymer Journal*, vol. 66, pp. 458–469, 2015.

[85] Andena, L., Rink, M., Marano, C., Briatico-Vangosa, F., Castellani, L.: Effect of processing on the environmental stress cracking resistance of high-impact polystyrene. *Polymer Testing*, vol. 54, pp. 40–47, 2016.

[86] Altstaedt, V., Keiter, S., Renner, M., Schlarb, A.: Environmental stress cracking of polymers monitored by fatigue crack growth experiments. *Macromolecular Symposia*, vol. 214, pp. 31–46, 2004.

[87] Kamaludin, M.A., Patel, Y., Williams, J.G., Blackman, B.R.K.: A fracture mechanics approach to characterising the environmental stress cracking behaviour of thermoplastics. *Theoretical and Applied Fracture Mechanics*, vol. 92, pp. 373–380, 2017.

[88] Arnold, J.C.: The influence of liquid uptake on environmental stress cracking of glassy polymers. *Materials Science and Engineering: A*, vol. 197, no. 1, pp. 119–124, 1995.

[89] Arnold, J.C.: The effects of diffusion on environmental stress crack initiation in PMMA. *Journal of Materials Science*, vol. 33, pp. 5193–5204, 1998.

[90] Higuchi, Y.: Observation of environmental stress cracking in polymethylmethacrylate by using the chemiluminescence method. *Materials Sciences and Applications*, vol. 6, pp. 1084–1088, 2015.

[91] Jansen, J.A.: Environmental stress cracking – the plastic killer. *Advanced Materials & Processes*, vol. 162, no. 7, pp. 50–53, 2004.

[92] Williams, J.G.: *Fracture mechanics of polymers*. Chichester: Limited, Ellis Horwood, 1984.

[93] Chang, P., Donovan, J.A.: Detergent assisted stress cracking in low density polyethylene. *Polymer Engineering & Science*, vol. 30, no. 22, pp. 1431–1441, 1990.

[94] DeCoste, J.B., Malm, F.S., Wallder, V.T.: Cracking of stressed polyethylene: effect of chemical environment. *Industrial and Engineering Chemistry*, vol. 43, no. 1, pp. 117–121, 1951.

[95] Frayer, P.D., Tong, P.P.-L., Dreher, W.W.: The role of intercrystalline links in the environmental stress cracking of high density polyethylene. *Polymer Engineering & Science*, vol. 17, no. 1, pp. 27–31, 1977.

[96] Brown, N.: A theory of the environmental stress cracking of polyethylene. *Polymer*, vol. 19, no. 10, pp. 1186–1188, 1978.

[97] Lustiger, A., Corneliusen, R.D.: The effect of an environmental stress cracking agent on interlamellar links in polyethylene. *Journal of Polymer Science Part B: Polymer Physics*, vol. 24, no. 7, pp. 1625–1629, 1986.

[98] Lagaron, J.M., Dixon, N.M., Reed, W., Pastor, J.M., Kip, B.J.: Morphological characterisation of the crystalline structure of cold- drawn HDPE used as a model material for the environmental stress cracking (ESC) phenomenon. *Polymer*, vol. 40, pp. 2569–2586, 1999.

[99] Isaksen, R.A., Newman, S., Clarck, R.J.: Mechanism of environmental stress cracking in linear polyethylene. *Journal of Applied Polymer Science*, vol. 7, no. 2, pp. 515–531, 1963.

[100] Deblieck, R.A.C., Van Beek, D.J.M., Remerie, K., Ward, I.M.: Failure mechanisms in polyolefines: The role of crazing, shear yielding and the entanglement network. *Polymer*, vol. 52, no. 14, pp. 2979–2990, 2011.

[101] Kambour, R.P., Romagosa, E.E., Gruner, C.L.: Swelling, Crazing, and Cracking of an Aromatic Copolyether-S'ulfone in Organic Media. *Moacromolecules*, vol. 5, no. 4, pp. 335–340, 1972.

[102] Kambour, R.P., Gruner, C.L., Romagosa, E.E.: Solvent crazing of "dry" polystyrene and "dry" crazing of plasticized polystyrene. *Journal of Polymer Science. Part B: Polymer Physics*, vol. 11, no. 10, pp. 1879–1890, 1973.

[103] Jacques, C.H.M., Wyzgoski, M.G.: Prediction of environmental stress cracking of polycarbonate from solubility considerations. *Journal of Applied Polymer Science*, vol. 23, no. 4, pp. 1153–1166, 1979.

[104] Mai, Y.W.: Environmental stress cracking of glassy polymers and solubility parameters. *Journal of materials science*, vol. 21, no. 3, pp. 904–916, 1986.

[105] Hansen, C.M.: On predicting environmental stress cracking in polymers. *Polymer Degradation and Stability*, vol. 77, no. 1, pp. 43–53, 2002.

[106] Nielsen, T.B., Hansen, C.M.: Surface wetting and the prediction of environmental stress cracking (ESC) in polymers. *Polymer Degradation and Stability*, vol. 89, no. 3, pp. 513–516, 2005.

[107] Robledo, N., Domínguez, C., García-Muñoz, R.A.: Alternative accelerated and short-term methods for evaluating slow crack growth in polyethylene resins with high crack resistance. *Polymer Testing*, vol. 62, pp. 366–372, 2017.

[108] O'Connell, P.A., Bonner, M.J., Duckett, R.A., Ward, I.M.: The relationship between slow crack propagation and tensile creep behaviour in polyethylene. *Polymer*, vol. 36, no. 12, pp. 2355–2362, 1995.

[109] O'Connell, P.A., Bonner, M.J., Duckett, R.A., Ward, I.M.: Effect of molecular weight and branch content on the creep behavior of oriented polyethylene. *Journal of Applied Polymer Science*, vol. 89, no. 6, pp. 1663–1670, 2003.

[110] Nezbedová, E., Hutař, P., Zouhar, M., Knésl, Z., Sadílek, J., Náhlík, L.: The applicability of the Pennsylvania Notch Test for a new generation of PE pipe grades. *Polymer Testing*, vol. 32, no. 1, pp. 106–114, 2013.

[111] Hosoda, S., Uemura, A.: Effect of the structural distribution on the mechanical properties of linear low-density polyethylenes. *Polymer Journal*, vol. 24, no. 9, pp. 939–949, 1992.

[112] Gueugnaut, D., Rousselot, D.: Detection of divergences in polyethylene resins fabrication by means of the modified stepwise isothermal segregation technique. *Journal of Applied Polymer Science*, vol. 73, no. 11, pp. 2103–2112, 1999.

[113] Huang, Y. L., Brown, N.: Dependence of slow crack growth in polyethylene on butyl branch density: Morphology and theory. *Journal of Polymer Science Part B: Polymer Physics*, vol. 29, no. 1, pp. 129–137, 1991.

[114] Brown, N., Lu, X., Huang, Y., Qian, R.: Slow crack growth in polyethylene-a review. *Macromolecular Symposia*, vol. 41, no. 1, pp. 55–67, 1991.

[115] Griffith, A.A.: The Phenomena of Rupture and Flow in Solids. *Phylosophical Transaction, Series A*, vol. 221, pp. 163–198, 1920.

[116] Irwin, G.R.: *Fracture dynamics*. In: Fracturing of metals. Cleveland: American Society for Metals, 1948, pp. 147–166.

[117] Irwin, G.R.: Onset of fast crack propagation in high strength steel and aluminum alloys. *Sagamore Research Conference Proceedings*, vol. 2, pp. 289–305, 1956.

[118] Westergaard, H.M.: Bearing pressures and cracks. *Journal of Applied Mechanics*, vol. 6, no. 2, pp. A49–A53, 1939.

[119] Irwin, G.R.: Analysis of stresses and strains near the end of a crack traversing a plate. *Journal of Applied Mechanics-Transactions of the ASME*, vol. E24, pp. 351–369, 1957.

[120] Irwin, G.R.: Plastic zone near a crack and fracture toughness. *Sagamore Research Conference Proceedings*, pp. 4–63, 1961.

[121] Barenblatt, G.I.: The mathematical theory of equilibrium cracks in brittle fracture. *Advances in Applied Mechanics*, vol. 7, pp. 55–129, 1962.

[122] Dugdale, D.S.: Yielding of steel sheets containing slits. *Journal of the Mechanics and Physics of Solids*, vol. 8, no. 2, pp. 100–104, 1960.

[123] Rice, J.R.: A path independent integral and the approximate analysis of strain concentration by notches and cracks. *Journal of Applied Mechanics*, vol. 35, pp. 379–386, 1968.

[124] Bradley, W., Cantwell, W.J., Kausch, H.H.: Viscoelastic Creep Crack Growth: A review of fracture mechanical analyses. *Mechanics of Time-Dependent Materials*, vol. 1, pp. 241–268, 1998.

[125] Frassine, R., Rink, M., Leggio, a., Pavan, a.: Experimental analysis of viscoelastic criteria for crack initiation and growth in polymers. *International Journal of Fracture*, vol. 81, no. 1, pp. 55–75, 1996.

[126] Schapery, R.A.: A theory of crack initiation and growth in viscoelastic media I. theoretical development. *International Journal of Fracture*, vol. 11, no. 1, pp. 141–159, 1975.

[127] Schapery, R. a.: A theory of crack initiation and growth in viscoelastic media II. Approximate methods of analysis. *International Journal of Fracture*, vol. 11, no. 3, pp. 369–388, 1975.

[128] Schapery, R.A.: A theory of crack initiation and growth in viscoelastic media III. Analysis of continuous growth. *International Journal of Fracture*, vol. 11, no. 4,
pp. 549–562, 1975.

[129] Williams, J.G.: *Fracture mechanics of anisotropic materials*. In: Application of fracture mechanics to composite materials (Editor: K. Friedrich). Amsterdam: Elsevier, 1989, pp. 3–38.

[130] Kies, J.A., Irwin, G.R.: Critical energy release rate analysis of fracture strength. *Welding Journal Research Supplement*, vol. 33, pp. 193–198, 1954.

[131] Anderson, T.L.: *Fracture mechanics, fundamentals and applications*. Boca Raton (Florida,U.S.A.), 1995.

[132] Andena, L., Rink, M., Frassine, R., Corrieri, R.: A fracture mechanics approach for the prediction of the failure time of polybutene pipes. *Engineering Fracture Mechanics*, vol. 76, no. 18, pp. 2666–2677, 2009.

[133] Rice, J.R.: *Mathematical analysis in the mechanics of fracture*. In: Fracture: An Advanced Treatise (Editor: H. Liebowitz). New York: Academic Press, 1968, pp. 191–311.

[134] Begley, J.A., Landes, J.D.: *The J-integral as a fracture criterion*. In: ASTM STP 514. Philadelphia: American Society for Testing and Materials, 1972, pp. 1–23.

[135] Landes, J.D., Begley, J.A.: *The Effect of specimen geometry on* J^{Ic}. In: ASTM STP 514. Philadelphia: American Society for Testing and Materials, 1972, pp. 24–29.

[136] Rice, J.R., Paris, P.C., Merkle, J.G.: *Some further results of J-integral analysis and estimates*. In: ASTM STP 536 - Progress in flaw growth and fracture toughness testing. Philadelphia: American Society for Testing and Materials, 1973, pp. 231–245.

[137] Sumpter, J.D.C., Turner, C.E.: *Method for laboratory determination of Jc*. In: ASTM STP 601. Philadelphia: American Society for Testing and Materials, 1976, pp. 3–18.

[138] Sharobeam, M.H., Landes, J.D.: The load separation criterion and methodology in ductile fracture mechanics. *International Journal of Fracture*, vol. 47, no. 2, pp. 81–104, 1991.

[139] Sharobeam, M.H., Landes, J.D.: The load separation and ηpl development in precracked specimen test recordsdevelopment in precracked specimen test records. *International Journal of Fracture*, vol. 59, no. 3, pp. 213–226, 1993.

[140] Bernal, C.R.; Montemartini, P.E.; Frontini, P.M..: The Use of Load Separation Criterion and Normalization Method in Ductile Fracture Characterization of Thermoplastic Polymers. *Journal of Polymer Science*, vol. 34, pp. 1869–1880, 1996.

[141] Bernal, C., Cassanelli, A., Frontini, P.: On the applicability of the load separation criterion to acrylonitrile/butadiene/styrene terpolymer resins. *Polymer*, vol. 37, no. 18, pp. 4033–4039, 1996.

[142] Wainstein, J., Frontini, P.M., Cassanelli, A.N.: J-R curve determination using the load separation parameter Spb method for ductile polymers. *Polymer Testing*, vol. 23, no. 5, pp. 591–598, 2004.

[143] Baldi, F., Riccò, T.: High-rate J-testing of toughened polyamide 6/6: Applicability of the load separation criterion and the normalization method. *Engineering Fracture Mechanics*, vol. 72, no. 14, pp. 2218–2231, 2005.

[144] Baldi, F., Agnelli, S., Riccò, T.: On the applicability of the load separation criterion in determining the fracture resistance (JIc) of ductile polymers at low and high loading rates. *International Journal of Fracture*, vol. 165, no. 1, pp. 105–119, 2010.

[145] Frontini, P.M., Fasce, L.A., Rueda, F.: Non linear fracture mechanics of polymers: Load Separation and Normalization methods. *Engineering Fracture Mechanics*, vol. 79, pp. 389–414, 2012.

[146] Baldi, F., Agnelli, S., Riccò, T.: On the determination of the point of fracture initiation by the load separation criterion in J-testing of ductile polymers. *Polymer Testing*, vol. 32, no. 8, pp. 1326–1333, 2013.

[147] Agnelli, S., Baldi, F., Blackman, B.R.K., Castellani, L., Frontini, P.M., Laiarinandrasana, L., Pegoretti, A., Rink, M., Salazar, A., Visser, H.A.: Application of the load separation criterion in J-testing of ductile polymers: A round-robin testing exercise. *Polymer Testing*, vol. 44, pp. 72–81, 2015.

[148] Agnelli, S., Baldi, F., Castellani, L., Pisoni, K., Vighi, M., Laiarinandrasana, L.: Study of the plastic deformation behaviour of ductile polymers: use of the material key curves. *Mechanics of Materials*, vol. 117, pp. 105–115, 2018.

[149] Marshall, G.P., Culver, L.E., Williams, J.G.: Environmental stress crack growth in low-density polyethylenes. *Plastics & Polymers*, vol. 38, no. 134, pp. 95–101, 1970.

[150] Marshall, G.P., Coutts, L.H., Williams, J.G.: Temperature effects in the fracture of PMMA. *Journal of Materials Science*, vol. 9, no. 9, pp. 1409–1419, 1974.

[151] Chan, M.K. V: *Fracture toughness testing and slow crack growth in polyethylenes*. Imperial College of Science & Technology, 1982.

[152] Chang, P., Donovan, J.A.: Crack size independence of the crack driving force in the buckled plate specimen. *Journal of Materials Science*, vol. 24, no. 3, pp. 816–820, 1989.

[153] Mariani, P., Frassine, R., Rink, M., Pavan, A.: Viscoelasticity of Rubber-Toughened Poly(Methyl Methacrylate). Part II: Fracture Behavior. *Polymer Engineering & Science*, vol. 3, no. 22, pp. 2758-2764, 1996.

[154] Pini, T., Briatico-Vangosa, F., Frassine, R., Rink, M.: Fracture toughness of acrylic resins: Viscoelastic effects and deformation mechanisms. *Polymer Engineering & Science*, vol. 58, no. 3, pp. 369–376, 2017.

[155] *EN ISO 527-3: Plastics - Determination of tensile properties - Part 3: Test conditions for films and sheets*. 1995.

[156] Mendogni, A.: *Studio del comportamento a frattura in ambiente attivo di polistirene antiurto*. Politecnico di Milano, 2011.

[157] Morelle, X.: *Mechanical characterization and physics- based modeling of highly-crosslinked epoxy resin*. Université catholique de Louvain, 2015.

[158] Khan, F., Krempl, E.: Pre-Necking and Post-Necking Relaxation and Creep Behavior of Polycarbonate: A Phenomenological Study. *Polymer Engineering & Science*, vol. 44, no. 9, pp. 1783–1791, 2004.

[159] Khan, F.: Loading History Effects on the Creep and Relaxation Behavior. *Journal of Engineering Materials and Technology*, vol. 128, no. 4, pp. 564–571, 2006.

[160] Khan, F., Yeakle, C.: Experimental investigation and modeling of non-monotonic creep behavior in polymers. *International Journal of Plasticity*, vol. 27, no. 4, pp. 512–521, 2011.

[161] Khan, F., Yeakle, C., Gomaa, S.: Characterization of the mechanical properties of a new grade of ultra high molecular weight polyethylene and modeling with the viscoplasticity based on overstress. *Journal of the Mechanical Behavior of Biomedical Materials*, vol. 6, pp. 174–180, 2012.

[162] Khan, F., Krempl, E.: Amorphous and Semicrystalline Solid Polymers : Experimental and Modeling Studies of Their Inelastic Deformation Behaviors. vol. 128, pp. 64–72, 2006.

[163] Krempl, E., Khan, F.: Rate (time) -dependent deformation behavior : an overview of some properties of metals and solid polymers. vol. 19, pp. 1069–1095, 2003.

[164] Ferry, J.D.: *Viscoelastic properties of polymers*. New York: John Wiley & Sons, 1970.

[165] Christensen, R.M.: *Theory of Viscoelasticity*. Mineola (New York): Dover Publications, Inc., 2003.

[166] *ISO 13586: Plastic - Determination of the fracture toughness (GIC and KIC) - Linear elastic fracture mechanics (LEFM) approach*. 2003.

[167] Stam, G.: The stress intensity factor for grooved DCB specimens loaded by splitting forces. *International Journal of Fracture*, vol. 76, no. 4, pp. 341–354, 1986.

[168] Machida, K.: JIG evaluation and effective thickness of thin specimens with and without side-grooves. *International Journal of Pressure Vessels and Piping*, vol. 71, pp. 1997, 1997.

[169] Rooke, D.P., Cartwright, D.J.: *Compendium of stress intensity factors*. Uxbridge (Middlesex,U.K.), 1976.

[170] Krishnaswamy, R.K.: Analysis of ductile and brittle failures from creep rupture testing of high-density polyethylene (HDPE) pipes. *Polymer*, vol. 46, no. 25, pp. 11664–11672, 2005.

[171] Saviello, D., Andena, L., Gastaldi, D., Toniolo, L., Goidanich, S.: Multi-analytical approach for the morphological, molecular, and mechanical characterization after photo-oxidation of polymers used in artworks. *Journal of Applied Polymer Science*, vol. 135, no. 17, 46194, 2018.

[172] Pinter, G., Lang, R.W.: Effect of Stabilization on Creep Crack Growth in High-Density Polyethylene. *Journal of Applied Polymer Science*, vol. 90, no. 12, pp. 3191-3207,2003.

[173] Pinter, G., Haager, M., Wolf, C., Lang, R.W.: Thermo-oxidative degradation during creep crack growth of PE-HD grades as assessed by FT-IR spectroscopy. *Macromolecular Symposia*, vol. 217, pp. 307–316, 2004.

ANNEX A: Calibration functions

A.1 Geometry calibration factor $\phi\left(\frac{a}{W}\right)$ for the four-point bending configuration

As described in Chapter 5 the compliance of a notched sample can be described as the product of the material creep compliance and of a geometry function ϕ can be written as:

$$\phi\left(\frac{a}{W}\right) = \frac{L}{BW}\cdot\left[\frac{15}{81}\cdot\frac{L^2}{W^2} + \frac{3}{8}\cdot(2+\nu) + \frac{2\pi L}{W}\int_0^{\frac{\bar{a}}{W}}\frac{a}{W}Y^2\left(\frac{a}{W}\right)d\frac{a}{W}\right] \tag{A.1.1}$$

where L is the span between the lower pins in a four-point bending test, B and W are the sample thickness and width respectively, ν is the Poisson's ratio and Y is the shape factor for the considered test configuration which for the four-point bending is equal to:

$$Y = 1.12 - 1.39\left(\frac{a}{W}\right) + 7.32\left(\frac{a}{W}\right)^2 - 13.1\left(\frac{a}{W}\right)^3 + 14.0\left(\frac{a}{W}\right)^4 \tag{A.1.2}$$

and whose square can be computed as:

$$\begin{aligned} Y^2\left(\frac{a}{W}\right) &= 1.2544 + 1.9321\left(\frac{a}{W}\right)^2 + 53.5824\left(\frac{a}{W}\right)^4 + 171.61\left(\frac{a}{W}\right)^6 + 196\left(\frac{a}{W}\right)^8 \\ &-3.1136\left(\frac{a}{W}\right) + 16.3968\left(\frac{a}{W}\right)^2 - 29.344\left(\frac{a}{W}\right)^3 + 31.36\left(\frac{a}{W}\right)^4 - 20.3496\left(\frac{a}{W}\right)^3 \\ &+36.418\left(\frac{a}{W}\right)^4 - 38.92\left(\frac{a}{W}\right)^5 - 191.784\left(\frac{a}{W}\right)^5 + 204.96\left(\frac{a}{W}\right)^6 - 366.8\left(\frac{a}{W}\right)^7 \end{aligned} \tag{A.1.3}$$

which, can be introduced in the integral of Equation (A.1.1) which hence can be rewritten as:

$$\begin{aligned} \int_0^{\frac{\bar{a}}{W}}\frac{a}{W}Y^2\left(\frac{a}{W}\right)d\frac{a}{W} &= \int_0^{\frac{\bar{a}}{W}}\Big[1.2544\left(\frac{a}{W}\right) - 3.1136\left(\frac{a}{W}\right)^2 + 18.3289\left(\frac{a}{W}\right)^3 \\ &-49.6936\left(\frac{a}{W}\right)^4 + 121.3604\left(\frac{a}{W}\right)^5 - 230.704\left(\frac{a}{W}\right)^6 + 376.57\left(\frac{a}{W}\right)^7 - 366.8\left(\frac{a}{W}\right)^8 \\ &+196\left(\frac{a}{W}\right)^9\Big]\,d\frac{a}{W} \end{aligned} \tag{A.1.3}$$

or

$$\int_0^{\frac{\bar{a}}{W}} \frac{a}{W} Y^2\left(\frac{a}{W}\right) d\frac{a}{W} = \left[\frac{1.2544}{2}\left(\frac{a}{W}\right)^2 - \frac{3.1136}{3}\left(\frac{a}{W}\right)^3 + \frac{18.3289}{4}\left(\frac{a}{W}\right)^4 - \frac{49.6936}{5}\left(\frac{a}{W}\right)^5 + \frac{121.3604}{6}\left(\frac{a}{W}\right)^6 - \frac{230.704}{7}\left(\frac{a}{W}\right)^7 + \frac{376.57}{8}\left(\frac{a}{W}\right)^8 - \frac{366.8}{9}\left(\frac{a}{W}\right)^9 + \frac{196}{10}\left(\frac{a}{W}\right)^{10}\right]_0^{\frac{\bar{a}}{W}} \quad \text{(A.1.4)}$$

Combining Equation (B.1.4) and (B.1.1) the explicit expression of the geometry calibration factor for the four-point bending configuration can be obtained:

$$\phi\left(\frac{a}{W}\right) = \frac{L}{BW} \cdot \left\{\frac{15}{81} \cdot \frac{L^2}{W^2} + \frac{3}{8} \cdot (2+\nu) + \frac{2\pi L}{W} \cdot \left[0.6272\left(\frac{a}{W}\right)^2 - 1.0379\left(\frac{a}{W}\right)^3 + 4.5822\left(\frac{a}{W}\right)^4 - 9.9387\left(\frac{a}{W}\right)^5 + 20.2267\left(\frac{a}{W}\right)^6 - 32.9577\left(\frac{a}{W}\right)^7 + 47.0713\left(\frac{a}{W}\right)^8 - 40.7556\left(\frac{a}{W}\right)^9 + 19.6\left(\frac{a}{W}\right)^{10}\right]_0^{\frac{\bar{a}}{W}}\right\} \quad \text{(A.1.5)}$$

A.2 Energy calibration factor $\psi\left(\frac{a}{W}\right)$ for the four-point bending configuration

The energy calibration factor can be computed as:

$$\psi\left(\frac{a}{W}\right) = \frac{C}{dC \Big/ d\left(\frac{a}{W}\right)} \quad \text{(A.2.1)}$$

where C can be expressed as:

$$C = D(t) \cdot \phi\left(\frac{a}{W}\right) \quad \text{(A.2.2)}$$

being $D(t)$ the material creep compliance and $\phi\left(\frac{a}{W}\right)$ the geometry calibration factor for the four-point bending configuration as per Equation (A.1.5). The derivative of the compliance $dC \Big/ d\left(\frac{a}{W}\right)$ can be evaluated as:

$$
\begin{aligned}
&{}^{dC}\Big/_{d\left(\frac{a}{W}\right)} = D \cdot \frac{d(\varphi)}{d\left(\frac{a}{W}\right)} \\
&= D\,\frac{L}{BW} \cdot \left\{\frac{2\pi L}{W}\left[1.2544\left(\frac{a}{W}\right) - 3.1136\left(\frac{a}{W}\right)^2 + 18.3289\left(\frac{a}{W}\right)^3 - 49.6936\left(\frac{a}{W}\right)^4\right.\right. \\
&\left.\left. +121.3604\left(\frac{a}{W}\right)^5 - 230.704\left(\frac{a}{W}\right)^6 + 376.57\left(\frac{a}{W}\right)^7 - 366.8\left(\frac{a}{W}\right)^8 + 196\left(\frac{a}{W}\right)^9\right\}\right.
\end{aligned}
\tag{A.2.3}
$$

which, if introduced in Equation (A.2.1), allows the evaluation of the explicit form of the energy calibration factor for the four-point bending configuration $\psi_{FPB}\left(\frac{a}{W}\right)$:

$$
\begin{aligned}
&\psi_{FPB}\left(\frac{a}{W}\right) = \left\{\frac{15}{81}\cdot\frac{L^2}{W^2} + \frac{3}{8}\cdot(2+\nu) + \frac{2\pi L}{W}\left[0.6272\left(\frac{a}{W}\right)^2 - 1.0379\left(\frac{a}{W}\right)^3\right.\right. \\
&\left.\left. +4.5822\left(\frac{a}{W}\right)^4 - 9.9387\left(\frac{a}{W}\right)^5 + 20.2267\left(\frac{a}{W}\right)^6 - 32.9577\left(\frac{a}{W}\right)^7\right.\right. \\
&\left.\left. +47.0713\left(\frac{a}{W}\right)^8 - 40.7556\left(\frac{a}{W}\right)^9 + 19.6\left(\frac{a}{W}\right)^{10}\right]\right\} \cdot \left\{\frac{2\pi L}{W}\left[1.2544\left(\frac{a}{W}\right)\right.\right. \\
&\left.\left. -3.1136\left(\frac{a}{W}\right)^2 + 18.3289\left(\frac{a}{W}\right)^3 - 49.6936\left(\frac{a}{W}\right)^4 + 121.3604\left(\frac{a}{W}\right)^5\right.\right. \\
&\left.\left. -230.704\left(\frac{a}{W}\right)^6 + 376.57\left(\frac{a}{W}\right)^7 - 366.8\left(\frac{a}{W}\right)^8 + 196\left(\frac{a}{W}\right)^9\right]\right\}^{-1}
\end{aligned}
\tag{A.2.4}
$$